



CMS-B2G-23-002

CERN-EP-2024-062  
2024/03/26

# Searches for Higgs boson production through decays of heavy resonances

The CMS Collaboration<sup>\*</sup>

## Abstract

The discovery of the Higgs boson has led to new possible signatures for heavy resonance searches at the LHC. Since then, search channels including at least one Higgs boson plus another particle have formed an important part of the program of new physics searches. In this report, the status of these searches by the CMS Collaboration is reviewed. Searches are discussed for resonances decaying to two Higgs bosons, a Higgs and a vector boson, or a Higgs boson and another new resonance, with proton-proton collision data collected at  $\sqrt{s} = 13$  TeV in the years 2016–2018. A combination of the results of these searches is presented together with constraints on different beyond-the-standard model scenarios, including scenarios with extended Higgs sectors, heavy vector bosons and extra dimensions. Studies are shown for the first time by CMS on the validity of the narrow-width approximation in searches for the resonant production of a pair of Higgs bosons. The potential for a discovery at the High Luminosity LHC is also discussed.

*To be submitted to Physics Reports*



## Contents

1	Introduction . . . . .	1
1.1	The Higgs boson at the LHC . . . . .	2
1.2	Resonant Higgs boson production in models beyond the SM . . . . .	6
2	Detector and analysis techniques . . . . .	15
2.1	The CMS Detector . . . . .	17
2.2	Physics objects . . . . .	17
2.3	Search for resonances in VH channels . . . . .	21
2.4	Search for resonances in the HH channel . . . . .	29
2.5	Search for resonances in the YH channel . . . . .	34
2.6	Statistical combination . . . . .	39
3	Upper limits on the cross sections . . . . .	39
3.1	The $X \rightarrow VH$ decays . . . . .	40
3.2	The $X \rightarrow HH$ decays . . . . .	41
3.3	The $X \rightarrow YH$ decays . . . . .	43
4	Model-specific interpretation . . . . .	46
4.1	Extended Higgs sector models . . . . .	46
4.2	Warped extra dimensions . . . . .	52
4.3	Heavy vector triplet models . . . . .	54
4.4	Effects of finite width and interference in resonant HH production . . . . .	54
5	Discovery potential at the HL-LHC . . . . .	62
5.1	Methodology for estimation of the discovery potential . . . . .	63
5.2	Discovery potential for $X \rightarrow HH$ . . . . .	64
5.3	Discovery potential for $X \rightarrow YH$ . . . . .	68
6	Summary . . . . .	74
A	The CMS Collaboration . . . . .	95

## 1 Introduction

The discovery of the Higgs (H) boson in 2012 [1–3], at a mass of about 125 GeV, represented a breakthrough for elementary particle physics. Its observation brought a direct confirmation of the principle of spontaneous symmetry breaking, which explains the origin of elementary particle masses, and is a cornerstone of today’s framework of the standard model (SM) of particle physics.

Since the H boson discovery, subsequent research has shown that the measured production and decay modes of the H boson are in agreement with the SM expectations [4]. Thanks to the high luminosity of the CERN Large Hadron Collider (LHC), the very sizable data set of proton-proton (pp) collisions at a centre-of-mass energy of 13 TeV accumulated during Run 2 (2015–2018), and the considerable advances in analysis methodology, the very elusive SM Higgs boson pair (HH) production process gradually comes into reach. The HH production allows the probing of the trilinear Higgs coupling and thus the investigation of the shape of the Higgs potential.

The H boson also provides an excellent instrument to probe hitherto unknown physics beyond the SM (BSM). A very striking feature of such extensions would be the existence of heavy

resonances coupling directly to the H boson, which might, even dominantly, decay into final states involving H bosons. This would lead to an additional source of H boson production in resonant topologies, which is absent in the SM. Given the small cross section of SM HH production due to the destructive interference between several contributing processes, an excess of HH production with respect to the SM prediction could reveal the existence of heavy BSM resonances. Similarly, the associated production of H and vector bosons could be significantly modified by resonant contributions.

Extended Higgs sectors, which comprise more than the single complex Higgs doublet of the SM, would provide natural candidates for heavy scalar bosons that decay into final states with one or more H bosons. Examples of such models are two-Higgs-doublet models (2HDM) [5–8], 2HDMs extended with a scalar singlet (2HDM+S) [9–11], and the two-real-singlet model (TRSM) [12]. Supersymmetry naturally incorporates extended Higgs sectors. The minimal supersymmetric model (MSSM) [13–16] features a 2HDM-type Higgs sector, while the next-to-minimal supersymmetric model (NMSSM) [17–19] includes a 2HDM+S-type Higgs sector.

Models of warped extra dimensions (WED) [20–29] predict the existence of an additional spatial dimension in which the field quanta of gravity, the gravitons, propagate. The Randall–Sundrum bulk model gives rise to heavy resonances such as the spin-0 radion, and a tower of Kaluza–Klein excitations of the spin-2 graviton, which might have sizable branching fractions into HH. In certain models, which might potentially solve the hierarchy problem, heavy vector resonances, like W' and Z', form a heavy vector triplet (HVT) [30]. They could manifest themselves through decays into ZH and WH, where W and Z denote the electroweak (EW) gauge bosons.

This report is organized as follows: Section 1 provides a brief introduction to the H boson and the theoretical concepts underlying the resonant production of H bosons. Section 2 summarizes the techniques of the respective CMS analyses on 13 TeV data. Section 3 presents a coherent picture of the results of these analyses, as well as combinations of these results. Section 4 is dedicated to interpretations of the results in the various models. Section 5 discusses projections towards higher integrated luminosities, including the potential for a discovery at the High-Luminosity LHC (HL-LHC). A summary is given in Section 6.

Tabulated results unique to this report are provided in a HEPData record [31].

## 1.1 The Higgs boson at the LHC

The Higgs boson was first proposed in the 1960s [32–34], and was finally discovered at the LHC in 2012, by the ATLAS [1] and CMS [2, 3] experiments.

In the SM, the Higgs field has a nonzero vacuum expectation value, which breaks the EW symmetry and generates the masses of the W and Z bosons, while leaving the photon massless. This process is called the EW symmetry breaking of the Brout–Englert–Higgs mechanism.

There are several ways that H bosons can be produced at the LHC in pp collisions, each with its own unique experimental signature. The production cross sections are shown in Fig. 1 (left).

The dominant H boson production mechanism is through the “gluon fusion” process (ggF), which involves the fusion of two gluons from the colliding protons. This process accounts for around 88% of all H bosons produced at the LHC. “Vector boson fusion” (VBF) describes the scattering of two vector bosons V (W or Z bosons) exchanged between the colliding protons, and accounts for around 8% of all Higgs bosons produced at the LHC. Other processes include associated H boson production with vector bosons (VH), with top quarks ( $t\bar{t}H$ ), or with bottom

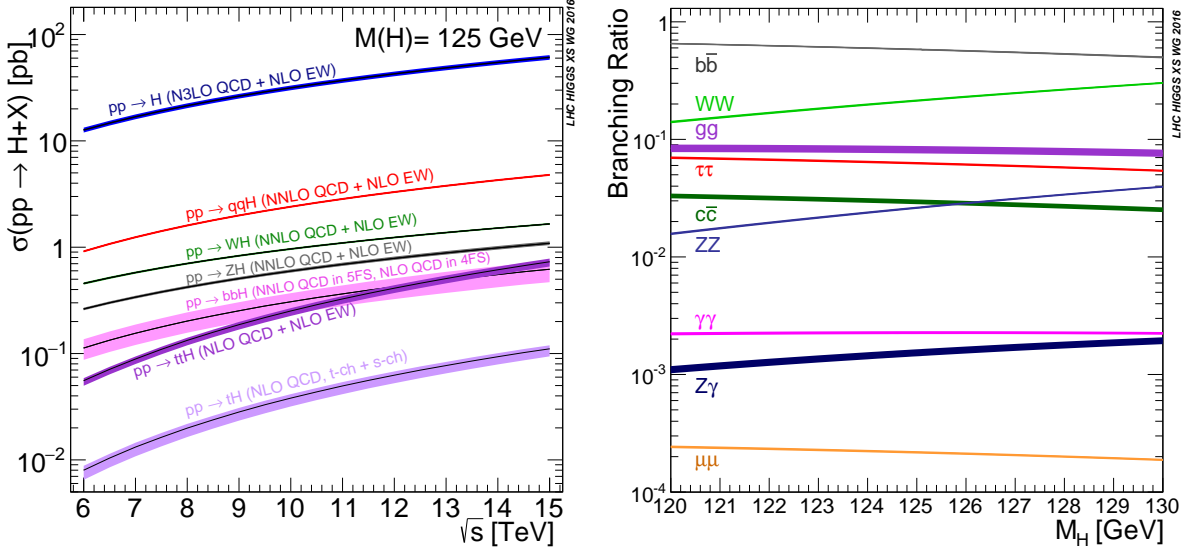


Figure 1: Higgs boson production cross sections in the SM as a function of the collider centre-of-mass energy (left), and Higgs boson branching fractions in the SM as a function of the Higgs boson mass (right). Both figures are taken from Ref. [35].

quarks ( $b\bar{b}H$ ).

Once produced, Higgs bosons can decay in various ways, each producing a different final state of particles. The most common and experimentally accessible  $H$  boson decay modes are to a pair of bottom quarks,  $W$  bosons,  $\tau$  leptons, and  $Z$  bosons as shown in Fig. 1 (right). The  $H$  boson does not directly couple to gluons or photons, but can decay into them via fermion or  $W$  boson loops.

The properties and couplings of the  $H$  boson have been extensively studied at the LHC. The SM does not predict the mass of the  $H$  boson, but once the mass is given, all its other properties are defined. The most recent and precise measurement of the  $H$  boson mass is  $m_H = 125.22 \pm 0.14$  GeV [36]. The CMS Collaboration has measured the  $H$  boson width to be  $\Gamma_H = 3.2^{+2.4}_{-1.7}$  MeV via off-shell production in the  $4\ell$  and  $2\ell + 2\nu$  final states [37]. This value is in agreement with the SM prediction of 4.1 MeV [38].

To quantify the agreement between the data and the SM predictions, the concept of a signal strength can be used, which is defined as  $\mu = \sigma/\sigma_{\text{SM}}$ , where  $\sigma$  is the measured production cross section and  $\sigma_{\text{SM}}$  is the SM prediction. After performing a combined fit of all the data collected at  $\sqrt{s} = 13$  TeV, in all production modes and decay channels, the observed  $H$  signal strength is  $\mu = 1.002 \pm 0.057$  [4], in agreement with the SM prediction. Figure 2 shows the CMS measurements of the signal strength parameter for each production mode,  $\mu_i = \sigma_i/\sigma_{i,\text{SM}}$ , and decay channels,  $\mu^f = \mathcal{B}^f/\mathcal{B}_{\text{SM}}^f$ , where  $\mathcal{B}$  is the branching fraction. The production modes  $ggF$ ,  $VBF$ ,  $WH$ ,  $ZH$ , and  $t\bar{t}H$  are all observed with a significance of five standard deviations (s.d.) or above [4].

To quantify the impact of new physics on the interaction between the  $H$  boson and other particles, we scale the coupling strengths as predicted in the SM by a factor  $\kappa_i$  (the coupling modifiers) [38], where  $i$  is the coupling which the modifier corresponds to. Two coupling modifiers are introduced,  $\kappa_V$  and  $\kappa_f$ , to scale the couplings to the EW gauge bosons and fermions, respectively. When differentiating between the two heavy gauge bosons  $W$  and  $Z$ , we can define  $\kappa_W$  and  $\kappa_Z$ . Equivalently, for the fermions we define  $\kappa_t$ ,  $\kappa_b$ ,  $\kappa_\tau$ , and  $\kappa_\mu$ . In extensions of the

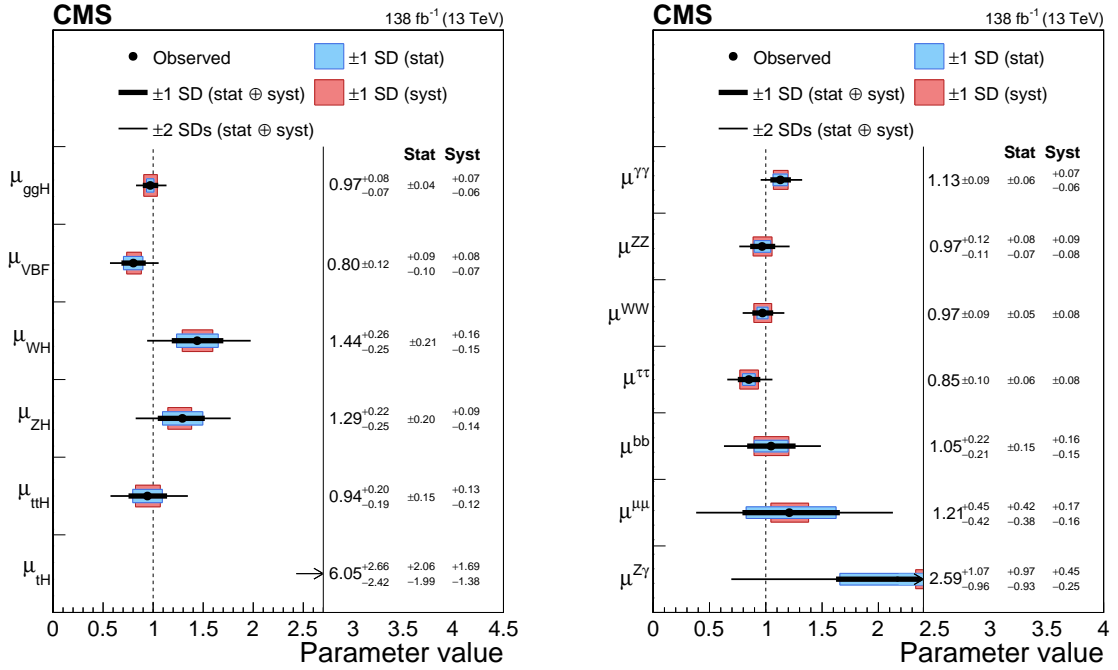


Figure 2: Signal strength parameters extracted for various production modes  $\mu_i$ , assuming the branching fractions  $\mathcal{B}^f = \mathcal{B}_{SM}^f$  (left), and decay channels  $\mu^f$ , assuming the production cross sections as predicted by the SM (right). The thick and thin black lines indicate the one and two s.d. confidence intervals (labelled by SD in the figures), with the systematic and statistical components of the former indicated by the red and blue bands, respectively. The vertical dashed line at unity represents the values of  $\mu_i$  (resp.  $\mu^f$ ) in the SM. Taken from Ref [4].

SM with new particles, loop-induced processes may receive additional contributions, therefore introducing additional modifiers for the effective couplings of the H boson to gluons ( $\kappa_g$ ), photons ( $\kappa_\gamma$ ), and  $Z\gamma$  ( $\kappa_{Z\gamma}$ ). According to the latest combined results on these effective couplings shown in Fig. 3, the measured coupling modifiers are compatible with the SM expectations within 1.5 s.d., with uncertainties around 10% for most couplings [4]. The invisible and undetected decays of the Higgs boson are also considered, where the latter expression refers to Higgs boson decays into final states that can not be distinguished from background processes, at the LHC.

The H boson trilinear self-coupling is a measure of the interaction strength between two H bosons and determines the shape of the Higgs field potential. The Higgs boson self-coupling can be accessed directly at the LHC via Higgs boson pair production. This rare process has a very low SM cross section because of the destructive interference of the two contributing processes at leading order (LO), the box and triangle diagrams shown in Fig. 4 (left and middle). Only the triangle diagram is sensitive to the H trilinear coupling. As a result, detecting the production of Higgs boson pairs and determining the trilinear self-coupling is a major experimental challenge.

The CMS Collaboration has constrained the coupling modifier for the trilinear H boson self-coupling to be within  $-1.25$  and  $6.85$  at 95% confidence level (CL) using pp data corresponding to an integrated luminosity of  $138 \text{ fb}^{-1}$ . The production cross section for inclusive HH production has been constrained to be smaller than 3.4 times the value predicted in the SM at 95% CL [4].

To understand the Higgs sector is essential for particle physics and cosmology. Determining

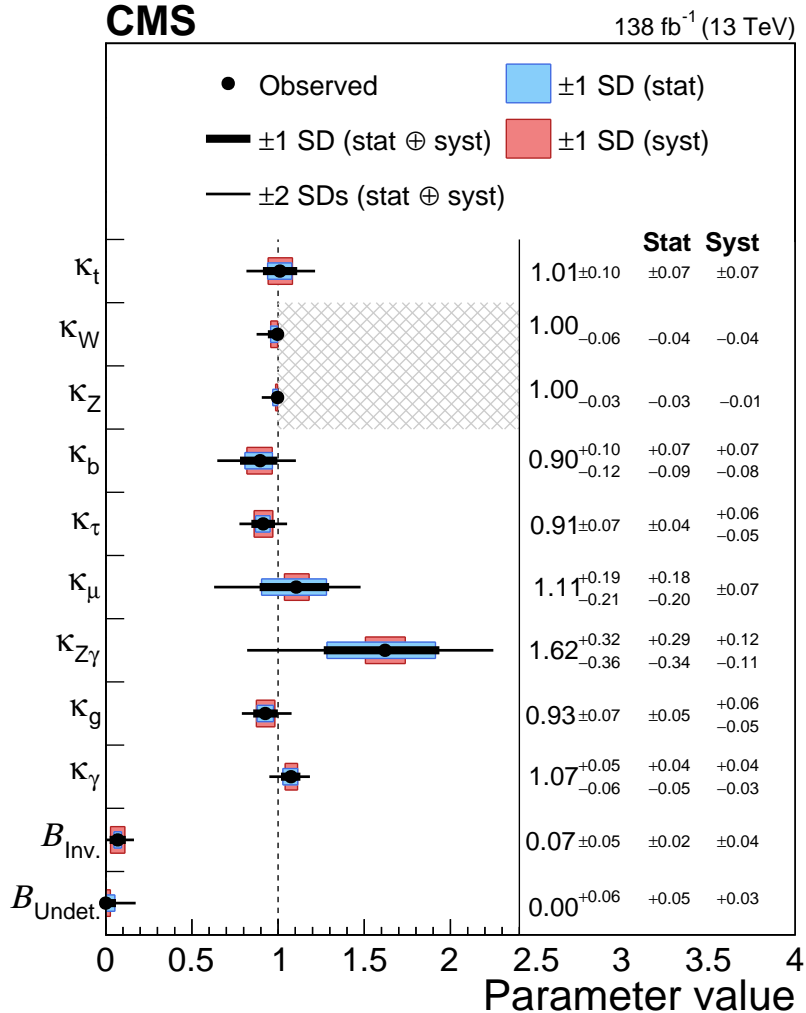


Figure 3: Measurements of the coupling modifiers  $\kappa_i$ , allowing both invisible and undetected decay modes, with the SM value used as an upper bound on both  $\kappa_W$  and  $\kappa_Z$ . The thick and thin black lines indicate the  $\pm 1$  and  $\pm 2$  s.d. confidence intervals, respectively, with the systematic and statistical components of the  $\pm 1$  s.d. interval indicated by the red and blue bands. The resulting branching fractions for invisible and undetected decay modes are also displayed. Taken from Ref. [4].

the exact behaviour of the Higgs field will help us understand the formation of structures in the early universe immediately after the Big Bang, and the stability of the vacuum. Some theories of inflation involve a scalar field as the inflaton, the field responsible for driving the expansion of the universe [39, 40].

The fact that the Higgs field is the only scalar field currently known motivates a theory based on the idea that the Higgs field caused inflation. In this case, the shape of the Higgs potential is tightly related to the problem of the stability of the vacuum. The behaviour of the Higgs field during the phase transition in the early universe can explain leptogenesis and baryogenesis and could potentially shed light on the matter-antimatter asymmetry we observe today [41]. However, the Higgs sector does not have to be minimal. The presence of additional fields would have an impact on the mechanism of inflation. Studying the Higgs interactions in detail and exploring the Higgs sector more broadly provide a promising avenue for discovering BSM physics and understanding the evolution of the early universe.

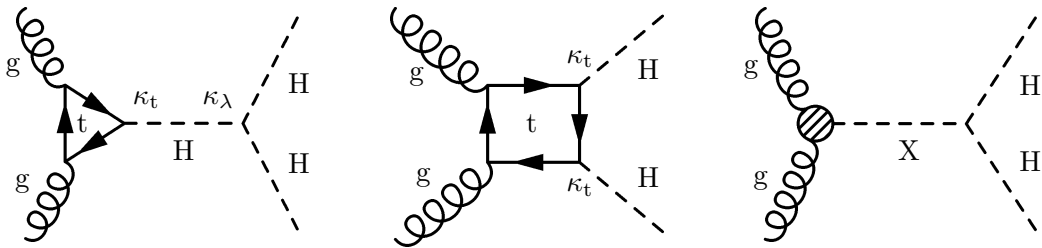


Figure 4: Leading order Feynman diagrams of Higgs boson pair production via gluon fusion. The left and middle parts of the figure show the “triangle” and “box” diagrams, respectively for nonresonant H production, as expected from the SM. The right part of the figure shows a diagram for H boson production through a new resonance of labeled as X.

## 1.2 Resonant Higgs boson production in models beyond the SM

The production of H bosons through the decay of heavy resonances is not possible within the SM. A generic example of a Feynman diagram for such a process is shown in Fig. 4 (right), where X denotes a sufficiently heavy resonance. In the following, we briefly review BSM models in which such production mechanisms occur.

### 1.2.1 Extended Higgs sectors

The SM Higgs sector consists of one complex Higgs doublet and leads to the prediction of one physical H boson. However, there is no guarantee that the Higgs sector is minimal. The SM Higgs sector can be extended with additional singlets, doublets, or triplets, or combinations thereof [6, 42–45]. Extended Higgs sectors imply the presence of additional Higgs bosons: Neutral Higgs bosons appear in singlet, doublet, and triplet extensions; charged Higgs bosons  $H^\pm$  appear in doublet and triplet extensions; and doubly charged Higgs bosons, like e.g.  $H^{++}$ , appear in triplet extensions. In this report, we focus on extensions with singlets and doublets since these lead to final states with SM-like H bosons. Furthermore, it is assumed that the singlets and doublets acquire a vacuum expectation value and couple to the SM particles.

The phenomenology of the additional neutral bosons also depends on their  $CP$  structure. Here, we only consider  $CP$  eigenstates: pure scalars are denoted by either X or Y, with  $m_X > m_Y$ , and pseudoscalars are denoted by A or a, with  $m_A > m_a$ . Depending on the structure of the extended Higgs sector and on the masses of the additional scalars and pseudoscalars, the following decays involve SM-like H bosons in the decay chain:

1. decays of a heavy neutral scalar to two SM-like Higgs bosons,  $X \rightarrow HH$ ,
2. decays of a heavy neutral scalar to an SM-like Higgs boson and another scalar,  $X \rightarrow YH$ ,
3. decays of a heavy pseudoscalar to an SM-like Higgs boson and another pseudoscalar,  $A \rightarrow Ha$ , and
4. decays of a heavy pseudoscalar to an SM-like Higgs boson and a Z boson,  $A \rightarrow ZH$ .
5. For large  $m_X$  and if  $m_Y \gtrsim 250\text{ GeV}$ , there can also be chained decays leading to the production of multiple H bosons,  $X \rightarrow YY \rightarrow HHHH$  and  $X \rightarrow YH \rightarrow HHH$ .

In general, the additional singlets and doublets mix with the SM doublet and therefore modify the couplings of the SM-like scalar H [46]. The couplings of the observed H boson agree well with the SM predictions, leading to significant constraints on the parameter space of extended Higgs models [4, 47–49].

**Additional singlets** The most straightforward extension of the SM Higgs sector is to introduce an additional real-singlet field  $S$  [50–53]. The ratio of the vacuum expectation values  $v$  of the SM complex doublet and of the singlet,  $\langle S \rangle$ , defines the parameter  $\tan \beta = v / \langle S \rangle$ . The real-singlet model leads to one additional scalar  $X$ , which can be heavier or lighter than  $H$ . When applying a  $\mathbb{Z}_2$  symmetry that requires invariance under transformation of the field  $S \rightarrow -S$ , the scalar  $X$  obtains its couplings to SM particles from mixing with the SM-like  $H$  boson, with a mixing angle  $\alpha$ . The couplings to SM particles hence correspond to those of the  $H$  boson, albeit suppressed by a factor  $\sin \alpha$  if  $m_X > m_H$ .

The decay rates of the scalar  $X$  hence correspond to those of an SM-like Higgs boson, unless  $m_X > 2m_H$ , in which case the decay  $X \rightarrow HH$  becomes kinematically possible. In this case, the decays to other SM particles are suppressed depending on the partial width of the  $X$  decay to  $HH$ , which depends on  $\tan \beta$ . In summary, the extension with a real additional scalar with  $\mathbb{Z}_2$  symmetry involves three new free parameters — the mass of the additional scalar  $m_X$ , the mixing angle  $\alpha$ , and the ratio of the two vacuum expectation values  $\tan \beta$  — and leads to  $X \rightarrow HH$  decays if kinematically possible, with a relative rate compared to the other decay modes depending on  $\tan \beta$ .

Adding a second real singlet field, again imposing  $\mathbb{Z}_2$  symmetry, defines the two real singlet model (TRSM) [12]. Compared to the real-singlet extension, the TRSM introduces four new parameters: the mass of a second new scalar  $Y$ , the mixing angles between the second real singlet field and the complex SM doublet as well as the other real singlet field, and the vacuum expectation value of the second real singlet field. The main difference in terms of phenomenology is that, depending on the masses of the additional Higgs bosons, decays of type  $X \rightarrow YH$ ,  $X \rightarrow HH$  (or  $Y \rightarrow HH$ ), and  $X \rightarrow YY$  become possible, including the chained decays  $X \rightarrow YY \rightarrow HHHH$  and  $X \rightarrow YH \rightarrow HHH$ . All of the decays involving  $H$  bosons can have large branching fractions and are hence of experimental interest. The final states that provide the most sensitivity after the decays of the  $H$  bosons depend on the branching fractions of  $H$  (discussed in Section 1.1) and  $Y$ . The  $Y$  branching fractions correspond to those of an SM-like Higgs boson of mass  $m_Y$ . Therefore, decays into  $W$  and  $Z$  bosons dominate above the  $WW$  and  $ZZ$  production thresholds, and decays to  $t\bar{t}$  become relevant above the  $t\bar{t}$  production threshold. This is different from 2HDMs where decays into fermions are dominant for a large fraction of the parameter space.

**Additional doublets** In 2HDMs, the SM is extended with a second Higgs doublet leading to the emergence of three neutral and two charged Higgs bosons [5–8]. Most commonly it is required that each Higgs doublet only couples to charged fermions of one type (up-type quarks, down-type quarks, or charged leptons) and  $CP$ -violating terms at the tree level are forbidden to evade constraints from flavor-changing neutral currents and the negative results of searches for  $CP$  violation in the Higgs sector. These constraints give rise to four types of 2HDMs that are distinguished by which of the Higgs doublet fields couples to which type of fermions:

1. Type I, with all charged fermions coupled to the second Higgs doublet,
2. Type II, with only up-type quarks coupled to the second Higgs doublet,
3. Lepton-specific (Type X), with only up-type and down-type quarks coupled to the second Higgs doublet, and
4. Flipped (Type Y), with only up-type quarks and charged leptons coupled to the second Higgs doublet.

The free parameters of the model can be expressed in terms of the masses of the Higgs bosons ( $m_H$ , with  $H$  being the SM-like Higgs boson, as well as  $m_X$ ,  $m_A$ , and  $m_{H^\pm}$ ), the vacuum expectation value of the SM-like doublet  $v$ , the ratio of the two vacuum expectation values  $\tan \beta$ , the mixing angle  $\alpha$ , and a parameter  $m_{12}$  that softly breaks the  $Z_2$  symmetry. Since  $m_H$  and  $v$  are known, there are six free parameters in these 2HDM scenarios. However, there are important constraints on the parameter space. Constraints from EW precision data require the masses of at least two of the additional Higgs bosons to be close to each other [54], which is why mass-degenerate scenarios are studied most frequently. In addition, flavor observables lead to strong constraints in the overall parameter space, and in particular to lower bounds on  $m_{H^\pm}$  of around 600 GeV in Type II and Type Y models. Furthermore, in the so-called alignment limit with  $\cos(\beta - \alpha) \rightarrow 0$  the  $H$  boson becomes SM-like. In turn, the measurements of the  $H$  boson couplings, which are consistent with the SM predictions within uncertainties [4, 49], lead to constraints on  $|\cos(\beta - \alpha)|$  between 0.02 and 0.3, depending on the type of 2HDM and on  $\tan \beta$  [47–49, 54].

The couplings of additional heavy Higgs bosons  $X$  and  $A$  that involve an  $H$  boson crucially depend on  $\cos(\beta - \alpha)$ . For  $\cos(\beta - \alpha) \rightarrow 0$ , the branching fractions for the decays  $X \rightarrow HH$  and  $A \rightarrow ZH$  vanish. While the couplings remain the same for different types of 2HDMs, the branching fractions can be different because these depend on the partial widths of all decay modes. Example branching fractions for 2HDMs of Type I and Type II are shown in Fig. 5. For non-mass-degenerate 2HDMs, decays of type  $A \rightarrow ZX$  and  $X \rightarrow ZA$  are possible. If allowed, these decays usually have large branching fractions that are not suppressed in the alignment limit.

An important special case of a 2HDM of Type II is the Higgs sector of the minimal supersymmetric standard model (MSSM) [13–16]. At the tree level, the MSSM Higgs sector can be described by two parameters,  $m_A$  and  $\tan \beta$ . The MSSM naturally predicts an  $H$  boson that has nearly SM-like couplings, in particular when  $m_A$  is large. Furthermore, it also predicts the mass of the SM-like  $H$  boson. For small values of  $\tan \beta$ , i.e.,  $\tan \beta \gtrsim 1$ , a large supersymmetry (SUSY) breaking scale is needed to achieve  $m_H = 125$  GeV. This is, however, consistent with the nonobservation of SUSY partners at the LHC.

Various MSSM benchmark scenarios have been proposed [35, 57–60, 63]. Searches for  $A/X \rightarrow \tau\tau$  exclude a large fraction of parameter space at medium to high  $\tan \beta$  [64], such that the phenomenologically interesting parameter space is at low to medium  $\tan \beta$ . Figure 6 shows the  $X \rightarrow HH$  branching fractions in two scenarios that are particularly designed to give non-excluded predictions at low  $\tan \beta$ . The branching fractions for masses below the  $t\bar{t}$  threshold can reach values of more than 80%, making this channel very important, though measurements of the  $H$  boson couplings indicate that  $m_A > 400$ –500 GeV [47, 48]. For intermediate values of  $\tan \beta$ , the branching fraction  $\mathcal{B}(X \rightarrow HH)$  can still be of order 10% and the search remains important, whereas  $\mathcal{B}(A \rightarrow ZH)$  becomes negligible.

**Models with additional singlets and doublets** Models that combine singlets and doublets include the next-to-minimal 2HDM (N2HDM), which extends the 2HDM with a real singlet, and the 2HDM+S, which extends the 2HDM with a complex singlet [9–11]. Considering only  $CP$ -conserving versions of the model, the N2HDM predicts three  $CP$ -even neutral Higgs bosons (again denoted as  $H$ ,  $X$ , and  $Y$ ), one  $CP$ -odd neutral Higgs boson  $A$ , and two charged Higgs bosons  $H^\pm$ . Compared to 2HDMs, the N2HDM adds four additional parameters [11]: two mixing angles  $\alpha_2$  and  $\alpha_3$ , responsible for the mixing of the additional singlet with the two doublets, the mass of the additional  $CP$ -even Higgs boson  $m_Y$ , and the vacuum expectation value of the real singlet  $v_S$ . The N2HDMs can be categorized in the same four scenarios as

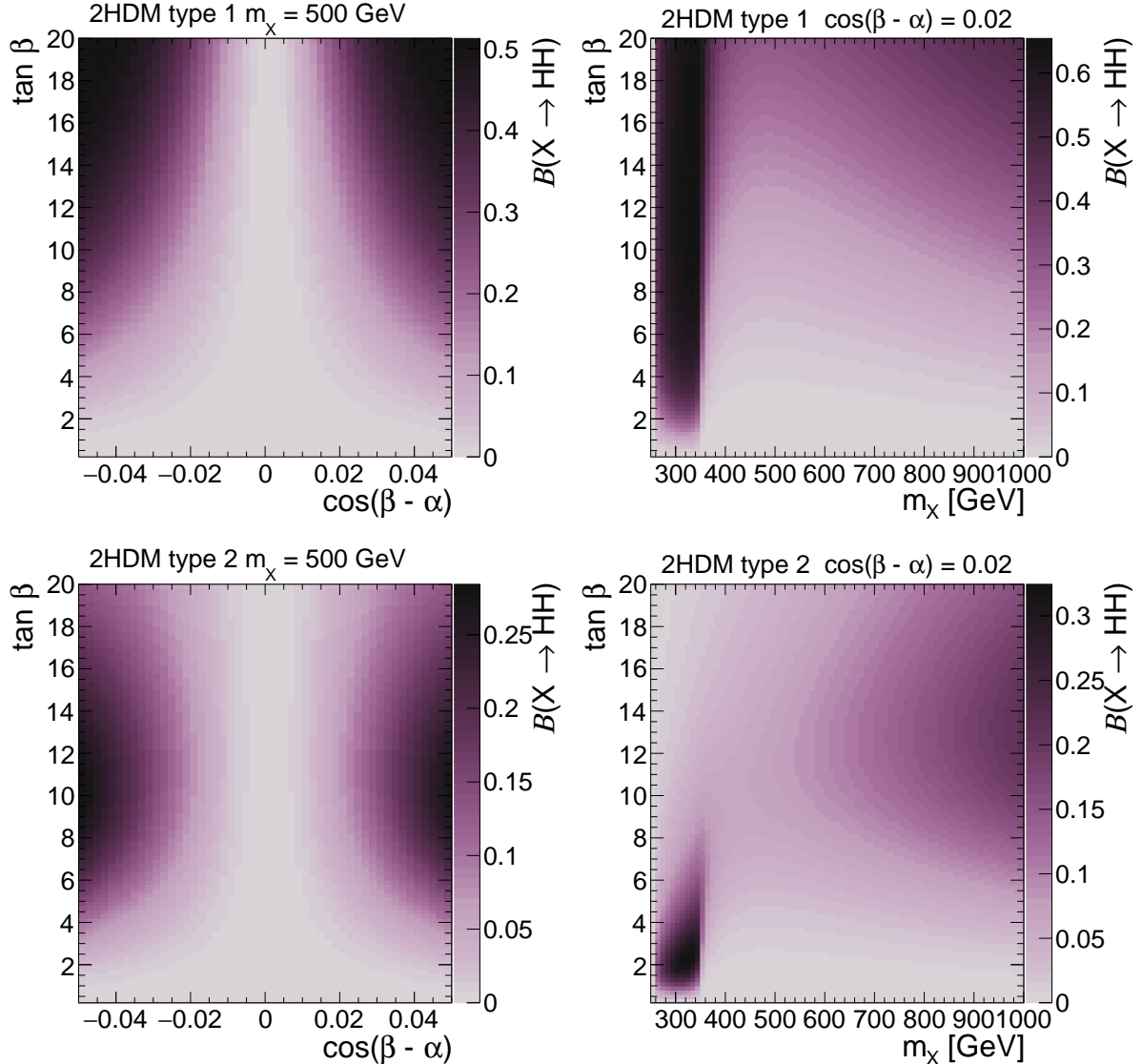


Figure 5: Branching fractions of  $X \rightarrow HH$  decays in 2HDMs of Type I (upper) and Type II (lower) in the  $\cos(\beta - \alpha)$ - $\tan \beta$  plane for  $m_X = 500$  GeV (left) and in the  $m_X$ - $\tan \beta$  plane for  $\cos(\beta - \alpha) = 0.02$  (right). The masses of all non-SM-like Higgs bosons are set to be the same,  $m_X = m_A$ , and  $m_{12}^2 = m_A^2 \tan \beta / (1 + \tan^2 \beta)$ . The branching fractions have been calculated with 2HDMC v1.8.0 [55, 56].

2HDMs, depending on the Yukawa couplings.

Phenomenologically, N2HDMs share many similarities and constraints with 2HDMs, in particular, those related to EW constraints and flavor observables. However, the singlet admixture can affect the couplings of the SM-like H boson. Most importantly, the additional scalar Y can either be produced directly or in decays of heavier Higgs bosons,  $X \rightarrow YH$  and  $X \rightarrow YY$ . Unlike decays to two SM-like Higgs bosons like  $X \rightarrow HH$ , these decays are not suppressed in the alignment limit, which is at least approximately realized given the SM-like nature of the H boson. The decays  $X \rightarrow YH$  and  $X \rightarrow YY$  can hence be dominant if kinematically allowed. The branching fractions of the Y boson to SM particles depend on the Yukawa type and the other model parameters. This leads to a variety of experimentally relevant final states [65, 66].

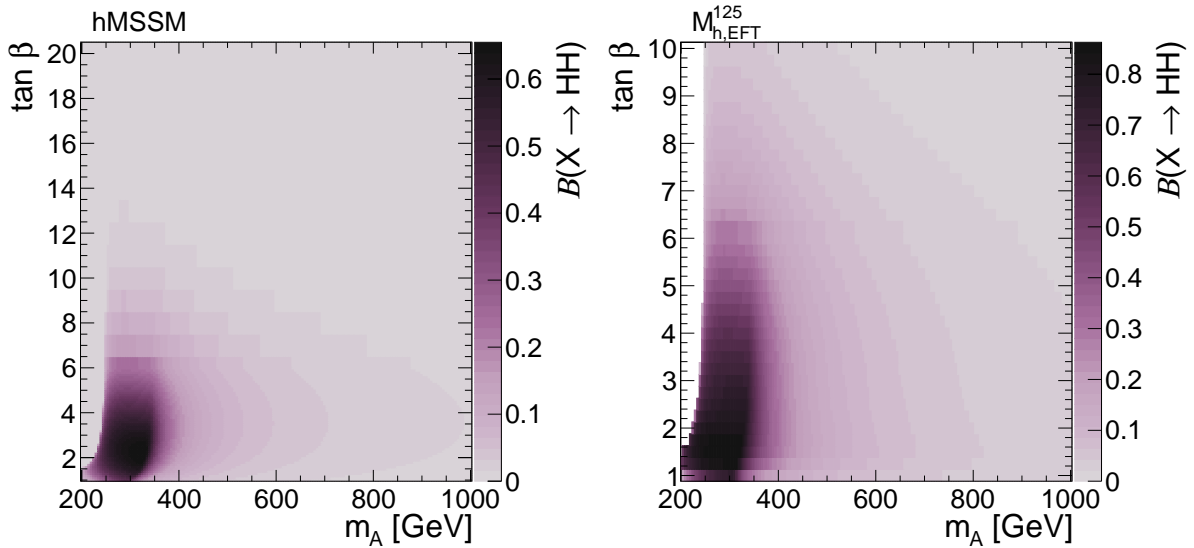


Figure 6: Branching fraction of  $X \rightarrow \text{HH}$  decays in the MSSM, for the hMSSM [57–59] (left) and the  $M_{h,\text{EFT}}^{125}$  [60] benchmarks, in the  $m_A$ – $\tan \beta$  plane. The branching fractions are taken from benchmark files produced by the MSSM subgroup of the LHC Higgs Working Group [61, 62].

The 2HDM+S model adds a second  $CP$ -odd Higgs boson, leading to the additional  $A \rightarrow Ha$  decay, which is experimentally consistent with the  $X \rightarrow \text{HY}$  signature [67]. The Higgs sector of the next-to-minimal MSSM (NMSSM) is a 2HDM+S of Type II [17–19]. The NMSSM generally leads to the same signatures as the N2HDM and 2HDM+S models, but, like the MSSM, is more constrained due to the characteristics of SUSY, and these constraints differ from the MSSM ones because of the additional particle content [52, 68, 69].

### 1.2.2 Warped extra dimensions (radion and Randall–Sundrum graviton)

Models with a warped extra dimension (WED), as proposed by Randall and Sundrum (RS) [20], postulate the existence of one extra spatial dimension compactified between two fixed “branes”. The region between the branes is referred to as bulk and controlled through an exponential metric. The gap between the two fundamental scales of nature, such as the Planck scale ( $M_{\text{Pl}}$ ) and the EW scale, is controlled by a warp factor ( $k$ ) in the metric, which corresponds to one of the fundamental parameters of the model. The brane where the extra-dimensional metric’s density is localized is called the “Planck brane”, while the other, where the Higgs field is localized, is called the “TeV brane”. This class of models predicts the existence of new particles that can decay to HH, such as the spin-0 radion  $R$  [21–23], and the first spin-2 Kaluza-Klein (KK) excitation of the graviton,  $G$  [24–26]. The radion is an additional element of WED models, needed to stabilize the size of the extra dimension  $l$  where the distance between the branes is connected to its vacuum expectation value [21].

There are two possible ways of describing a KK graviton in WED models, that depend on the localization choice for the SM matter fields, as shown in Fig. 7. In the RS1 model, only gravity is allowed to propagate in the extra-dimensional bulk. In this model, the KK graviton couplings to matter fields are controlled by the dimensionless quantity  $\tilde{k} = k/\bar{M}_{\text{Pl}}$  [20], with the reduced Planck mass  $\bar{M}_{\text{Pl}}$  defined by  $M_{\text{Pl}}/\sqrt{8\pi}$ . The second possibility is to have SM particles propagate in the bulk, the bulk-RS model. In this scenario, the KK graviton couplings to the matter fields depend on the localization of the SM fields in the bulk. This report uses the phenomenology of Ref. [27]. The SM particles are allowed to propagate in the bulk and follow the SM gauge group’s characteristics, with the right-handed top quark localized very near the TeV brane (the

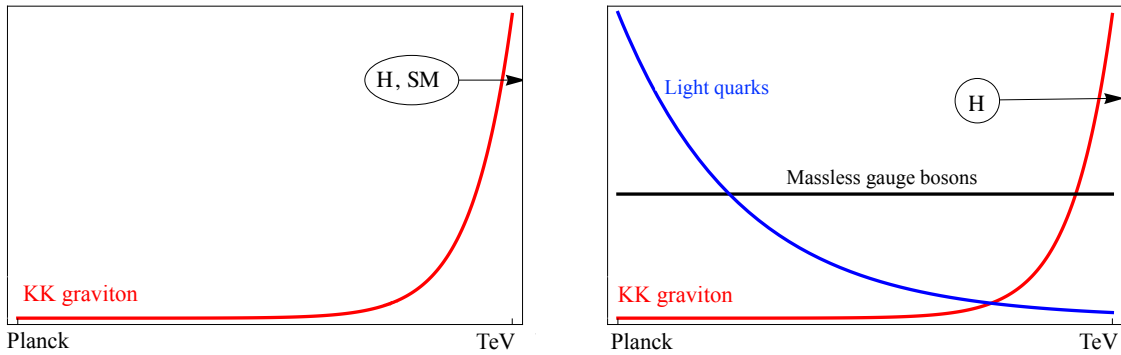


Figure 7: Localization of fields on the branes, in different types of the Randall-Sundrum (RS) model: RS1 (left) and bulk-RS (right). The  $x$ -axis represents the 5th dimension with the Planck brane on the left and the TeV brane on the right. The  $y$ -axis is the probability density. Adapted from Ref. [28].

so-called elementary top quark hypothesis).

It is common practice to express the benchmark points of the model in terms of  $\tilde{k}$ , and the mass scale  $\Lambda_R = \sqrt{6} e^{-kL} M_{Pl}$ , where the latter is interpreted as the ultraviolet cutoff of the model [29]. The addition of a scalar-curvature term can induce mixing between the scalar R and the H boson [29, 70, 71]. Precision EW studies suggest that this mixing is small [72], so we neglect the possibility of R-H mixing in this report.

The choice of localization of the SM matter fields for the KK-graviton resonance impacts the kinematics of the signal and drastically modifies its production and decay properties [73], so that a distinction of the RS1 and bulk-RS models is necessary for G. In contrast, the physics of the radion depends only very weakly on the choice of the model [29], which obviates the need to distinguish the RS1 and bulk-RS possibilities for R. More details on WED models can be found in Ref. [28].

In RS1, with all the SM fields localized on the TeV brane, a heavy graviton would decay to a wide range of final states with significant branching fractions as shown in Fig. 8 (top left), and constraints on the RS1 model are mainly obtained from fermionic channels [74]. In the bulk-RS model, the maximum branching fraction to a pair of Higgs bosons is below 10% under the hypothesis of an elementary H boson, as shown in Fig. 8 (top right). Accordingly, the HH final state is usually not the most important one for placing constraints on the bulk-RS model, where the largest sensitivity arises from searches in WW, ZZ, or  $t\bar{t}$  signatures. However, the branching fraction to HH can reach 25% if the top quark coupling becomes small, such that investigations of HH signatures are necessary in the context of bulk-RS models, because the branching fractions are very model dependent.

The dominant R decay modes are into pairs of massive gauge bosons, H bosons, and top quarks, as shown in Fig. 8 (right). Since the couplings are determined by the masses of the final-state particles, and these masses arise from the H boson localized on the TeV brane, the RS1 and bulk-RS couplings are identical at LO. For large resonance mass  $m_X$ , the corresponding widths are

$$\Gamma(R \rightarrow HH) = \Gamma(R \rightarrow ZZ) = \Gamma(R \rightarrow WW)/2 = \frac{1}{32\pi} \frac{m_X^3}{\Lambda_R^2} \quad (1)$$

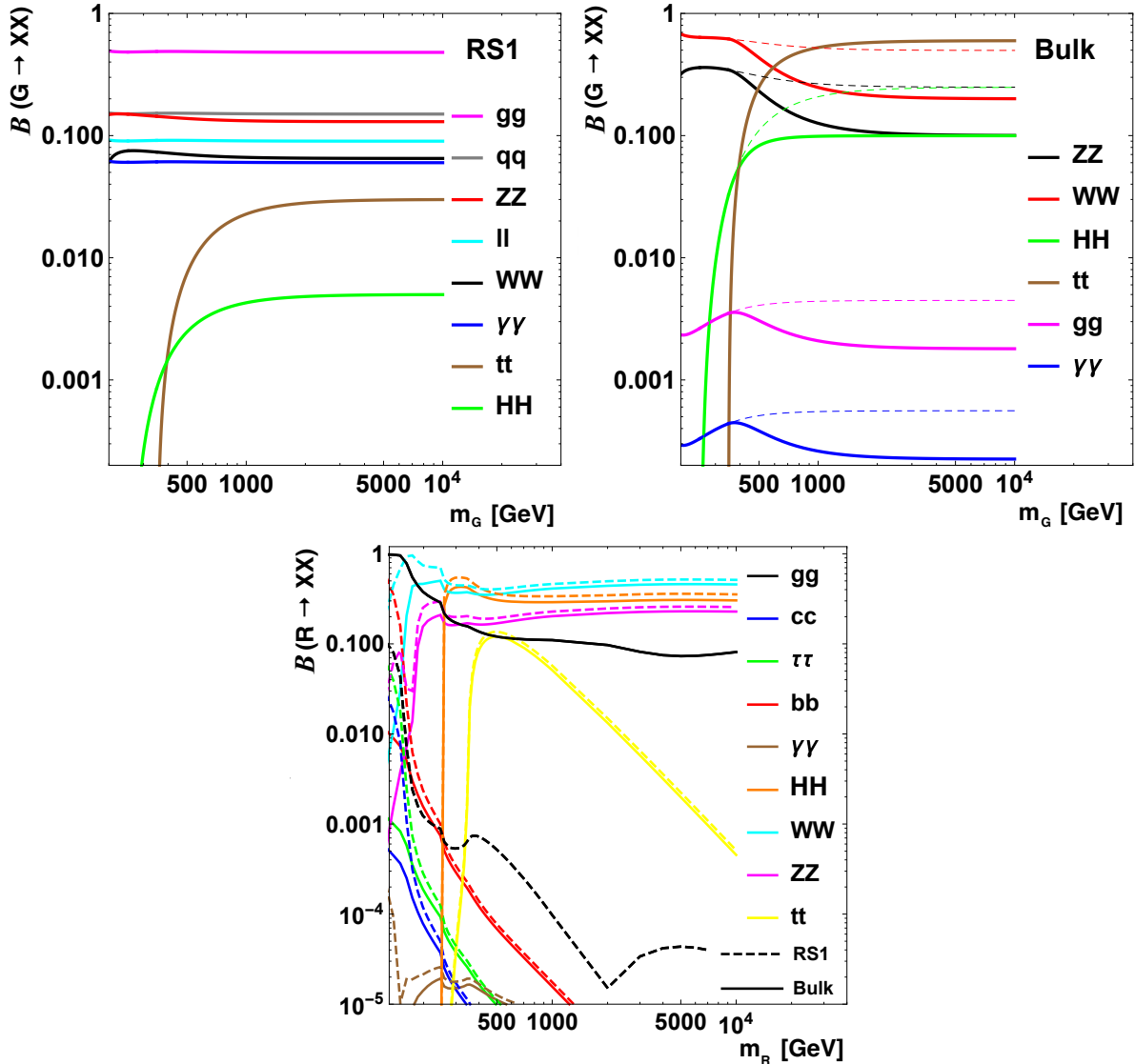


Figure 8: The decay branching fractions of an RS1 graviton (top left), bulk graviton (upper right), and radion (lower). Solid lines assume a fully elementary top quark, while the dashed lines ignore the coupling of the graviton to top quarks. Adapted from Ref. [28].

and

$$\Gamma(R \rightarrow t\bar{t}) = \frac{3}{8\pi} \left( \frac{m_t}{m_X} \right)^2 \frac{m_X^3}{\Lambda_R^2}. \quad (2)$$

For large radion masses, the branching fraction to HH is approximately 25%, independent of  $\Lambda_R$ , because the contribution from decays to  $t\bar{t}$  is suppressed by  $(m_t/m_X)^2$ . This makes the  $R \rightarrow HH$  channel an important one in the search for a radion resonance.

### 1.2.3 Heavy vector triplet (W' and Z')

A class of models extending the gauge groups of the SM predicts new force-carrying vector bosons. They may form a heavy vector triplet (HVT) [30] consisting of W' and Z', in analogy with the carriers of the weak force. Examples of such theories include weakly coupled W' and Z' models [75–77], little Higgs models [78, 79], and composite Higgs scenarios [80–84]. The latter are of particular interest as they offer a potential solution to the hierarchy problem. In

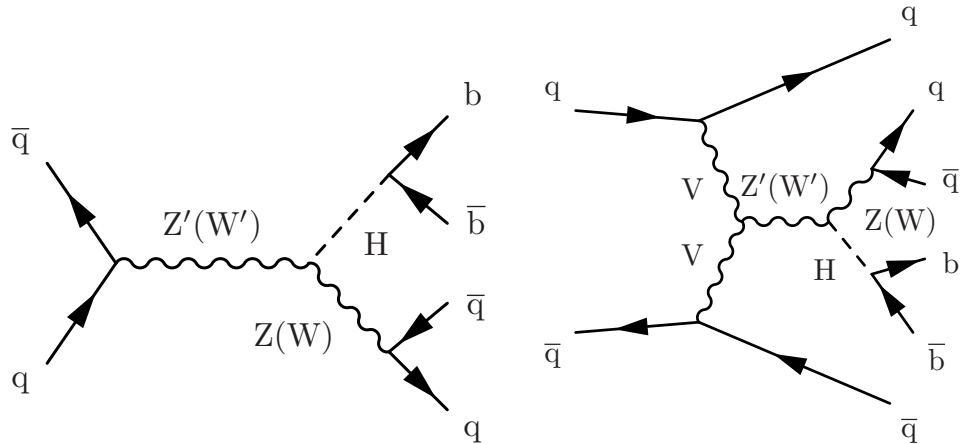


Figure 9: Feynman diagrams for the production of  $Z'$  and  $W'$  bosons produced through the (left) Drell–Yan and (right) vector boson fusion process. The  $Z'$  (resp.  $W'$ ) boson subsequently decays into  $ZH$  and  $WH$ , respectively.

these scenarios, the  $H$  boson is a strongly coupled bound state, a pseudo-Nambu–Goldstone boson, sharing constituents with new heavy vector bosons. One possible signature of such models at the LHC is  $H$  boson production through new heavy vector resonances.

The phenomenology of models including an HVT can be deduced from a simplified Lagrangian [30]. The HVT model is characterized in terms of four parameters: the masses of the  $W'$  and  $Z'$  resonances, which are degenerate, a coefficient  $c_F$ , which scales the  $W'$  and  $Z'$  couplings to fermions, another coefficient  $c_H$ , which scales the  $W'$  and  $Z'$  couplings to the  $H$  boson and longitudinally polarized SM vector bosons, and  $g_V$ , which represents the typical strength of the new vector boson interaction.

The two main  $W'$  and  $Z'$  production modes at the LHC and their decays to  $VH$  are shown in Fig. 9. The triplet field, which mixes with the SM gauge bosons, couples to the fermionic current through the combination of parameters  $g_F = g^2 c_F / g_V$  and to the  $H$  and  $V$  bosons through  $g_H = g_V c_H$ , where  $g$  is the  $SU(2)_L$  gauge coupling, taken to be  $2m_W/v = 0.6534$  with the  $W$  boson mass  $m_W$  and the vacuum expectation value  $v$  from Ref. [45]. We will derive the constraints on the couplings  $g_H$  and  $g_F$  for several values of  $g_V$  below.

Three benchmark scenarios are typically considered in searches.

- Model A, with  $g_V = 1$ ,  $c_H = -0.556$ , and  $c_F = -1.316$ , corresponding to  $g_F = -0.562$  and  $g_H = -0.556$ . This scenario reproduces a model with a weakly coupled extended gauge theory [85].
- Model B, with  $g_V = 3$ ,  $c_H = -0.976$ , and  $c_F = 1.024$ , corresponding to  $g_F = 0.146$  and  $g_H = -2.928$ . It mimics a minimal strongly coupled composite Higgs model [81].
- Model C, with  $g_V = 1$ ,  $c_H = 1 - 3$ , and  $c_F = 0$ , is a model where couplings to fermions are suppressed, such that no production via a Drell–Yan (DY) process is possible at the LHC and the production of  $W'$  and  $Z'$  bosons happens exclusively via VBF.

In all three scenarios, fermion universality is assumed. In model A, the vector resonances have larger couplings to fermions than to bosons, with the branching fractions to quarks enhanced by the colour factor in QCD. Thus, searches for resonances in fermion pair production are most sensitive. Models B and C have large branching fractions to boson pairs, while the fermionic

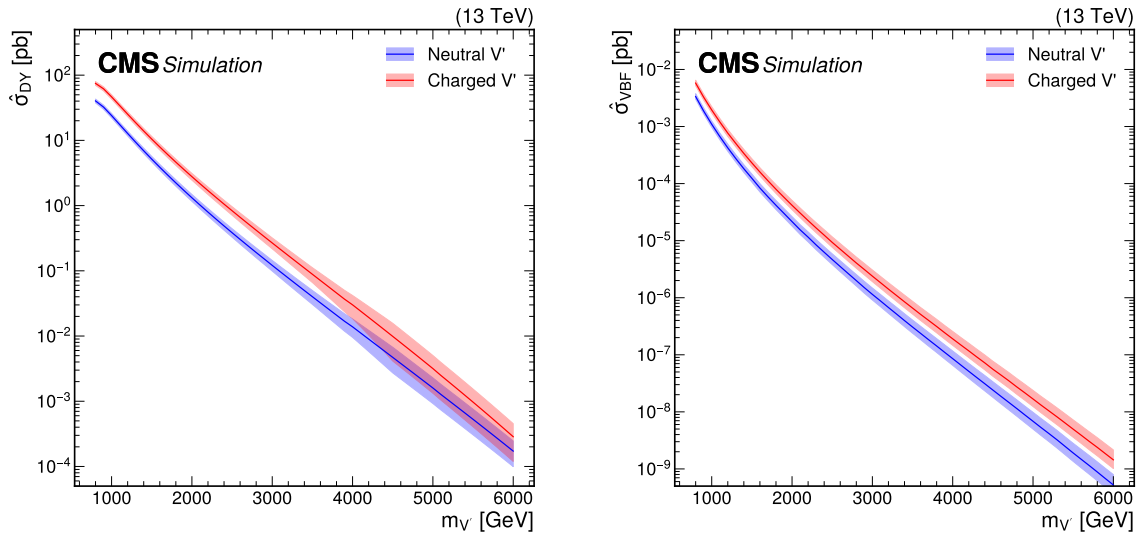


Figure 10: Cross sections for (left) Drell–Yan production ( $\hat{\sigma}_{\text{DY}}$ ) and (right) production through vector boson fusion ( $\hat{\sigma}_{\text{VBF}}$ ), as defined in Eqs. (3) and (4), for  $Z'$  and  $W'$  bosons in the heavy vector triplet (HVT) model B at  $\sqrt{s} = 13 \text{ TeV}$ . Calculations are based on the work of Ref. [30].

couplings are suppressed.

The analyses discussed in this paper derive results using the narrow-width approximation. In this approximation, the production of a certain final state through the  $W'$  and  $Z'$  resonances can be factorized into the production of the  $W'$  and  $Z'$  resonances, followed by the decay with the respective branching fractions to the final state under consideration. We parametrise the  $W'$  and  $Z'$  production cross sections as

$$\sigma_{\text{DY}}(g_F, g_H, g_V) = g_F^2 \hat{\sigma}_{\text{DY}} \quad (3)$$

$$\sigma_{\text{VBF}}(g_F, g_H, g_V) = g_H^2 \hat{\sigma}_{\text{VBF}} \quad (4)$$

where  $\hat{\sigma}_{\text{DY}}$  and  $\hat{\sigma}_{\text{VBF}}$  for model B are shown in Fig. 10. Compared to the production cross sections of heavy scalar resonances discussed in Section 1.2.1, where the smallness of the cross sections restricts the sensitivity at the LHC to masses of order 1 TeV, the  $W'$  and  $Z'$  cross sections are large enough to probe masses of multiple TeV.

The branching fractions of  $W'$  and  $Z'$  bosons as functions of the coupling parameter  $g_H$  times the sign of  $g_F$  are shown in Fig. 11. These are computed for  $g_F$  values corresponding to the benchmarks models A and B, and for two distinct resonance masses of 1 and 2 TeV. For a resonance mass of 1 TeV, a subtle distinction between positive and negative values of  $g_F$  is observed, whereas branching fractions are symmetric with respect to the sign of  $g_F$  for higher masses. When  $g_H$  is small, the branching fractions for decays into quark final states are large. The leptonic decay modes are suppressed due to the QCD colour factors. Conversely, for large values of  $g_H$ , the bosonic decay modes dominate the branching fractions, indicating that the searches for VH resonances have the best sensitivity together with searches for VV resonances.

The dependence of the branching fraction of the decay  $Z' \rightarrow VH$  on the parameter  $g_F$  is shown in Fig. 12 (left) for a resonance with a mass of 2 TeV. This branching fraction increases for decreasing  $g_F$ , asymptotically approaching the maximum value of about 50% as  $g_H$  increases. The total width of the  $Z'$  boson is shown in Fig. 12 (right) for a resonance mass of 2 TeV. The

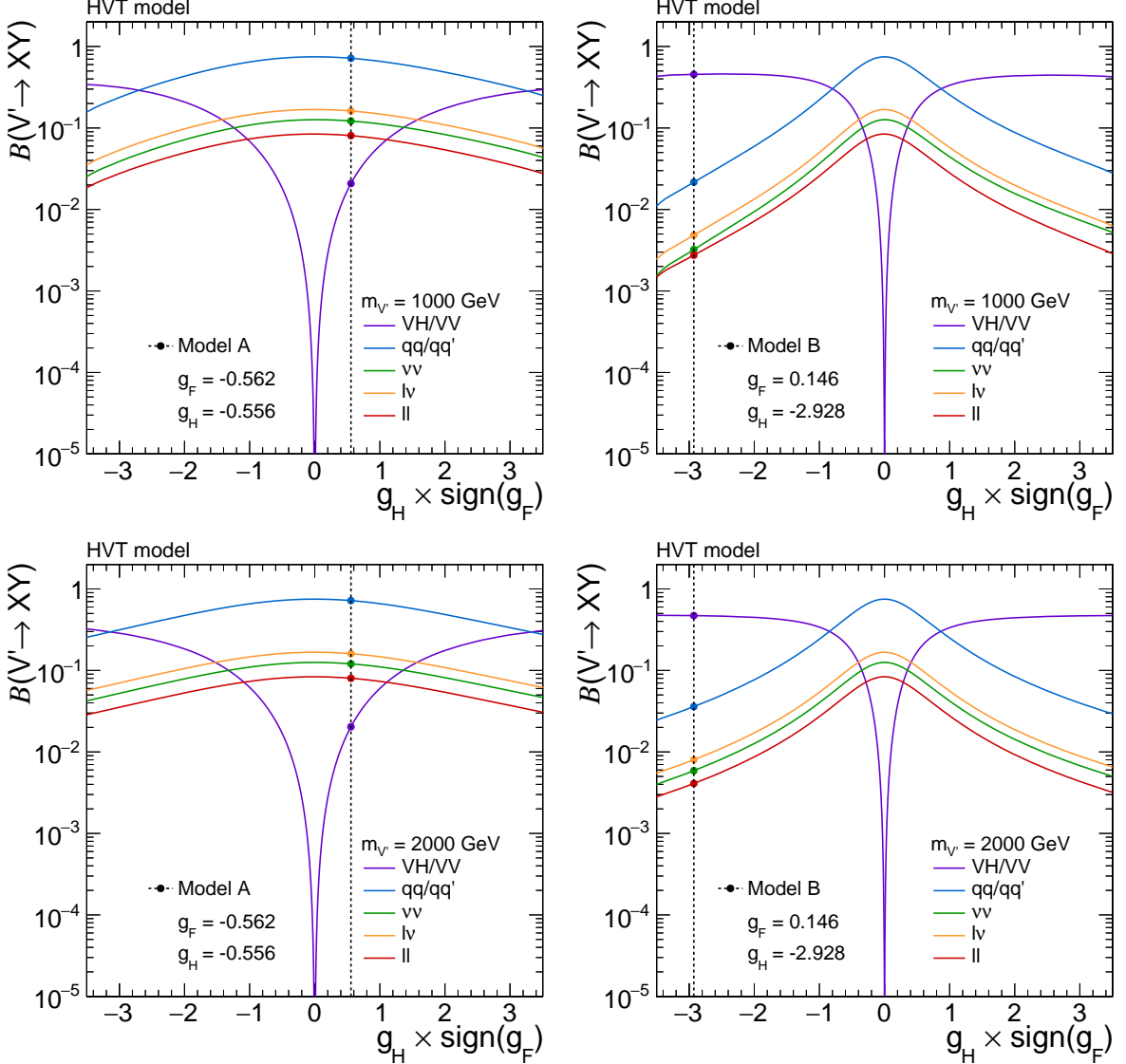


Figure 11: Branching fractions for heavy vector triplet (HVT) bosons with masses of (upper) 1 and (lower) 2 TeV for values of the parameter  $g_F$  corresponding to models (left) A and (right) B. The exact branching fractions of each model are indicated by the crossing points of the individual curves with the dashed vertical lines. Calculations are based on the work of Ref. [30].

width increases for increasing values of  $g_F$  and  $g_H$ . For small values of  $g_F$ , the width changes more rapidly as a function of  $g_H$ . The  $W'$  boson branching fractions and decay widths exhibit very similar behavior as a function of  $g_F$  and  $g_H$  to those of  $Z'$  bosons, and are not shown here. Previous searches by the CMS and ATLAS Collaborations in the VH channel have not observed significant deviations from the SM [86–100].

## 2 Detector and analysis techniques

The analyses described in the following sections are searches for a new heavy resonance X in the  $X \rightarrow HH$ ,  $X \rightarrow VH$ , and  $X \rightarrow YH$  decays, where V denotes a W or Z boson, H the observed Higgs boson, and Y another new particle like an additional Higgs boson, as predicted in several extensions of the SM Higgs sector. This report focuses on analyses by the CMS Collaboration;

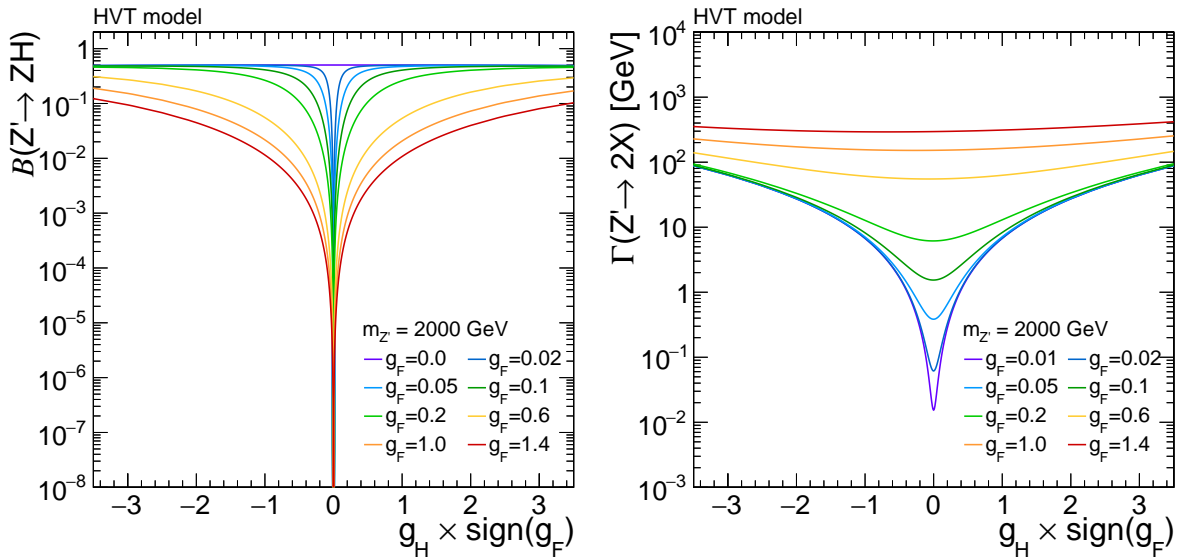


Figure 12: (left) Branching fraction for the decay  $Z' \rightarrow ZH$ , and (right) total width of the  $Z'$  boson, for a resonance with 2 TeV mass, for different values of the parameter  $g_F$ . Calculations are based the work of Ref. [30].

related results from the ATLAS Collaboration can be found in Refs. [94, 101–106].

In most analyses, the intermediate particles V or Y are targeted in decay modes involving b quarks, leptons or photons. This choice is made to profit from the accuracy with which these particles can be reconstructed and identified to distinguish the resulting final states from the overwhelming large amount of purely hadronic processes at the LHC. In all searches the natural decay widths of the X and Y particles are assumed to be small compared to the experimental resolution. Implications of this assumption are discussed in Section 4.4.

The search signatures are rich in characteristic features, most notably there are three resonance masses in the full decay chain, of which the masses of the V bosons and  $m_H$  are known to a precision of better than 1%. To include this information in the process description, we introduce a notation where the final-state particles are associated with the V, H, or Y particles. For example, with this notation the decay  $X \rightarrow Y(bb)H(\tau\tau)$  indicates the subsequent decays of  $Y \rightarrow bb$  and  $H \rightarrow \tau\tau$ . An overview is given in Table 1 of all the analyses discussed in the following sections and the kinematic ranges of their sensitivity.

The analyses span resonance mass ranges of  $90 < m_X < 6000$  GeV and  $60 < m_Y < 2800$  GeV. Such large ranges in mass require different reconstruction techniques even for the same final state [118]. In the case of small  $m_X$ , the decay products of Y and H are produced with large angular distances and can be reconstructed as separate objects. This characterizes a regime with fully resolved final states. In contrast, for large  $m_X$  and sufficiently small  $m_Y$ , the decay products of Y and H are strongly collimated because of the large Lorentz boost, such kinematic regimes are referred to as boosted throughout this report. Final state objects being part of such collimated decays are referred to as merged. In the boosted regime, the hadronic decay products of the intermediate resonances, e.g.  $H(bb)$ , are reconstructed as a single large- $R$  jet with substructure identification and grooming of soft and large-angle radiation [119–121], where the parameter  $R$  denotes the distance parameter of the jet finding algorithm, as described in Section 2.2.1. Typically for the values of  $R$  used in this paper, the resolved regime corresponds to  $m_X \lesssim 1$  TeV, and the boosted regime to  $m_X \gtrsim 1$  TeV with  $m_Y \ll m_X$ . For  $m_X \approx 1$  TeV both merged and resolved final states might be encountered depending on the helicity angles of the

Table 1: Summary of all analyses discussed in Section 2. Note that the list of sub-channels is not exhaustive in all cases. All analyses listed under YH also contribute to the HH measurements.

Target final state		Ref.	Mass coverage (GeV)	Comment	
V	H		$m_X$		
$Z(\ell\ell)$	$\tau\tau$	[107]	220–400		
$Z(\ell\ell + \nu\nu)$	bb	[108]	225–1000	resolved jets	
$W(\ell\nu)$	bb	[109]	1000–4500	$W \rightarrow \ell\nu$ and merged bb jet	
$Z(\ell\ell)$	bb	[110]	800–4600	$Z \rightarrow \ell\ell/\nu\nu$ and merged bb jet	
$Z(qq)$	bb	[111]	1300–6000	two merged jets	
H	H		$m_X$		
bb	$W(\ell\nu)W(\ell\nu + qq)$	[112]	250–900	resolved + merged	
bb	$W(\ell\nu)W(\ell\nu + qq)$	[113]	800–4500	merged	
$WW + \tau\tau$	$WW + \tau\tau$	[114]	250–1000	multilepton final state	
Y	H		$m_X$	$m_Y$	
bb	$\tau\tau$	[115]	240–3000	60–2800	resolved jets and $\tau$ leptons
bb	$\gamma\gamma$	[116]	300–1000	90–800	resolved jets and photons
bb	bb	[117]	900–4000	60–600	two merged bb jets

boson decays.

Unless stated otherwise, all analyses are based on pp collision data collected between 2016 and 2018, at a center-of-mass energy of 13 TeV, corresponding to an integrated luminosity of 137–138 fb<sup>-1</sup>.

## 2.1 The CMS Detector

The central feature of the CMS apparatus is a superconducting solenoid of 6 m internal diameter, providing a magnetic field of 3.8 T. Within the solenoid volume are a silicon pixel and strip tracker, a lead tungstate crystal electromagnetic calorimeter (ECAL), and a brass and scintillator hadron calorimeter (HCAL), each composed of a barrel and two endcap sections. Forward calorimeters extend the pseudorapidity coverage provided by the barrel and endcap detectors. Muons are measured in gas-ionization detectors embedded in the steel flux-return yoke outside the solenoid. A more detailed description of the CMS detector, together with a definition of the coordinate system used and the relevant kinematic variables, can be found in Ref. [122].

Events of interest are selected using a two-tiered trigger system. The first level, composed of custom hardware processors, uses information from the calorimeters and muon detectors to select events at a rate of around 100 kHz within a fixed latency of 4  $\mu$ s [123]. The second level, known as the high-level trigger, consists of a farm of processors running a version of the full event reconstruction software optimized for fast processing, and reduces the event rate to around 1 kHz before data storage [124].

## 2.2 Physics objects

The reconstruction of the pp collision products is based on the particle-flow (PF) algorithm [125], combining the available information from all CMS subdetectors to reconstruct individual particle candidates, categorized into charged and neutral hadrons, electrons, photons, and muons. The average number of interactions per bunch crossing was 23 in the year 2016 and 32 in the years 2017–2018. The fully recorded detector data of a bunch crossing define an event for further processing. The primary interaction vertex (PV) is taken to be the vertex corresponding

to the hardest scattering in an event, evaluated using tracking information alone, as described in Ref. [126]. Secondary vertices, which are detached from the PV, might be associated with decays of long-lived particles emerging from the PV. Any other collision vertices in an event are associated with additional mostly soft inelastic pp collisions referred to as pileup (PU).

### 2.2.1 Jets and missing transverse momentum

**AK4 and AK8 jets** All PF candidates are clustered into jets using the anti- $k_T$  clustering algorithm [127] as implemented in the FASTJET software package [128]. By default, a distance parameter of  $R = 0.4$  is used. The resulting jet collection will be referred to as AK4 jets. Ideally, the kinematic properties of AK4 jets resemble those of the single quarks or gluons initiating them. In the boosted regime the fragmentation products of the individual quarks, resulting from hadronic V, H, or Y decays, start to overlap and cannot be properly reconstructed as AK4 jets. For this purpose, a second collection of large- $R$  jets is obtained with a distance parameter of 0.8, referred to as AK8 jets. The larger jet radius allows the inclusion of all hadronic decay products in a single jet, and subsequently jet substructure techniques can be applied to identify the boosted decay within this jet, as explained in the following.

In each case, the jet momenta are determined from the vectorial sum of the momenta of all PF candidates contained in a jet. The value of this sum is measured to be within 5 to 10% of the same quantity calculated from the momenta of stable particles inside equally clustered generated jets in simulation, which holds over the entire transverse momentum ( $p_T$ ) spectrum and geometrical detector acceptance. Jet energy corrections to the stable-particle level are obtained from simulation, and are confirmed with *in situ* measurements of the energy balance in dijet, multijet,  $\gamma$ +jets, and Z+jets events, where the Z boson decays into light leptons [129]. Residual corrections to the simulated energies to match the observed spectra usually amount to no more than 2–3%.

The AK4 jets are restricted to  $p_T > 30\text{ GeV}$ . Depending on the analysis, these are either used in a range of  $|\eta| < 2.4$ , well contained in the coverage of the tracker, or in a range of  $|\eta| < 4.7$ , where the extension is based on the calorimeters but not covered by the tracker. The AK8 jets are restricted to  $p_T > 200\text{ GeV}$  and  $|\eta| < 2.4$  or 2.5, depending on the analysis, where the higher value in  $|\eta|$  has been used after the upgrade of the silicon pixel detector from 2017 on. Ideally, their properties match those of the decaying resonance. In a first step, AK8 jets are used for the selection of events of interest. In a second step, their specific properties are used to distinguish signal from background processes, based on dedicated algorithms, as discussed below. To reduce the dependence of the related observables on PU, the pileup-per-particle identification (PUPPI) algorithm [130, 131] is applied to the AK8 jets, weighting all PF candidates by their probability to originate from the PV [132]. For AK4 jets the charged-hadron subtraction (CHS) technique, as described in Refs. [125, 131] is used. In addition, both AK4 and AK8 jets are required to pass tight identification requirements [133] to remove jets originating from calorimetric noise and track misreconstruction. Several properties of the selected jets are of importance for the analyses described in this report and will be discussed in more detail in the following.

**Mass of AK8 jets** The mass of the hadronically decaying boson resonance associated with an AK8 jet is estimated using the “soft-drop” mass  $m_{\text{SD}}$  [134], obtained with the soft-drop algorithm with an angular exponent  $\beta = 0$ , soft-cutoff threshold  $z_{\text{cut}} = 0.1$ , and characteristic radius  $R_0 = 0.8$ . The soft-drop algorithm is a generalization of the modified mass-drop algorithm [135, 136], which is identical to soft drop for  $\beta = 0$ . The reconstruction of  $m_{\text{SD}}$  is tested and calibrated in  $t\bar{t}$ -enriched event selections, where the mass of hadronically decaying

$W$  bosons can be reconstructed with a resolution of 10%.

**Identification of b jets** To identify jets resulting from the hadronisation of b quarks (b jets) several strategies and tagging algorithms are used, depending on the analysis. These algorithms comprise the DEEPCSV [137] and DEEPJET [137, 138] algorithms, which are applied either to AK4 jets or to the subjets of the selected AK8 jet. The subjets are obtained with the soft drop algorithm, where the Cambridge–Aachen algorithm [139, 140] is reversed until the soft drop condition [134] is fulfilled. The two resulting clusters are identified as subjets of the AK8 jet. Alternatively, the “double-b tagger” [137], the DEEPAK8 jet tagging [141], or the PARTICLENET [142] algorithms are used to identify AK8 jets that are consistent with being initiated by two b quarks, a process referred to as “double-b tagging”. These algorithms usually result in a multiclass output from which a composed discriminant is built. This discriminant is used to distinguish AK8 jets produced from light-flavor quarks or gluons versus AK8 jets from two near-collinear b quarks. All algorithms use secondary vertex and impact parameter information, as well as the multiplicities and kinematic properties of the clustered PF candidates. The resonance tagging algorithms are usually trained to be insensitive to the mass of the corresponding resonance. For all algorithms, predefined working points corresponding to an expected b jet identification efficiency for a given misidentification rate for jets initiated by light-flavor quarks or gluons, as defined in Ref. [143], are used, exhibiting efficiencies of 70–90% for misidentification rates of 1–10%.

**Jet substructure** To exploit the substructure of a selected AK8 jet, the ratio  $\tau_{21} = \tau_2/\tau_1$  is used, where  $\tau_1$  and  $\tau_2$  are the 1- and 2-subjettiness observables [144], respectively. The quantity  $\tau_{21}$  takes lower values for jets originating from two-prong V, H, or Y decays and larger values for one-prong jets initiated, e.g., by single quarks or gluons. However, a selection on  $\tau_{21}$  alters the distribution in  $m_{\text{SD}}$ , such that the monotonically falling distribution might feature a resonant structure after selecting jets with a minimum value of  $\tau_{21}$ . This feature prevents typical background estimation methods from working for important background processes, like  $W+\text{jets}$  production [109]. To overcome this drawback, we use the “designing decorrelated tagger” (DDT) procedure [145] leading to

$$\tau_{21}^{\text{DDT}} = \tau_{21} + 0.08 \log \left( \frac{m_{\text{SD}}^2}{p_T \mu} \right), \quad (5)$$

where  $p_T$  refers to the transverse momentum of the AK8 jet and  $\mu = 1 \text{ GeV}$ . A selection based on  $\tau_{21}^{\text{DDT}}$  does not alter the distribution in  $m_{\text{SD}}$ , such that the shape of this distribution can be derived from control regions (CRs) to estimate the background from SM processes in signal regions (SRs).

**Event observables** The two-dimensional vector in the  $x$  and  $y$  coordinates,  $\vec{p}_T^{\text{miss}}$ , describes the missing transverse momentum and is computed as the negative  $\vec{p}_T$  sum of all PF candidates in the event [132]. The magnitude of  $\vec{p}_T^{\text{miss}}$  is referred to as  $p_T^{\text{miss}}$ . It is used for the event selection and in the calculation of the transverse mass

$$m_T = \sqrt{2 p_T p_T^{\text{miss}} (1 - \cos \Delta\phi)}, \quad (6)$$

where  $\Delta\phi$  refers to the azimuthal angular difference between the transverse momentum vector  $\vec{p}_T$  of the visible decay product of the particle whose transverse mass is to be estimated, and  $\vec{p}_T^{\text{miss}}$ . Depending on the analysis, sometimes the PUPPI algorithm is used to mitigate PU effects on  $\vec{p}_T^{\text{miss}}$ . Alternatively, the quantity  $H_T^{\text{miss}}$  is used, defined as the magnitude of the  $\vec{p}_T$  sum of

all AK4 jets with  $p_T > 30\text{ GeV}$  and  $|\eta| < 3.0$ . In the same context also the observable  $H_T$  is used, which corresponds to the scalar  $p_T$ -sum of all selected AK4 jets. It indicates the overall magnitude of hadronic activity in an event.

## 2.2.2 Leptons and photons

**Electrons, muons, and photons** Electron candidates are reconstructed from matching clusters of energy deposits in the ECAL with tracks, which are fitted to form hits in the tracker [146, 147]. To increase their purity, reconstructed electrons are required to pass a multivariate electron identification discriminant, which combines information on the track quality, shower shape, and kinematic quantities [147]. Predefined working points corresponding to electron identification efficiencies of 70–90% and misidentification rates of 2–15% are used. Energy deposits in the ECAL that are not linked to any charged-particle trajectory associated with a pp collision are identified as photons.

Muons in an event are reconstructed by performing a simultaneous track fit to hits in the tracker and in the muon chambers [148, 149]. The presence of hits in the muon chambers already leads to a strong suppression of particles misidentified as muons. Additional identification requirements on the track-fit quality and the compatibility of individual track segments with the fitted track reduce the misidentification rate further.

The contributions from backgrounds to the electron and muon selections are usually further reduced by requiring the corresponding lepton to be isolated from any hadronic activity in the detector. This property is quantified by an isolation variable

$$I_{\text{rel}} = \frac{1}{p_T^\ell} \left( \sum p_T^{\text{charged}} + \max \left( 0, \sum E_T^{\text{neutral}} + \sum E_T^\gamma - p_T^{\text{PU}} \right) \right), \quad (7)$$

where  $p_T^\ell$  corresponds to the measured electron or muon  $p_T$ . The variables  $\sum p_T^{\text{charged}}$ ,  $\sum E_T^{\text{neutral}}$ , and  $\sum E_T^\gamma$  are calculated from the sum over  $p_T$  or transverse energy  $E_T$  of all charged particles, neutral hadrons, and photons, respectively. These sums include all particles in a predefined cone of radius  $\Delta R = \sqrt{(\Delta\eta)^2 + (\Delta\phi)^2}$  around the lepton direction at the PV, where  $\Delta\eta$  and  $\Delta\phi$  are the angular distances between the corresponding particle and the lepton in the  $\eta$  and azimuthal  $\phi$  directions. The lepton itself is excluded from the calculation of  $I_{\text{rel}}$ . Typical values for cone sizes are  $\Delta R = 0.3$  and  $0.4$  for electrons and muons, respectively. To mitigate effects from PU on  $I_{\text{rel}}$ , only charged particles with tracks associated with the PV are taken into account. Since for neutral hadrons and photons an unambiguous association with the PV or PU is not possible, an estimate of the contribution from PU ( $p_T^{\text{PU}}$ ) is subtracted from the sum of  $\sum E_T^{\text{neutral}}$  and  $\sum E_T^\gamma$ . This estimate is obtained from tracks not associated with the PV in the case of muons, and from the mean energy flow per unit area in the case of electrons. If the sum is negative, the result is set to zero. The  $I_{\text{rel}}$  selection threshold is optimized for each analysis separately. If a lepton isolation requirement is imposed in an analysis, leptons failing this requirement are not considered further.

**Hadronic  $\tau$  lepton decays** The reconstruction of hadronic  $\tau$  lepton decays ( $\tau_h$ ) starts from AK4 jets, further exploiting their substructure with the hadrons-plus-strips algorithm [150]. This algorithm acts like a tagger, with different working points as defined in [150]. The decays into one or three charged hadrons with up to two neutral pions with  $p_T > 2.5\text{ GeV}$  are used. The neutral pions are reconstructed as strips in the ECAL with a dynamic size in  $\eta\text{-}\phi$  from reconstructed electrons and photons contained in a jet, where the strip size varies as a function of

the  $p_T$  of the electron or photon candidate. Electrons, which may emerge from photon conversions, are considered in the reconstruction of the strips. The  $\tau_h$  decay mode is then obtained by combining the charged hadrons with the strips.

To distinguish  $\tau_h$  candidates from jets originating from the hadronisation of quarks or gluons, and from electrons or muons, the DEEPTAU (DT) algorithm [151] is used. This algorithm exploits basic tracking and clustering information in the tracker, ECAL, and HCAL, the kinematic and object-identification properties of both the PF candidates forming the  $\tau_h$  candidate and all remaining PF candidates in the vicinity of the  $\tau_h$  candidate, and several characterizing quantities of the whole event. It results in a multiclassification output  $y_\alpha^{\text{DT}}$ , where  $\alpha = \tau, \text{jet}, e, \mu$ . The output can be identified with a Bayesian probability of the  $\tau_h$  candidate to originate from a genuine  $\tau$  lepton decay, the hadronisation of a quark or gluon, an isolated electron, or an isolated muon. From this output three discriminants are built according to

$$D_i = \frac{y_\tau^{\text{DT}}}{y_\tau^{\text{DT}} + y_i^{\text{DT}}} \quad \text{with} \quad i = \text{jet, e, or } \mu. \quad (8)$$

For the identification of  $\tau_h$  candidates based on  $D_i$  predefined working points with varying efficiencies for given misidentification rates are used as described in Ref. [151]. For  $D_{\text{jet}}$  the efficiencies vary within 50–70% for misidentification rates of <0.5%. For  $D_e$  and  $D_\mu$ , the efficiencies vary within 80–99% for misidentification rates between 0.05 and 2.50%.

## 2.3 Search for resonances in VH channels

Searches for VH resonances are optimized either for the mass range up to about 1 TeV, motivated by neutral members of an extended Higgs sector, or masses greater than 1 TeV, where heavy vector bosons might be found. The latter case corresponds to the boosted regime, where the V and H bosons are strongly Lorentz-boosted and dedicated reconstruction and identification techniques are applied.

All searches presented in the following target the  $H \rightarrow bb$  or  $H \rightarrow \tau\tau$  decays. The V bosons are reconstructed either through the leptonic decays  $W(\ell\nu)$  [109],  $Z(\ell\ell)$  or  $Z(\nu\nu)$  [107, 108, 110], or by the hadronic decays  $V(qq)$  [111]. Where allowed by the signal signature, the trigger selection is based on the presence of a single high- $p_T$  electron or muon within the geometrical acceptance of  $|\eta| < 2.4$  (2.5) for electrons (muons), large  $p_T^{\text{miss}}$ , or large  $H_T^{\text{miss}}$ . Also, dilepton triggers are used. Otherwise, triggers based on the presence of high- $p_T$  AK4 jets or large values of  $H_T$  are required. Offline, search regions are defined by the presence of exactly one ( $1\ell$  category), two ( $2\ell$  category), or no ( $0\ell$  category) charged leptons. This categorization ensures that the analyses are mutually exclusive, allowing for a combined statistical interpretation subsequently to the completion of all analyses.

### 2.3.1 The sub-TeV mass region

The analyses searching for  $CP$ -odd Higgs bosons through their  $A \rightarrow ZH$  decay, in the mass region below 1 TeV, are based on the 2016 data set. The H boson is reconstructed in the  $H \rightarrow bb$  [108] and  $H \rightarrow \tau\tau$  [107] decay channels.

In the  $H \rightarrow bb$  case, the two b jet candidates with the highest b tagging scores are selected to form the H boson candidate. Both gluon-gluon fusion and b quark-associated production are considered. In the  $0\ell$  category, which targets decays of the Z boson into neutrinos, the mass of the A resonance cannot be reconstructed directly. In this case, its mass is estimated by computing the transverse mass  $m_{ZH}^T$  using Eq. (6). It is calculated using  $\vec{p}_T^{\text{miss}}$  and the four-momentum of the H boson candidate, and must be larger than 500 GeV. The resulting efficiency

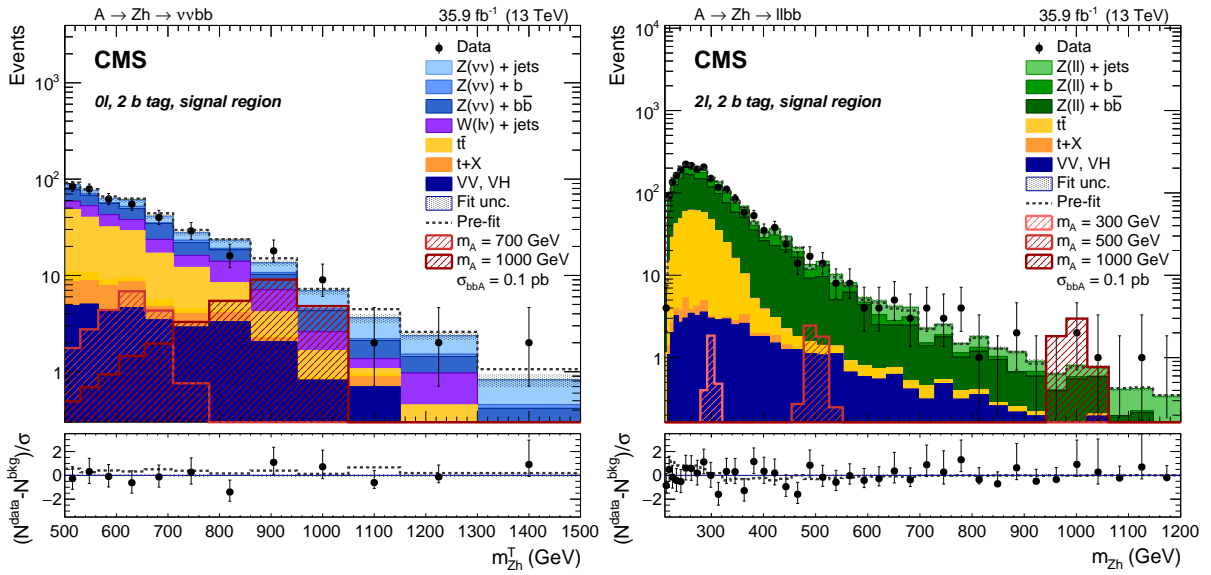


Figure 13: Search for  $X \rightarrow VH(bb)$ : Distributions of the  $m_{Z_H}^T$  and  $m_{Z_H}$  variables, as introduced in the text, in the (left)  $0\ell$  and (right)  $2\ell$  categories, in the 2 b tag signal region of the  $A \rightarrow ZH(bb)$  analysis [108]. In the  $2\ell$  categories, the contributions of the  $2e$  and  $2\mu$  channels have been summed. The gray dotted line represents the sum of all background processes before the fit to data; the shaded area represents the post-fit uncertainty. The hatched red histograms represent signal hypotheses for b quark associated X production corresponding to  $\sigma_A \mathcal{B}(A \rightarrow ZH) \mathcal{B}(H \rightarrow bb) = 0.1 \text{ pb}$ . The lower panels depict  $(N_{\text{data}} - N_{\text{bkg}})/\sigma$  in each bin, where  $\sigma$  refers to the statistical uncertainty in the given bin. Figure from Ref. [108].

for signal events with  $m_A \lesssim 500 \text{ GeV}$  is small because the  $p_T$  of the Z boson is not sufficient to produce a  $p_T^{\text{miss}}$  large enough to pass this selection. Therefore, the sensitivity of the  $0\ell$  category is significant only for large values of  $m_A$ .

In the  $2e$  and  $2\mu$  categories, events are required to have at least two isolated electrons or muons within the detector's geometrical acceptance. The Z boson candidate is formed from the two highest  $p_T$ , opposite-sign, same-flavor leptons, and must have an invariant mass  $m_{\ell\ell}$  between 70 and 110 GeV. The  $m_{\ell\ell}$  selection lowers the contamination from  $t\bar{t}$  dileptonic decays and significantly reduces the contribution from  $Z \rightarrow \tau\tau$  decays. The A boson candidate is reconstructed from the invariant mass  $m_{ZH}$  of the Z and H boson candidates.

If the two jets originate from an H boson, their invariant mass is expected to peak close to 125 GeV. Events with a dijet invariant mass  $m_{jj}$  between 100 and 140 GeV enter the SRs; otherwise, if  $m_{jj} < 400 \text{ GeV}$ , they fall in the dijet mass sidebands, which are used as CRs to estimate the contributions of the main backgrounds. The SRs are further divided by the number of jets passing the b tagging requirement (1, 2, or at least 3 b tags). The 3 b tag category has been defined to select the additional b quarks from b quark associated production. In this region, at least one additional jet, other than the two used to reconstruct the H boson, has to pass the kinematic selections and b tagging requirements. Comparisons between data and background predictions, together with examples for signal distributions are shown in Fig. 13 in the 2 b tag SR for the  $0\ell$  and  $2\ell$  categories. The data are well described by the backgrounds expected from SM processes. The  $0\ell$  and  $2\ell$  categories can be combined using the known branching fractions of the Z boson.

In the  $H \rightarrow \tau\tau$  case, only the dielectron and dimuon decays of the Z boson are used. For the

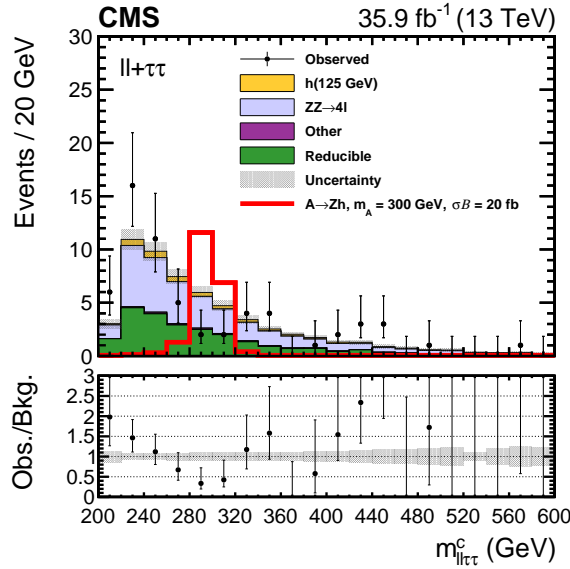


Figure 14: Search for  $X \rightarrow VH(\tau\tau)$ : Distribution of the  $m_{\ell\ell\tau\tau}^c$  variable, as introduced in the text, of the  $A \rightarrow ZH(\tau\tau)$  analysis [107], after a fit of the background-only hypothesis in all eight final states. While the fit is based on corresponding distributions, for each final state individually, these have been combined into a single distribution, for visualization purposes for this figure. Uncertainties include both statistical and systematic components. The expected contribution from the  $A \rightarrow ZH$  signal process is shown for a pseudoscalar Higgs boson with  $m_A = 300$  GeV with the product of the cross section and branching fraction of 20 fb. Figure from Ref. [107].

H boson reconstruction, the  $e\tau_h$ ,  $\mu\tau_h$ ,  $e\mu$ , and  $\tau_h\tau_h$  topologies are considered. The leptons associated with the H boson decay are required to have opposite signs. In case of the  $e\tau_h$ ,  $\mu\tau_h$ , and  $e\mu$  decay channels, tighter selection criteria are applied to the light leptons to decrease the background contributions from Z+jets and other reducible backgrounds. These four  $H \rightarrow \tau\tau$  decay patterns are combined with the Z boson decays into two light leptons, i.e.,  $Z \rightarrow \ell\ell$  with  $\ell = e, \mu$ , resulting in eight distinct final states of the A boson decay.

The mass resolution of the reconstructed A boson candidate can be significantly improved by accounting for the neutrinos associated with the leptonic and hadronic  $\tau$  decays. We use the SVFIT algorithm [152] to estimate the mass of the H boson, denoted as  $m_{\tau\tau}^{\text{fit}}$ . The SVFIT algorithm combines the  $\vec{p}_T^{\text{miss}}$  with the four-vectors of both  $\tau$  candidates ( $e$ ,  $\mu$ , or  $\tau_h$ ), resulting in an improved estimate of the four-vector of the H boson, which is further improved by giving the measured mass of the Higgs boson (125 GeV) as an input to the SVFIT algorithm. This yields a constrained estimate of the four-vector of the H boson, which results in an even more precise estimate of the A boson candidate mass, denoted as  $m_{\ell\ell\tau\tau}^c$ . The resolution of  $m_{\ell\ell\tau\tau}^c$  is as good as 3% at 300 GeV, which improves the expected 95% CL model-independent limits by approximately 40% compared to using the visible mass of the A boson  $m_{\ell\ell\tau\tau}^{\text{vis}}$  as the discriminating variable.

The resulting distribution in  $m_{\ell\ell\tau\tau}^c$ , summed over all eight categories, is shown in Fig. 14, together with the expected signal shape for  $m_A = 300$  GeV. No excess above the SM background expectation is observed in the data.

### 2.3.2 The high-mass region: leptonic V boson decays

In the high-mass analyses targeting leptonic V boson decays, the presence of an isolated electron with  $p_T > 115 \text{ GeV}$  and  $|\eta| < 2.4$  or muon with  $p_T > 55 \text{ GeV}$  and  $|\eta| < 2.5$  is required. The high  $p_T$  thresholds are imposed to guarantee a sufficiently high selection efficiency at the trigger level.

For  $W(\ell\nu)$  decays, this selection is complemented by the requirement of  $p_T^{\text{miss}} > 80 \text{ GeV}$  in the electron channel and  $p_T^{\text{miss}} > 40 \text{ GeV}$  in the muon channel. Events with additional leptons fulfilling looser selection criteria are discarded from the selection. To reconstruct a  $W(\ell\nu)$  boson candidate, the  $\vec{p}_T^{\text{miss}}$  is used as an estimate of the  $\vec{p}_T$  of the neutrino. The longitudinal component  $p_z$  of the neutrino momentum is estimated by imposing the constraint that the mass of the system formed from the selected lepton and the neutrino should equal  $m_W$ . This leads to a quadratic equation in  $p_z$ , of which the solution with the smallest magnitude is chosen. When no real solution is found, only the real part of the two complex solutions is considered.

For  $Z(\ell\ell)$  decays, a second lepton with the same flavor and  $\eta$  range as the first lepton, and  $p_T > 20 \text{ GeV}$  is required. The system formed by the two leptons is used to reconstruct the  $Z$  boson candidate. It must have  $p_T^{\ell\ell} > 200 \text{ GeV}$  and  $70 < m_{\ell\ell} < 110 \text{ GeV}$ . The window in  $m_{\ell\ell}$  has not been chosen tighter, since a narrowing would reduce the signal efficiency while not improving its relation to the main background from  $Z+\text{jets}$  events. In all cases, all leptons are required to have a large enough distance in  $\Delta R$  to any AK4 jet. For the  $Z(\nu\nu)$  channel, the absence of leptons and a value of  $p_T^{\text{miss}} > 250 \text{ GeV}$  are required.

In addition to the identification of the reconstructed objects forming the V boson candidate, all events are required to have an AK8 jet with  $p_T > 200 \text{ GeV}$  and  $|\eta| < 2.4$  [109] or 2.5 [110]. In the case that more than one AK8 jet is found in an event, the leading one in  $p_T$  is interpreted to originate from the  $H \rightarrow bb$  decay, hence referred to as the H candidate.

In the  $W(\ell\nu)$  channel [109], the H candidate is required to have a distance of  $\Delta R > \pi/2$  from the selected lepton and a distance larger than 2 in  $\Delta\phi$  from both  $\vec{p}_T^{\text{miss}}$  and the  $W(\ell\nu)$  candidate. Furthermore, it is required to have a value of  $\tau_{21}^{\text{DDT}} < 0.8$ . All accepted events are assigned to 24 high-purity (HP) and low-purity (LP) event categories according to the flavor of the selected lepton ( $e$  or  $\mu$ ), the value of the double-b-tagger output of the H candidate, the distance between the  $W(\ell\nu)$  and the H candidate in rapidity  $|\Delta y| < 1$  (LDy) or  $|\Delta y| > 1$  (HDy), a tightened requirement of  $\tau_{21}^{\text{DDT}} < 0.5$  (defining the HP and LP categories), and a VBF tag requiring the pseudorapidity difference of the two VBF jets  $|\Delta\eta| > 4$  and the dijet mass larger than  $500 \text{ GeV}$ . The VBF tag is imposed to increase the sensitivity of the search to the production of the VH system through VBF. The categorization in  $\Delta y$  is imposed to tag different spin hypotheses for X. A two-dimensional (2D) discriminant composed of  $m_{\text{SD}}$  of the H candidate and an estimate of  $m_X$  obtained from the four-vectors of the H and the  $W(\ell\nu)$  candidates is used for the final signal extraction in these categories. We note that this analysis is not restricted to the VH process, which is the subject of this report, but extends towards VV final states as well. The data are interpreted under both signal hypotheses each time considering all event categories, including those enriched and depleted in VH and VV by the value of the double-b tagger of the H candidate.

Distributions of  $m_{\text{SD}}$  and the reconstructed  $m_X$  in the event category with a selected muon,  $\tau_{21}^{\text{DDT}} < 0.5$ , double-b tag, and  $|\Delta y| > 1$  are shown in Fig. 15. The background processes are split into two categories: (i) processes exhibiting resonant structures close to the t quark and/or V boson mass in  $m_{\text{SD}}$  ( $W + V/t$ ), comprising  $t\bar{t}$ , single-t quark, and diboson production, and (ii) processes without resonant structure in the  $m_{\text{SD}}$  distribution, dominated by  $W+\text{jets}$  events. All

backgrounds are characterized by a falling spectrum in  $m_X$ . These are estimated with the help of simulation, where the smoothness of the background shape is ensured by using conditional probability density functions in  $m_{SD}$  and the reconstructed  $m_X$ , as detailed in Ref. [109].

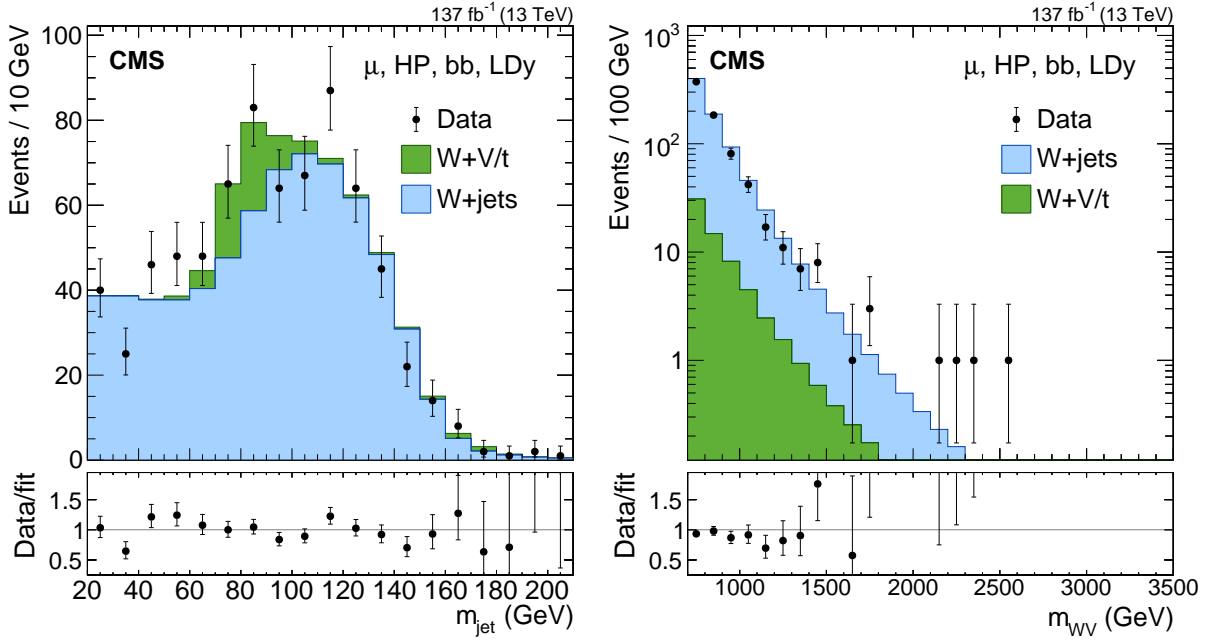


Figure 15: Search for  $X \rightarrow VH(bb)$ : Distributions of (left) the jet soft drop mass of a boosted Higgs boson candidate, labeled  $m_{jet}$ , and (right) the mass of the  $X$  resonance candidate, labeled  $m_{WV}$  in the  $W(\ell\nu)H(bb)$  channel. The notation  $m_{WV}$  is used as a shorthand since the analysis also searches for resonances in the WW and WZ final states. Figures from Ref. [109].

In the  $Z(\ell\ell)$  channel, the  $H$  candidate is required to have a distance of  $\Delta R > 0.8$  from each selected lepton. For the  $Z(\nu\nu)$  channel  $\Delta R(\vec{p}_T^{\text{miss}}, H) > 2$  and a ratio of  $p_T^{\text{miss}}/p_T^H > 0.6$  are required. Finally, the value of  $m_{SD}$  of the  $H$  candidate is required to lie within  $105 < m_{SD} < 135$  GeV, compatible with  $m_H$ . All remaining events are assigned to 12 event categories based on the flavor of the selected leptons ( $\mu\mu$ , ee, or  $\nu\nu$ ), the number of b-tagged subjets of the  $H$  candidate ( $\leq 1$ , or 2), and a VBF tag identical to the one defined above. The DEEPCSV algorithm is applied to the two subjets of the AK8 jet with the highest  $p_T$ . The signal is extracted in the  $Z(\ell\ell)$  channel from the distribution in  $m_X$ , obtained from the four-vectors of the  $H$  and the  $Z$  candidates. In the  $Z(\nu\nu)$  channel the variable  $m_T$ , as obtained from  $\vec{p}_T^H$  and  $\vec{p}_T^{\text{miss}}$ , is chosen. Distributions of  $m_{SD}$ ,  $m_X$ , and  $m_T$  in the  $\mu\mu$  and  $\nu\nu$  event categories with two b-tagged subjets, and no VBF tag are shown in Fig. 16. The dominant background in this search is from  $Z+jets$  events, which is estimated from data using low-mass (LSB) and high-mass (HSB) CRs in  $m_{SD}$ . A veto region with  $65 < m_{SD} < 105$  GeV is excluded from the analysis to minimize the event overlap with dedicated searches in the VV decay channel [153–155]. Minor backgrounds originate from  $t\bar{t}$ , single t quark, and SM VH production. In all cases, analytical functions are fitted to the observed distributions in  $m_X$  in the LSB and HSB CRs, where the functions are predefined with the help of simulation. For the minor backgrounds from diboson (including VH) production these functions are purely determined from simulation. For  $t\bar{t}$  production and for the dominating background from  $Z+jets$  events, these are fitted to the data in dedicated sideband regions, after subtracting the estimates of the minor backgrounds in these regions. The functions are then extrapolated to the SR through transfer functions, which have been obtained from simulation. This method has been validated with slightly modified sideband

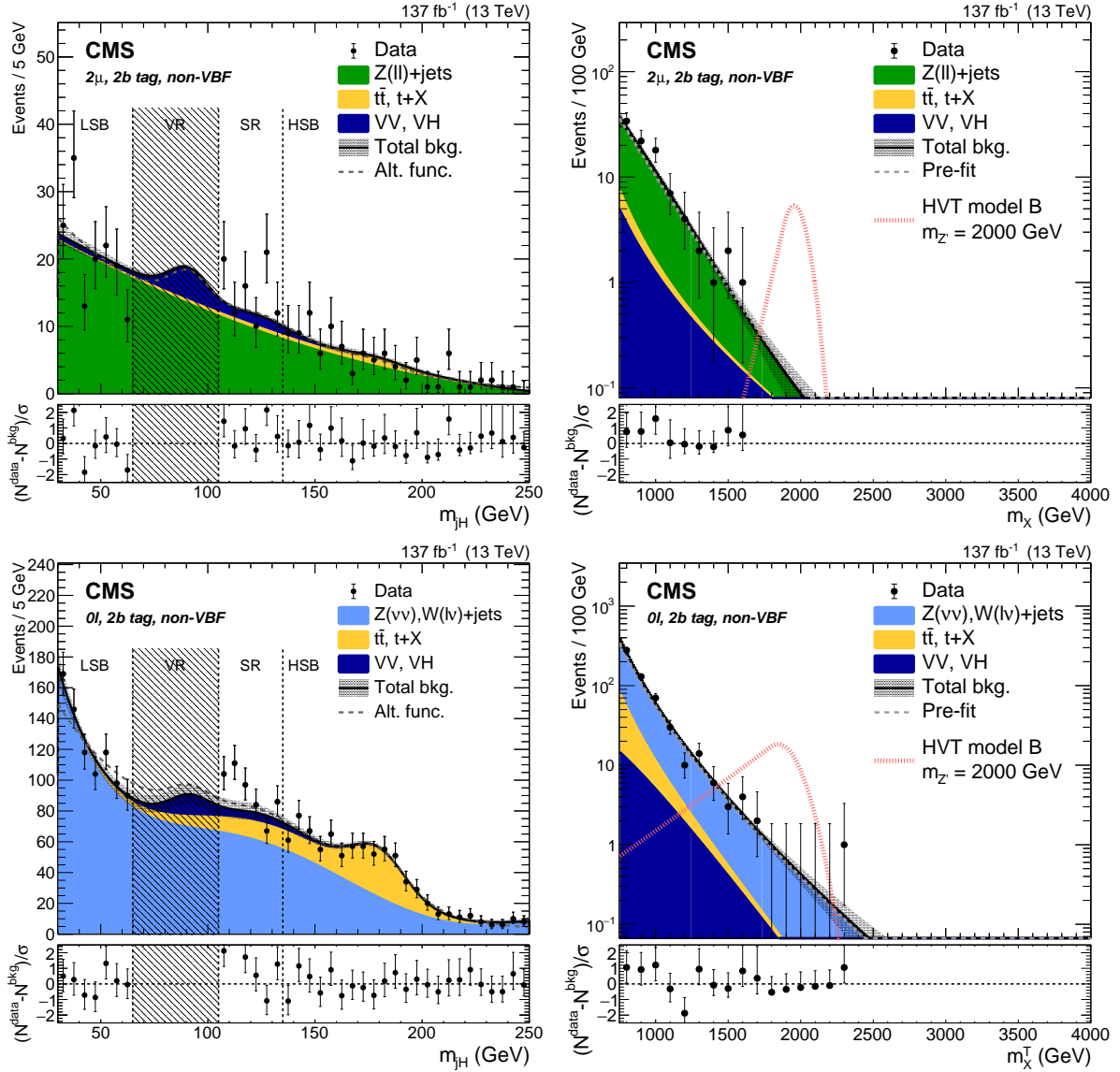


Figure 16: Search for  $X \rightarrow VH(bb)$ : Distributions of (left) the jet soft drop mass of a boosted Higgs boson candidate, labeled  $m_{jH}$ , and (right) the mass or transverse mass of the  $X$  resonance candidate, labeled  $m_X$  and  $m_X^T$ , respectively, in the  $Z(\ell\ell)H(bb)$  (upper) and  $Z(\nu\nu)H(bb)$  channels (lower). The shaded area depicts a veto region excluded from the analysis to minimize the event overlap with dedicated searches in the  $VV$  decay channel. Figures from Ref. [110].

definitions providing independent control regions close to the SRs. Several functional forms have been tested and a bias test has been conducted to ensure that the method is capable of describing the data in the validation regions and that no spurious signal may emerge this way.

### 2.3.3 The high-mass region: hadronic V boson decays

In the high-mass analysis targeting hadronic V boson decays [111], the presence of two AK8 jets with  $p_T > 200 \text{ GeV}$  and  $|\eta| < 2.5$  is required. In cases where more than two AK8 jets are found in an event, the leading ones in  $p_T$  are interpreted to originate from the  $V \rightarrow qq$  and  $H \rightarrow bb$  decays. To guarantee an efficiency of  $>99\%$  of the trigger selection, the invariant mass of the selected AK8 jets is required to be larger than  $m_{jj}^{\text{AK8}} > 1250 \text{ GeV}$ . Furthermore, the jets are required to have a distance  $\Delta R > 0.8$  from any reconstructed electron or muon with  $p_T > 20$  or  $30 \text{ GeV}$  satisfying identification criteria optimized for high-momentum leptons, respectively.

To reduce the background from events with purely QCD-induced light-quark and gluon jets, referred to as QCD multijet production in the following, the selected AK8 jets are required to be separated by no more than  $|\Delta\eta_{jj}^{\text{AK8}}| < 1.3$ . In addition,  $55 < m_{SD} < 215 \text{ GeV}$  and a loose requirement of

$$\rho = \log(m_{SD}^2 / p_T^2) < 1.8 \quad (9)$$

are imposed. The requirement on  $\rho$  is imposed to prevent high values for  $m_{SD}$  while the  $p_T$  of the AK8 jet is low. In those cases, the cone size of  $\Delta R = 0.8$  is too small to contain the full jet, affecting both the  $m_{SD}$  resolution and the efficiency to assign each AK8 jet to a W, Z, or H boson.

The DEEPAK8 jet tagging algorithm [141] is used to identify AK8 jets originating from a W, Z, or H boson. The algorithm consists of a staggered two-step deep neural network (NN) architecture, based on the properties of the clustered PF candidates, such as the  $p_T$ , charge, and angular distance to the jet axis, as well as track and secondary vertex information. The latter is used to infer whether a jet contains heavy-quark decays or not. The input features of both, the PF candidates and the secondary vertices and tracks are processed in two independent convolutional NNs. The outputs of these NNs are passed to a third, fully connected deep NN (DNN) to assign a jet to one of the following classes: single quark or gluon, W boson decaying to cq or qq, and H or Z boson, each decaying into bb, cc, or light flavor quarks. For the reported analysis two discriminants are of relevance, both discriminating between signal jets and jets from single quarks or gluons. A qq discriminant is built to identify the decay of a W or Z boson into light quarks, and a bb discriminant is built to identify the H and Z boson decays into bb.

The strategy of the search is to distinguish the signal, which is peaking in three distributions, namely  $m_{SD}$  of each selected AK8 jet and the dijet mass of the two AK8 jets  $m_{jj}^{\text{AK8}}$ , from the considered backgrounds that exhibit a smoothly falling spectrum in at least one of these observables. To guarantee that the  $m_{SD}$  distributions of the considered background processes are not kinematically biased by the selection based on the DEEPAK8 tagger, an adversarial training of the NNs is performed that leads to a reduced correlation between  $m_{SD}$  and the output of the tagger [141]. The remaining correlations are further suppressed by a DDT method [145] applied on the tagger output. Eventually, the selection of the output of the DEEPAK8 tagger is chosen such that it yields a constant tagging rate as a function of  $p_T$  and  $m_{SD}$  for the quark or gluon jets with the highest  $p_T$  in QCD multijet production, based on simulation.

The qq tagging efficiency, and the probability of hadronic t quark decays to be misidentified by the qq tagger are calibrated in a  $t\bar{t}$  event selection enriched in hadronic W boson decays.

The bb discriminant is calibrated in an event sample enriched with jets from  $g \rightarrow bb$  splitting using a double-muon tag, as described in Ref. [137].

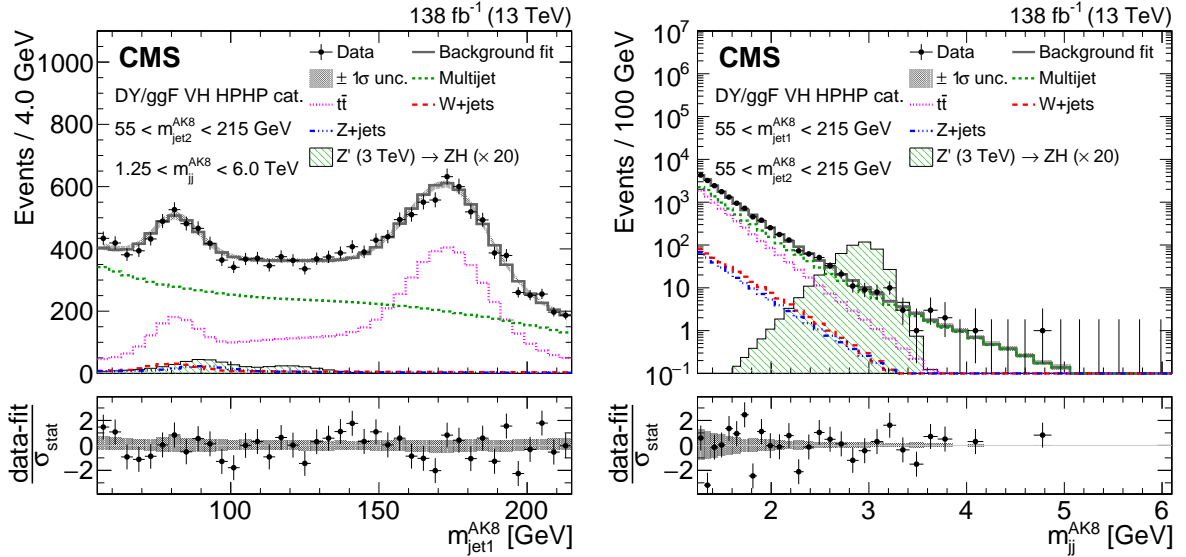


Figure 17: Search for  $X \rightarrow V(q\bar{q})H(bb)$ : Distributions of (left) the soft drop mass  $m_{SD}$  variable, labelled as  $m_{jet1}^{AK8}$ , and (right) the dijet mass  $m_{jj}^{AK8}$  in the  $V(q\bar{q})H(bb)$  channel [111]. The individual contributions of the background model are shown by open histograms with different colours and line styles. The signal of a  $Z'$  boson with a mass of 3 TeV decaying via  $Z \rightarrow q\bar{q}$  and  $H \rightarrow bb$  is also shown, by a green filled histogram. Figure from Ref. [111].

To increase the sensitivity of the search after selection, all remaining events are assigned to one of 10 mutually exclusive event categories based on a VBF tag and the outputs of the qq and bb discriminants from each of the selected AK8 jets. The VBF tag is defined by requiring at least two AK4 jets with  $p_T > 30$  GeV and  $|\eta| < 5.0$  that do not overlap with the selected AK8 jets within  $\Delta R < 1.2$ . For the two AK4 jets, which are leading in  $p_T$ ,  $m_{jj} > 800$  GeV and a separation of  $|\Delta\eta| > 4.5$  are required. The event categories target VV and VH decays.

Distributions of  $m_{SD}$  and  $m_{jj}^{AK8}$  in the non-VBF VH event category, where one of the selected AK8 jets (the V candidate) exhibits a high-purity classification score in the qq discriminant, while the other one (the H candidate) exhibits a high purity classification score in the bb discriminant, are shown in Fig. 17. To simplify the modelling of the three-dimensional (3D) ( $m_{jj}^{AK8}$ ,  $m_{SD}^{jet1}$ ,  $m_{SD}^{jet2}$ ) shapes, the assignment of AK8 jets to “Jet 1” and “Jet 2” is performed randomly, so that both  $m_{SD}$  distributions exhibit the same shape. The largest background originates from QCD multijet production, which is estimated from a parametric functional form obtained through a forward-folding technique applied to a set of simulated samples at the level of stable particles [156]. This functional form can be constrained through nuisance parameters attached to physics-motivated alternative shapes. All other processes are obtained from simulation. The production of  $t\bar{t}$  events is expected to contribute 40%, the expected background from  $W+jets$  and  $Z+jets$  production amounts to up to 4% of the selected events. Backgrounds from single t quark and diboson production are expected to contribute less than 1.5%. While all backgrounds are nonresonant in  $m_{jj}^{AK8}$ , some exhibit one or two resonant structures at different values in the  $m_{SD}$  distribution of only one or both AK8 jets. The signal is obtained from analytic functional forms as in the case of the analyses described in Section 2.3.2.

## 2.4 Search for resonances in the HH channel

This section describes searches for resonances decaying into two H bosons with a mass of 125 GeV. Various further decay mode combinations are covered by the more general searches in the  $X \rightarrow YH$  analyses, and are discussed in Section 2.5.

### 2.4.1 The $X \rightarrow H(bb)H(WW)$ decay in resolved jet topology

For a pair of Higgs bosons, the  $bbWW$  decay channel has the second-largest branching fraction of all  $HH$  decay modes, of about 24%. The analysis described in this section focuses on the single lepton (SL)  $bbl\nu qq$  and dilepton (DL)  $bbl\nu\ell\nu$  final states [112].

The data have been collected with a combination of single- and double-lepton triggers. The event selection requires one or two isolated leptons, in the second case with opposite signs. The analysis considers  $H \rightarrow bb$  in both resolved and merged jet topologies, and requires suitable numbers of AK4 and AK8 jets. Jets associated with the  $H \rightarrow bb$  candidate are b tagged by passing the medium working point of the DEEPJET algorithm [138] in the AK4 case, or the medium working point of the DEEPCSV algorithm [137] in case of AK8 subjets.

The selection vetoes pairs of leptons, which according to their invariant mass are likely to originate from quarkonia or Z boson decays. Overlap with events selected by the analysis in the  $bb\tau\tau$  channel (discussed in Section 2.5.1) is removed by vetoing events containing at least one  $\tau_h$  candidate passing the selection described in Ref. [115].

The events are classified into processes based on the output of multiclass deep neural networks (DNNs), separately trained for the SL and DL cases. The DNNs feature output nodes for a number of backgrounds and one signal node. The DNNs are trained on all signal samples; they are parameterized in the nominal signal mass and contain five background nodes for the SL and seven for the DL category. Depending on the highest scoring node, events are subdivided into signal and background categories. The network inputs include a number of high-level features, such as invariant masses and the hadronic activity of the event, but in addition also the output of a Lorentz-boost network [157] performing automated feature engineering based on the four-momenta of selected leptons and jets. Due to similarity of the DNN score distributions for various background classes, they are merged into process groups prior to the signal extraction.

The signal categories are further divided into subcategories according to the b jet topology and multiplicity, referred to as resolved 1b, resolved 2b, and merged. The merged jet subcategories are excluded in the  $HH$  combination (Section 2.6) as they would overlap with the analysis described in Section 2.4.2. Background contributions dominantly originating from  $t\bar{t}$  production are estimated from simulation, with two exceptions: contributions arising from jets misidentified as leptons are estimated with the misidentification-factor method [158], while the DY background is addressed with a different method using the 0b CR in data and transfer factors determined in the Z boson peak region.

In the SL case, the signal extraction is performed by a simultaneous maximum likelihood fit to the distributions of the DNN outputs of the signal and the background process groups. In the DL case, the DNN output of the signal category is combined into an unrolled 2D variable with the output of a heavy-mass estimator (HME) [159], a variable that estimates the most likely invariant mass of the  $HH$  system considering the presence of two neutrinos and the  $\vec{p}_T^{\text{miss}}$  measurement.

Examples of the signal extraction are shown in Fig. 18. The distribution in the DNN score (SL case) and the unrolled combination of the DNN score and the HME bin (DL case) are shown

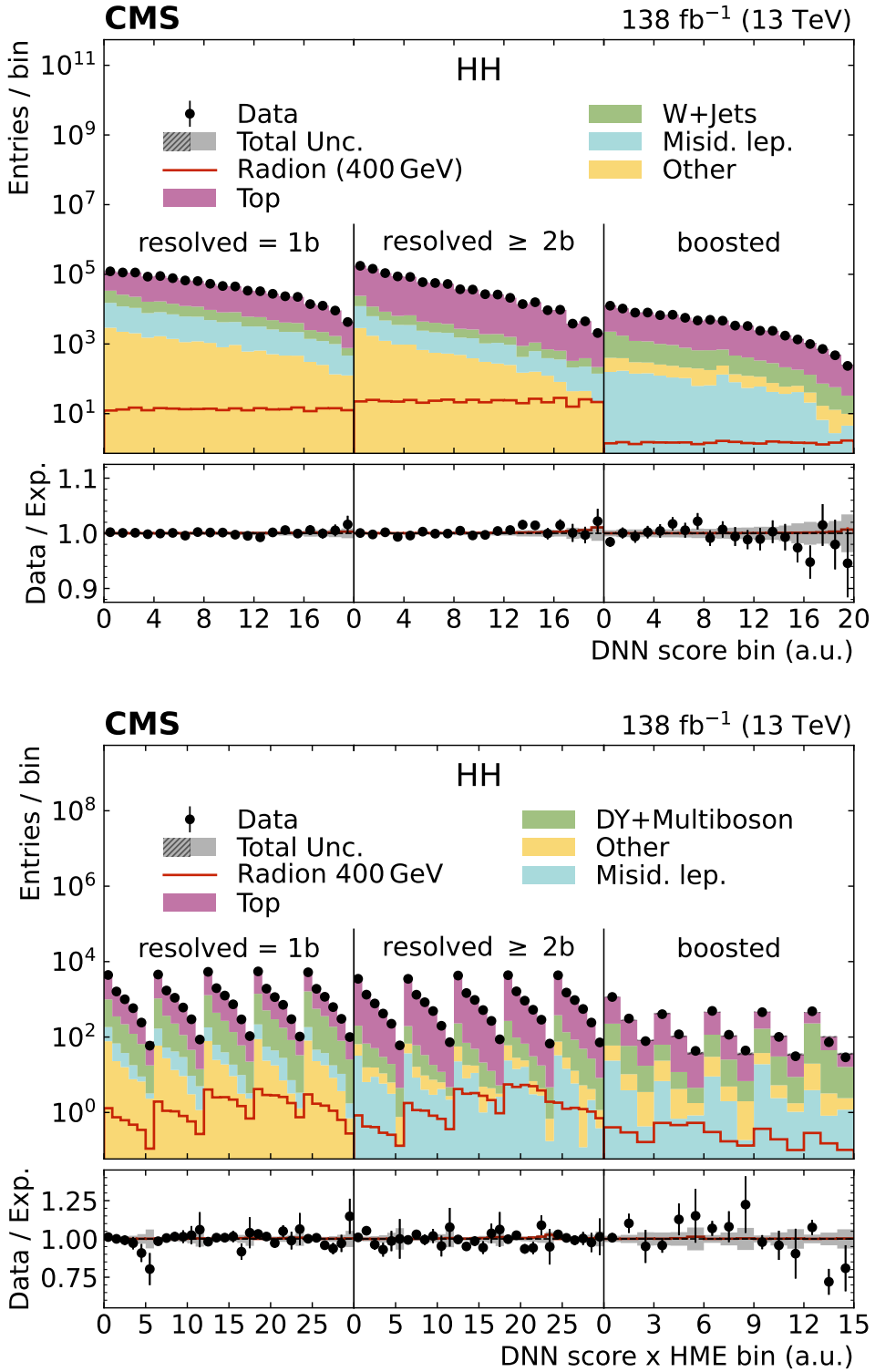


Figure 18: Search for  $X \rightarrow H(\text{bb})H(\text{WW})$ : Distributions of the DNN output for events in the signal nodes of the (upper) SL and (lower) DL categories of the  $H(\text{bb})H(\text{WW})$  analysis based on merged and resolved jets [112]. The distributions for a signal of a resonant radion with a mass of 400 GeV is also shown, by an open red histogram. Figure from Ref. [112].

for the SR for the three event categories, for an assumed resonance mass of  $m_X = 400\text{ GeV}$ . The signal expected for a radion of this mass with a cross section of 1 pb is also displayed. The observed distributions agree well with the expectation from SM backgrounds and no significant signal is observed.

#### 2.4.2 The $X \rightarrow H(bb)H(WW)$ decay in merged-jet topology

This study extends the search in the bbWW channel towards higher X masses [113]. As in Section 2.4.1, the SL selection targets the  $HH \rightarrow bbWW \rightarrow bbl\nu qq$  decay mode. The DL selection covers both the  $HH \rightarrow bbWW \rightarrow bbl\nu l\nu$  and the  $HH \rightarrow bb\tau\tau \rightarrow bbl\nu\nu l\nu\nu$  decay modes, and the latter comprises 30–35% of the total expected DL signal yield. As this analysis targets resonance masses of  $m_X > 0.8\text{ TeV}$ , the H bosons emerge with a large Lorentz boost with respect to the laboratory rest frame, and their decay products are contained in collimated cones. For this reason, the hadronically decaying H and W bosons are each reconstructed with a single AK8 jet.

The signal is searched for in the two-dimensional distribution in the  $(m_{bb}, m_{HH})$  mass plane, hence the kinematics of both Higgs boson candidates need to be reconstructed.

In the SL final state, the highest  $p_T$  lepton in the event is selected as the lepton candidate from the leptonic W decay. The W(qq) decay is reconstructed with a high- $p_T$  AK8 jet. The AK8 jet nearest to the lepton satisfying  $\Delta R < 1.2$  is taken to be the W candidate. The H  $\rightarrow$  WW decay chain is reconstructed using a likelihood-based technique, which provides an estimate of the neutrino momentum vector and also a correction to the  $p_T$  of the W(qq) candidate jet.

In the DL final state, two opposite-sign light leptons with the highest  $p_T$  are taken to be the leptons arising from the H  $\rightarrow$  WW decay.

Due to the collimation of the Higgs boson decay products, the polar angles of the dineutrino and dilepton systems can be assumed to be the same. Using this assumption, and by approximating the invariant mass of the two neutrinos with its expected mean value of 55 GeV, the sum of the four-momenta of the two neutrinos is estimated using  $p_T^{\text{miss}}$ . These assumptions are guided by simulation studies. The leptons are required to be close by satisfying  $\Delta R < 1$ , and their invariant mass is required to be in the range of 6–75 GeV to reduce contamination from DY production. Events are required to have large  $p_T^{\text{miss}}$ , pointing in approximately the same direction in the transverse plane as the dilepton system, satisfying  $\Delta\phi < \pi/2$ .

In all considered final states, the H  $\rightarrow$  bb decay is reconstructed as a single AK8 jet with two-prong substructure and high  $p_T$ . The double-b tagging is performed with the DEEPAK8 algorithm. The SR is defined by requiring  $m_{SD}$  of the H  $\rightarrow$  bb candidate to be within 30–210 GeV. This allows us to also capture the neighboring background, which is important for the signal extraction described below. Events containing any b-tagged AK4 jets outside the H  $\rightarrow$  bb candidate AK8 jet are vetoed, as they are likely to arise from t̄t production.

Events with the production of one or more top quarks constitute the majority of the background, where particles from a hadronic top quark decay are captured in the H  $\rightarrow$  bb candidate jet, particularly in the SL final state. The invariant mass distributions of such backgrounds may resonate in  $m_t$ ,  $m_W$ , or neither, depending on which daughter partons are captured, and the backgrounds are classified accordingly. Events originating from other processes, primarily from W+jets and QCD multijet production in the SL channel and DY production in the DL channel, are taken as a separate component.

Events are divided into twelve categories according to the lepton flavor, the purity of the

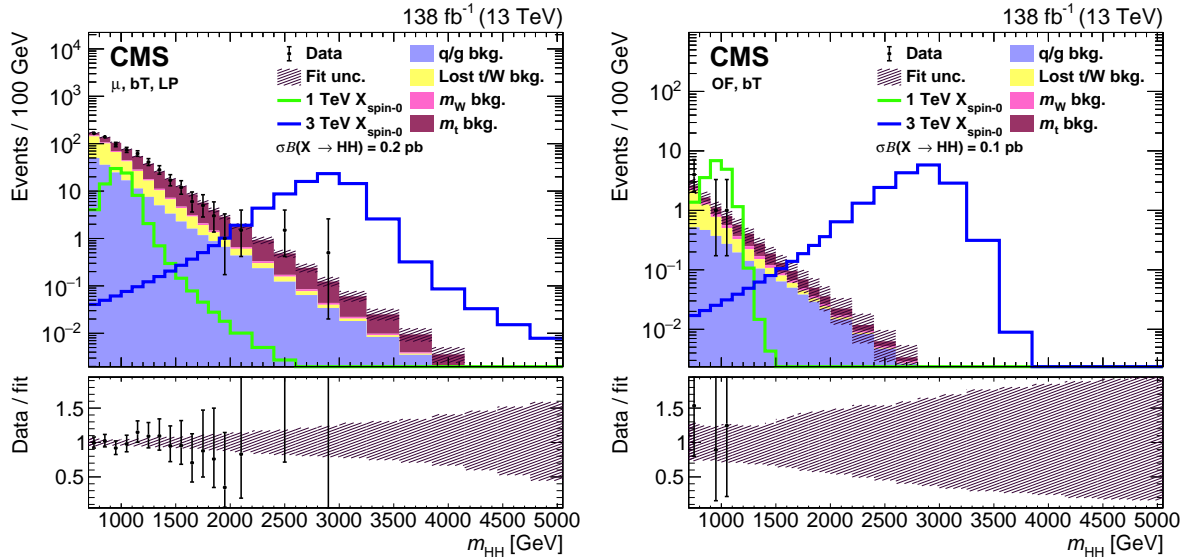


Figure 19: Search for  $X \rightarrow H(bb)H(WW)$ : Distributions of the  $m_{HH}$  variable, in the (left) SL and (right) DL categories of the  $H(bb)H(WW)$  analysis with merged jets [113]. Expected signal distributions from a spin-0 resonance with a mass of 1 or 3 TeV are also shown, by the open green and blue histograms. Figure from Ref. [113].

$H \rightarrow bb$  flavor tagging, and, for the SL final states, the purity of the  $H \rightarrow WW$  decay reconstruction. Results are extracted by performing a maximum likelihood fit in the 2D ( $m_{bb}$ ,  $m_{HH}$ ) mass plane. The background-only model is found to describe the observed distributions well. The distributions of events projected into  $m_{HH}$  for two selected categories in SL and DL final states are shown in Fig. 19. In both cases high purity of the  $H \rightarrow bb$  flavor tagging (bT) is required. The chosen SL category is further characterized by a muon and a low purity (LP) requirement of the  $H \rightarrow WW$  decay reconstruction. The DL category is characterized by different flavors.

#### 2.4.3 The $X \rightarrow HH$ decays into multilepton final states

The analysis of multilepton final states [114] does not assume at least one  $H \rightarrow bb$  decay, unlike all other HH analyses discussed in this report, and thus gains access to various hitherto uncovered HH signatures. This search is focused on resonant HH production in the  $WWWW$ ,  $WW\tau\tau$ , and  $\tau\tau\tau\tau$  decay modes. The chosen final states provide a good compromise between a relatively large HH branching fraction and a clean leptonic event signature. The latter provides a series of almost background-free categories with low event counts, which are especially sensitive at low resonance masses. The data are collected using triggers combining single and multiple lepton and  $\tau_h$  signatures.

The selected events are split into seven event categories with different multiplicities of reconstructed leptons and hadronically decaying taus, denoted as  $2\ell ss$  (same sign),  $3\ell$ ,  $4\ell$ ,  $3\ell + 1\tau_h$ ,  $2\ell + 2\tau_h$ ,  $1\ell + 3\tau_h$ , and  $4\tau_h$ . The lower multiplicity  $2\ell ss$  and  $3\ell$  categories also require additional jets, as expected from hadronic W boson decays. To reduce the impact of backgrounds involving the decay of top quarks, such as  $t\bar{t}$  production, and to avoid overlap with other HH analyses, events with b jets reconstructed with the DEEPJET algorithm [138] are explicitly vetoed. Similarly, events with two opposite-sign same-flavor lepton pairs and a combined invariant mass below 140 GeV are vetoed to avoid overlap with the  $HH \rightarrow bbZZ$  signature. To exclude phase space regions enriched in low mass resonances, which are not well modelled in simulation, and to reduce the impact of backgrounds involving Z boson decays, events con-

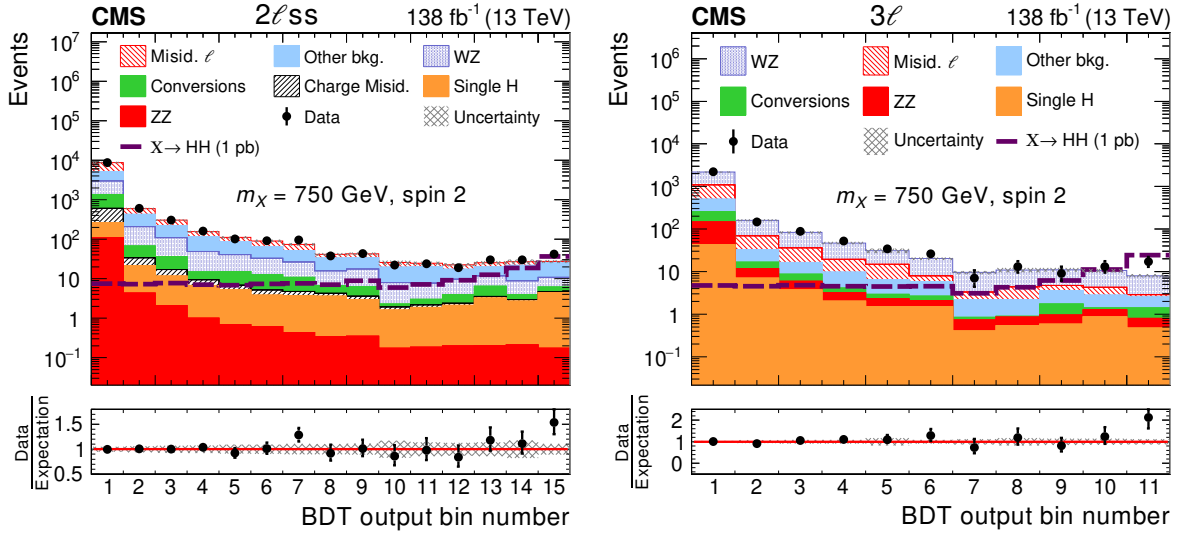


Figure 20: Search for  $X \rightarrow \text{HH}$  in multi-lepton final states: Distributions of the BDT classifier output for events in the (left)  $2\ell\text{ss}$  and (right)  $3\ell$  categories of the  $H(WW + \tau\tau)H(WW + \tau\tau)$  analysis in multilepton final states [114]. The expected signal for a spin-2 resonance with a mass of 750 GeV resonant HH signal is shown, by the open dashed histogram. The signal is normalized to a cross section of 1 pb. The distributions of the estimated background processes and corresponding uncertainties are shown after a fit of the signal plus background hypothesis to the data. Figure from Ref. [114].

taining DL pairs with a mass of  $m_{\ell\ell} < 12$  GeV or in the vicinity of the Z boson mass are vetoed as well.

The main backgrounds arise from genuine multiboson processes, such as ZZ production in all categories, as well as WZ production in the  $2\ell\text{ss}$  and  $3\ell$  categories. These backgrounds, as well as smaller backgrounds, such as contributions from DY,  $t\bar{t}$ , and single H production together with backgrounds from photon conversions in the detector material are estimated from the simulation. Background events from charge misidentification in the  $2\ell\text{ss}$  category, however, are also estimated from data extrapolating events with opposite-sign electrons from  $Z \rightarrow ee$  decays into the SR. In most categories, backgrounds arising from jets misidentified as either leptons or  $\tau_h$  also play an important role; these are estimated with the misidentification-rate factor method [158].

The signal extraction is based on maximum likelihood fits to the distributions of boosted decision tree (BDT) discriminants. The BDTs are trained to discriminate signal from background in each of the seven categories and for each resonance spin assumption (spin 0 or 2). The BDTs are parameterized in the nominal resonance mass.

The selection of BDT input variables is optimized for each signal category, and includes kinematic variables of  $\ell$  and  $\tau_h$  candidates as well as angular separations and invariant masses of their combinations. Also, the reconstructed HH mass is used. All noninteger variables are decorrelated from the signal hypothesis, improving the usage of the available training data set. The fits also include two kinematic distributions in control regions enriched in the dominant prompt backgrounds from ZZ and WZ production.

As an example of the SR composition, Fig. 20 shows the BDT output in the two highest signal yield categories  $2\ell\text{ss}$  and  $3\ell$  for a spin-2 particle with  $m_X = 750$  GeV. A small excess is observed

in both distributions in the rightmost bin of both distributions, amounting to a local significance of about 2.1 standard deviations in both categories. This leads to a mild local excess of the observed limits corresponding to about 1.5–2 standard deviations for masses above 600 GeV, which is visible in Fig. 27.

## 2.5 Search for resonances in the YH channel

Recently, direct searches for new physics in the Higgs sector have been extended towards YH decays, where Y denotes another unknown bosonic resonance. Such decays are expected, e.g., in 2HDM+S models like the NMSSM, where X and Y can be identified with additional heavy or light Higgs bosons. In cases where Y carries a large singlet component its couplings to SM particles are suppressed and its dominant production at the LHC proceeds via the decay  $X \rightarrow YH$ . The first analysis presenting such a search was performed in  $Y(bb)H(\tau\tau)$  final states [115], covering mass ranges of  $260 < m_X < 3000$  GeV and  $60 < m_Y < 2800$  GeV. Later on, this analysis was complemented by similar searches in the  $Y(bb)H(bb)$  [117] and  $Y(bb)H(\gamma\gamma)$  [116] final states. The search in the  $Y(bb)H(bb)$  final state covers mass ranges of  $900 < m_X < 4000$  GeV and  $60 < m_Y < 600$  GeV, targeting kinematic regimes where both bb decays are reconstructed as large- $R$  AK8 jets. The  $Y(bb)H(\gamma\gamma)$  analysis covers mass ranges of  $300 < m_X < 1000$  GeV and  $90 < m_Y < 800$  GeV, where the upper bound on  $m_X$  is implied by the requirement that it should be possible to resolve the b quarks originating from the Y decay as two distinct AK4 jets. All final states have the  $Y(bb)$  decay in common. The  $H(bb)$  decay utilizes the large branching fraction of the H boson to b quarks; the  $H(\tau\tau)$  decay comprises the second largest branching fraction with advantageous reconstruction and identification properties; the  $H(\gamma\gamma)$  decay contributes through the excellent mass resolution of the ECAL.

### 2.5.1 The $X \rightarrow Y(bb)H(\tau\tau)$ decays

The analysis in  $Y(bb)H(\tau\tau)$  final states evolved from an analysis of  $H \rightarrow \tau\tau$  [160], adding loose requirements on the  $Y \rightarrow bb$  decay where the b quarks are reconstructed as AK4 jets. For the  $H(\tau\tau)$  decay the  $e\tau_h, \mu\tau_h$ , and  $\tau_h\tau_h$  final states are considered. These final states have been shown to have the largest sensitivity to this signature, while the contribution from  $\tau\tau$  decays into an e and  $\mu$ , mostly due to the large background from  $t\bar{t}$  production in the kinematic phase space with additionally selected b jets is marginal.

The trigger selection of the events proceeds via the presence of high- $p_T$  electrons, muons, or  $\tau_h$  decays, or combinations of those at the trigger level. Due to the trigger requirements evolving with time, the offline  $p_T$  thresholds range from 25–33 GeV for electrons, from 20–25 GeV for muons, and from 30–40 GeV for  $\tau_h$  candidates, the latter depending also on the  $\tau\tau$  final state. The  $\tau_h$  candidates are identified using the DEEPTAU algorithm [151], as discussed in Section 2.2. Jets are b tagged using the DEEPJET algorithm, with a working point of 80% efficiency with a misidentification rate for light-flavor or gluon jets of  $\approx 1\%$  [137, 138]. For the event selection, a  $\tau\tau$  pair in one of the targeted  $\tau\tau$  final states and at least one b jet are required. Events that contain only one b jet and no other jet are discarded from the analysis. If more than two b jets are found, the  $Y(bb)$  decay is built from those jets that are leading in  $p_T$ . If only one b jet exists, the Y candidate is built from this b jet and the jet with the highest b jet score of the DEEPJET algorithm, even if this lies below the threshold of the chosen working point. The energies of the jets used to form the Y candidate are corrected using the multivariate energy-momentum regression [161].

Depending on the  $\tau\tau$  final state, all selected events are then passed through one of three NNs exploiting multiclass classification to distinguish signal, for given values of  $m_X$  and  $m_Y$ , from four background classes: (i) events with genuine  $\tau$  pairs in the final state; (ii) events with quark-

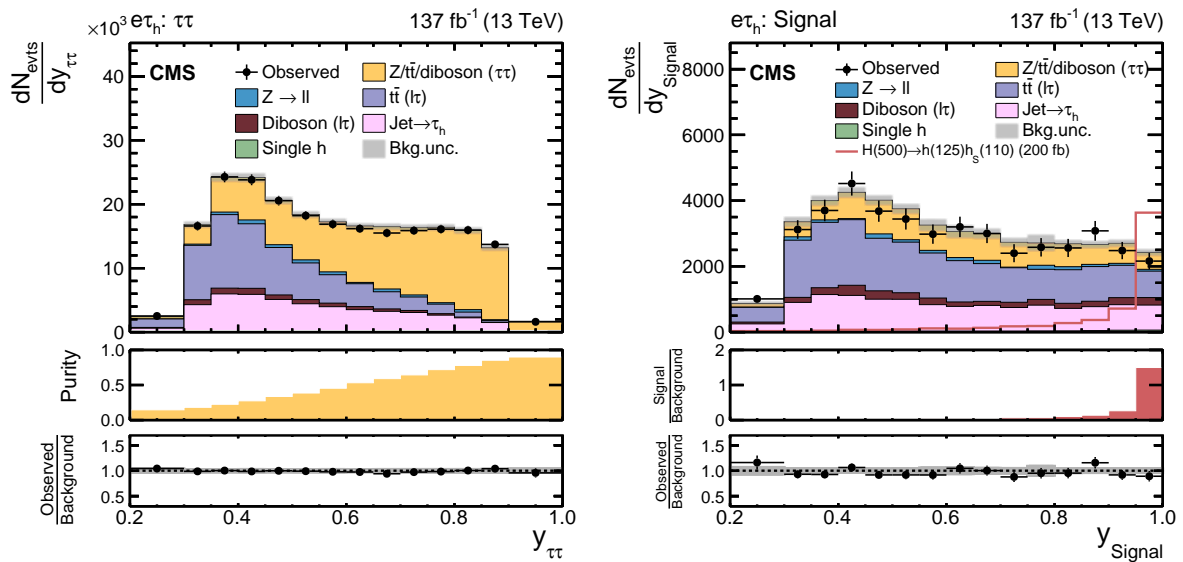


Figure 21: Search for  $X \rightarrow Y(bb)H(\tau\tau)$ : Distributions of the NN output scores  $y_i$ , in different event categories after NN classification, based on a training for a resonance  $X$  with  $m_X = 500$  GeV and a resonance  $Y$  with  $100 \leq m_Y < 150$  GeV in the  $e\tau_h$  final state of the  $H(\tau\tau)Y(bb)$  analysis [115]. Shown are the (left)  $\tau\tau$  and (right) signal categories. For these figures, the data of all years have been combined. The uncertainty bands correspond to the combination of statistical and systematic uncertainties after the fit of the signal plus background hypothesis for  $m_X = 500$  GeV and  $m_Y = 110$  GeV to the data. In the lower panels of the figures the (left) purity and (right) fraction of the expected signal over background yields for a signal with a cross section of 200 fb, as well as the ratio of the obtained yields in data over the expectation based on only the background model, are shown. Figure from Ref. [115].

or gluon-induced jets misidentified as  $\tau_h$  candidates; (iii)  $t\bar{t}$  events where the intermediate  $W$  bosons in the decay chain decays into any combination of electrons and muons or into a single  $\tau$  lepton and an electron or muon (not included in (i) or (ii)); (iv) events from remaining background processes that are of minor importance for the analysis and not yet included in any of the previous classes. This last class comprises single  $H$ , single  $t$  quark, and diboson production, as well as  $Z$  boson decays into electrons or muons. For single  $H$  production, rates and branching fractions as predicted by the SM are assumed.

Inputs to the NNs are 20–25 features, of which the following estimates have been identified to be most discriminating, according to an unambiguous metric as given in Ref. [162]: the invariant masses of the  $bb$ ,  $\tau\tau$ , and  $bb\tau\tau$  systems, and the  $\chi^2$ -value of a kinematic fit to the data of the signal hypothesis for given values of  $m_X$  and  $m_Y$ . Since the discrimination depends on the signal hypothesis, individual NNs have been trained for 68 groups of kinematically adjacent and similar signal hypotheses. Each event has been assigned to the class with the highest NN output score. Eventually, the NN output scores have been chosen as discriminating variables for a maximum likelihood fit in 45 individual event categories, split by  $\tau\tau$  final state and data-taking year. Typical output distributions are shown in Fig. 21.

### 2.5.2 The $X \rightarrow Y(bb)H(\gamma\gamma)$ decays

As in the previous case, the analysis in the  $Y(bb)H(\gamma\gamma)$  final state [116] starts from the well-identified  $H \rightarrow \gamma\gamma$  decay complemented by the selection of two additional AK4 jets to form the  $Y(bb)$  candidate.

The trigger selection proceeds through the requirement of two photons with thresholds of  $p_T > 30 \text{ GeV}$  for the leading ( $\gamma_1$ ) and  $p_T > 18 \text{ GeV}$  for the subleading ( $\gamma_2$ ) photon in  $p_T$ , for data taken in 2016. For data taken in the years 2017–2018, the requirement on  $\gamma_2$  is raised to  $p_T > 22 \text{ GeV}$  because of the larger amount of PU in data. The photons are required to pass identification and isolation criteria, already through the trigger selection, and the mass of the two photons is required to be  $m_{\gamma\gamma} > 90 \text{ GeV}$ .

In the offline selection, the photons from which the H candidate is formed are required to be well contained in the ECAL and tracker fiducial volumes of  $|\eta| < 2.5$ , excluding the transition region of  $1.44 < |\eta| < 1.57$  between the ECAL barrel and endcaps, and to fulfill kinematic requirements of  $100 < m_{\gamma\gamma} < 180 \text{ GeV}$ ,  $p_T^{\gamma_1}/m_{\gamma\gamma} > 1/3$ , and  $p_T^{\gamma_2}/m_{\gamma\gamma} > 1/4$ . In addition to the photons at least two AK4 jets originating from the same PV as the photons are required, where the assignment of the photons to the PV is achieved with the help of an MVA technique, as described in Ref. [163]. The jets must fulfill identification requirements as described in Section 2.2, have  $p_T > 25 \text{ GeV}$  and  $|\eta| < 2.4$  or 2.5, for the data taken in 2016 and 2017–2018, respectively, and be separated from each of the selected photons by  $\Delta R > 0.4$ . Of all jets in an event that match these criteria, those with the highest sum of their DEEPJET discriminant scores are chosen to form the Y candidate with a requirement on the dijet mass of  $70 < m_{jj} < 1200 \text{ GeV}$ . The lower bound on  $m_{jj}$  is implied by the kinematic turn-on in the  $m_{jj}$  distribution, the upper bound is defined by the transition towards Lorentz-boosted regimes, where the bb system may not be resolved by two spatially separated AK4 jets.

The X candidate is reconstructed from the jets and photons forming the H and Y candidates. To improve the resolution, its mass  $m_X$  is estimated from

$$\tilde{m}_X = m_{\gamma\gamma jj} - (m_{\gamma\gamma} - m_H) - (m_{jj} - m_Y), \quad (10)$$

where  $m_{\gamma\gamma jj}$  is the mass calculated from the two jets and the two photons. It is corrected by subtracting  $m_{\gamma\gamma}$  and  $m_{jj}$ , with their values replaced by the hypothesised masses  $m_H$  and  $m_Y$ . This estimate has been shown to lead to a 30 to 90% improvement in signal resolution compared to  $m_{\gamma\gamma jj}$  alone, in the high- and low- $m_X$  regimes, respectively. For the signal extraction, events are required to be located inside a window in  $\tilde{m}_X$ , depending on the  $m_X$  hypothesis under test. The width of this window has been defined such that it contains at least 60% of the signal.

Resonant backgrounds to the analysis originate from single H production, which is strongly suppressed already by the selection in  $\tilde{m}_X$ . For hypotheses of  $m_X < 550 \text{ GeV}$  a sizeable contribution from t̄tH production is further reduced by an NN-based discriminant developed for the search for nonresonant H( $\gamma\gamma$ )H(bb) production [164], exploiting the presence of W boson decays in an event, which arises from the t̄t decay chains.

Nonresonant backgrounds in this search mostly originate from the production of one ( $\gamma$ +jets) and two ( $\gamma\gamma$ +jets) photons in association with jets. To separate these backgrounds from the signal a BDT with three output classes, one for each background and one for signal, and 22 input features is used. The input features comprise kinematic and identification observables of the selected jets and photons, estimates of the mass, energy, and  $p_T$  resolutions, and an estimate of the  $p_T$  density from PU. For training, six exclusive kinematic regions are defined, based on the hypothesised values of  $m_X$  and  $m_Y$ , where in each region all contained signal samples and the two background processes in question, as obtained from simulation, are used with equal weight. These training regions are defined to resemble similar kinematic properties for signals inside the given  $m_X$ – $m_Y$  window. For each kinematic region, three event categories are defined, based on the output of the corresponding BDT. These categories are introduced to indicate regimes of varying signal purity. For each  $m_X$  hypothesis the signal is inferred from an

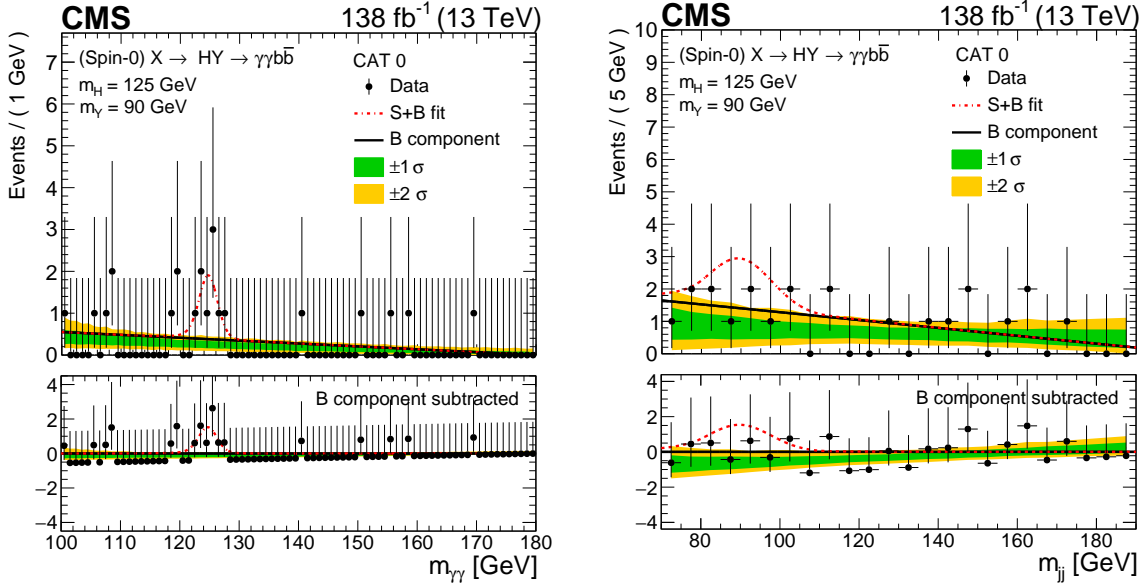


Figure 22: Search for  $X \rightarrow Y(bb)H(\gamma\gamma)$ : Marginal distributions of the (left)  $m_{\gamma\gamma}$  and (right)  $m_{jj}$  variables, in the high-purity SR (labeled “CAT 0”) of the  $Y(bb)H(\gamma\gamma)$  analysis [116]. The figure is shown, for a hypothesis of  $m_X = 650$  GeV and  $m_Y = 90$  GeV, for which the largest excess of events over the background model is observed. In the lower panels, the numbers of background-subtracted events are shown after the fit of the background model to the data. Figure from Ref. [116].

unbinned likelihood fit of a parametric model to the data in the 2D discriminating distributions given by the values of  $m_{\gamma\gamma}$  and  $m_{jj}$ , in each of the BDT categories. The data are found to be compatible with the SM predictions. In Fig. 22 the marginal distributions of  $m_{\gamma\gamma}$  and  $m_{jj}$  in the BDT category with the highest expected signal purity for a selection corresponding to  $m_X = 650$  GeV and  $m_Y = 90$  GeV, are shown together with the results of the fit to the data. For these mass values, the largest deviation from the background-only hypothesis is observed, with a local (global) significance of 3.8 (2.8) standard deviations.

In Fig. 22 the marginal distributions of  $m_{\gamma\gamma}$  and  $m_{jj}$  in the BDT category with the highest expected signal purity are shown together with the results of the fit to data. A hypothesised signal for  $m_X = 650$  GeV and  $m_Y = 90$  GeV with an arbitrary normalization is also shown.

### 2.5.3 The $X \rightarrow Y(bb)H(bb)$ decays in merged jet topology

This analysis in the  $Y(bb)H(bb)$  final state [117] explicitly targets ranges in  $m_X$  and  $m_Y$  where both, the  $Y(bb)$  and  $H(bb)$  decays can be reconstructed with AK8 jets, as described in Section 2.2.

The trigger selection proceeds through a logical OR of a mixture of trigger paths requiring the presence of high- $p_T$  AK8 jets, large values of  $H_T$ , or combinations of those. In addition, b tagging requirements and a requirement on the mass of the two leading jets, in cases where more than one AK8 jet is present in an event, are imposed. This setup aims at a trigger efficiency close to 100% for the offline selected events. Residual corrections to the trigger efficiency have been derived from CRs. These corrections usually range below 5%.

In the offline selection, the events are required to contain at least two AK8 jets with  $p_T > 350$  GeV and  $|\eta| < 2.4$  for the data taken in 2016 and  $p_T > 400$  GeV and  $|\eta| < 2.5$  for data taken in 2017–2018. The dominant backgrounds for this analysis arise from  $t\bar{t}$  production in

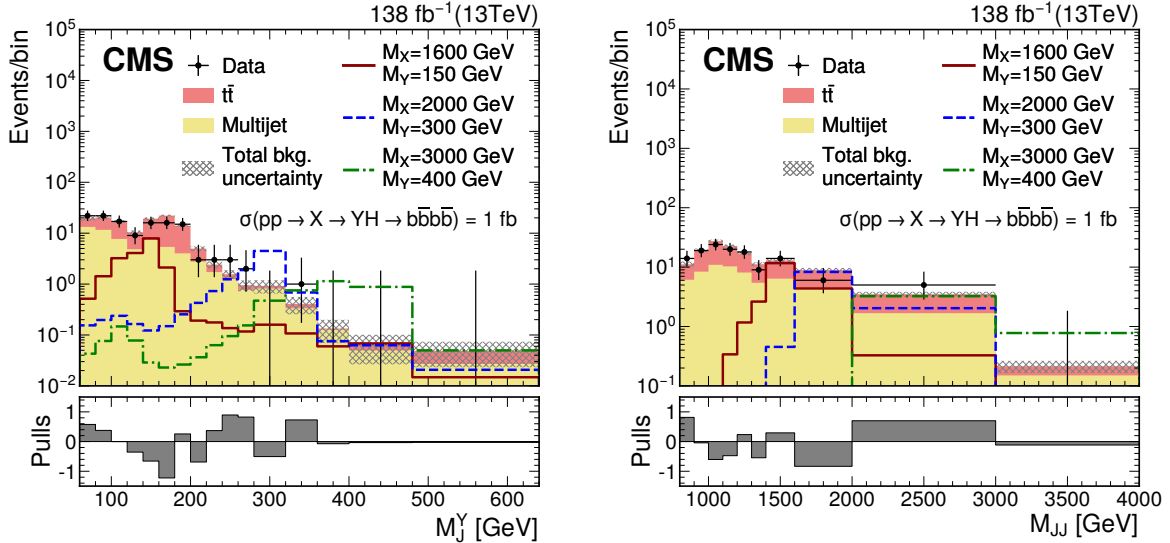


Figure 23: Search for  $X \rightarrow Y(bb)H(bb)$ : Distributions of the (left) soft-drop mass of the boosted  $Y$  candidate, labeled  $M_J^Y$ , and (right) the dijet mass of the  $Y$  and  $H$  candidates,  $M_{JJ}$ , in the high-purity SR of the  $Y(bb)H(bb)$  analysis with two merged  $bb$  jets [117]. The distributions as expected for signals with three different values of  $m_X$  and  $m_Y$  (labeled  $M^X$  and  $M^Y$ ) are also shown. In the lower panels the statistical pull in each bin is displayed. Figure from Ref. [117].

the all-hadronic decay of the intermediate  $W$  bosons and QCD multijet production. To further suppress the latter an additional pairwise requirement of  $|\Delta\eta| < 1.3$  for the selected AK8 jets is imposed. Eventually the two leading jets in  $p_T$  are identified as the  $H$  and  $Y$  candidates, where requirements of  $110 < m_{SD} < 140$  GeV for the  $H$  candidate and  $m_{SD} > 60$  GeV for the  $Y$  candidate are imposed. When both AK8 jets satisfy the first mass requirement, the  $Y$  jet is chosen at random. The  $H$  and  $Y$  candidates are then passed to the PARTICLENET algorithm [142] to discriminate the decays of a boosted resonance,  $H(bb)$  or  $Y(bb)$ , from light-flavor quark or gluon jets.

Based on the output of the PARTICLENET algorithm for each of the AK8 jets, a loose and a tight SR, with varying expected signal purity, are defined. In addition, corresponding sideband regions for the estimation of the background from QCD multijet production and a series of regions to validate this background estimate are constructed. The background from  $t\bar{t}$  production is estimated from simulation and monitored in a dedicated CR in data, obtained from a selection of either an isolated electron or muon with  $p_T > 40$  GeV and  $|\eta| < 2.4$ , and an AK4 jet tagged as a  $b$  jet with the DEEPJET algorithm, with a distance of  $\Delta R < 1.5$  from the selected lepton. For this purpose, a working point of the DEEPJET algorithm with an efficiency of 90% with a misidentification rate of  $\approx 10\%$  has been chosen. In addition, requirements of  $p_T^{\text{miss}} > 60$  GeV and  $H_T > 500$  GeV are imposed. The lepton,  $p_T^{\text{miss}}$ , and the  $b$ -tagged jet provide the signature of a leptonically decaying  $t$  quark. A hadronically decaying  $t$  quark candidate is reconstructed from an AK8 jet fulfilling the same kinematic requirement as in the SR and  $m_{SD} > 60$  GeV. In addition the selected AK8 jet must have a distance of  $\Delta R > 2$  from the selected lepton. This selection reaches a purity in  $t\bar{t}$  events of greater than 90%. The signal is obtained from a fit of the signal and background models to the observed 2D distribution in the  $(m_J^Y, m_{JJ})$  plane, where  $m_J^Y$  is the soft-drop mass of the  $Y$  boson candidate, and  $m_{JJ}$  is the invariant mass of the  $H$  and  $Y$  boson candidates. The loose and tight SRs are fit jointly with the corresponding CRs that

constrain the QCD multijet and  $t\bar{t}$  backgrounds. Distributions in  $m_J^Y$  and  $m_{JJ}$  in the high-purity signal region are shown in Fig. 23.

## 2.6 Statistical combination

A combined likelihood analysis, based on all search results presented in this report, is performed for the HH and YH decay channels, whose results will be presented in Section 3. For this analysis, those systematic variations that should act in the same way for each individual search in consideration, are treated as correlated. A typical example of that kind is the uncertainty in the integrated luminosities of the used data sets. According to the values of  $m_X$  and  $m_Y$ , different channels may contribute at different levels of relative sensitivity. This is because of differences in the selection efficiency, the acceptance of the CMS detector, the trigger efficiency and the branching fractions. Therefore a combination might be either dominated by one channel or benefit from the joint effect of many channels with similar sensitivity depending on the phase-space region.

For the  $X \rightarrow HH$  decay, the combination is performed separately for the spin-0 and spin-2 hypotheses on the X boson. For the  $X \rightarrow YH$  case, spin-0 is assumed for both the X and Y bosons. For all measurements described in the following, the H boson mass is fixed to  $m_H = 125$  GeV. The branching fractions of the H boson are assumed to equal the SM prediction for an H boson with  $m_H = 125$  GeV. In case of the  $Y(bb)H(\tau\tau)$  analysis (Section 2.5.1), for which no limits at  $m_Y = 125$  GeV are available, we use  $m_Y = 130$  GeV instead to estimate the result for the HH case. This is justified by the limited mass resolution. We make this particular choice because a comparison of the limits with  $m_Y = 120$  GeV and  $m_Y = 130$  GeV shows that the latter choice yields more conservative limits.

For the combination, the same measurement is performed in all individual channels with their specific final states. The combination is achieved by translating the measured upper limits on the product of cross section and branching fraction into a limit on the HH production cross section by correcting for the branching fraction of the particular H boson decays. Theoretical uncertainties in the branching fractions and in the HH cross sections are taken into account [35]. For the YH combination, only final states with  $Y \rightarrow bb$  are considered. Therefore, in order to stay as model-independent as possible, a correction is only done for the branching fraction of the H boson.

The used grids in points of  $m_X$  and  $(m_X, m_Y)$  can differ across the various analyses. In general, the combination is performed only for the points common to all analyses considered in the combination.

As theoretical systematic uncertainties, we consider normalization uncertainties related to PDF, QCD scale, and  $\alpha_S$  in the total cross section for the main backgrounds and for the single H production process, which follows the recommendations by the LHC cross section working group [35]. These uncertainties are considered to be uncorrelated across processes, and fully correlated across channels that share the same process.

## 3 Upper limits on the cross sections

We now turn to the results of the searches for heavy resonances X decaying into VH, HH, and YH channels. Each search features at least one instance of the H boson at a mass of 125 GeV originating from the decay of a heavy resonance X. The analyses are performed in a variety of final states with complementary sensitivity in the masses  $m_X$  and  $m_Y$ .

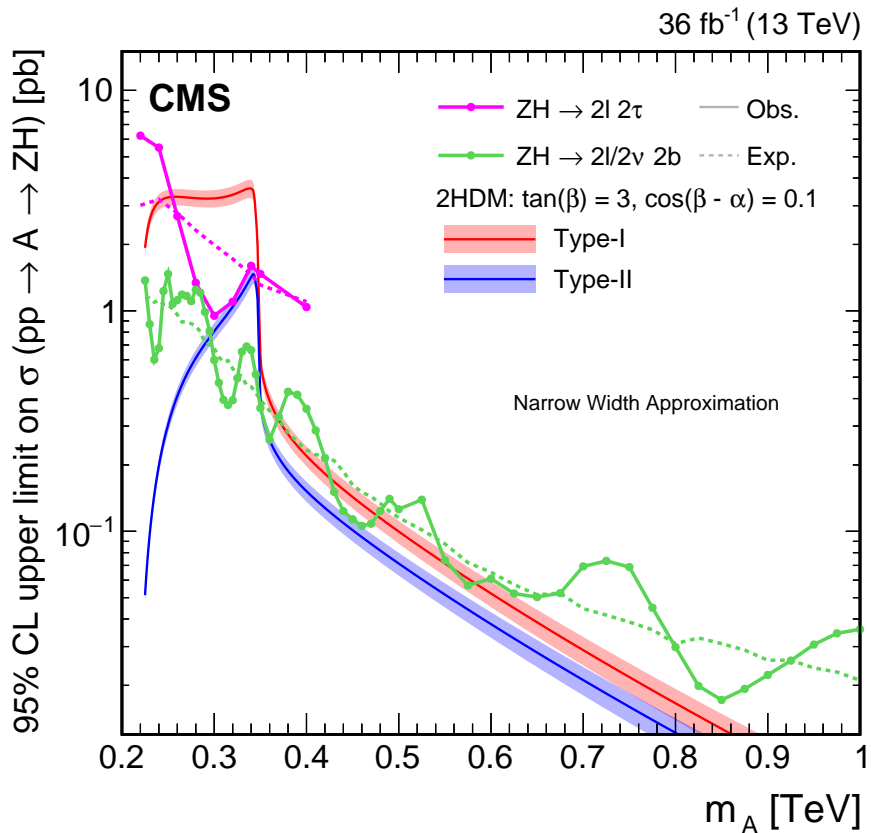


Figure 24: Search for  $X \rightarrow ZH$ : Observed and expected 95% CL upper limits on the product of the cross section  $\sigma$  for the production of an  $A$  boson, via gluon-gluon fusion and the branching fraction  $\mathcal{B}$  for the  $A \rightarrow ZH$  decay. The limits are given in pb as functions of  $m_A$ . The markers connected with solid lines (dashed lines) indicate the observed (expected) limits. The green (magenta) lines refer to the  $Z(\ell\ell + \nu\nu)H(bb)$  [108] ( $Z(\ell\ell)H(\tau\tau)$  [107]) analysis. The red and blue solid lines indicate the product  $\sigma\mathcal{B}$  as expected by the 2HDM Type I and Type II models, respectively, for the parameters  $\tan\beta = 3$  and  $\cos(\beta - \alpha) = 0.1$ . The shaded areas associated with these predictions indicate the corresponding model uncertainties. The results and model predictions have been adapted from Refs. [107, 108].

The observed data for all searches are found to be in agreement with the SM expectations in the corresponding SRs. We set upper limits on the product of the production cross section of the resonance and the branching fraction,  $\sigma\mathcal{B}$ . The upper limits are set at 95% CL, using the  $CL_s$  criterion [165–167]. Statistical combinations of the different HH and YH analyses are performed as described in Section 2.6 to extract the maximum information from the data.

### 3.1 The $X \rightarrow VH$ decays

Five searches for VH resonances are presented in Section 2.3. These target final states with 0, 1, and 2 leptons, originating from the decay of the vector boson (W or Z) produced together with the H boson. The H boson is assumed to either decay to bb or  $\tau_h\tau_h$ . The results are shown as upper limits on  $\sigma\mathcal{B}$  as functions of the resonance mass X. This can either be a scalar particle, which can occur, e.g., in 2HDM models, or models with vector resonances, such as W' and Z', as predicted in the HVT models.

Figure 24 shows the upper limits on  $\sigma(pp \rightarrow A)\mathcal{B}(A \rightarrow ZH)$  as functions of the mass of the CP-odd Higgs boson A, using H decays to bb [108] and  $\tau\tau$  [107], obtained with the data set

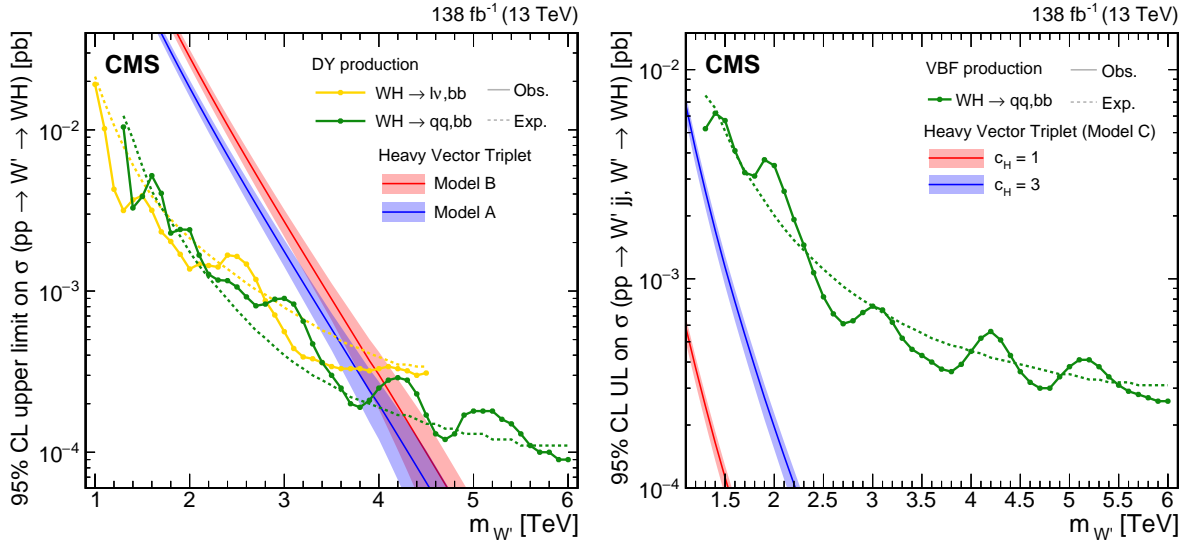


Figure 25: Search for  $X \rightarrow WH$ : Observed and expected 95% CL upper limits on the product of the cross section  $\sigma$  for the production of a  $W'$  spin-1 resonance, via (left) DY production or (right) vector boson fusion and the branching fraction  $\mathcal{B}$  for the  $W' \rightarrow WH$  decay. The solid lines represent the observed and the dotted lines the expected limits. The theory predictions from the heavy vector triplet models A, B, and C are also shown.

recorded in 2016. This plot also shows the expected cross sections for  $A$  bosons in two typical 2HDM scenarios. These feature a drop beyond the  $t\bar{t}$  threshold because of the  $A \rightarrow t\bar{t}$  channel opening up.

Figures 25 and 26 show the upper limits on  $\sigma\mathcal{B}$  for spin-1  $W'$  and  $Z'$  resonances, as a function of the masses  $m_{W'}$  and  $m_{Z'}$ , respectively. The limits are derived for DY (left) and VBF (right) production separately. The exclusion limits reach values of  $\sigma\mathcal{B}$  below 0.1 and 0.3 fb for the DY and VBF topologies, respectively. In DY production the results from searches with leptons in the final state yield a stronger exclusion for  $m_{W'}$  masses below 1.7 TeV and  $m_{Z'}$  below 3.2 TeV. For higher masses, the fully hadronic final state shows higher sensitivity. The interpretations of these upper limits on  $\sigma\mathcal{B}$  in HVT models will be discussed in detail in Section 4.3.

### 3.2 The $X \rightarrow HH$ decays

The six searches for  $X \rightarrow HH$  discussed in Section 2.4 target a variety of final states with b jets, photons, light leptons, and  $\tau_h$  leptons. The searches study spin-0 and spin-2 resonances in the mass range 0.28–4.5 TeV. We denote the spin-0 resonance as  $X$  since interpretations in warped extra dimension and extended Higgs sector models are both possible. We denote the spin-2 resonance as  $G$  having a graviton in mind.

Figure 27 shows the upper limits on  $\sigma\mathcal{B}$  as functions of the resonance mass for both spin hypotheses. The exclusion in terms of  $\sigma\mathcal{B}$  ranges down to 0.2 fb for both spin scenarios probed. The best sensitivity at low masses is obtained by the diphoton search, while at high masses the two searches with b-tagged merged jets show the best sensitivity. The results of the statistical combination as described in Section 2.6 are shown as red lines. These combined results are presented again separately in Fig. 28 along with the  $\pm 1$  and  $\pm 2$  s.d. intervals on the expected limits. No deviation larger than 2 s.d. from the expected limits is observed. Large improvements in sensitivity relative to the best individual channel are achieved in the range of  $m_X \sim 0.5$ –1 TeV, where many channels contribute with about the same weight to the com-

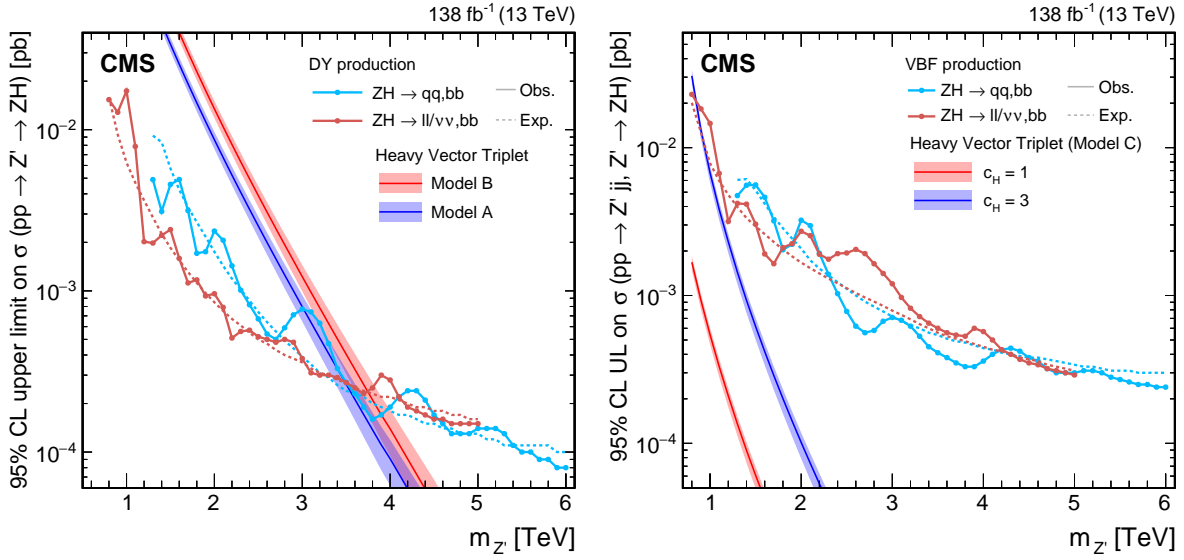


Figure 26: Search for  $X \rightarrow ZH$ : Observed and expected 95% CL upper limits on the product of the cross section  $\sigma$  for the production of a  $Z'$  spin-1 resonance, via (left) DY production or (right) vector boson fusion and the branching fraction  $\mathcal{B}$  for the  $Z' \rightarrow ZH$  decay. The solid lines represent the observed and the dotted lines the expected limits. The theory predictions from the heavy vector triplet models A, B and C are also shown.

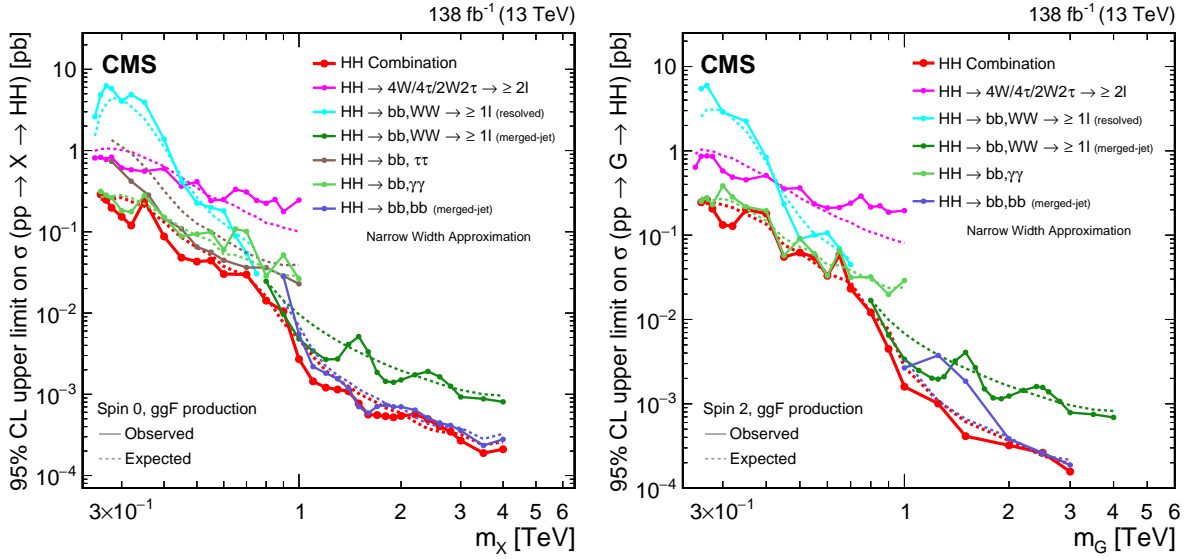


Figure 27: Search for  $X \rightarrow HH/G \rightarrow HH$ : Observed and expected 95% CL upper limits on the product of the cross section  $\sigma$  for the production of a (left) spin-0 resonance  $X$  and (right) a spin-2 resonance  $G$ , via gluon-gluon fusion and the branching fraction  $\mathcal{B}$  for the corresponding  $HH$  decay. The results of the individual analyses presented in this report and the result of their combined likelihood analysis are shown. The observed limits are indicated by markers connected with solid lines and the expected limits by dashed lines.

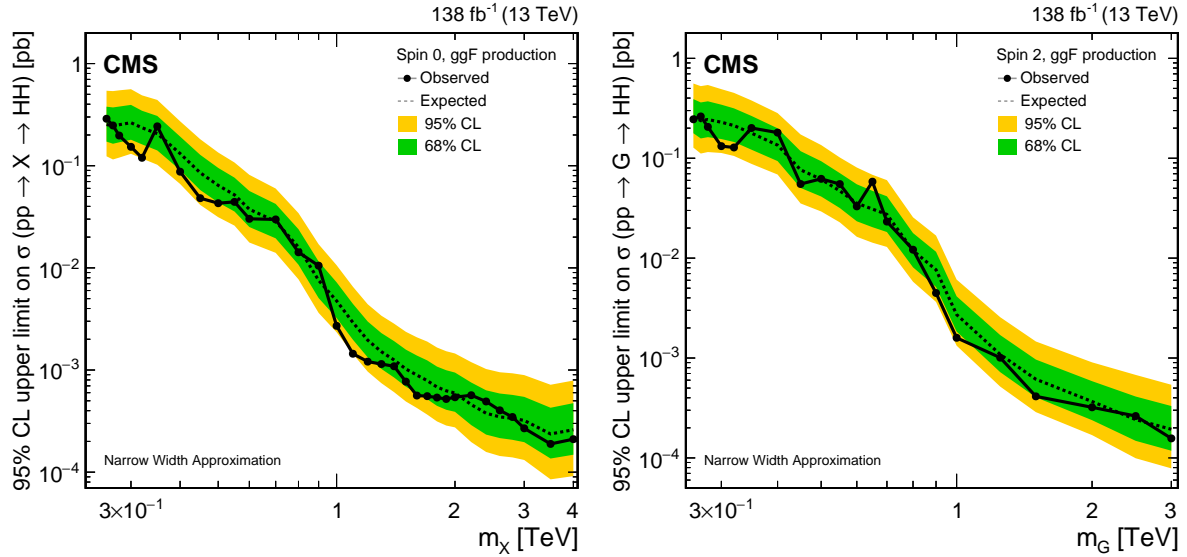


Figure 28: Search for  $X \rightarrow HH/G \rightarrow HH$ : Observed and expected 95% CL upper limits on the product of the cross section  $\sigma$  for the production of a (left) spin-0 resonance  $X$  and (right) a spin-2 resonance  $G$ , via gluon-gluon fusion, and the branching fraction  $\mathcal{B}$  for the corresponding  $HH$  decay, as obtained from the combined likelihood analysis of all contributing individual analyses presented in this report and shown in Fig. 27. In addition to the limit from the combined likelihood analysis the 68 and 95% central intervals for the expected upper limits in the absence of a signal are shown as coloured bands.

bination. Below masses of 0.32 TeV and above 0.8 TeV, this combination gives the strongest observed limits to date on resonant  $HH$  production. A recent combination of  $HH$  searches performed by the ATLAS Collaboration can be found in Ref. [168].

### 3.3 The $X \rightarrow YH$ decays

Three searches target the  $X \rightarrow YH$  decay. Two are dedicated to lower masses with the  $H$  boson decaying to  $\gamma\gamma$  or  $\tau\tau$  with two b-tagged AK4 jets for the reconstruction of the  $Y$  boson (as discussed in Section 2.5). The search in the fully hadronic final state with two double-b-tagged AK8 jets targets the high-mass regime. As the  $Y$  boson always decays to  $bb$  in all cases considered, this allows for a direct comparison of the results from these three searches, without the assumption of a specific model. Furthermore, this makes a model-independent combination possible, where only the branching fractions of the  $H$  boson need to be taken into account.

Figures 29 and 30 show the upper limits on  $\sigma\mathcal{B}$  as functions of the  $m_Y$  for  $m_X \leq 1$  TeV and for  $m_X \geq 1.2$  TeV, respectively. The results have been achieved by adjusting each channel to the corresponding SM branching fraction of the  $H$  boson decay under consideration. No correction has been made for the unknown branching fraction of  $Y \rightarrow bb$ , which is the same in all searches.

At low  $m_X$ , the  $Y(bb)H(\tau\tau)$  and  $Y(bb)H(\gamma\gamma)$  analyses provide the best sensitivity. For  $m_X = 1$  TeV and higher, the  $Y(bb)H(bb)$  in the merged jet topology dominates for small and medium values of  $m_Y$ . At the largest values of  $m_Y$ , however, approaching the kinematic limit, the sensitivity of the  $Y(bb)H(bb)$  analysis is reduced because the Lorentz boost of the  $Y$  boson rest frame is too small for the fragmentation products of the two b quarks to merge into a single jet.

The four analyses are statistically combined as described in Section 2.6, and the resulting ex-

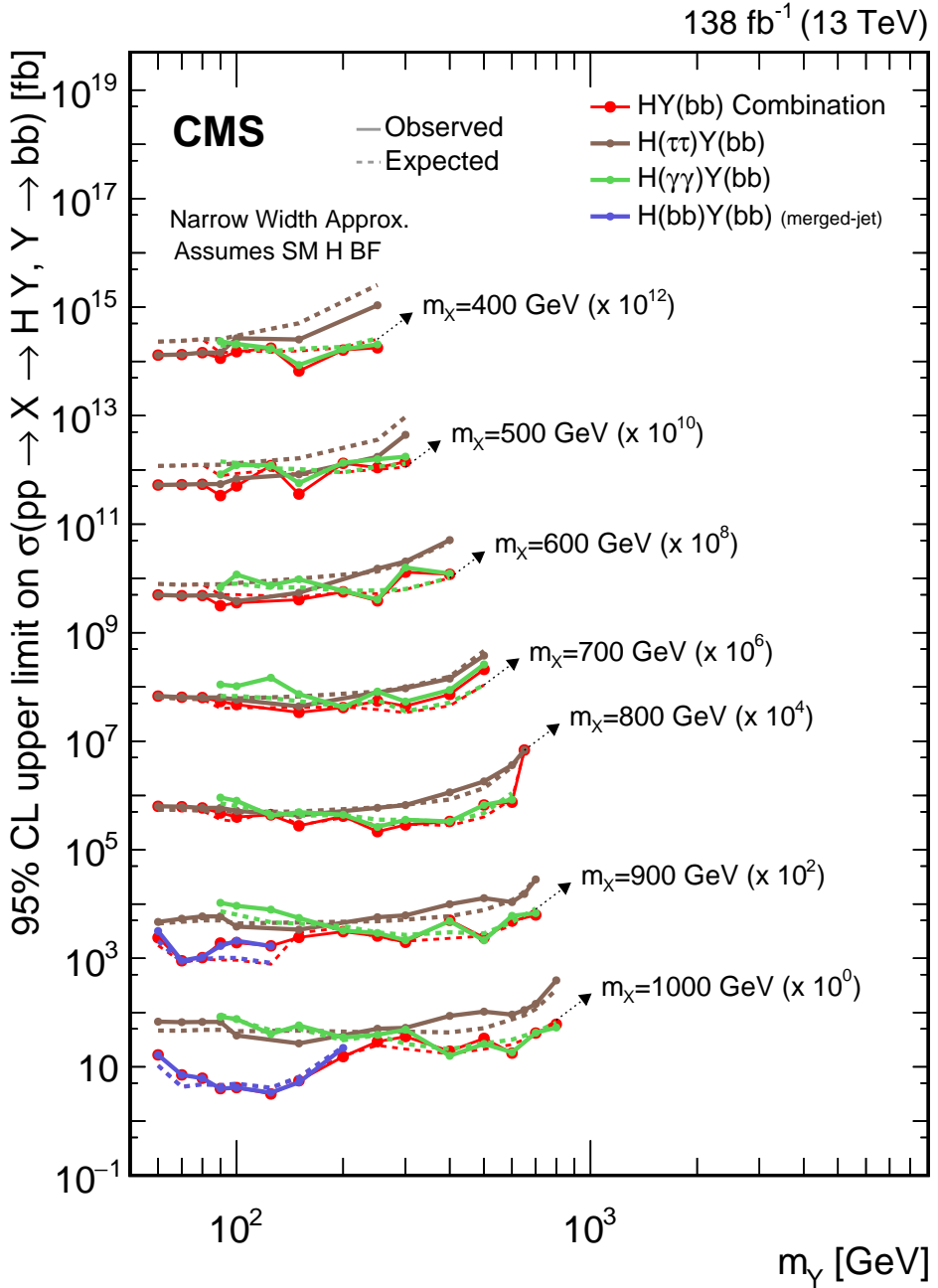


Figure 29: Search for  $X \rightarrow YH$ : Observed and expected upper limits, at 95% CL, on the product of the cross section  $\sigma$  for the production of a resonance  $X$  via gluon-gluon fusion and the branching fraction  $\mathcal{B}$  for the  $X \rightarrow Y(bb)H$  decay. For the branching fractions of the  $H \rightarrow \tau\tau$ ,  $H \rightarrow \gamma\gamma$  and  $H \rightarrow bb$  decays, the SM values are assumed. The results derived from the individual analyses presented in this report and the result of their combined likelihood analysis are shown as functions of  $m_Y$  and  $m_X$  for  $m_X \leq 1 \text{ TeV}$ . Observed limits are indicated by markers connected with solid lines, expected limits by dashed lines. For presentation purposes, the limits have been scaled in successive steps by two orders of magnitude, each. For each set of graphs, a black arrow points to the  $m_X$  related legend.

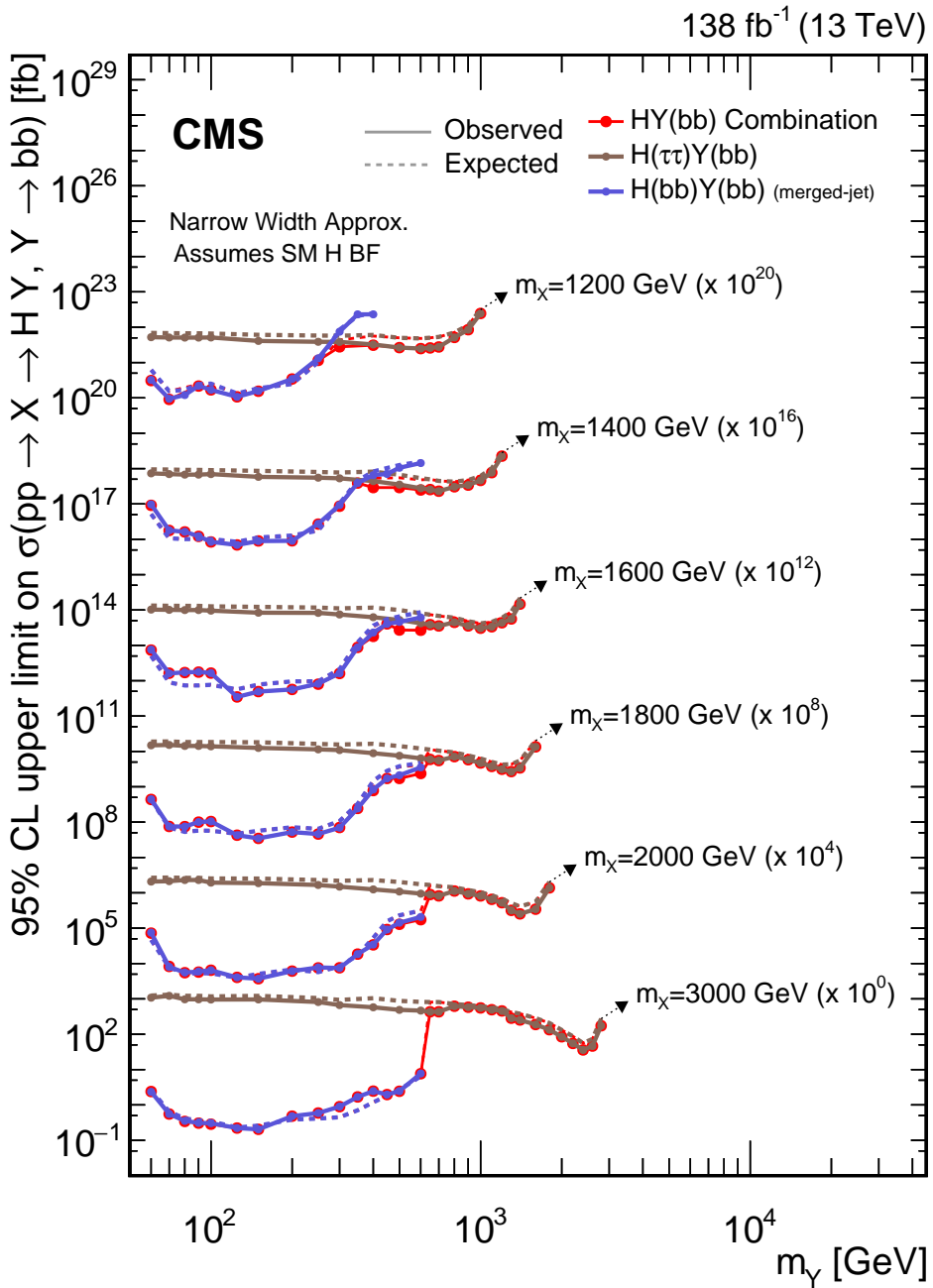


Figure 30: Search for  $X \rightarrow YH$ : Observed and expected upper limits, at 95% CL, on the product of the cross section  $\sigma$  for the production of a resonance  $X$  via gluon-gluon fusion and the branching fraction  $\mathcal{B}$  for the  $X \rightarrow Y(bb)H$  decay. For the branching fractions of the  $H \rightarrow \tau\tau$  and  $H \rightarrow bb$  decays, the SM values are assumed. The results derived from the individual analyses presented in this report and the result of their combined likelihood analysis are shown as functions of  $m_Y$  and  $m_X$  for  $m_X \geq 1.2 \text{ TeV}$ . Observed limits are indicated by markers connected with solid lines, expected limits by dashed lines. For presentation purposes, the limits have been scaled in successive steps by four orders of magnitude, each. For each set of graphs, a black arrow points to the  $m_X$  related legend.

pected and observed limits are shown in Figs. 29 and 30. Covering the full mass grid, however, is beyond the scope of this review paper. This combination is shown as an example for the given mass points, and a separate publication in the near future will include a full combination featuring a larger set of decay modes. The typical exclusion upper limits on  $\sigma\mathcal{B}$  are about 50, 5, and 0.3 fb for  $m_X = 0.5, 1$ , and  $3 \text{ TeV}$ , respectively. No excess larger than two s.d. above the expected limit is observed at any of these mass points. A two-dimensional representation of the experimental limits in the  $(m_X, m_Y)$  parameter space is shown as part of the interpretation in Section 4.1.3.

## 4 Model-specific interpretation

We interpret the results of the individual searches and their combinations in specific models. The interpretations highlight the coverage of the analyses in the corresponding parameter space and show which regions are excluded by the current data. The first three subsections address how the measurements can constrain the parameter space of models with an extended Higgs sector, warped extra dimensions, and in a HVT framework. Section 4.4 is dedicated to studies going beyond the narrow-width approximation (NWA), where we investigate the effects of non-negligible resonance widths and interference.

### 4.1 Extended Higgs sector models

#### 4.1.1 The MSSM

The decays  $X \rightarrow HH$  and  $A \rightarrow ZH$  can have sizable branching fractions in models with two complex Higgs doublets. However, as discussed previously, the branching fractions get suppressed when approaching the alignment limit, where the H boson becomes SM-like. Searches for  $HH$  and  $ZH$  can nonetheless set important constraints in these models, in particular at low to intermediate values of  $\tan\beta$ , and for masses below or near the  $t\bar{t}$  threshold,  $m_{X/A} \lesssim 350 \text{ GeV}$ .

Figure 31 shows exclusion regions in the  $(m_A, \tan\beta)$  plane of the hMSSM [57–59, 62]. For this and the following model interpretations, the version numbers of the corresponding tools are documented in Ref. [62]. The branching fractions are obtained with HDECAY [171, 172]. The gluon fusion cross section is obtained with SUSHI [173, 174], which includes higher-order QCD corrections [175–181] and EW effects from light quarks [182, 183]. The  $X \rightarrow HH$  searches result in an exclusion for  $\tan\beta \lesssim 6$  for  $m_A$  just above the  $HH$  production threshold of  $250 \text{ GeV}$ , decreasing to  $\tan\beta \lesssim 1$  for  $m_A \approx 600 \text{ GeV}$ . This is complementary to the exclusion regions from searches for fermionic decays, such as  $A \rightarrow \tau\tau$ , which excludes regions of large  $\tan\beta$ . The  $A \rightarrow ZH$  search in the  $H \rightarrow \tau\tau$  channel provides sensitivity for  $220 < m_A < 350 \text{ GeV}$  and excludes regions below  $\tan\beta = 3.6$  for  $m_A \lesssim 330 \text{ GeV}$ . Compared to other direct searches, there is a unique sensitivity of the  $X \rightarrow HH$  searches for  $m_A \gtrsim 450 \text{ GeV}$  and  $\tan\beta < 5$ . At the same time, the constraints derived from the measurements of the H boson couplings are somewhat more stringent, albeit these place only indirect constraints on this model.

The frequently used  $M_h^{125}$  benchmark model is not very suitable for interpretations of results from  $X \rightarrow HH$  searches as these exclude regions at low  $\tan\beta$  where the SM-like scalar has a mass inconsistent with  $125 \text{ GeV}$  and thus with the observed H boson. Instead, we choose to interpret these results in the  $M_{h,\text{EFT}}^{125}$  scenario [60, 62]. Higgs boson masses and mixings are obtained with FEYNHIGGS [15, 184–190]. The branching fraction calculations make use of both FEYNHIGGS, HDECAY, and PROPHECY4F [191, 192]. The cross section for gluon fusion production is obtained from the same tools and predictions as in the hMSSM scenario. The resulting exclusion regions in the  $(m_A, \tan\beta)$  plane are shown in Fig. 32. In this scenario, the

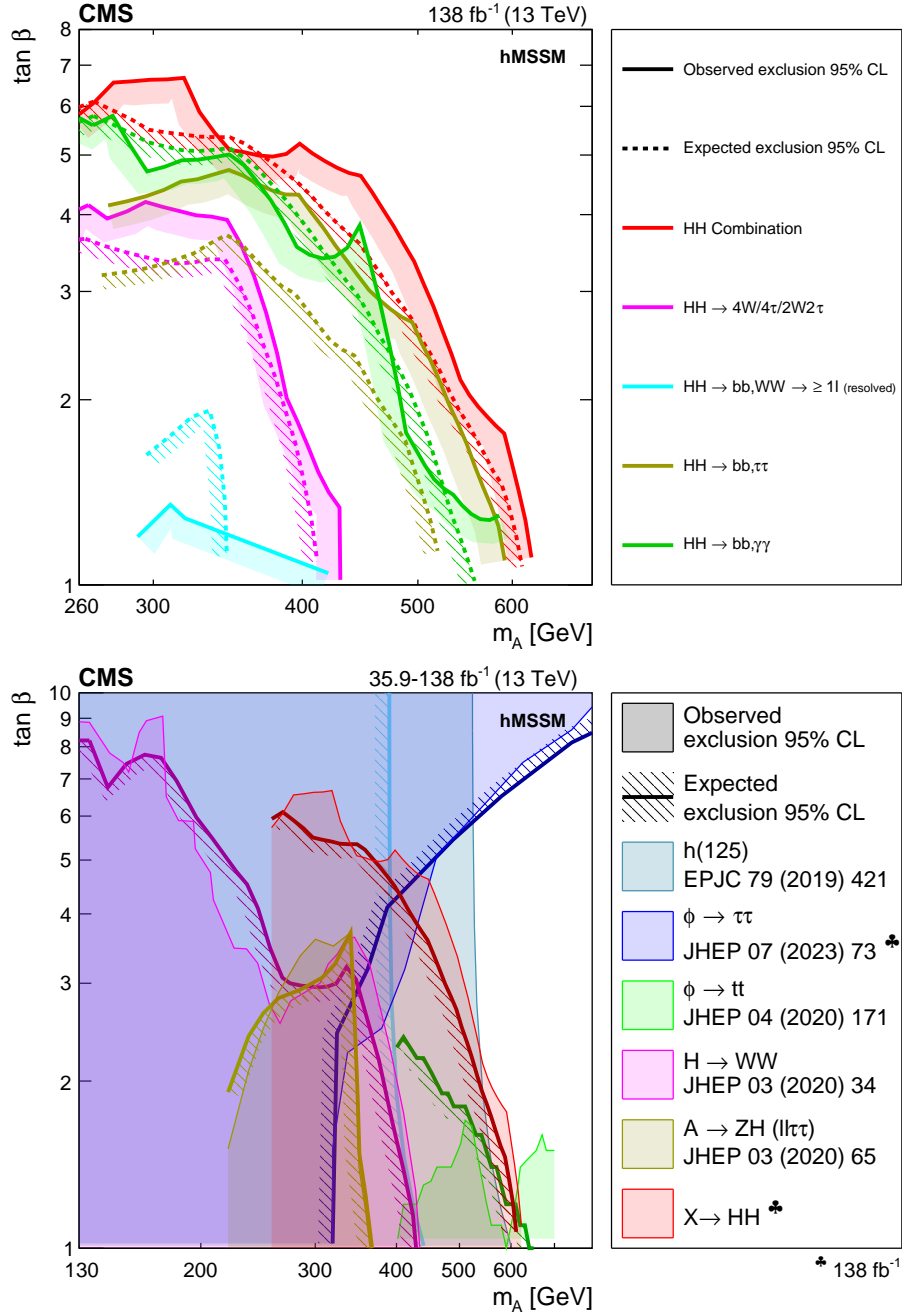


Figure 31: Interpretation of the results from the searches for the  $X \rightarrow HH$  decay, in the hMSSM model. In the upper part of the figure, the observed and expected exclusion contours at 95% CL, in the  $(m_A, \tan \beta)$  plane, from the individual HH analyses presented in this report and their combined likelihood analysis are shown. In the lower part of the figure, a comparison of the region excluded by the combined likelihood analysis shown in the upper part of the figure with selected results from other searches for the production of heavy scalar bosons in the hMSSM, in  $\tau\tau$  [64],  $tt$  [169] and  $WW$  [170] decays is shown. Also shown, are the results from one representative search for  $A \rightarrow ZH$  [107] and indirect constraints obtained from measurements of the coupling strength of the observed H boson [47]. Results not marked by a club symbol are based on an integrated luminosity of  $35.9 \text{ fb}^{-1}$ .

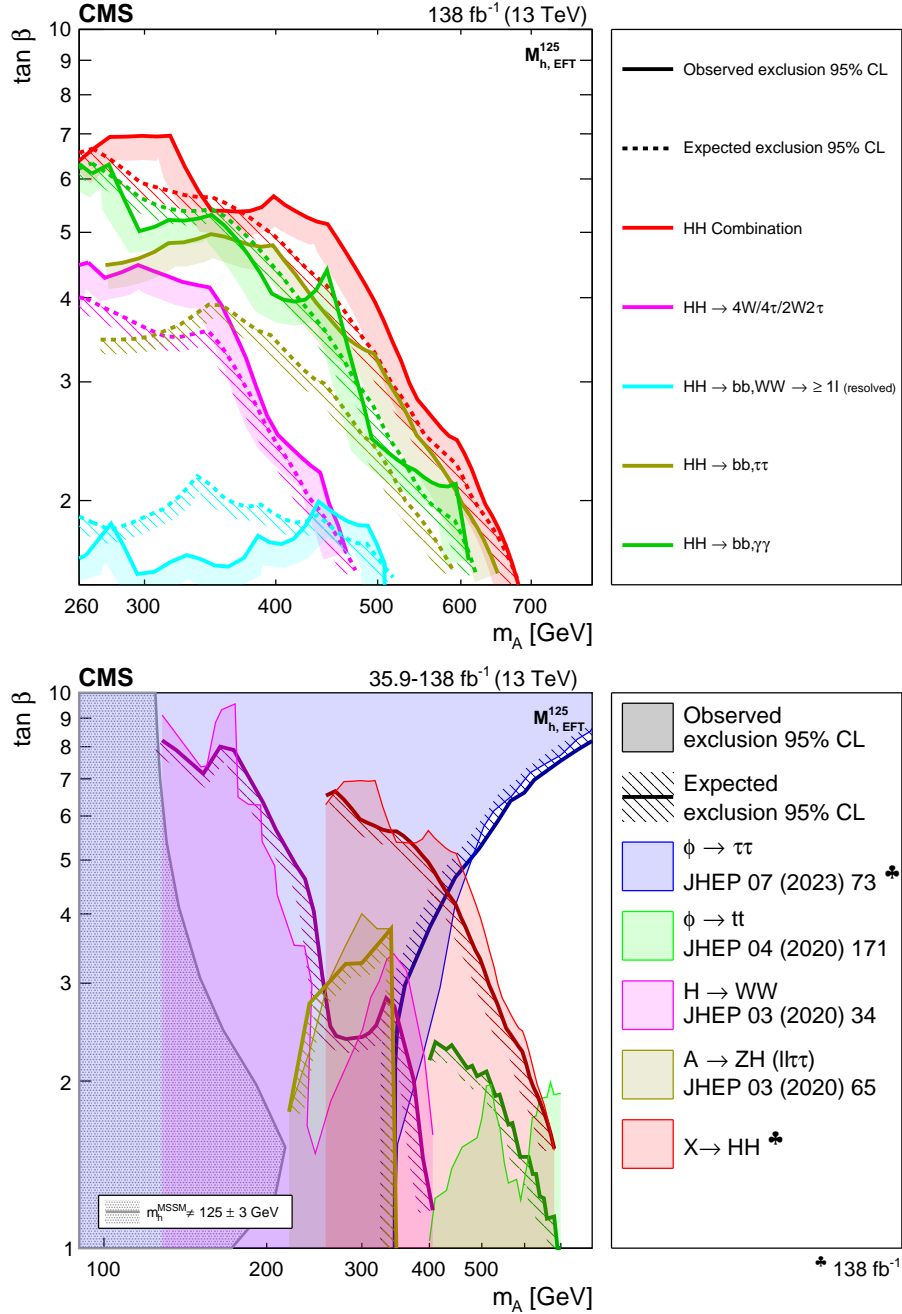


Figure 32: Interpretation of the results from the searches for the  $X \rightarrow HH$  decay, in the  $M_{h,\text{EFT}}^{125}$  benchmark scenario. In the upper part of the figure, the observed and expected exclusion contours at 95% CL are shown, in the  $(m_A, \tan \beta)$  plane from the individual  $HH$  analyses presented in this report and their combined likelihood analysis. In the lower part of the figure, a comparison of the region excluded by the combined likelihood analysis shown in the upper part of the figure with selected results from other searches for the production of heavy scalar bosons in the  $M_{h,\text{EFT}}^{125}$  scenario, in  $\tau\tau$  [64],  $t\bar{t}$  [169] and  $WW$  [170] decays is shown. Also shown, are the results from one representative search for  $A \rightarrow ZH$  [107]. The parameter region in which the mass of the lightest MSSM Higgs boson does not coincide with 125 GeV within a 3 GeV margin is indicated by the dark hatched area. Results not marked by a club symbol are based on an integrated luminosity of  $35.9 \text{ fb}^{-1}$ .

parameter regions excluded by the HH combination are found not to be in conflict with the measured H boson mass. For  $m_A \gtrsim 400$  GeV the results from the combination provide unique exclusions. Otherwise, the overall picture is similar to the hMSSM scenario.

#### 4.1.2 The 2HDM

Exclusion limits in the 2HDM are derived from the results of the search for  $A \rightarrow ZH(bb)$  [108]. The 2HDM cross sections and branching fractions are computed with 2HDMC [55] and SUSHI, respectively. The light H boson mass is set to 125 GeV and  $m_H = m_{H^\pm} = m_A$  is used. The Z boson branching fractions are set to the measured values [45]. Figure 33 shows the constraints in the  $(\tan \beta, \cos(\beta - \alpha))$  plane for  $m_A = 300$  GeV [108]. The search excludes nearly the whole region of low  $\tan \beta$  in all four 2HDM scenarios, except for a narrow region around  $\cos(\beta - \alpha) = 0$  for which the branching fraction goes to zero, another narrow region at negative  $\cos(\beta - \alpha)$  for the Type I and lepton-specific scenarios, and at positive  $\cos(\beta - \alpha)$  for the other two scenarios. At high  $\tan \beta$ , the excluded region widens in the Type II and flipped scenarios, whereas there is no sensitivity in the Type I and lepton-specific scenarios because the production cross section for the A boson becomes too small.

#### 4.1.3 The NMSSM and TRSM models

The searches for  $X \rightarrow YH$  decays are interpreted in the NMSSM and TRSM models. In both models, there are various free parameters besides the masses of the additional X and Y bosons that affect the cross sections and branching fractions. To check whether the searches are sensitive to a point in the  $(m_X, m_Y)$  plane, a parameter scan is performed to determine the maximally allowed cross section, taking all previous constraints on the models into account.

In the NMSSM case, we obtain the maximally allowed cross section values for  $\sigma(X \rightarrow YH \rightarrow bbbb)$  from the scans in Ref. [193], which are based on version 5.6.2 of the program NMSSMTOOLS [193]. These numbers are divided by the corresponding branching fraction  $\mathcal{B}(H \rightarrow bb)$  to obtain an approximation for the maximally allowed values of  $\sigma(X \rightarrow Y(bb)H)$ . Uncertainties arising from the precision of the measured branching fractions of the H boson are neglected.

Figure 34 shows the observed and expected upper limits at 95% CL on  $\sigma\mathcal{B}$  of the combined  $X \rightarrow YH$  searches (upper panel), together with the maximally allowed model values (lower panel). While the experimental limits appear to touch the model predictions in several places, there is not much additional exclusion. This is expected because many relevant measurements, including the CMS searches for  $X \rightarrow Y(bb)H(\tau\tau)$  and  $X \rightarrow Y(bb)H(bb)$  presented in this article, are already accounted for in this version of NMSSMTOOLS, which lowers the maximally allowed NMSSM cross sections correspondingly. Therefore, no new constraints are expected from these channels compared to those in the original publications [116, 117, 160].

Comparisons of the measured limits for  $X \rightarrow Y(bb)H(bb)$  in merged final states with the maximally allowed TRSM values can be found in Ref. [117]. The measurement excludes part of the allowed TRSM parameter space in a wedge-shaped region between  $m_X \approx 1000$ –1300 GeV and around  $m_Y \approx 125$  GeV. An interpretation of the  $X \rightarrow Y(bb)H(\tau\tau)$  measurements within the TRSM benchmark planes can be found in Ref. [194].

#### 4.1.4 The real-singlet extension

The additional scalar boson X predicted in the real-singlet model has the same relative couplings to SM particles as the SM H boson. Most searches for  $X \rightarrow HH$  assume that the width of the X boson is much smaller than the reconstructed mass resolution, such that the NWA holds. We use the real-singlet model for a dedicated study of nonnegligible width and interference

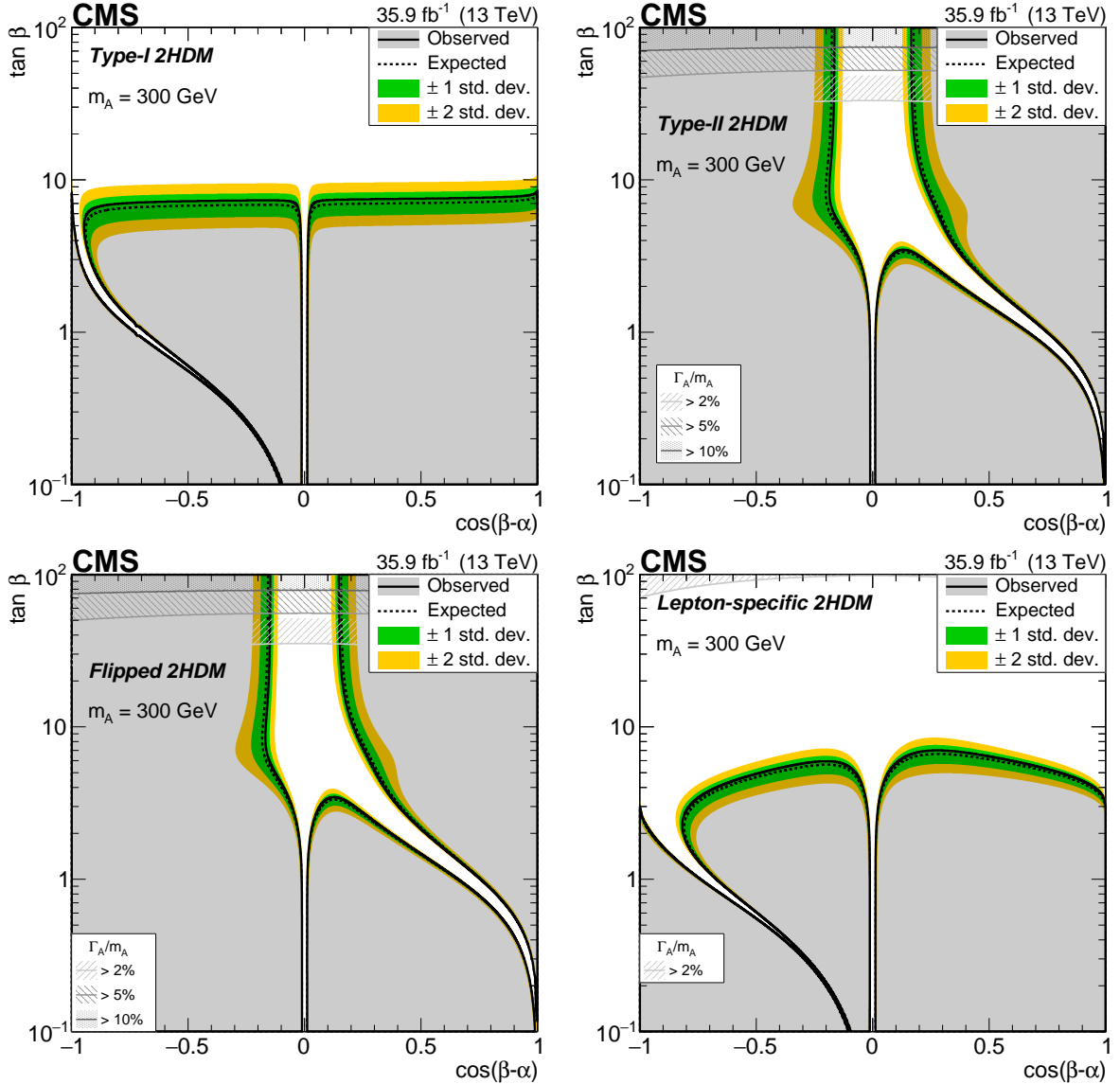


Figure 33: Interpretation of the results of the  $A \rightarrow ZH(bb)$  analysis [108], in the (upper left) Type I, (upper right) Type II, (lower left) flipped, and (lower right) lepton-specific 2HDM models. In each case observed and expected exclusion contours at 95% CL, in the plane defined by  $\cos(\beta - \alpha)$  and  $\tan \beta$ , are shown. The excluded regions are represented by the shaded gray areas. The 68 and 95% central intervals of the expected exclusion contours in the absence of a signal are indicated by the green and yellow bands. Contours are derived from the projection on the corresponding 2HDM parameter space for  $m_A = 300 \text{ GeV}$ . The regions of parameter space where the natural width of the  $A$  boson  $\Gamma_A$  is comparable to or larger than the experimental resolution and thus the narrow-width approximation is not valid are represented by hatched gray areas. Figure from Ref. [108].

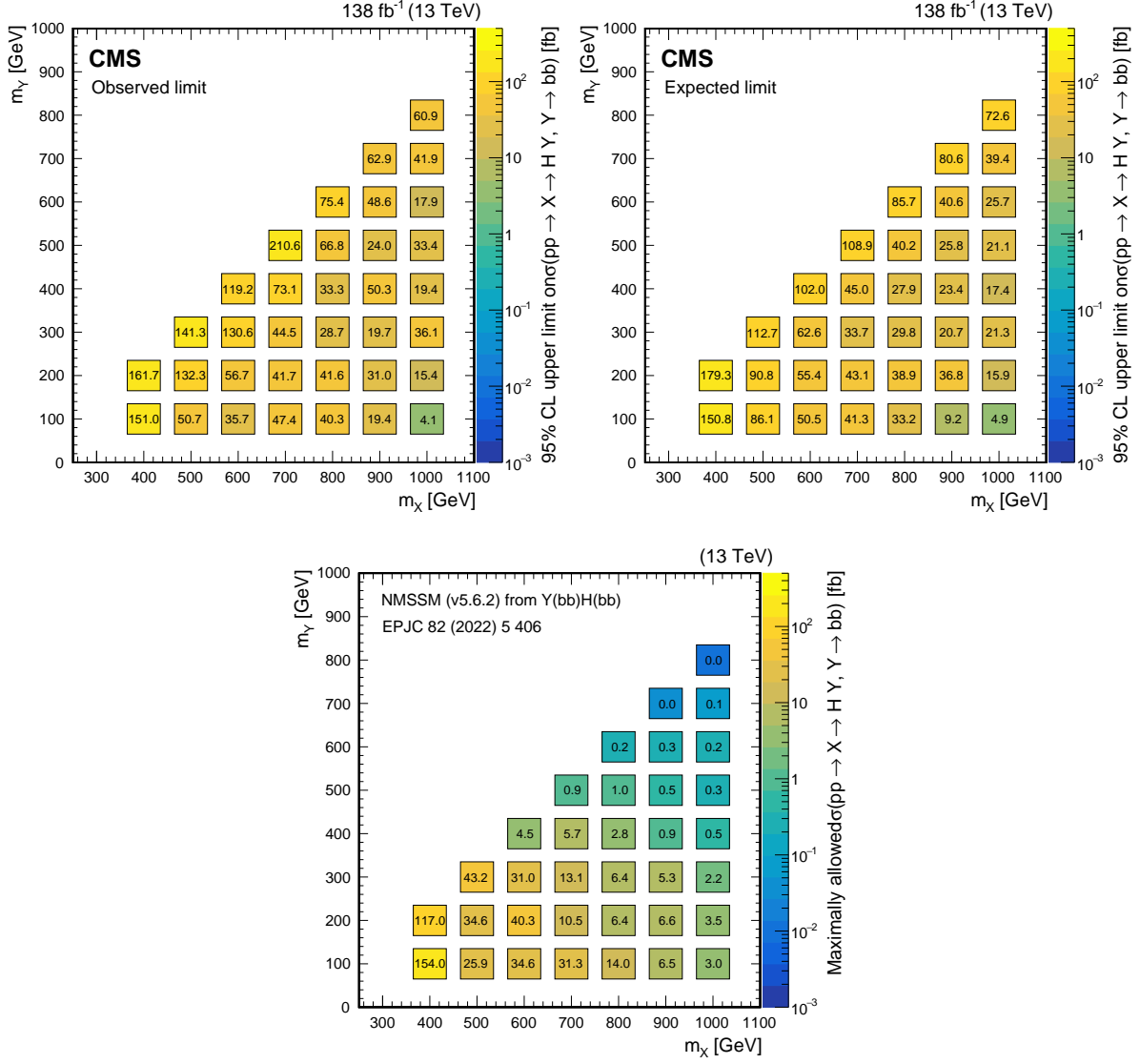


Figure 34: (Upper left) Observed and (upper right) expected upper limits at 95% CL, on the product of the cross section  $\sigma$  for the production of a resonance  $X$  via gluon-gluon fusion and the branching fraction  $\mathcal{B}$  for the  $X \rightarrow Y(bb)H$  decay, as obtained from a combined likelihood analysis of the individual analyses presented in this report and shown in Fig. 29. The results are presented in a plane defined by  $m_X$  and  $m_Y$ . The limits have been evaluated in discrete steps corresponding to the centers of the boxes. The numbers in the boxes are given in  $\text{fb}$ . The corresponding maximally allowed values of  $\sigma\mathcal{B}$  in the NMSSM are also shown for comparison (lower plot), as adapted from Ref. [193].

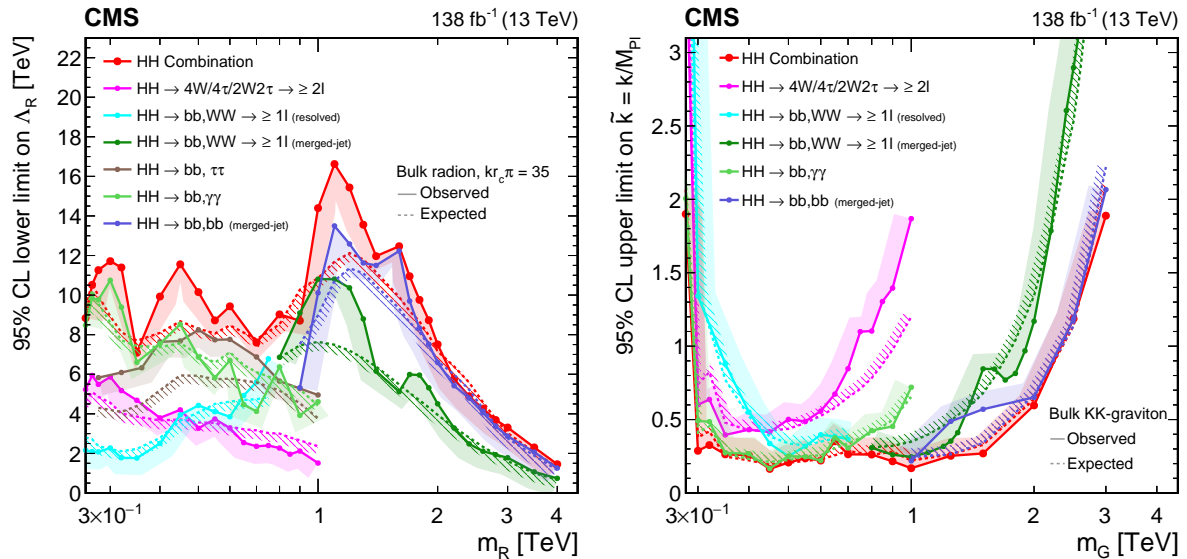


Figure 35: Observed and expected limits, at 95% CL, on the parameters of models with warped extra dimensions, as obtained from the  $X \rightarrow HH$  analyses presented in this report and their combined likelihood analysis. Shown are lower limits (left) on the bulk radion ultraviolet cutoff parameter  $\Lambda_R$ , as a function of the radion mass  $m_R$ , and upper limits (right) on the parameter  $\tilde{k}$  of the spin-2 bulk graviton  $G$ , as a function of  $m_G$ . Excluded areas are indicated by the direction of the hatching along the exclusion contours.

effects and present the results in Section 4.4. The corresponding model interpretations for the  $X \rightarrow HH$  combination in the real-singlet model are presented there.

## 4.2 Warped extra dimensions

The measured upper limits on resonant  $HH$  production can also be interpreted in the context of WED models (as discussed in Section 1.2.2). Figure 35 (left) shows the lower limit on the bulk radion ultraviolet cutoff parameter  $\Lambda_R$  as a function of the radion mass  $m_R$  for all presented  $HH$  analyses and their combination. The individual analyses with the best sensitivity are from the searches of  $X \rightarrow H(bb)H(\gamma\gamma)$  for  $m_X \lesssim 1$  TeV, and  $X \rightarrow H(bb)H(bb)$  for  $m_X \gtrsim 1$  TeV. In the regions  $0.5 \lesssim m_X \lesssim 1$  TeV and  $1 \lesssim m_X \lesssim 1.5$  TeV, the  $X \rightarrow H(bb)H(\tau\tau)$  and  $X \rightarrow H(bb)H(WW)$  analyses contribute significantly to the combination. In the mass region below 1 TeV, the expected lower limit from the combination ranges from 8 to 10 TeV, with observed limits reaching up to 12 TeV. The strongest exclusion limits of about 12 TeV expected and 16 TeV observed are reached near  $m_R = 1.2$  TeV. The combination improves the sensitivity over the full mass range probed. Figure 35 (right) shows the corresponding upper limits of the parameter  $\tilde{k}$  of the spin-2 bulk graviton  $G$ . The combination excludes values of  $\tilde{k}$  larger than about 0.3 at 95% CL for the large mass range  $0.3 < m_G < 1.5$  TeV.

We compare the limits obtained from the  $HH$  combination with limits from searches for  $X \rightarrow ZZ$  [195–197] and  $X \rightarrow WW$  [109, 111, 170] in Fig. 36. The  $HH$  combination is found to be very competitive, and it places stronger constraints on the WED models in some mass regions. For radions, shown on the left, the  $HH$  combination shows about the same sensitivity as the  $Z(\ell\ell)Z(qq/vv/\ell\ell)$  final state [195] for  $m_R \lesssim 1$  TeV. The  $HH$  combination has the best sensitivity in the region  $1 < m_R < 2$  TeV, and for higher masses it has a comparable sensitivity as searches in final states from hadronic and semileptonic  $WW$  decays [109, 111]. For gravitons, the  $HH$  combination places the best upper limits on  $\tilde{k}$  for  $250 < m_G < 450$  GeV and  $700 < m_G < 2000$  GeV.

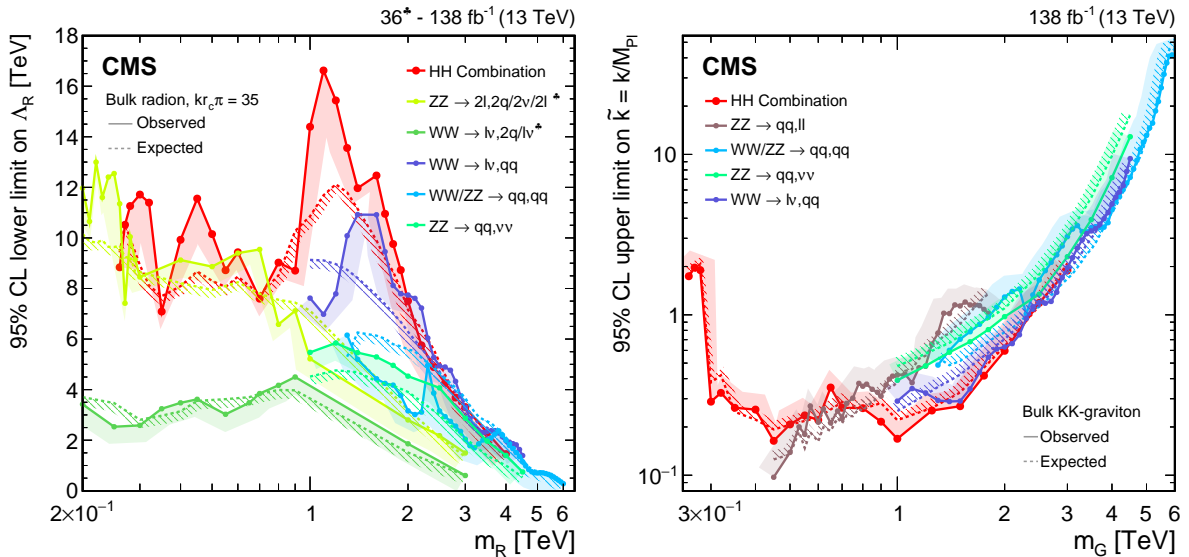


Figure 36: Observed and expected limits, at 95% CL, on the parameters of models with warped extra dimensions, as obtained from the combined likelihood analysis of the individual  $X \rightarrow HH$  analyses presented in this report and shown in Fig. 35. The exclusion contours obtained from the combined likelihood analysis are compared to similar exclusions obtained from individual searches in the decays  $Z(\ell\ell)Z(qq/vv/\ell\ell)$  [195],  $W(\ell\nu)W(\ell\nu/qq)$  [170],  $W(\ell\nu)W(qq)$  [109],  $V(qq)V(qq)$  [111], and  $Z(vv)Z(qq)$  [196], in case of the radion interpretation, and from individual searches in the decays  $Z(qq)Z(\ell\ell)$  [197],  $V(qq)V(qq)$  [111],  $Z(vv)Z(qq)$  [196], and  $W(\ell\nu)W(qq)$  [109], in the case of the graviton interpretation. Excluded areas are indicated by the direction of the hatching along the exclusion contours.

### 4.3 Heavy vector triplet models

The three searches for  $X \rightarrow VH$  introduced in Section 2.3 probe for a new vector boson  $V'$  (either  $W'$  or  $Z'$ ) in final states with 0, 1, and 2 leptons. The resulting upper limits on  $\sigma\mathcal{B}$  presented in Section 3.1 are now interpreted in the HVT model. The theoretical cross sections are calculated at NLO in QCD with the models detailed in Ref. [28, 30]. The theory predictions with the corresponding  $\mathcal{B}(W' \rightarrow WH)$  and  $\mathcal{B}(Z' \rightarrow ZH)$  in the models A, B, and C, where couplings of  $V'$  to bosons are enhanced, have been shown in Figs. 25 and 26. The upper limits on  $\sigma\mathcal{B}$  are translated into lower limits on the vector boson masses. The  $W'$  and  $Z'$  masses are excluded up to 4.1 and 3.9 TeV, respectively, in model B interpretations.

Figure 37 shows the upper limits on the DY production cross section of  $V'$  in the  $WH$  and  $ZH$  channels, compared to those obtained from  $VV$  [109, 111, 196, 197] and fermion pair production channels [198–201] assuming branching fractions of the HVT models A and B. The corresponding theory predictions are overlaid. The all-jets channels are sensitive to both  $W'$  and  $Z'$  production and are thus interpreted in combined  $V'$  production. While in model A, searches for fermion pair production dominate the sensitivity, in model B, where couplings of  $V'$  to bosons are large, the  $VV$  and  $VH$  searches are most sensitive.

For four resonance mass hypotheses, the cross section exclusion limits from DY production are translated into two-dimensional upper limits on the coupling parameters for fermions and bosons of the HVT model. Figure 38 shows only the constraints from  $VH$  production, while Fig. 39 includes also  $VV$  and fermion pair production channels for comparison. The constraints from  $VH$  searches are most stringent, apart from the region with small boson couplings, where the complementary searches with fermion final states provide stronger constraints.

In model C, where the  $V'$  is produced exclusively via VBF, the data set is not sufficient to exclude couplings below  $g_H = 3$  in any range of  $m_{V'}$ . The corresponding results are shown in Fig. 40.

### 4.4 Effects of finite width and interference in resonant $HH$ production

Most of the  $HH$  and  $YH$  analyses performed by the CMS Collaboration make use of the NWA, where the width of BSM particles is neglected and no interference with nonresonant Higgs boson pair production occurs. However, in general, interference effects can strongly impact the  $HH$  cross section. The interference can be either constructive or destructive, enhancing or decreasing the  $HH$  production rate [202, 203], and have a nonnegligible effect in BSM exclusion limits. We study the impact of the interference between nonresonant and resonant production in the inclusive  $pp \rightarrow HH$  production, which can receive contributions from resonant  $X \rightarrow HH$  production. This work provides the first measure of interference effects, identifying phase space regions where the NWA is valid. We use as a benchmark a simplified scenario based on the real-singlet model introduced in Section 1.2.1, as it includes the smallest number of additional free parameters [204]. We note that interference effects are model dependent and may be different for other BSM scenarios.

For this specific study, we modify the singlet model by not imposing the  $\mathbb{Z}_2$  symmetry. The  $\mathbb{Z}_2$  symmetry precludes terms of odd powers of the additional singlet scalar field, which are known to be responsible for a stronger first-order EW phase transition [205, 206]. Exploiting EW symmetry breaking on the singlet model scalar potential, we are left with two mixing states. After mass diagonalization, the identification of one of the states with the SM H boson reduces the number of uncorrelated parameters further from seven to five. The other state is

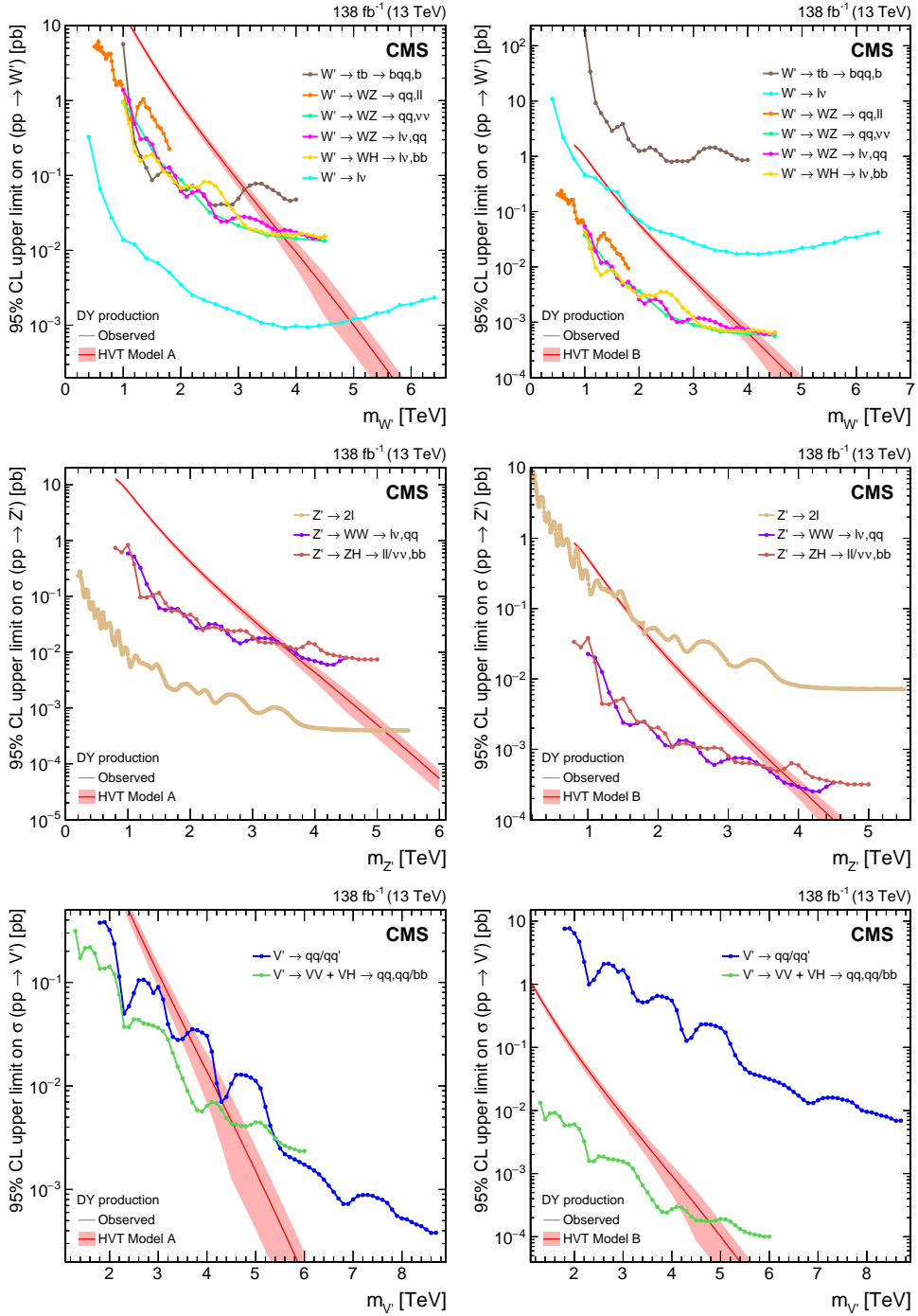


Figure 37: Observed upper limits, at 95% CL, on the Drell-Yan production cross section of (upper)  $W'$ , (middle)  $Z'$ , and (lower) combined  $V'$  spin-1 resonances assuming branching fractions of the heavy vector triplet models (left) A and (right) B. The theory predictions from these models are also shown. Results from the VH [109–111] and VV channels [109, 111, 196, 197], as well as results from dijet [201], tb [199],  $\ell\ell$  [198], and  $\ell\nu$  [200] final states are also shown, for comparison.

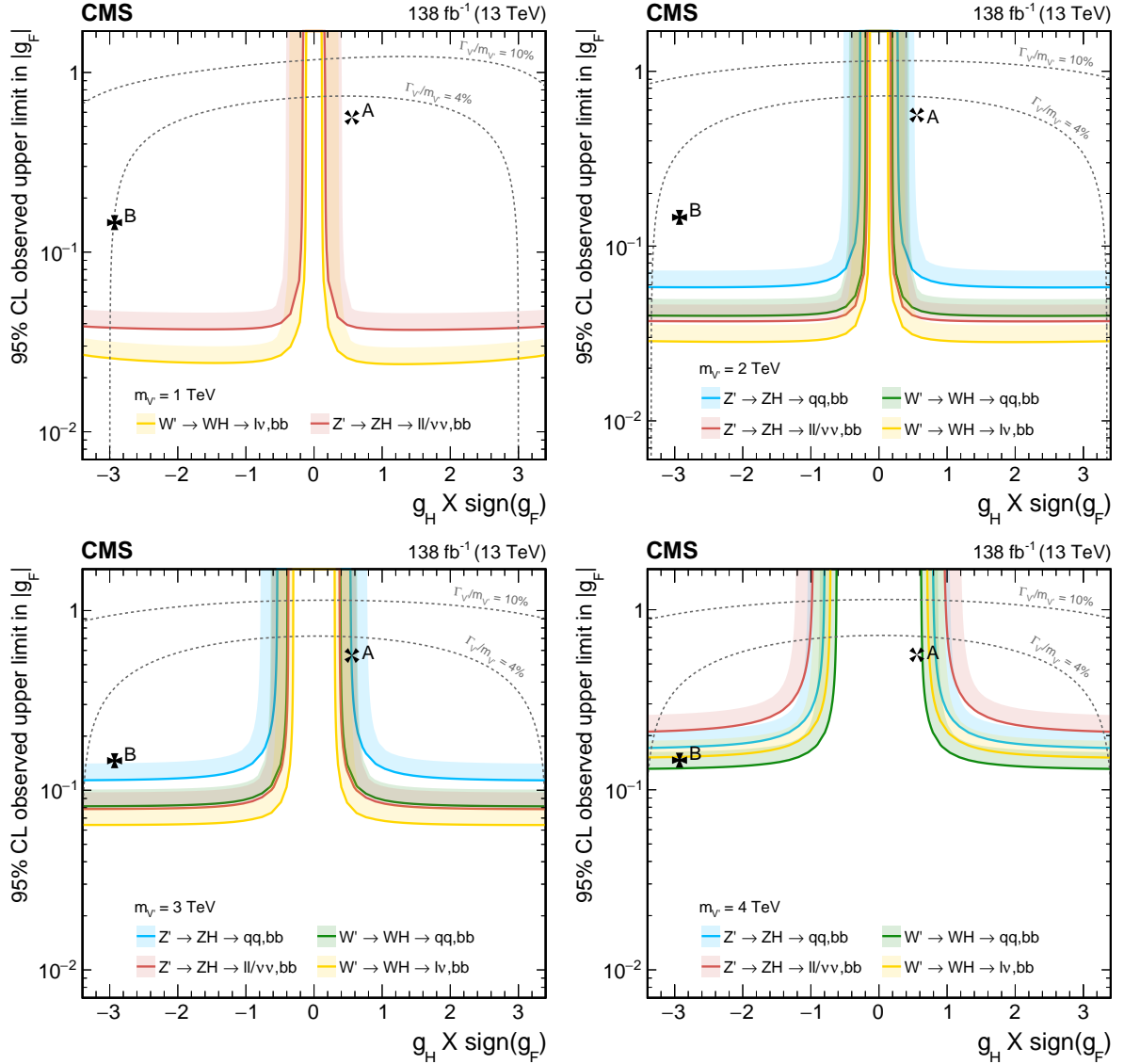


Figure 38: Observed upper limits, at 95% CL, on the  $V'$  couplings  $g_F$  and  $g_H$  within the HVT model for  $V'$  masses of (upper left) 1, (upper right) 2, (lower left) 3, and (lower right) 4 TeV, from DY production, derived from VH channels of Refs. [109–111] discussed in this report. Excluded areas are indicated by the direction of the shading along the exclusion contours. The dotted lines denote coupling values above which the relative width of the resonance,  $\Gamma_{V'}/m_{V'}$ , exceeds 4 and 10%, respectively, implying that the narrow width approximation no longer applies. The couplings corresponding to the heavy vector triplet models A and B are indicated by cross markers.

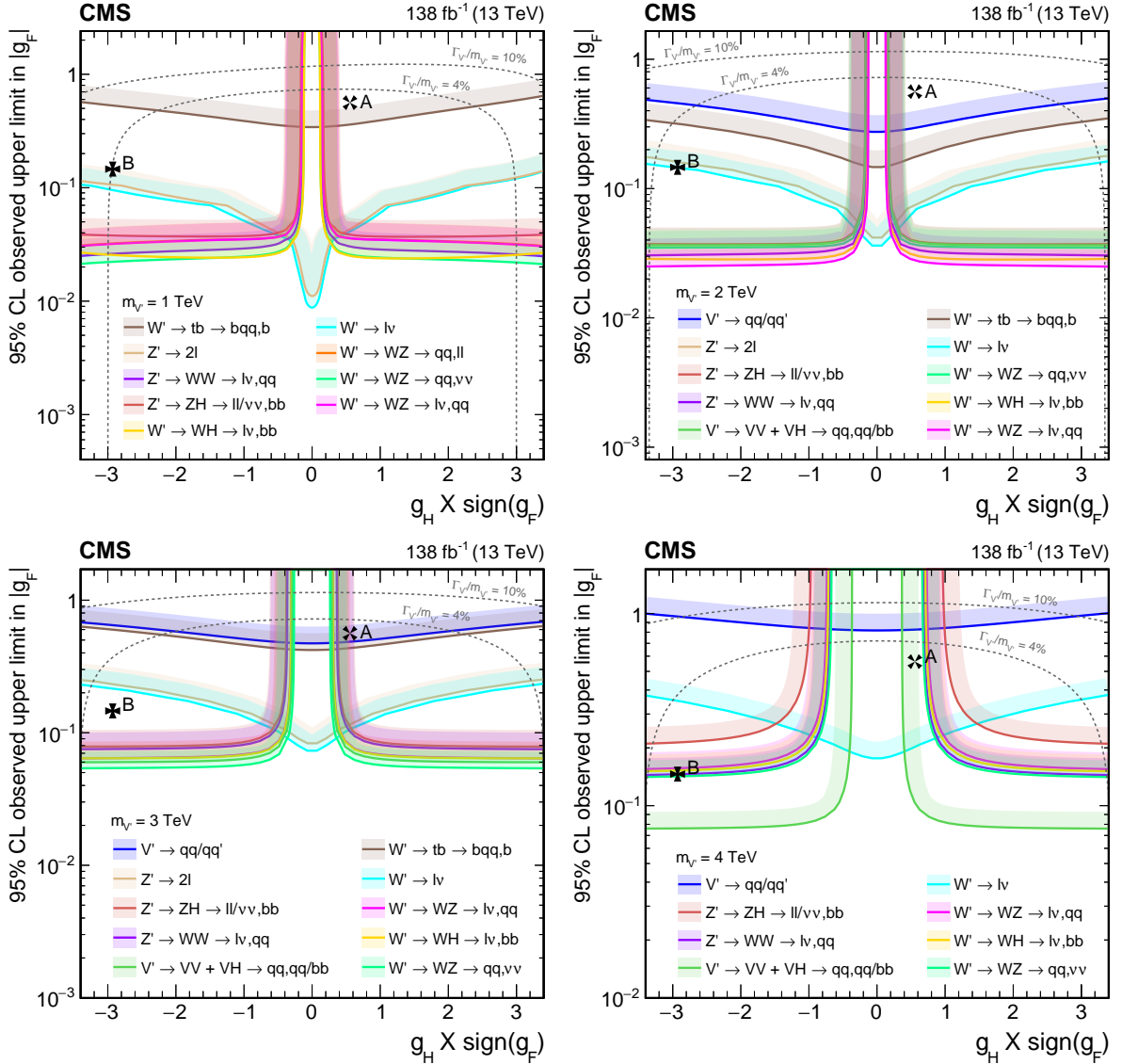


Figure 39: Observed upper limits, at 95% CL, on the  $V'$  couplings  $g_F$  and  $g_H$  within the HVT model for  $V'$  masses of (upper left) 1, (upper right) 2, (lower left) 3, and (lower right) 4 TeV, from DY production, derived from VH channels of Refs. [109–111] discussed in this report and the VV channels of Refs. [109, 111, 196, 197], as well as results from dijet [201],  $tb$  [199],  $\ell\ell$  [198] and  $\ell\nu$  [200] final states. Excluded areas are indicated by the direction of the shading along the exclusion contours. The dotted lines denote coupling values above which the relative width of the resonance,  $\Gamma_{V'}/m_{V'}$ , exceeds 4 and 10%, respectively, implying that the narrow width approximation no longer applies. The couplings corresponding to the heavy vector triplet models A and B are indicated by cross markers.

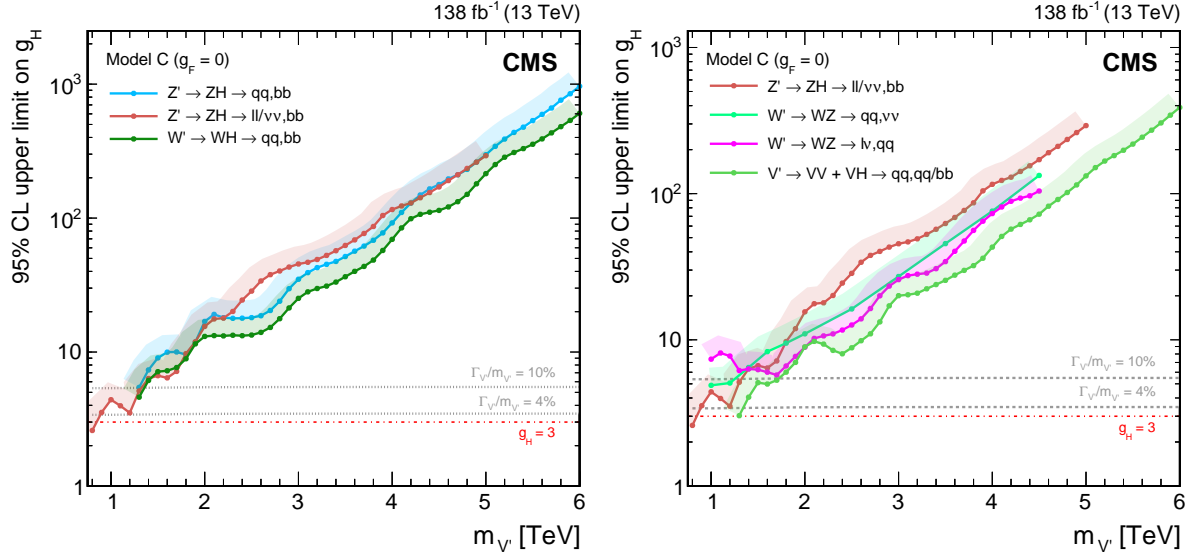


Figure 40: Observed upper limits, at 95% CL, on the coupling  $g_H$  within the heavy vector triplet model, as a function of the  $V'$  mass. The limits are shown for the vector boson fusion production mode in the context of model C, in which  $g_F = 0$ . The results are shown (left) for the WH and ZH analyses of Refs. [109–111], individually, and for a combination with the WZ final states of Refs. [109, 111, 196] (right), where the WH and ZH results from all-hadronic final states have been combined with the corresponding VV channels. The dotted lines denote coupling values above which the relative width of the resonance,  $\Gamma_{V'}/m_{V'}$ , exceeds 4 and 10%, respectively, implying the narrow width approximation no longer applies.

associated with a new particle X. The couplings of the H boson and the X particle are given by

$$g_{Hkk} = g_{Hkk}^{\text{SM}} \cos \alpha \quad \text{and} \quad g_{Xkk} = -g_{Hkk}^{\text{SM}} \sin \alpha, \quad (11)$$

where  $\alpha$  is the mixing angle, and  $k$  represents any SM particle. For  $m_X > 2m_H$  the width of the X resonance can be calculated as

$$\Gamma_X = \sin^2 \alpha \Gamma^{\text{SM}}(m_X) + \frac{\lambda_{\text{HHX}}^2 \sqrt{1 - 4m_H^2/m_X^2}}{8\pi m_X}, \quad (12)$$

where  $\lambda_{\text{HHX}}$  is the trilinear coupling between two H bosons and the new particle X, and  $\Gamma^{\text{SM}}(m_X)$  represents the width of a scalar boson of mass  $m_X$  with the same decay modes as the SM H boson. The latter has been calculated by interpolating the values published in Ref. [35]. In addition to  $\alpha$ ,  $m_X$  and  $\lambda_{\text{HHX}}$ , this singlet model also depends on the trilinear H coupling  $k_\lambda \equiv \lambda_{\text{HHH}}/\lambda_{\text{HHH}}^{\text{SM}}$ , and on an additional scalar coupling.

We use the MADGRAPH5\_aMC@NLO generator version 2.9.7 [207], to simulate inclusive HH events in the singlet model at LO. A custom universal FERMIRULES [208] output (UFO) model based on Ref. [205] adds a heavy scalar boson to the SM with couplings to SM particles as defined in Eq. (11). The samples are created according to the following parameter grid with  $k_\lambda = 1$ :

- $m_X$  [GeV]: 280, 300, 400, 500, 600, 700, 800, 900, 1000,
- $\sin \alpha$ : 0.00, 0.10, 0.20, 0.30, 0.40, 0.50, 0.60, 0.70, 0.80, 0.90, 0.95, 0.99,
- $\lambda_{\text{HHX}}$  [GeV]: -600, -500, -400, -300, -200, -100, -50, 0, 50, 100, 200, 300, 400, 500, 600,

where  $m_X$  is chosen based on the signal samples used in the HH combination presented in Section 3.2. The resonant, nonresonant, and total cross sections for each combination of grid points are generated separately. We perform a parameter scan in the parameters  $m_X$ ,  $\sin \alpha$ , and  $\lambda_{\text{HHX}}$  of the interference ratio defined as

$$R_{\text{int}} = \frac{\sigma^{\text{full}} - (\sigma^{\text{resonant-only}} + \sigma^{\text{nonresonant}})}{\sigma^{\text{resonant-only}} + \sigma^{\text{nonresonant}}}. \quad (13)$$

We obtain the nonresonant cross section by setting the coupling  $g_{Xkk}$  defined in Eq. (11) to zero, and the resonant-only cross section by setting the coupling  $g_{Hkk}$  to zero. The variable  $R_{\text{int}}$  provides information concerning the relative strength of the interference between the SM and BSM processes. The larger the deviation of  $R_{\text{int}}$  from zero, the stronger the modification of the cross section due to the interference. We consider the gluon fusion production mode due to its dominant contribution to the cross section. The UFO model and procedure are validated using the program HPAIR [203, 209] where the results varying  $k_\lambda$  in the nonresonant scenario are found to agree with the NLO predictions of Ref. [4].

Exact conclusions from this study naturally depend on the allowed size of  $R_{\text{int}}$  and the relative width  $\Gamma_X/m_X$ . In the following, we choose as benchmark points  $R_{\text{int}} = \pm 10$  and  $\pm 20\%$ , and  $\Gamma_X/m_X = 5, 10$  and  $20\%$ . The corresponding contours and exclusion limits derived from the HH combination in the singlet model are shown in Fig. 41.

Contours of positive and negative interference ratios are shown in green (for  $R_{\text{int}} = \pm 10\%$ ) and blue (for  $R_{\text{int}} = \pm 20\%$ ). They are found to swap positions at  $m_X = 400 \text{ GeV}$ , likely because of the peak of the nonresonant HH distribution. The dotted lines denote coupling value combinations beyond which the relative width of the resonance,  $\Gamma_X/m_X$ , exceeds 5 and 10%, respectively, implying the narrow width approximation not being accurate anymore. For a given  $m_X$ , the quadratic dependence of  $\Gamma_X$  on both  $\sin \alpha$  and  $\lambda_{\text{HHX}}$  according to Eq. (12) leads to elliptical isolines of constant  $\Gamma_X/m_X$ . The experimental bound from the HH combination discussed in Section 3.2 is obtained from the 95% CL upper limit on  $\sigma(\text{pp} \rightarrow X)\mathcal{B}(X \rightarrow \text{HH})$ , with the X production cross section growing with increasing  $\sin \alpha$ , and  $\mathcal{B}(X \rightarrow \text{HH})$  growing with increasing  $\lambda_{\text{HHX}}$ . We note that large values of  $\sin \alpha$ , corresponding to regions where the H boson is less SM-like, also tend to be excluded by precision measurements of the H boson.

For most of the studied mass points, sizable interference ratios occur only in parameter regions to which the current measurements are not yet sensitive. However, there are regions at intermediate  $m_X$  where the interpretation of NWA-based limits for HH derived in the singlet model would solicit some care already in the Run 2 combination (e.g.  $m_X = 500 \text{ GeV}$ ,  $\sin \alpha = 0.2$  and  $\lambda_{\text{HHX}} = 400 \text{ GeV}$ ). On the other hand, exclusion limits for  $m_X$  above  $600 \text{ GeV}$  are very loose. Interference effects are small for large resonance masses, and might only play a role when the full data set from the HL-LHC [210] becomes available, as discussed in Section 5.3.

The differential cross sections as a function of  $m_{\text{HH}}$  are shown for exemplary points from the  $(\sin \alpha, \lambda_{\text{HHX}})$  parameter space in Fig. 42 for  $m_X = 280 \text{ GeV}$ , and in Fig. 43 for  $m_X = 500 \text{ GeV}$ . The parameters are chosen such that  $\Gamma_X/m_X = 5\%$ , which is well below the detector resolution, and  $R_{\text{int}} = \pm 10$  or  $\pm 20\%$  so that sizable interference effects are expected. The lineshapes show points in parameter space where the  $R_{\text{int}}$  contours intersect with lines of constant  $\Gamma_X/m_X = 5\%$  in Fig. 41.

The mass points of  $m_X = 280$  and  $500 \text{ GeV}$  have been chosen because these values are on the left- and right-hand side of the peak in the  $m_{\text{HH}}$  distribution for nonresonant SM HH production. The line shapes are in general not affected strongly, especially for small  $m_X$ . The signature indicating the presence of the X resonance, including interference effects, can be assessed as

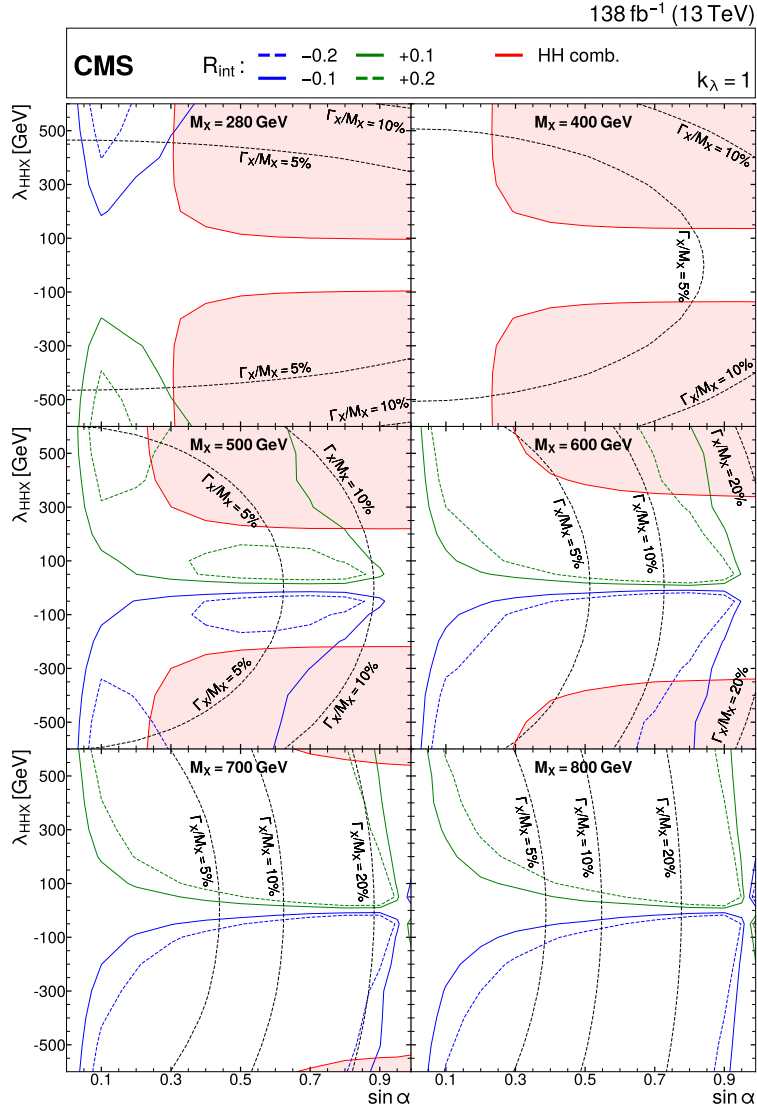


Figure 41: Contours of the variable  $R_{\text{int}}$  as defined in Eq. (13) and discussed in the text, in the  $(\sin \alpha, \lambda_{\text{HHX}})$  plane for the singlet model with  $k_\lambda = 1$  and different resonance masses  $m_X$  between (upper left) 280 and (lower right) 800 GeV. Contours are shown for  $R_{\text{int}}$  values of (dashed blue)  $-0.2$ , (solid blue)  $-0.1$ , (solid green)  $+0.1$ , and (dashed green)  $+0.2$ . Regions that are excluded, at 95% CL, from the combined likelihood analysis of the HH analyses presented in this report are indicated by red filled areas. Dashed black lines indicate constant relative widths of 5, 10, and 20%.

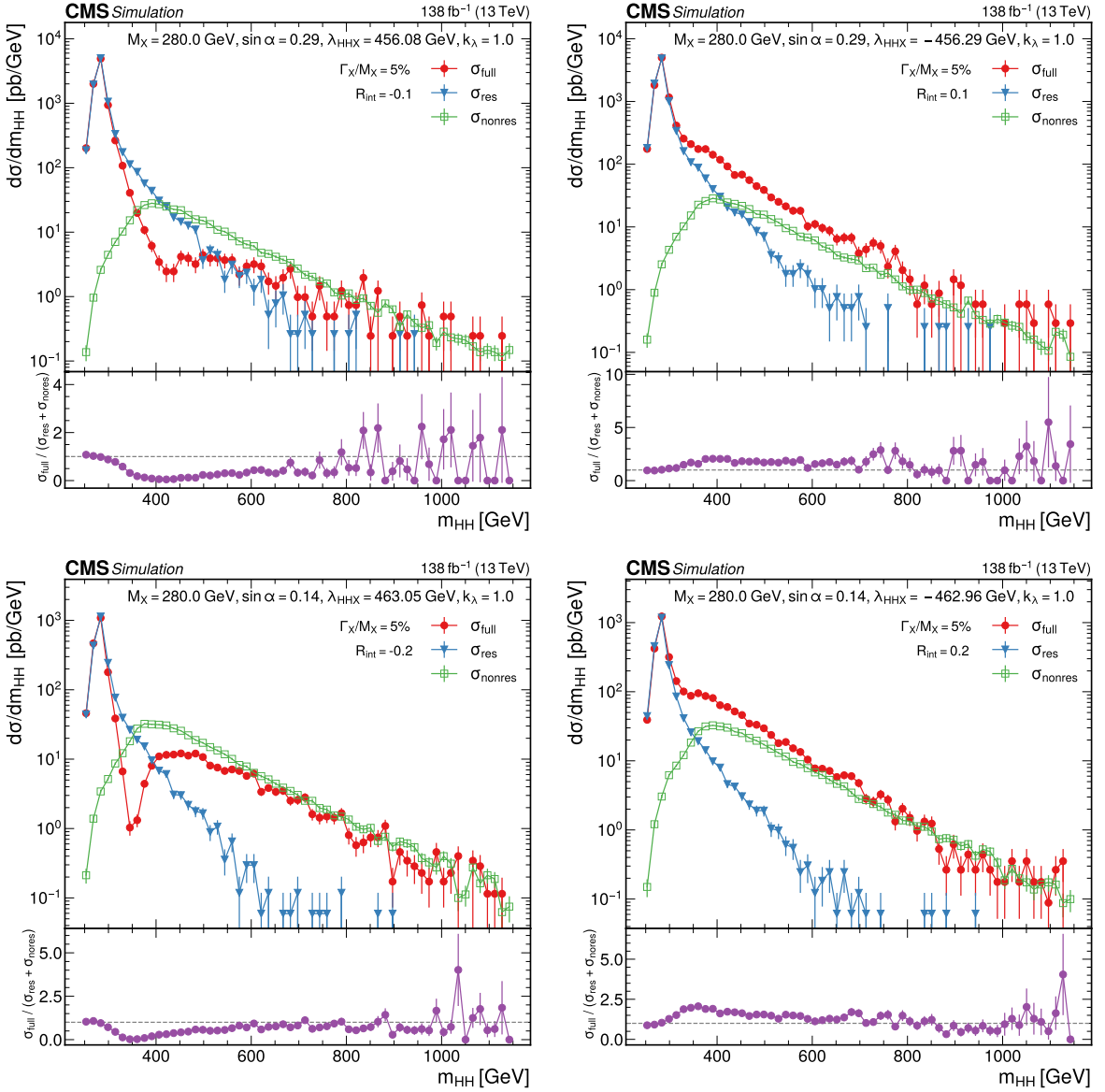


Figure 42: Expected differential cross sections for HH production, as a function of  $m_{\text{HH}}$ , for the real-singlet model with  $m_X = 280 \text{ GeV}$  and  $\Gamma_X/m_X = 5\%$ . The parameters  $\sin \alpha$  and  $\lambda_{\text{HHX}}$  have been chosen such that (upper row)  $R_{\text{int}} = \pm 10\%$  and (lower row)  $R_{\text{int}} = \pm 20\%$ , for (left) negative and (right) positive values of  $R_{\text{int}}$ . The total cross section for HH production  $\sigma^{\text{full}}$  (red line, labelled as  $\sigma_{\text{full}}$ ) is compared to the cross sections  $\sigma^{\text{resonant-only}}$  (blue line, labelled as  $\sigma_{\text{res}}$ ) and  $\sigma^{\text{nonresonant}}$  (green line, labelled as  $\sigma_{\text{nonres}}$ ) considering only resonant and nonresonant production. In the lower panels the ratio of  $\sigma^{\text{full}}$  over  $(\sigma^{\text{resonant-only}} + \sigma^{\text{nonresonant}})$  is shown.

the difference between  $\sigma^{\text{full}}$  (red graph) and  $\sigma^{\text{nonresonant}}$  (green graph). For  $m_X = 280 \text{ GeV}$ , this signature develops a peak-dip structure for a negative interference ratio, and a shoulder-like enhancement towards large masses for a positive interference ratio. Similar effects, albeit on reversed sides of the peak, are visible for  $m_X = 500 \text{ GeV}$ . Although the expected interference effects clearly depend on the underlying model, they can be expected to be of mounting importance in the future as the LHC data set increases.

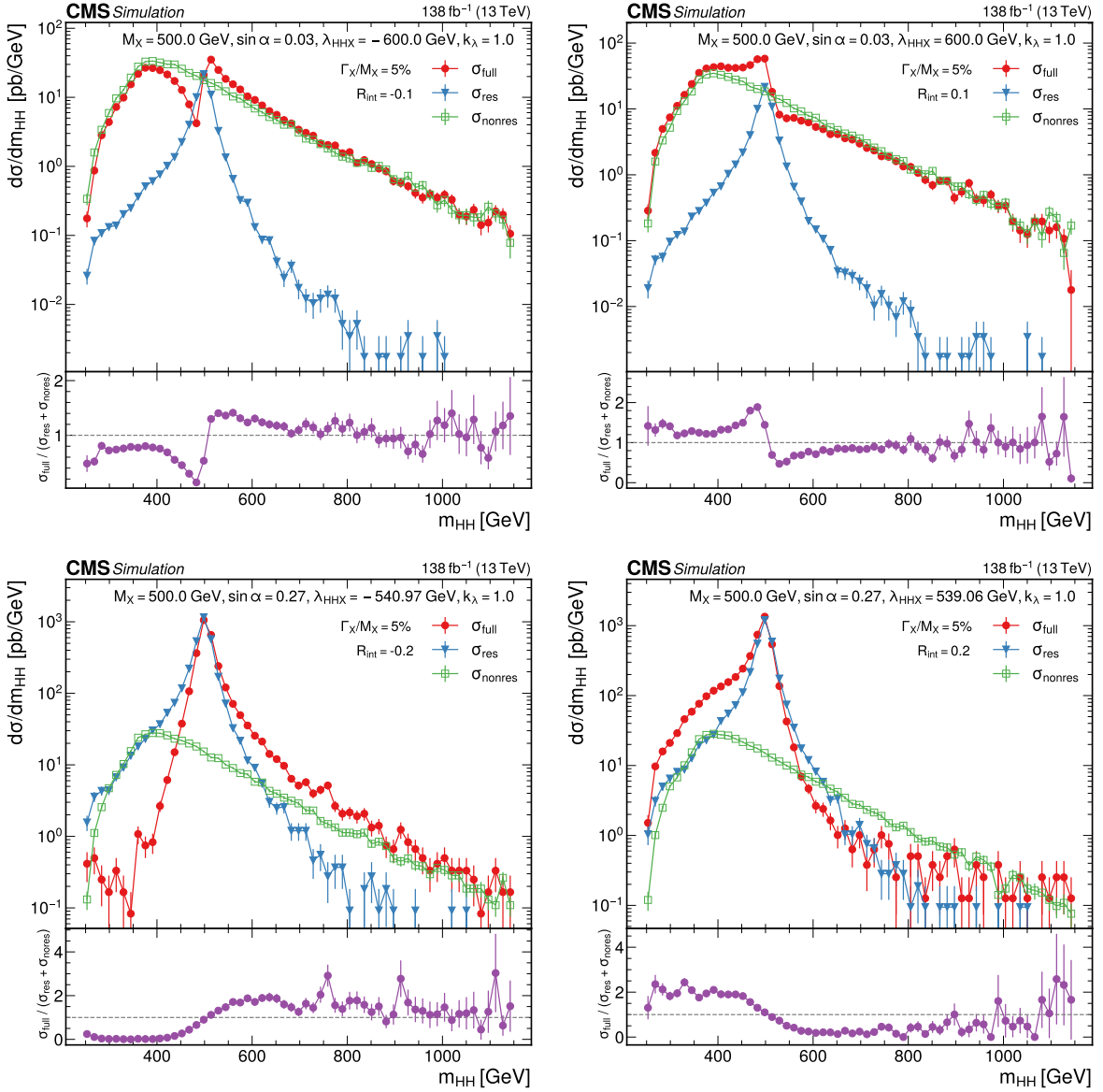


Figure 43: Expected differential cross sections for HH production, as a function of  $m_{\text{HH}}$  for the real-singlet model with  $m_X = 500 \text{ GeV}$  and  $\Gamma_X/m_X = 5\%$ . The parameters  $\sin \alpha$  and  $\lambda_{\text{HHX}}$  have been chosen such that (upper row)  $R_{\text{int}} = \pm 10\%$  and (lower row)  $R_{\text{int}} = \pm 20\%$ , for (left) negative and (right) positive values of  $R_{\text{int}}$ . The total cross section for HH production  $\sigma^{\text{full}}$  (red line, labelled as  $\sigma^{\text{full}}$ ) is compared to the cross sections  $\sigma^{\text{resonant-only}}$  (blue line, labelled as  $\sigma^{\text{res}}$ ) and  $\sigma^{\text{nonresonant}}$  (green line, labelled as  $\sigma^{\text{nonres}}$ ) considering only resonant and nonresonant production. In the lower panels the ratio of  $\sigma^{\text{full}}$  over  $(\sigma^{\text{resonant-only}} + \sigma^{\text{nonresonant}})$  is shown.

## 5 Discovery potential at the HL-LHC

The HL-LHC [211] is planned to start in 2029 and aims to deliver a pp collision data set corresponding to about  $3000 \text{ fb}^{-1}$  of integrated luminosity in the baseline scenario, and up to  $4000 \text{ fb}^{-1}$  in the ultimate scenario, at an unprecedented centre-of-mass energy of 14 TeV. The CMS detector will be upgraded to cope with the large size of 140 (200) PU events on average for the baseline (ultimate) scenario. The upgraded detector will also meet the challenges from the adverse effects due to the radiation dose to which the detector components are exposed, which

Table 2: Searches for resonant HH and YH production considered for the projection study.

Final state	Reference	Section
$bb\tau\tau$	[115]	2.5.1
$bb\gamma\gamma$	[116]	2.5.2
$bbbb$ (merged-jet)	[117]	2.5.3

is one order of magnitude higher than at the current LHC. Furthermore, major improvements of the software for the online and offline event reconstruction are under development to fully exploit the potential of the upgraded detector. Searches for scalars X decaying to HH or YH are among the most relevant targets of research at the HL-LHC, and thus projection studies are very important to motivate the ongoing hardware and software upgrades. Meanwhile, such studies can provide an estimate of the sensitivity to the relevant BSM theories which can be achieved with the HL-LHC data.

This section describes the perspectives for the searches for X boson resonances decaying to HH or YH at the HL-LHC, in the most sensitive decay channels  $bb\gamma\gamma$ ,  $bb\tau\tau$ , and  $bbbb$ , in the baseline scenario of the HL-LHC. Using the combined likelihood method, individual channels are statistically combined to exploit their complementarity in sensitivity to different regions in parameter space of the tested BSM theories. The expected upper limits at 95% CL on the cross sections of the BSM processes of interest are provided as functions of the masses of the BSM scalars. The expected exclusion in the parameters of the relevant BSM theories is estimated, as well as the expected discovery significance for benchmark BSM signals.

## 5.1 Methodology for estimation of the discovery potential

The projection studies are based on the resonant HH and YH searches in the most sensitive channels from the CMS Run 2 data set corresponding to an integrated luminosity of  $138 \text{ fb}^{-1}$ , as summarized in Table 2. Descriptions of the Run 2 HH and YH searches are given in the sections indicated in the table.

Using the same approach as studies in Ref. [210], searches using the Run 2 data set are projected to an integrated luminosity of  $3000 \text{ fb}^{-1}$ . Where appropriate, the signal cross sections have been scaled to the centre-of-mass energy of  $14 \text{ TeV}$  [35]. As the upgraded CMS detector will ensure a performance comparable to Run 2, the efficiency in the reconstruction and identification of photons, leptons, jets and b jets, as well as the resolution in their energy and momentum measurements are assumed to be unchanged. The experimental sensitivity expected at the HL-LHC is derived using the following three systematic uncertainty scenarios.

- S1: All the systematic uncertainties are assumed to remain the same as in Run 2. This is an over-conservative scenario because the CMS detector upgrade, the progress in the reconstruction techniques, and the very large data set available for the experimental calibrations are expected to bring a substantial reduction of several systematic uncertainties. Furthermore, progress in the theory calculations is expected to reduce the uncertainties in the predictions.
- S2: The theory uncertainties are halved, while the experimental uncertainties are set according to the recommendations of Ref. [212].

Statistical only: The results are derived considering only the statistical uncertainty in data.

The projected results from the channels considered are statistically combined following the same procedure as adopted for the Run 2 combination which is described in Section 2.6. In particular, the systematic uncertainties affecting multiple channels, such as the uncertainties in

the luminosity and on the b jet identification efficiency, are treated as correlated among all the input channels.

## 5.2 Discovery potential for $X \rightarrow HH$

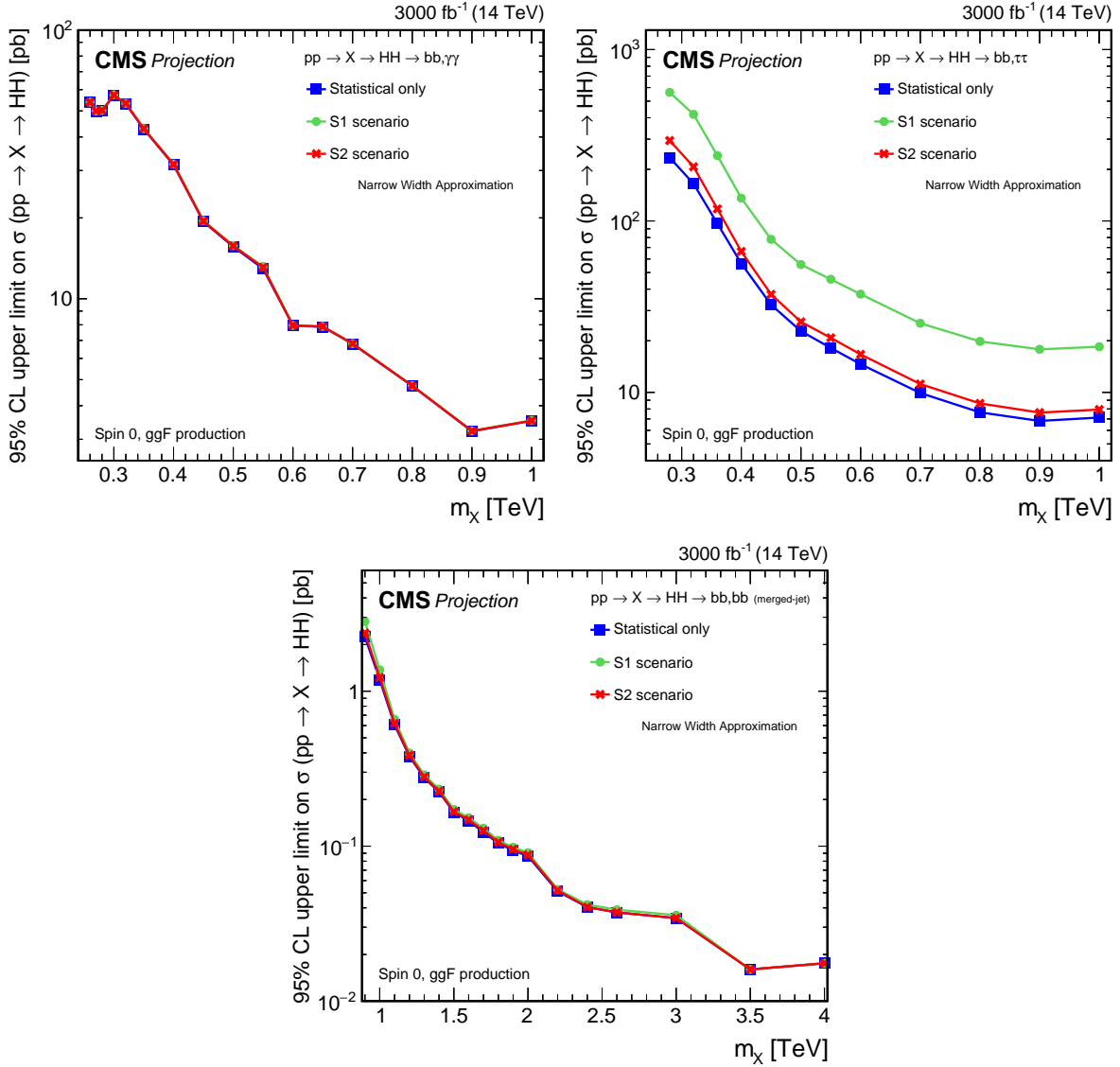


Figure 44: Expected upper limits at 95% CL, on the product of the cross section for the production of a spin-0 resonance  $X$  and the branching fraction  $\mathcal{B}(X \rightarrow HH)$ , as functions of  $m_X$  from the (upper left)  $bb\tau\tau$  [115], (upper right)  $bb\gamma\gamma$  [116], and (lower)  $bbbb$  with two merged  $bb$  jets [117] analyses discussed in this report, projected to an integrated luminosity of  $3000 \text{ fb}^{-1}$  under the assumption of different systematic uncertainty scenarios, as discussed in the text. All estimates include the anticipated statistical uncertainties.

The expected upper limits at 95% CL on the  $X \rightarrow HH$  cross section from the channels considered projected to  $3000 \text{ fb}^{-1}$  are shown for the three different systematic uncertainty scenarios in Fig. 44. The projected upper limits from the  $bb\gamma\gamma$  decay mode range between 60 and 3 fb for  $m_X$  within 300–1000 GeV. The overall impact of the systematic uncertainties on the  $bb\gamma\gamma$  upper limits is below 1% because of the small uncertainty on the background modeling thanks to the estimation procedure based on the fit to the data in sideband regions.

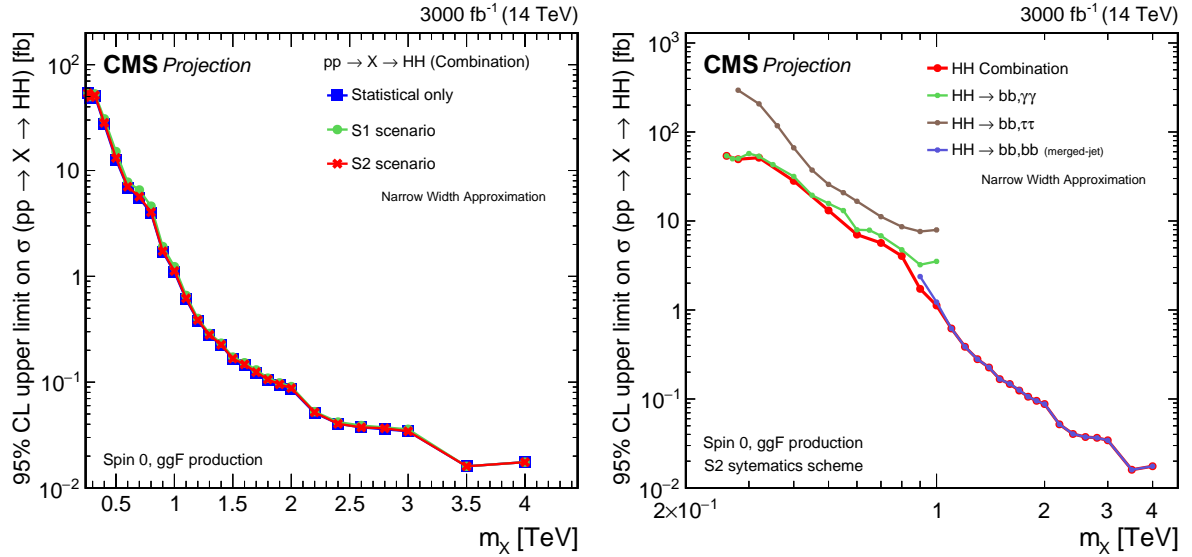


Figure 45: Expected upper limits at 95% CL, on the product of the cross section for the production of a spin-0 resonance  $X$  and the branching fraction  $\mathcal{B}(X \rightarrow HH)$ , as a function of  $m_X$ , for an integrated luminosity of  $3000 \text{ fb}^{-1}$  and the combination of the three analyses shown in Fig. 44. Shown are the effects of the different systematic uncertainty scenarios (left), and the reach of the individual analyses for the S2 systematic scenario (right). All estimates include the anticipated statistical uncertainties.

The  $bb\tau\tau$  channel provides upper limits on the cross section at 95% CL between 300 and 7 fb for  $m_X$  within 300–1000 GeV. The systematic uncertainty with the largest impact in the S1 scenario has its origin in the limited size of the MC simulation used for the background estimation. In the S2 scenario, the statistical uncertainties on the simulated events are assumed to be negligible and the main systematic uncertainties arise from the efficiencies of the b jet and  $\tau$  identification and misidentification.

The  $bbbb$  channel in the boosted regime, in the following simply referred to as  $bbbb$ , covers  $m_X$  values between 900 and 4000 GeV, and is expected to provide upper limits between 0.04 and 0.02 fb at an integrated luminosity of  $3000 \text{ fb}^{-1}$ . The impact of the systematic uncertainties is very small, as the sensitivity of the analysis is mainly limited by the statistical uncertainty in the data.

The results of the combination of the resonant HH searches considered are shown in Fig. 45 in the different systematic uncertainty scenarios, and in comparison to the results from the individual channels. The  $bb\gamma\gamma$  channel is found to dominate the sensitivity in the region  $m_X < 500$  GeV; around 900 GeV the channel with the best sensitivity is  $bbbb$ , followed by  $bb\gamma\gamma$  and  $bb\tau\tau$ . For  $m_X > 1000$  GeV the only channel considered is  $bbbb$  which is expected to be the most sensitive in this kinematic region. Thanks to the small impact of the systematic uncertainties on the  $bb\gamma\gamma$  and  $bbbb$  channels, the differences between the three systematic uncertainty scenarios are rather small.

### 5.2.1 Perspectives for the discovery of BSM benchmark signals

The expected significance for the discovery of a benchmark BSM signal from a spin-0 resonance with a mass of 1 TeV is calculated for several signal cross sections and represented as a function of the integrated luminosity in Fig. 46. Based on the three channels considered in this projection, the significance of a signal of  $X \rightarrow HH$  with a cross section of 10 fb corresponds to about

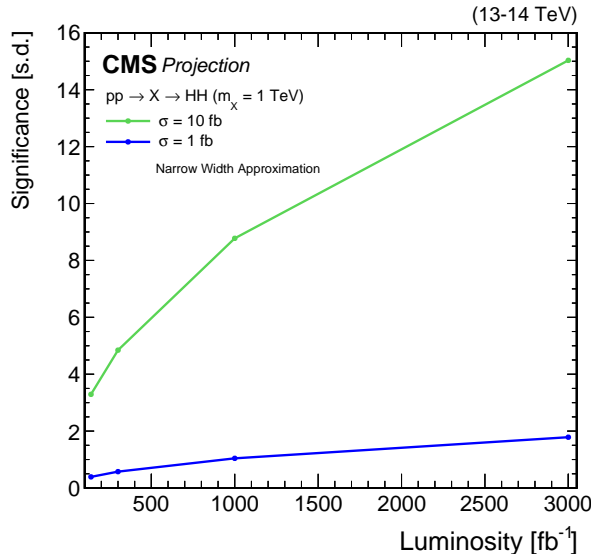


Figure 46: Expected discovery significance for a spin-0 resonance  $X$  with  $m_X = 1 \text{ TeV}$  and cross sections of 1 and  $10 \text{ fb}$ , obtained for the combined likelihood analysis of the resonant HH searches as discussed in Section 5 and shown in Figs. 44 and 45, shown as function of the integrated luminosity.

three standard deviations at Run 2, while an integrated luminosity of  $300 \text{ fb}^{-1}$  would yield 4.8 standard deviations, indicating an attractive discovery potential already for Run 3 and its combination with Run 2. The significance of the same signal would reach about 15 standard deviations at  $3000 \text{ fb}^{-1}$ . A signal with a cross section of  $3 \text{ fb}$  would be sufficient to reach an observation at the level of five standard deviations with  $3000 \text{ fb}^{-1}$ .

### 5.2.2 Perspectives for MSSM scenarios

The projected exclusions limits at 95% CL of the hMSSM and  $M_{h,\text{EFT}}^{125}$  benchmark scenarios from resonant HH searches are shown in Fig. 47. The S1 systematic uncertainty scenario is used for the Run 2 result and conservatively also for the result with  $300 \text{ fb}^{-1}$ , while the S2 systematic uncertainty scenario is used for the projected 1000 and  $3000 \text{ fb}^{-1}$  results. Over the full accessible range in  $\tan\beta$ , the exclusion in  $m_A$  increases by about 250–300 GeV when moving from the Run 2 integrated luminosity to  $3000 \text{ fb}^{-1}$ , for both the hMSSM and  $M_{h,\text{EFT}}^{125}$  scenarios. This exclusion from the resonant HH searches will complement the searches for  $X$  decaying to a pair of fermions or vector bosons.

### 5.2.3 Perspectives for the WED bulk scenario

The expected lower limits at 95% CL on the bulk radion parameter  $\Lambda_R$  as a function of the radion mass  $m_R$  are shown in Fig. 48. The limits are obtained from the combination of resonant HH searches in the WED bulk scenario. The S1 systematic uncertainty scenario is used for the Run 2 result and conservatively also for the result with  $300 \text{ fb}^{-1}$ , while the S2 systematic uncertainty scenario is used for the projected 1000 and  $3000 \text{ fb}^{-1}$  results. Over the full range in  $m_R$ , the limit on  $\Lambda_R$  is expected to increase by a factor of at least two with the full HL-LHC data set.

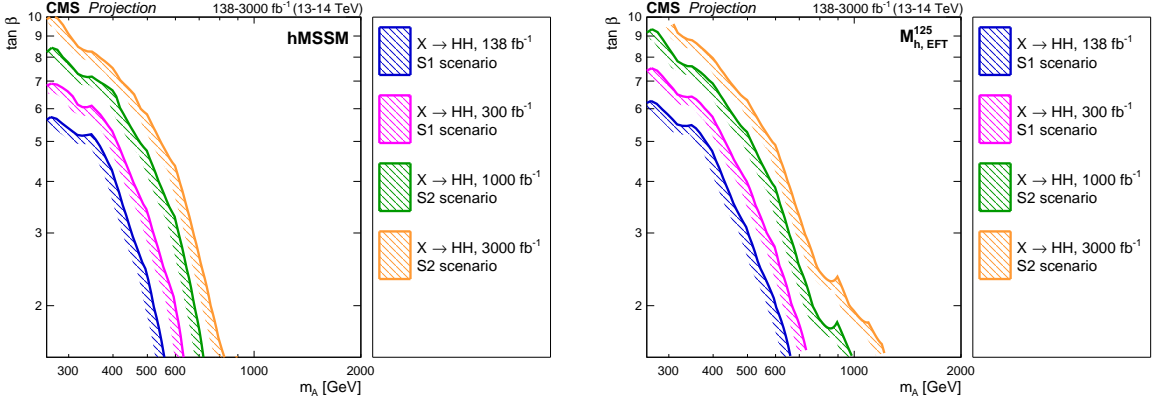


Figure 47: Expected exclusion contours at 95% CL, in the  $(\tan \beta, m_A)$  plane of the (left) hMSSM and (right)  $M_{h,\text{EFT}}^{125}$  scenarios obtained from the combined likelihood analysis of the HH searches discussed in Section 4.1 and shown in Figs. 31 and 32, for different integrated luminosities and compared to the Run 2 result obtained at  $\sqrt{s} = 13$  TeV. The projections assume  $\sqrt{s} = 14$  TeV.

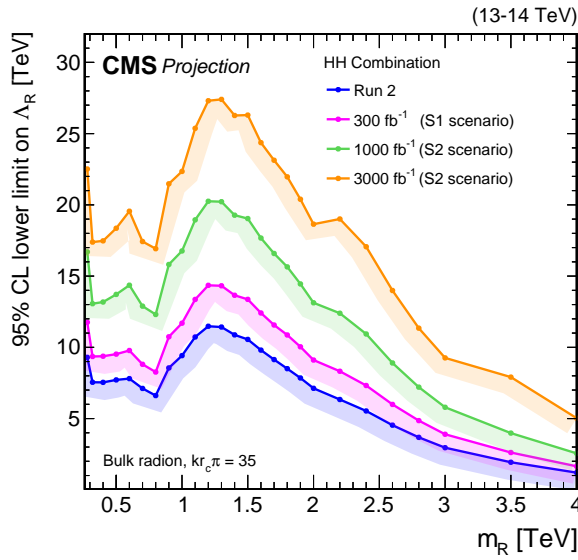


Figure 48: Expected lower limit at 95% CL, on  $\Lambda_R$  in the warped extra dimensions bulk scenario for the production of a radion  $R$ , as a function of  $m_R$ . The limits are derived from the combined likelihood analysis of the HH searches discussed in Section 4.2 and shown in Fig. 35, for different values of the integrated luminosity. Excluded areas are indicated by the direction of the hatching along the exclusion contours.

### 5.2.4 Perspectives for the singlet scenarios

In the singlet model of Section 4.4 with  $k_\lambda = 1$ , limits are derived in the  $(\sin \alpha, \lambda_{\text{HHX}})$  plane from the combination of resonant HH searches. Resonance masses between 280 and 1000 GeV are probed using Run 2 data and projected to integrated luminosities corresponding to 300, 1000, and  $3000 \text{ fb}^{-1}$ . Projected exclusion regions at 95% CL are shown in Fig. 49. The HL-LHC dataset of  $3000 \text{ fb}^{-1}$  has the potential to considerably expand the present exclusion regions in the  $(\sin \alpha, \lambda_{\text{HHX}})$  plane for all values of  $m_X$ . Compared to the present limits, the largest improvement is observed for large masses,  $m_X = 600 \text{ GeV}$  and higher, where large regions of the  $(\sin \alpha, \lambda_{\text{HHX}})$  plane can be probed, and part of the plane even for  $m_X = 1 \text{ TeV}$ .

## 5.3 Discovery potential for $X \rightarrow YH$

The upper limits on the cross section for  $X \rightarrow YH$  are also projected to an integrated luminosity of  $3000 \text{ fb}^{-1}$  for the three systematic uncertainty scenarios. The projections are derived for the individual channels in the  $bb\gamma\gamma$ ,  $bb\tau\tau$ , and  $bbbb$  final states, and for a combination with the assumption of SM H boson branching fractions, where we use the same procedure as for the HH projections. The differences between the upper limits in the S1, S2, and statistical-only scenarios are analogous to the findings for the corresponding channels in the  $X \rightarrow \text{HH}$  projections.

The results of the  $X \rightarrow YH$  projections are presented in Figs. 50 and 51 for  $m_X$  up to and above 1 TeV, respectively. The regions of the  $(m_X, m_Y)$  parameter space with the largest ratios of  $m_Y/m_X$  correspond to a Y particle with low transverse momentum, and can be probed with the  $bb\gamma\gamma$  channel. In the regions with small ratios of  $m_Y/m_X$ , the Y particle receives a large Lorentz boost, such that the  $bbbb$  boosted channel has the highest sensitivity and only this final state is considered. In the intermediate region, the  $bb\gamma\gamma$  and  $bb\tau\tau$  channels provide comparable sensitivity and about equal weight in the combination.

Selected bins of the projections from the YH combination are used for presenting expected upper limits as functions of  $m_X$  and  $m_Y$ , and are shown in Fig. 52. In comparison with Fig. 34, the improvement is clearly visible.

### 5.3.1 Perspectives for the NMSSM and TRSM

We compare the maximally allowed cross sections predicted by the NMSSM model scans with the expected upper limits at 95% CL on the  $X \rightarrow YH$  cross sections, projected to an integrated luminosity of  $3000 \text{ fb}^{-1}$ . The NMSSM model scans are obtained with NMSSMTOOLS version 5.6.2 [193], as described in Section 4.1.3, and take many relevant experimental constraints from Run 2 into account. Figure 53 shows the projected exclusion contours for the final states  $Y(bb)H(\gamma\gamma)$  (upper left),  $Y(bb)H(\tau\tau)$  (upper right), and  $Y(bb)H(bb)$  in the merged-jet topology (lower left). The maximized model  $\sigma\mathcal{B}$  values may depend non-monotonically on  $m_Y$  which can reflect in the contours. Substantial regions of the parameter space can be excluded in the probed mass region with  $m_X = 500\text{--}1000 \text{ GeV}$  and  $m_Y = 100\text{--}350 \text{ GeV}$ , as well as up to  $m_Y = 200 \text{ GeV}$  for  $m_X = 1100\text{--}1500 \text{ GeV}$ . This indicates a huge increase in sensitivity for the HL-LHC compared to the results from Run 2. Similarly, we compare the predictions of the TRSM model [12] with the projected results from the  $Y(bb)H(bb)$  channel in the merged-jet topology in Fig. 53 (lower right), which results in a sizable exclusion region for  $m_X = 900\text{--}1500 \text{ GeV}$  and  $m_Y = 110\text{--}135 \text{ GeV}$ .

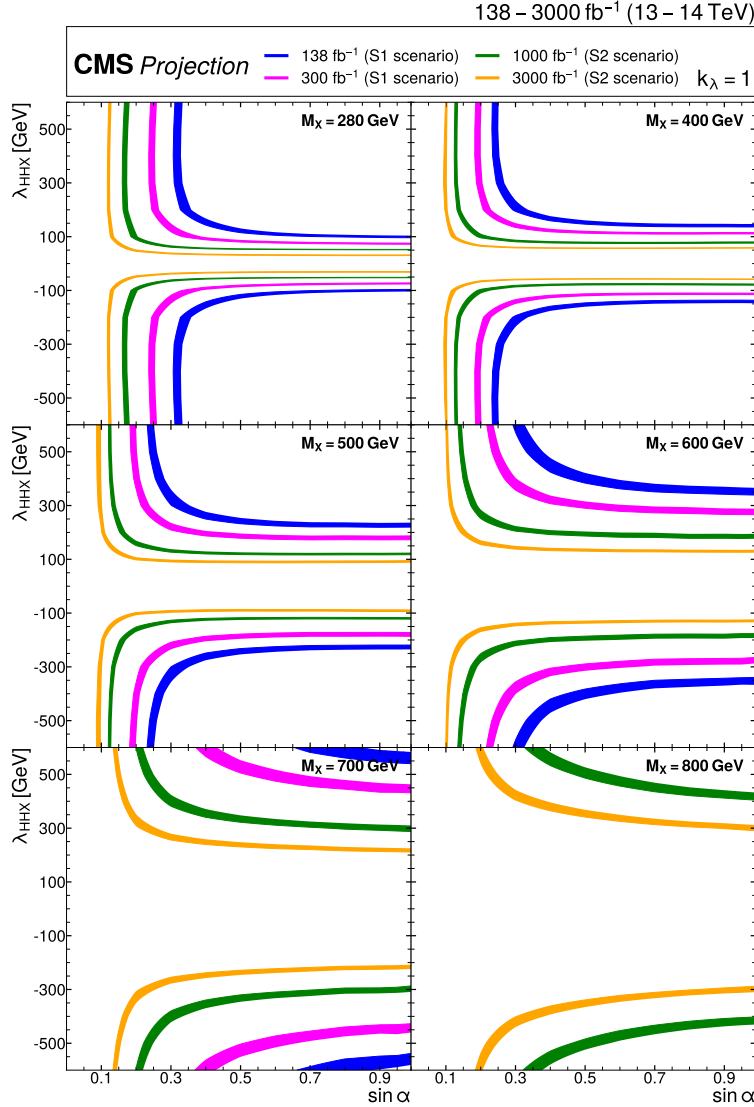


Figure 49: Exclusion contours at 95% CL, in the  $(\sin \alpha, \lambda_{\text{HHX}})$  plane for  $k_\lambda = 1$  in the real-singlet model. These contours are obtained from the combined likelihood analysis of the HH searches discussed in Section 4.1 for (upper left to lower right)  $m_X = 280, 400, 500, 600, 700$ , and  $1000 \text{ GeV}$ . The expected limits from the Run 2 dataset have been projected to integrated luminosities of  $300, 1000$ , and  $3000 \text{ fb}^{-1}$ . Excluded areas are indicated by the direction of the hatching along the exclusion contours.

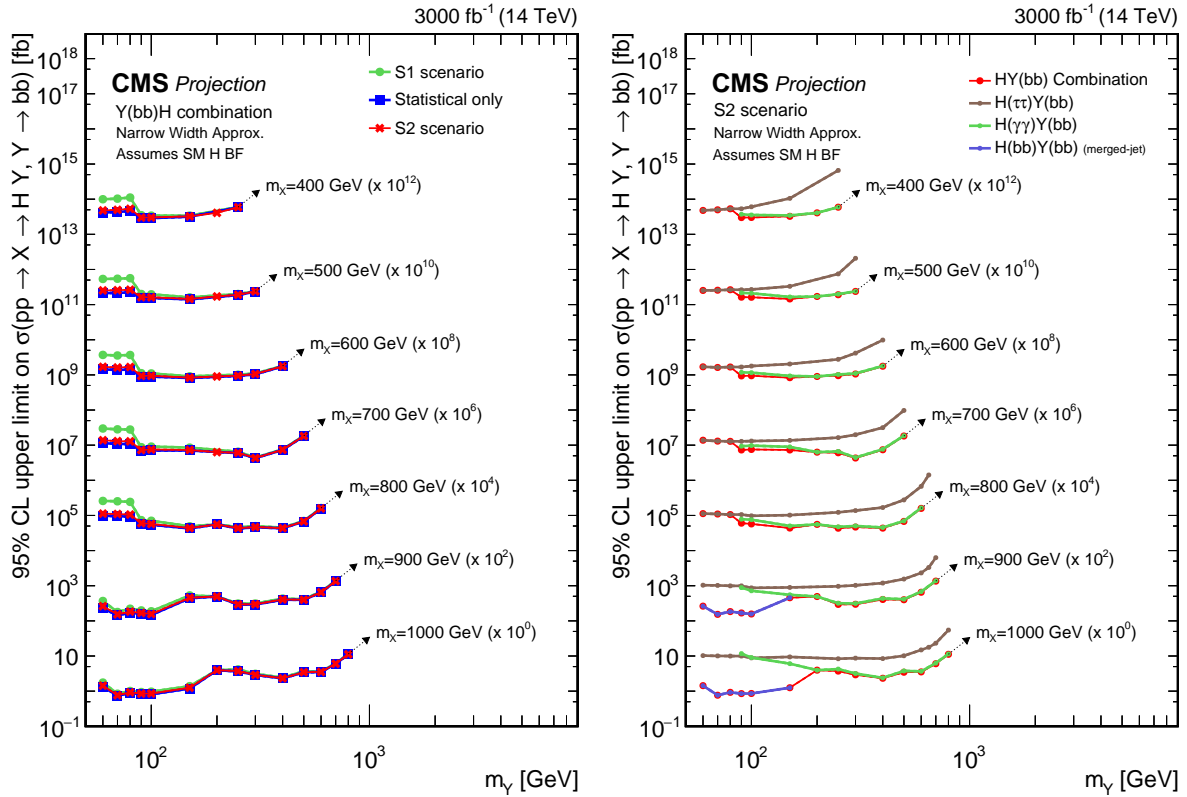


Figure 50: Expected upper limits at 95% CL, on the product of the cross section  $\sigma$  for the production of a resonance  $X$  via gluon-gluon fusion and the branching fraction  $\mathcal{B}$  for the  $X \rightarrow Y(bb)H$  decay, as functions of  $m_Y$ , for  $m_X \leq 1 \text{ TeV}$ . For the branching fractions of the  $H \rightarrow \tau\tau$ ,  $H \rightarrow \gamma\gamma$  and  $H \rightarrow bb$  decays, the SM values are assumed. The limits are obtained from the combined likelihood analysis of all analyses discussed in Section 3.3 and shown in Fig. 29, projected to an integrated luminosity of  $3000 \text{ fb}^{-1}$ . Shown are the projections for the combined likelihood analysis for different systematic uncertainty scenarios (left), and the projections for the combined likelihood analysis and the individual contributing analyses assuming the S2 scenario (right). For presentation purposes, the limits have been scaled in successive steps by two orders of magnitude. For each set of graphs, a black arrow points to the  $m_X$  related legend.

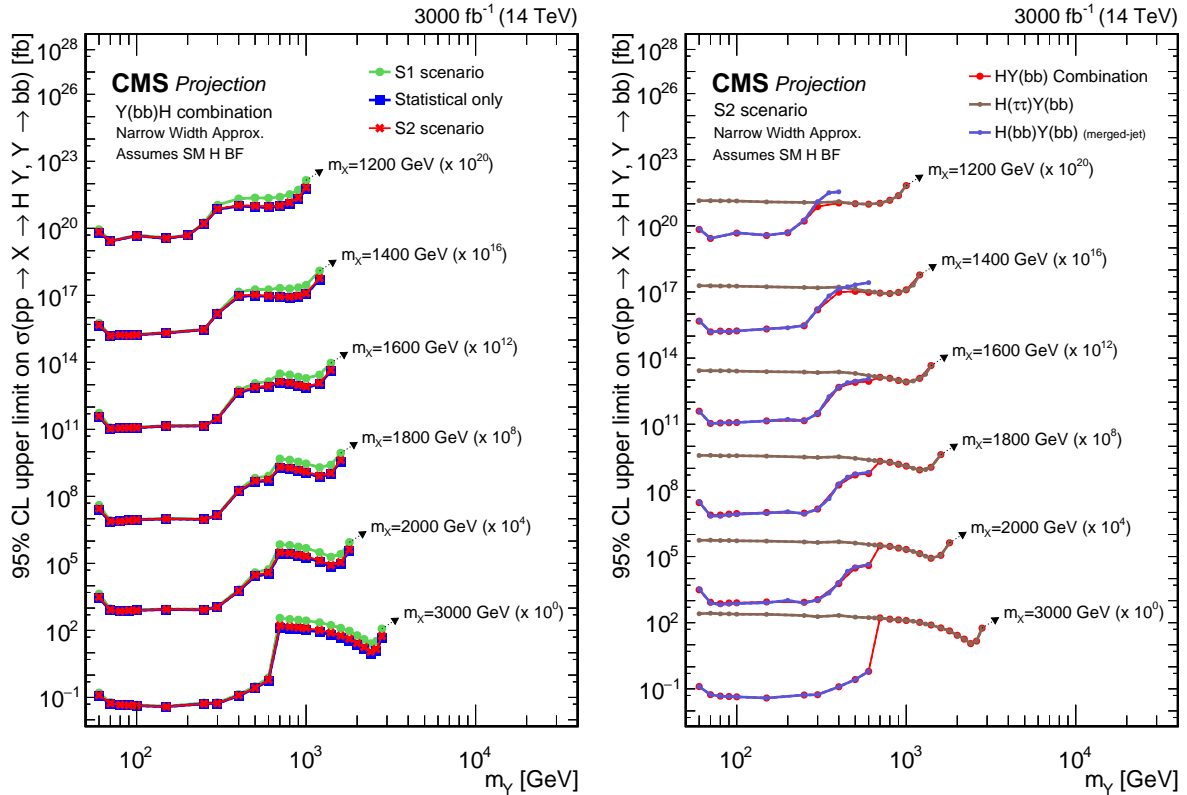


Figure 51: Expected upper limits at 95% CL, on the product of the cross section  $\sigma$  for the production of a resonance  $X$  via gluon-gluon fusion and the branching fraction  $\mathcal{B}$  for the  $X \rightarrow Y(bb)H$  decay, as functions of  $m_Y$ , for  $m_X \geq 1.2$  TeV. For the branching fractions of the  $H \rightarrow \tau\tau$  and  $H \rightarrow bb$  decays, the SM values are assumed. The limits are obtained from the combined likelihood analysis of all analyses discussed in Section 3.3 and shown in Fig. 30, projected to an integrated luminosity of  $3000 \text{ fb}^{-1}$ . Shown are the projections for the combined likelihood analysis for different systematic uncertainty scenarios (left), and the projections for the combined likelihood analysis and the individual contributing analyses assuming the S2 scenario (right). For presentation purposes, the limits have been scaled in successive steps by four orders of magnitude. For each set of graphs, a black arrow points to the  $m_X$  related legend.

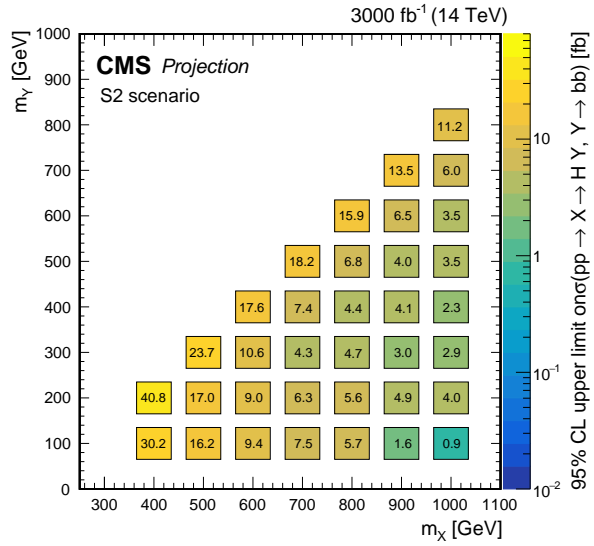


Figure 52: Expected upper limits at 95 % CL on the product of the cross section  $\sigma$  for the production of a resonance  $X$  via gluon-gluon fusion and the branching fraction  $\mathcal{B}$  for the  $X \rightarrow Y(b\bar{b})H$  decay, as obtained from the combined likelihood analysis of the individual analyses presented in Section 3.3 and Figure 29. The results are shown in the plane spanned by  $m_Y$  and  $m_X$  for  $m_X \leq 1$  TeV, and projected to an integrated luminosity of  $3000 \text{ fb}^{-1}$ , assuming the S2 systematic uncertainty scenario. The numbers in the boxes are given in fb.

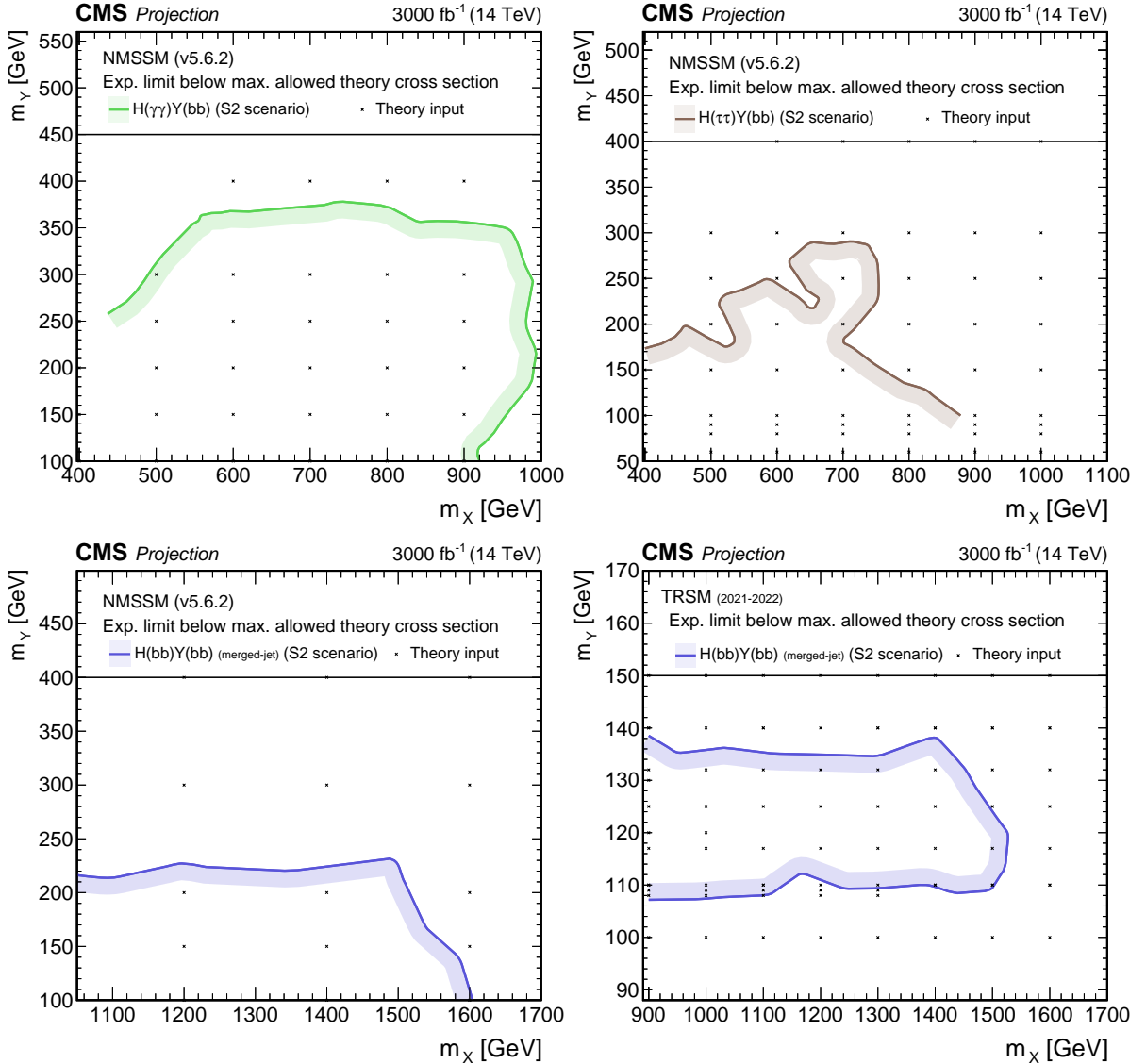


Figure 53: Interpretation of the upper limits at 95% CL, on the product of the cross section  $\sigma$  for the production of a resonance  $X$  via gluon-gluon fusion and the branching fraction  $\mathcal{B}$  for the  $X \rightarrow Y(bb)H$  decay, obtained from the projections to an integrated luminosity of  $3000 \text{ fb}^{-1}$  of the (upper left)  $Y(bb)H(\gamma\gamma)$  [116], (upper right)  $Y(bb)H(\tau\tau)$  [115], and (lower row)  $Y(bb)H(bb)$  [117] analyses, assuming the S2 systematic uncertainty scenario. The projected limits are mapped onto the  $(m_X, m_Y)$  plane, and compared with the maximally allowed cross sections of the NMSSM (left and upper right), and TRSM models (lower right) discussed in Section 4.1.3. The points indicate the available theory predictions. The mass dependences of both the projected experimental limits and the maximally allowed theory cross sections have been interpolated to obtain approximate exclusion contours. The NMSSM predictions based on NMSSMTOOLS version 5.6.2 are adapted from Ref. [193], whereas the TRSM is described in Ref. [12]. In both cases, the model predictions have been scaled to  $\sqrt{s} = 14 \text{ TeV}$ .

## 6 Summary

The analyses searching for the production of the Higgs ( $H$ ) boson through decays of heavy resonances, performed by the CMS Collaboration using the Run 2 data set, are reviewed. This review covers final states with two bosons with at least one an  $H$  boson, namely an  $H$  boson and a vector boson ( $VH$ ), a pair of  $H$  bosons ( $HH$ ), and an  $H$  boson joined by a new boson  $Y$  ( $YH$ ), where  $V$  represents a  $W$  or a  $Z$  boson.

The analyses cover a wide range of  $H$  boson decay modes, in particular, decays into photons,  $b$  quarks,  $\tau$  leptons, and  $W$  bosons. The  $Y$  boson is exclusively searched for in  $b$  quark final states. Topologies involving both resolved and merged jet objects are used to cover a wide range of the phase space. Multivariate methods are employed in various ways to improve the performance.

The results are presented as summary plots which show the sensitivity of all channels in direct comparison. For the  $HH$  and  $YH$  final states, the results obtained by combining all decay channels are presented for the first time.

The results are interpreted in the context of relevant beyond-the-standard model scenarios for resonances decaying into  $VH$ ,  $HH$  and  $YH$  final states. These include various extended Higgs sector models, warped extra-dimension models, and heavy vector triplet models. The results from resonant  $H$  boson production searches are compared with results from searches in other channels.

While all presented analyses assume the validity of the narrow-width approximation, a dedicated study of the impact of finite width and interference is performed for the first time in CMS for the real singlet extension of the standard model. This study shows the modification of the  $HH$  cross section and line shape in regions of the parameter space where the narrow-width approximation is not valid anymore.

The expected sensitivity of the analyses in the  $HH$  and  $YH$  final states is estimated for future data sets with integrated luminosities of 300, 1000, and  $3000\text{ fb}^{-1}$ , the last number corresponding to the baseline scenario of the High-Luminosity LHC (HL-LHC) over its full lifetime. The expected upper limits for resonant  $HH$  production for the HL-LHC scenario range from about  $50\text{ fb}$  at a resonance mass of  $300\text{ GeV}$  to nearly  $0.01\text{ fb}$  for masses of  $3\text{ TeV}$  and above. The exclusions in terms of  $\tan\beta$  in the hMSSM and  $M_{h,\text{EFT}}^{125}$  scenarios are expanded by almost a factor of two compared to the Run 2 data set.

This review shows how the specific strengths of many different experimental signatures can be combined to chart very thoroughly the territory where resonant Higgs boson production might reveal beyond the standard model physics, and gives a promising outlook towards the achievement potential of future measurements in this sector.

## Acknowledgments

We congratulate our colleagues in the CERN accelerator departments for the excellent performance of the LHC and thank the technical and administrative staffs at CERN and at other CMS institutes for their contributions to the success of the CMS effort. In addition, we gratefully acknowledge the computing centres and personnel of the Worldwide LHC Computing Grid and other centres for delivering so effectively the computing infrastructure essential to our analyses. Finally, we acknowledge the enduring support for the construction and operation of the LHC, the CMS detector, and the supporting computing infrastructure provided

by the following funding agencies: the Armenian Science Committee, project no. 22rl-037; the Austrian Federal Ministry of Education, Science and Research and the Austrian Science Fund; the Belgian Fonds de la Recherche Scientifique, and Fonds voor Wetenschappelijk Onderzoek; the Brazilian Funding Agencies (CNPq, CAPES, FAPERJ, FAPERGS, and FAPESP); the Bulgarian Ministry of Education and Science, and the Bulgarian National Science Fund; CERN; the Chinese Academy of Sciences, Ministry of Science and Technology, the National Natural Science Foundation of China, and Fundamental Research Funds for the Central Universities; the Ministerio de Ciencia Tecnología e Innovación (MINCIENCIAS), Colombia; the Croatian Ministry of Science, Education and Sport, and the Croatian Science Foundation; the Research and Innovation Foundation, Cyprus; the Secretariat for Higher Education, Science, Technology and Innovation, Ecuador; the Estonian Research Council via PRG780, PRG803, RVTT3 and the Ministry of Education and Research TK202; the Academy of Finland, Finnish Ministry of Education and Culture, and Helsinki Institute of Physics; the Institut National de Physique Nucléaire et de Physique des Particules / CNRS, and Commissariat à l'Énergie Atomique et aux Énergies Alternatives / CEA, France; the Shota Rustaveli National Science Foundation, Georgia; the Bundesministerium für Bildung und Forschung, the Deutsche Forschungsgemeinschaft (DFG), under Germany's Excellence Strategy – EXC 2121 "Quantum Universe" – 390833306, and under project number 400140256 - GRK2497, and Helmholtz-Gemeinschaft Deutscher Forschungszentren, Germany; the General Secretariat for Research and Innovation and the Hellenic Foundation for Research and Innovation (HFRI), Project Number 2288, Greece; the National Research, Development and Innovation Office (NKFIH), Hungary; the Department of Atomic Energy and the Department of Science and Technology, India; the Institute for Studies in Theoretical Physics and Mathematics, Iran; the Science Foundation, Ireland; the Istituto Nazionale di Fisica Nucleare, Italy; the Ministry of Science, ICT and Future Planning, and National Research Foundation (NRF), Republic of Korea; the Ministry of Education and Science of the Republic of Latvia; the Research Council of Lithuania, agreement No. VS-19 (LMTLT); the Ministry of Education, and University of Malaya (Malaysia); the Ministry of Science of Montenegro; the Mexican Funding Agencies (BUAP, CINVESTAV, CONACYT, LNS, SEP, and UASLP-FAI); the Ministry of Business, Innovation and Employment, New Zealand; the Pakistan Atomic Energy Commission; the Ministry of Education and Science and the National Science Centre, Poland; the Fundação para a Ciência e a Tecnologia, grants CERN/FIS-PAR/0025/2019 and CERN/FIS-INS/0032/2019, Portugal; the Ministry of Education, Science and Technological Development of Serbia; MCIN/AEI/10.13039/501100011033, ERDF "a way of making Europe", Programa Estatal de Fomento de la Investigación Científica y Técnica de Excelencia María de Maeztu, grant MDM-2017-0765, projects PID2020-113705RB, PID2020-113304RB, PID2020-116262RB and PID2020-113341RB-I00, and Plan de Ciencia, Tecnología e Innovación de Asturias, Spain; the Ministry of Science, Technology and Research, Sri Lanka; the Swiss Funding Agencies (ETH Board, ETH Zurich, PSI, SNF, UniZH, Canton Zurich, and SER); the Ministry of Science and Technology, Taipei; the Ministry of Higher Education, Science, Research and Innovation, and the National Science and Technology Development Agency of Thailand; the Scientific and Technical Research Council of Turkey, and Turkish Energy, Nuclear and Mineral Research Agency; the National Academy of Sciences of Ukraine; the Science and Technology Facilities Council, UK; the US Department of Energy, and the US National Science Foundation.

Individuals have received support from the Marie-Curie programme and the European Research Council and Horizon 2020 Grant, contract Nos. 675440, 724704, 752730, 758316, 765710, 824093, 101115353, 101002207, and COST Action CA16108 (European Union) the Leventis Foundation; the Alfred P. Sloan Foundation; the Alexander von Humboldt Foundation; the Belgian Federal Science Policy Office; the Fonds pour la Formation à la Recherche dans l'Industrie

et dans l’Agriculture (FRIA-Belgium); the Agentschap voor Innovatie door Wetenschap en Technologie (IWT-Belgium); the F.R.S.-FNRS and FWO (Belgium) under the “Excellence of Science – EOS” – be.h project n. 30820817; the Beijing Municipal Science & Technology Commission, No. Z191100007219010 and USTC Research Funds of the Double First-Class Initiative No. YD2030002017 (China); the Ministry of Education, Youth and Sports (MEYS) of the Czech Republic; the Shota Rustaveli National Science Foundation, grant FR-22-985 (Georgia); the Hungarian Academy of Sciences, the New National Excellence Program - ÚNKP, the NKFIH research grants K 131991, K 133046, K 138136, K 143460, K 143477, K 146913, K 146914, K 147048, 2020-2.2.1-ED-2021-00181, and TKP2021-NKTA-64 (Hungary); the Council of Scientific and Industrial Research, India; ICSC – National Research Centre for High Performance Computing, Big Data and Quantum Computing, funded by the EU NexGeneration program, Italy; the Latvian Council of Science; the Ministry of Education and Science, project no. 2022/WK/14, and the National Science Center, contracts Opus 2021/41/B/ST2/01369 and 2021/43/B/ST2/01552 (Poland); the Fundação para a Ciência e a Tecnologia, grant FCT CEECIND/01334/2018; the National Priorities Research Program by Qatar National Research Fund; the Programa Estatal de Fomento de la Investigación Científica y Técnica de Excelencia María de Maeztu, grant MDM-2017-0765 and projects PID2020-113705RB, PID2020-113304RB, PID2020-116262RB and PID2020-113341RB-I00, and Programa Severo Ochoa del Principado de Asturias (Spain); the Chulalongkorn Academic into Its 2nd Century Project Advancement Project, and the National Science, Research and Innovation Fund via the Program Management Unit for Human Resources & Institutional Development, Research and Innovation, grant B37G660013 (Thailand); the Kavli Foundation; the Nvidia Corporation; the SuperMicro Corporation; the Welch Foundation, contract C-1845; and the Weston Havens Foundation (USA).

## References

- [1] ATLAS Collaboration, “Observation of a new particle in the search for the standard model Higgs boson with the ATLAS detector at the LHC”, *Phys. Lett. B* **716** (2012) 1, doi:10.1016/j.physletb.2012.08.020, arXiv:1207.7214.
- [2] CMS Collaboration, “Observation of a new boson at a mass of 125 GeV with the CMS experiment at the LHC”, *Phys. Lett. B* **716** (2012) 30, doi:10.1016/j.physletb.2012.08.021, arXiv:1207.7235.
- [3] CMS Collaboration, “Observation of a new boson with mass near 125 GeV in pp collisions at  $\sqrt{s} = 7$  and 8 TeV”, *JHEP* **06** (2013) 081, doi:10.1007/JHEP06(2013)081, arXiv:1303.4571.
- [4] CMS Collaboration, “A portrait of the Higgs boson by the CMS experiment ten years after the discovery”, *Nature* **607** (2022) 60, doi:10.1038/s41586-022-04892-x, arXiv:2207.00043.
- [5] T. D. Lee, “A theory of spontaneous  $T$  violation”, *Phys. Rev. D* **8** (1973) 1226, doi:10.1103/PhysRevD.8.1226.
- [6] G. C. Branco et al., “Theory and phenomenology of two-Higgs-doublet models”, *Phys. Rept.* **516** (2012) 1, doi:10.1016/j.physrep.2012.02.002, arXiv:1106.0034.
- [7] H. E. Haber and O. Stål, “New LHC benchmarks for the  $\mathcal{CP}$ -conserving two-Higgs-doublet model”, *Eur. Phys. J. C* **75** (2015) 491, doi:10.1140/epjc/s10052-015-3697-x, arXiv:1507.04281. [Erratum: doi:10.1140/epjc/s10052-016-4151-4].

- [8] F. Kling, J. M. No, and S. Su, “Anatomy of exotic Higgs decays in 2HDM”, *JHEP* **09** (2016) 093, doi:10.1007/JHEP09(2016)093, arXiv:1604.01406.
- [9] G. Chalons and F. Domingo, “Analysis of the Higgs potentials for two doublets and a singlet”, *Phys. Rev. D* **86** (2012) 115024, doi:10.1103/PhysRevD.86.115024, arXiv:1209.6235.
- [10] C.-Y. Chen, M. Freid, and M. Sher, “Next-to-minimal two Higgs doublet model”, *Phys. Rev. D* **89** (2014) 075009, doi:10.1103/PhysRevD.89.075009, arXiv:1312.3949.
- [11] M. Mühlleitner, M. O. P. Sampaio, R. Santos, and J. Wittbrodt, “The N2HDM under theoretical and experimental scrutiny”, *JHEP* **03** (2017) 094, doi:10.1007/JHEP03(2017)094, arXiv:1612.01309.
- [12] T. Robens, T. Stefaniak, and J. Wittbrodt, “Two-real-scalar-singlet extension of the SM: LHC phenomenology and benchmark scenarios”, *Eur. Phys. J. C* **80** (2020) 151, doi:10.1140/epjc/s10052-020-7655-x, arXiv:1908.08554.
- [13] J. F. Gunion and H. E. Haber, “Higgs bosons in supersymmetric models (I)”, *Nucl. Phys. B* **272** (1986) 1, doi:10.1016/0550-3213(86)90340-8.
- [14] J. F. Gunion and H. E. Haber, “Higgs bosons in supersymmetric models (II). Implications for phenomenology”, *Nucl. Phys. B* **278** (1986) 449, doi:10.1016/0550-3213(86)90050-7. [Erratum: doi:10.1016/0550-3213(93)90654-8].
- [15] G. Degrassi et al., “Towards high precision predictions for the MSSM Higgs sector”, *Eur. Phys. J. C* **28** (2003) 133, doi:10.1140/epjc/s2003-01152-2, arXiv:hep-ph/0212020.
- [16] A. Djouadi, “The anatomy of electroweak symmetry breaking Tome II: The Higgs bosons in the minimal supersymmetric model”, *Phys. Rept.* **459** (2008) 1, doi:10.1016/j.physrep.2007.10.005, arXiv:hep-ph/0503173.
- [17] M. Maniatis, “The next-to-minimal supersymmetric extension of the standard model reviewed”, *Int. J. Mod. Phys. A* **25** (2010) 3505, doi:10.1142/S0217751X10049827, arXiv:0906.0777.
- [18] U. Ellwanger, C. Hugonie, and A. M. Teixeira, “The next-to-minimal supersymmetric standard model”, *Phys. Rept.* **496** (2010) 1, doi:10.1016/j.physrep.2010.07.001, arXiv:0910.1785.
- [19] S. F. King, M. Mühlleitner, and R. Nevzorov, “NMSSM Higgs benchmarks near 125 GeV”, *Nucl. Phys. B* **860** (2012) 207, doi:10.1016/j.nuclphysb.2012.02.010, arXiv:1201.2671.
- [20] L. Randall and R. Sundrum, “Large mass hierarchy from a small extra dimension”, *Phys. Rev. Lett.* **83** (1999) 3370, doi:10.1103/PhysRevLett.83.3370, arXiv:hep-ph/9905221.
- [21] W. D. Goldberger and M. B. Wise, “Modulus stabilization with bulk fields”, *Phys. Rev. Lett.* **83** (1999) 4922, doi:10.1103/PhysRevLett.83.4922, arXiv:hep-ph/9907447.

- [22] O. DeWolfe, D. Z. Freedman, S. S. Gubser, and A. Karch, “Modeling the fifth dimension with scalars and gravity”, *Phys. Rev. D* **62** (2000) 046008, doi:10.1103/PhysRevD.62.046008, arXiv:hep-th/9909134.
- [23] C. Csáki, M. Graesser, L. Randall, and J. Terning, “Cosmology of brane models with radion stabilization”, *Phys. Rev. D* **62** (2000) 045015, doi:10.1103/PhysRevD.62.045015, arXiv:hep-ph/9911406.
- [24] H. Davoudiasl, J. L. Hewett, and T. G. Rizzo, “Phenomenology of the Randall–Sundrum gauge hierarchy model”, *Phys. Rev. Lett.* **84** (2000) 2080, doi:10.1103/PhysRevLett.84.2080, arXiv:hep-ph/9909255.
- [25] C. Csaki, M. L. Graesser, and G. D. Kribs, “Radion dynamics and electroweak physics”, *Phys. Rev. D* **63** (2001) 065002, doi:10.1103/PhysRevD.63.065002, arXiv:hep-th/0008151.
- [26] K. Agashe, H. Davoudiasl, G. Perez, and A. Soni, “Warped gravitons at the CERN LHC and beyond”, *Phys. Rev. D* **76** (2007) 036006, doi:10.1103/PhysRevD.76.036006, arXiv:hep-ph/0701186.
- [27] A. L. Fitzpatrick, J. Kaplan, L. Randall, and L.-T. Wang, “Searching for the Kaluza-Klein graviton in bulk RS models”, *JHEP* **09** (2007) 013, doi:10.1088/1126-6708/2007/09/013, arXiv:hep-ph/0701150.
- [28] A. Oliveira, “Gravity particles from warped extra dimensions, predictions for LHC”, 2014. arXiv:1404.0102.
- [29] G. F. Giudice, R. Rattazzi, and J. D. Wells, “Graviscalars from higher-dimensional metrics and curvature-Higgs mixing”, *Nucl. Phys. B* **595** (2001) 250, doi:10.1016/S0550-3213(00)00686-6, arXiv:hep-ph/0002178.
- [30] D. Pappadopulo, A. Thamm, R. Torre, and A. Wulzer, “Heavy vector triplets: Bridging theory and data”, *JHEP* **09** (2014) 060, doi:10.1007/JHEP09(2014)060, arXiv:1402.4431.
- [31] “HEPData record for this analysis”, 2024. doi:10.17182/hepdata.146897.
- [32] P. W. Higgs, “Broken symmetries, massless particles and gauge fields”, *Phys. Lett.* **12** (1964) 132, doi:10.1016/0031-9163(64)91136-9.
- [33] P. W. Higgs, “Spontaneous symmetry breakdown without massless bosons”, *Phys. Rev.* **145** (1966) 1156, doi:10.1103/PhysRev.145.1156.
- [34] F. Englert and R. Brout, “Broken symmetry and the mass of gauge vector mesons”, *Phys. Rev. Lett.* **13** (1964) 321, doi:10.1103/PhysRevLett.13.321.
- [35] M. Cepeda et al., “Handbook of LHC Higgs cross sections: 4. Deciphering the nature of the Higgs sector”, CERN Report CERN-2017-002-M, 2016. doi:10.23731/CYRM-2017-002, arXiv:1610.07922.
- [36] ATLAS Collaboration, “Measurement of the Higgs boson mass with  $H \rightarrow \gamma\gamma$  decays in  $140 \text{ fb}^{-1}$  of  $\sqrt{s} = 13 \text{ TeV}$  pp collisions with the ATLAS detector”, *Phys. Lett. B* **847** (2023) 138315, doi:10.1016/j.physletb.2023.138315, arXiv:2308.07216.

- [37] CMS Collaboration, “Measurement of the Higgs boson width and evidence of its off-shell contributions to ZZ production”, *Nature Phys.* **18** (2022) 1329, doi:10.1038/s41567-022-01682-0, arXiv:2202.06923.
- [38] LHC Higgs Cross Section Working Group, “Handbook of LHC Higgs Cross Sections: 3. Higgs Properties: Report of the LHC Higgs Cross Section Working Group”. Number CERN-2013-004 in CERN Yellow Reports: Monographs. CERN, 2013. doi:10.5170/CERN-2013-004.
- [39] F. Bezrukov and M. Shaposhnikov, “Inflation, LHC and the Higgs boson”, *C. R. Phys.* **16** (2015) 994, doi:10.1016/j.crhy.2015.08.005.
- [40] F. L. Bezrukov and M. Shaposhnikov, “The standard model Higgs boson as the inflaton”, *Phys. Lett. B* **659** (2008) 703, doi:10.1016/j.physletb.2007.11.072, arXiv:0710.3755.
- [41] Y. Hamada and M. Yamada, “Baryogenesis in false vacuum”, *Eur. Phys. J. C* **77** (2017) 643, doi:10.1140/epjc/s10052-017-5215-9, arXiv:1605.06897.
- [42] I. P. Ivanov, “Building and testing models with extended Higgs sectors”, *Prog. Part. Nucl. Phys.* **95** (2017) 160, doi:10.1016/j.ppnp.2017.03.001, arXiv:1702.03776.
- [43] S. Dawson, C. Englert, and T. Plehn, “Higgs Physics: It ain’t over till it’s over”, *Phys. Rept.* **816** (2019) 1, doi:10.1016/j.physrep.2019.05.001, arXiv:1808.01324.
- [44] J. Steggemann, “Extended scalar sectors”, *Ann. Rev. Nucl. Part. Sci.* **70** (2020) 197, doi:10.1146/annurev-nucl-032620-043846.
- [45] Particle Data Group, “Review of particle physics”, *Prog. Theor. Exp. Phys.* **2022** (2022) 083C01, doi:10.1093/ptep/ptac097.
- [46] C. Englert et al., “Precision measurements of Higgs couplings: Implications for new physics scales”, *J. Phys. G* **41** (2014) 113001, doi:10.1088/0954-3899/41/11/113001, arXiv:1403.7191.
- [47] CMS Collaboration, “Combined measurements of Higgs boson couplings in proton–proton collisions at  $\sqrt{s} = 13$  TeV”, *Eur. Phys. J. C* **79** (2019) 421, doi:10.1140/epjc/s10052-019-6909-y, arXiv:1809.10733.
- [48] ATLAS Collaboration, “Combined measurements of Higgs boson production and decay using up to  $80 \text{ fb}^{-1}$  of proton-proton collision data at  $\sqrt{s} = 13$  TeV collected with the ATLAS experiment”, *Phys. Rev. D* **101** (2020) 012002, doi:10.1103/PhysRevD.101.012002, arXiv:1909.02845.
- [49] ATLAS Collaboration, “A detailed map of Higgs boson interactions by the ATLAS experiment ten years after the discovery”, *Nature* **607** (2022) 52, doi:10.1038/s41586-022-04893-w, arXiv:2207.00092. [Erratum: doi:10.1038/s41586-022-05581-5].
- [50] A. Datta and A. Raychaudhuri, “Next-to-minimal Higgs: Mass bounds and search prospects”, *Phys. Rev. D* **57** (1998) 2940, doi:10.1103/PhysRevD.57.2940, arXiv:hep-ph/9708444.

- [51] V. Barger et al., “Complex singlet extension of the standard model”, *Phys. Rev. D* **79** (2009) 015018, doi:10.1103/PhysRevD.79.015018, arXiv:0811.0393.
- [52] R. Costa, M. Mühlleitner, M. O. P. Sampaio, and R. Santos, “Singlet extensions of the standard model at LHC Run 2: Benchmarks and comparison with the NMSSM”, *JHEP* **06** (2016) 034, doi:10.1007/JHEP06(2016)034, arXiv:1512.05355.
- [53] T. Robens and T. Stefaniak, “Status of the Higgs singlet extension of the standard model after LHC Run 1”, *Eur. Phys. J. C* **75** (2015) 104, doi:10.1140/epjc/s10052-015-3323-y, arXiv:1501.02234.
- [54] J. Haller et al., “Update of the global electroweak fit and constraints on two-Higgs-doublet models”, *Eur. Phys. J. C* **78** (2018) 675, doi:10.1140/epjc/s10052-018-6131-3, arXiv:1803.01853.
- [55] D. Eriksson, J. Rathsman, and O. Stal, “2HDMC: Two-Higgs-doublet model calculator physics and manual”, *Comput. Phys. Commun.* **181** (2010) 189, doi:10.1016/j.cpc.2009.09.011, arXiv:0902.0851.
- [56] R. Harlander et al., “Interim recommendations for the evaluation of Higgs production cross sections and branching ratios at the LHC in the two-Higgs-doublet model”, 2013. arXiv:1312.5571.
- [57] A. Djouadi and J. Quevillon, “The MSSM Higgs sector at a high  $M_{\text{SUSY}}$ : Reopening the low  $\tan \beta$  regime and heavy Higgs searches”, *JHEP* **10** (2013) 028, doi:10.1007/JHEP10(2013)028, arXiv:1304.1787.
- [58] A. Djouadi et al., “The post-Higgs MSSM scenario: Habemus MSSM?”, *Eur. Phys. J. C* **73** (2013) 2650, doi:10.1140/epjc/s10052-013-2650-0, arXiv:1307.5205.
- [59] A. Djouadi et al., “Fully covering the MSSM Higgs sector at the LHC”, *JHEP* **06** (2015) 168, doi:10.1007/JHEP06(2015)168, arXiv:1502.05653.
- [60] H. Bahl, S. Liebler, and T. Stefaniak, “MSSM Higgs benchmark scenarios for Run 2 and beyond: The low  $\tan \beta$  region”, *Eur. Phys. J. C* **79** (2019) 279, doi:10.1140/epjc/s10052-019-6770-z, arXiv:1901.05933.
- [61] E. A. Bagnaschi et al., “Benchmark scenarios for MSSM Higgs boson searches at the LHC”, Technical Report LHCHWG-2021-001, 2021.
- [62] LHC Higgs Working Group – MSSM subgroup, “LHCHWG MSSM ROOT files”, 2022.
- [63] E. Bagnaschi et al., “MSSM Higgs boson searches at the LHC: Benchmark scenarios for Run 2 and beyond”, *Eur. Phys. J. C* **79** (2019) 617, doi:10.1140/epjc/s10052-019-7114-8, arXiv:1808.07542.
- [64] CMS Collaboration, “Searches for additional Higgs bosons and for vector leptoquarks in  $\tau\tau$  final states in proton-proton collisions at  $\sqrt{s} = 13$  TeV”, *JHEP* **07** (2023) 073, doi:10.1007/JHEP07(2023)073, arXiv:2208.02717.
- [65] I. Engeln, M. Mühlleitner, and J. Wittbrodt, “N2HDECAY: Higgs boson decays in the different phases of the N2HDM”, *Comput. Phys. Commun.* **234** (2019) 256, doi:10.1016/j.cpc.2018.07.020, arXiv:1805.00966.

- [66] H. Abouabid et al., “Benchmarking di-Higgs production in various extended Higgs sector models”, *JHEP* **09** (2022) 011, doi:10.1007/JHEP09(2022)011, arXiv:2112.12515.
- [67] S. Baum and N. R. Shah, “Two Higgs doublets and a complex singlet: Disentangling the decay topologies and associated phenomenology”, *JHEP* **12** (2018) 044, doi:10.1007/JHEP12(2018)044, arXiv:1808.02667.
- [68] U. Ellwanger and M. Rodriguez-Vazquez, “Simultaneous search for extra light and heavy Higgs bosons via cascade decays”, *JHEP* **11** (2017) 008, doi:10.1007/JHEP11(2017)008, arXiv:1707.08522.
- [69] S. Baum, N. R. Shah, and K. Freese, “The NMSSM is within reach of the LHC: Mass correlations & decay signatures”, *JHEP* **04** (2019) 011, doi:10.1007/JHEP04(2019)011, arXiv:1901.02332.
- [70] D. Dominici, B. Grzadkowski, J. F. Gunion, and M. Toharia, “The scalar sector of the Randall–Sundrum model”, *Nucl. Phys. B* **671** (2003) 243, doi:10.1016/j.nuclphysb.2003.08.020, arXiv:hep-ph/0206192.
- [71] I. Antoniadis and R. Sturani, “Higgs graviscalar mixing in type I string theory”, *Nucl. Phys. B* **631** (2002) 66, doi:10.1016/S0550-3213(02)00214-6, arXiv:hep-th/0201166.
- [72] N. Desai, U. Maitra, and B. Mukhopadhyaya, “An updated analysis of radion-Higgs mixing in the light of LHC data”, *JHEP* **10** (2013) 093, doi:10.1007/JHEP10(2013)093, arXiv:1307.3765.
- [73] A. Oliveira and R. Rosenfeld, “Graviscalars from higherdimensional metrics and curvature-Higgs mixing”, *Phys. Lett. B* **702** (2011) 201, doi:10.1016/j.physletb.2011.06.086, arXiv:1009.4497.
- [74] CMS Collaboration, “Search for high-mass resonances in dilepton final states in proton-proton collisions at  $\sqrt{s} = 13$  TeV”, *JHEP* **06** (2018) 120, doi:10.1007/JHEP06(2018)120, arXiv:1803.06292.
- [75] C. Grojean, E. Salvioni, and R. Torre, “A weakly constrained  $W'$  at the early LHC”, *JHEP* **07** (2011) 002, doi:10.1007/JHEP07(2011)002, arXiv:1103.2761.
- [76] E. Salvioni, G. Villadoro, and F. Zwirner, “Minimal  $Z'$  models: Present bounds and early LHC reach”, *JHEP* **11** (2009) 068, doi:10.1088/1126-6708/2009/11/068, arXiv:0909.1320.
- [77] G. Altarelli, B. Mele, and M. Ruiz-Altaba, “Searching for new heavy vector bosons in  $p\bar{p}$  colliders”, *Z. Phys. C* **45** (1989) 109, doi:10.1007/BF01556677. [Erratum: doi:10.1007/BF01552335].
- [78] M. Schmaltz and D. Tucker-Smith, “Little Higgs review”, *Ann. Rev. Nucl. Part. Sci.* **55** (2005) 229, doi:10.1146/annurev.nucl.55.090704.151502, arXiv:hep-ph/0502182.
- [79] N. Arkani-Hamed, A. G. Cohen, E. Katz, and A. E. Nelson, “The littlest Higgs”, *JHEP* **07** (2002) 034, doi:10.1088/1126-6708/2002/07/034, arXiv:hep-ph/0206021.

- [80] B. Bellazzini, C. Csáki, and J. Serra, “Composite Higgses”, *Eur. Phys. J. C* **74** (2014) 2766, doi:[10.1140/epjc/s10052-014-2766-x](https://doi.org/10.1140/epjc/s10052-014-2766-x), arXiv:[1401.2457](https://arxiv.org/abs/1401.2457).
- [81] R. Contino, D. Marzocca, D. Pappadopulo, and R. Rattazzi, “On the effect of resonances in composite Higgs phenomenology”, *JHEP* **10** (2011) 081, doi:[10.1007/JHEP10\(2011\)081](https://doi.org/10.1007/JHEP10(2011)081), arXiv:[1109.1570](https://arxiv.org/abs/1109.1570).
- [82] D. Marzocca, M. Serone, and J. Shu, “General composite Higgs models”, *JHEP* **08** (2012) 013, doi:[10.1007/JHEP08\(2012\)013](https://doi.org/10.1007/JHEP08(2012)013), arXiv:[1205.0770](https://arxiv.org/abs/1205.0770).
- [83] D. Greco and D. Liu, “Hunting composite vector resonances at the LHC: Naturalness facing data”, *JHEP* **12** (2014) 126, doi:[10.1007/JHEP12\(2014\)126](https://doi.org/10.1007/JHEP12(2014)126), arXiv:[1410.2883](https://arxiv.org/abs/1410.2883).
- [84] K. Lane and L. Pritchett, “The light composite Higgs boson in strong extended technicolor”, *JHEP* **06** (2017) 140, doi:[10.1007/JHEP06\(2017\)140](https://doi.org/10.1007/JHEP06(2017)140), arXiv:[1604.07085](https://arxiv.org/abs/1604.07085).
- [85] V. D. Barger, W.-Y. Keung, and E. Ma, “A gauge model with light W and Z bosons”, *Phys. Rev. D* **22** (1980) 727, doi:[10.1103/PhysRevD.22.727](https://doi.org/10.1103/PhysRevD.22.727).
- [86] CMS Collaboration, “Search for heavy resonances decaying into two Higgs bosons or into a Higgs boson and a W or Z boson in proton-proton collisions at 13 TeV”, *JHEP* **01** (2019) 051, doi:[10.1007/JHEP01\(2019\)051](https://doi.org/10.1007/JHEP01(2019)051), arXiv:[1808.01365](https://arxiv.org/abs/1808.01365).
- [87] CMS Collaboration, “Search for heavy resonances decaying into a vector boson and a Higgs boson in final states with charged leptons, neutrinos and b quarks at  $\sqrt{s} = 13 \text{ TeV}$ ”, *JHEP* **11** (2018) 172, doi:[10.1007/JHEP11\(2018\)172](https://doi.org/10.1007/JHEP11(2018)172), arXiv:[1807.02826](https://arxiv.org/abs/1807.02826).
- [88] CMS Collaboration, “Search for heavy resonances that decay into a vector boson and a Higgs boson in hadronic final states at  $\sqrt{s} = 13 \text{ TeV}$ ”, *Eur. Phys. J. C* **77** (2017) 636, doi:[10.1140/epjc/s10052-017-5192-z](https://doi.org/10.1140/epjc/s10052-017-5192-z), arXiv:[1707.01303](https://arxiv.org/abs/1707.01303).
- [89] CMS Collaboration, “Search for heavy resonances decaying into a vector boson and a Higgs boson in final states with charged leptons, neutrinos, and b quarks”, *Phys. Lett. B* **768** (2017) 137, doi:[10.1016/j.physletb.2017.02.040](https://doi.org/10.1016/j.physletb.2017.02.040), arXiv:[1610.08066](https://arxiv.org/abs/1610.08066).
- [90] CMS Collaboration, “Search for massive WH resonances decaying into the  $\ell\nu b\bar{b}$  final state at  $\sqrt{s} = 8 \text{ TeV}$ ”, *Eur. Phys. J. C* **76** (2016) 237, doi:[10.1140/epjc/s10052-016-4067-z](https://doi.org/10.1140/epjc/s10052-016-4067-z), arXiv:[1601.06431](https://arxiv.org/abs/1601.06431).
- [91] CMS Collaboration, “Search for a massive resonance decaying into a Higgs boson and a W or Z boson in hadronic final states in proton-proton collisions at  $\sqrt{s} = 8 \text{ TeV}$ ”, *JHEP* **02** (2016) 145, doi:[10.1007/JHEP02\(2016\)145](https://doi.org/10.1007/JHEP02(2016)145), arXiv:[1506.01443](https://arxiv.org/abs/1506.01443).
- [92] CMS Collaboration, “Search for narrow high-mass resonances in proton-proton collisions at  $\sqrt{s} = 8 \text{ TeV}$  decaying to a Z and a Higgs boson”, *Phys. Lett. B* **748** (2015) 255, doi:[10.1016/j.physletb.2015.07.011](https://doi.org/10.1016/j.physletb.2015.07.011), arXiv:[1502.04994](https://arxiv.org/abs/1502.04994).
- [93] ATLAS Collaboration, “Search for heavy resonances decaying into a Z or W boson and a Higgs boson in final states with leptons and b jets in  $139 \text{ fb}^{-1}$  of pp collisions at  $\sqrt{s} = 13 \text{ TeV}$  with the ATLAS detector”, *JHEP* **06** (2023) 016, doi:[10.1007/JHEP06\(2023\)016](https://doi.org/10.1007/JHEP06(2023)016), arXiv:[2207.00230](https://arxiv.org/abs/2207.00230).

- [94] ATLAS Collaboration, “Search for resonances decaying into a weak vector boson and a Higgs boson in the fully hadronic final state produced in proton–proton collisions at  $\sqrt{s} = 13$  TeV with the ATLAS detector”, *Phys. Rev. D* **102** (2020) 112008, doi:10.1103/PhysRevD.102.112008, arXiv:2007.05293.
- [95] ATLAS Collaboration, “Combination of searches for heavy resonances decaying into bosonic and leptonic final states using  $36\text{ fb}^{-1}$  of proton-proton collision data at  $\sqrt{s} = 13$  TeV with the ATLAS detector”, *Phys. Rev. D* **98** (2018) 052008, doi:10.1103/PhysRevD.98.052008, arXiv:1808.02380.
- [96] ATLAS Collaboration, “Search for heavy resonances decaying to a photon and a hadronically decaying Z/W/H boson in pp collisions at  $\sqrt{s} = 13$  TeV with the ATLAS detector”, *Phys. Rev. D* **98** (2018) 032015, doi:10.1103/PhysRevD.98.032015, arXiv:1805.01908.
- [97] ATLAS Collaboration, “Search for heavy resonances decaying into a W or Z boson and a Higgs boson in final states with leptons and b-jets in  $36\text{ fb}^{-1}$  of  $\sqrt{s} = 13$  TeV pp collisions with the ATLAS detector”, *JHEP* **03** (2018) 174, doi:10.1007/JHEP03(2018)174, arXiv:1712.06518. [Erratum: doi:10.1007/JHEP11(2018)051].
- [98] ATLAS Collaboration, “Search for a new resonance decaying to a W or Z boson and a Higgs boson in the  $\ell\ell/\ell\nu/\nu\nu + b\bar{b}$  final states with the ATLAS detector”, *Eur. Phys. J. C* **75** (2015) 263, doi:10.1140/epjc/s10052-015-3474-x, arXiv:1503.08089.
- [99] ATLAS Collaboration, “Search for new resonances decaying to a W or Z boson and a Higgs boson in the  $\ell^+\ell^-b\bar{b}$ ,  $\ell v b\bar{b}$ , and  $\nu\bar{\nu} b\bar{b}$  channels with pp collisions at  $\sqrt{s} = 13$  TeV with the ATLAS detector”, *Phys. Lett. B* **765** (2017) 32, doi:10.1016/j.physletb.2016.11.045, arXiv:1607.05621.
- [100] ATLAS Collaboration, “Search for high-mass diboson resonances with boson-tagged jets in proton-proton collisions at  $\sqrt{s} = 8$  TeV with the ATLAS detector”, *JHEP* **12** (2015) 055, doi:10.1007/JHEP12(2015)055, arXiv:1506.00962.
- [101] ATLAS Collaboration, “Search for a heavy Higgs boson decaying into a Z boson and another heavy Higgs boson in the  $\ell\ell bb$  and  $\ell\ell WW$  final states in pp collisions at  $\sqrt{s} = 13$  TeV with the ATLAS detector”, *Eur. Phys. J. C* **81** (2021) 396, doi:10.1140/epjc/s10052-021-09117-5, arXiv:2011.05639.
- [102] ATLAS Collaboration, “Search for Higgs boson pair production in the two bottom quarks plus two photons final state in pp collisions at  $\sqrt{s} = 13$  TeV with the ATLAS detector”, *Phys. Rev. D* **106** (2022) 052001, doi:10.1103/PhysRevD.106.052001, arXiv:2112.11876.
- [103] ATLAS Collaboration, “Search for resonant and non-resonant Higgs boson pair production in the  $b\bar{b}\tau^+\tau^-$  decay channel using 13 TeV pp collision data from the ATLAS detector”, *JHEP* **07** (2023) 040, doi:10.1007/JHEP07(2023)040, arXiv:2209.10910.
- [104] ATLAS Collaboration, “Search for resonant pair production of Higgs bosons in the  $b\bar{b}b\bar{b}$  final state using pp collisions at  $\sqrt{s} = 13$  TeV with the ATLAS detector”, *Phys. Rev. D* **105** (2022) 092002, doi:10.1103/PhysRevD.105.092002, arXiv:2202.07288.

- [105] ATLAS Collaboration, “Search for a new heavy scalar particle decaying into a Higgs boson and a new scalar singlet in final states with one or two light leptons and a pair of  $\tau$ -leptons with the ATLAS detector”, *JHEP* **10** (2023) 009, doi:10.1007/JHEP10(2023)009, arXiv:2307.11120.
- [106] ATLAS Collaboration, “Anomaly detection search for new resonances decaying into a Higgs boson and a generic new particle X in hadronic final states using  $\sqrt{s} = 13$  TeV pp collisions with the ATLAS detector”, *Phys. Rev. D* **108** (2023) 052009, doi:10.1103/PhysRevD.108.052009, arXiv:2306.03637.
- [107] CMS Collaboration, “Search for a heavy pseudoscalar Higgs boson decaying into a 125 GeV Higgs boson and a Z boson in final states with two tau and two light leptons at  $\sqrt{s} = 13$  TeV”, *JHEP* **03** (2020) 065, doi:10.1007/JHEP03(2020)065, arXiv:1910.11634.
- [108] CMS Collaboration, “Search for a heavy pseudoscalar boson decaying to a Z and a Higgs boson at  $\sqrt{s} = 13$  TeV”, *Eur. Phys. J. C* **79** (2019) 564, doi:10.1140/epjc/s10052-019-7058-z, arXiv:1903.00941.
- [109] CMS Collaboration, “Search for heavy resonances decaying to WW, WZ, or WH boson pairs in the lepton plus merged jet final state in proton-proton collisions at  $\sqrt{s} = 13$  TeV”, *Phys. Rev. D* **105** (2022) 032008, doi:10.1103/PhysRevD.105.032008, arXiv:2109.06055.
- [110] CMS Collaboration, “Search for a heavy vector resonance decaying to a Z boson and a Higgs boson in proton-proton collisions at  $\sqrt{s} = 13$  TeV”, *Eur. Phys. J. C* **81** (2021) 688, doi:10.1140/epjc/s10052-021-09348-6, arXiv:2102.08198.
- [111] CMS Collaboration, “Search for new heavy resonances decaying to WW, WZ, ZZ, WH, or ZH boson pairs in the all-jets final state in proton-proton collisions at  $\sqrt{s} = 13$  TeV”, *Phys. Lett. B* **844** (2023) 137813, doi:10.1016/j.physletb.2023.137813, arXiv:2210.00043.
- [112] CMS Collaboration, “Search for Higgs boson pair production in the bbWW decay mode in proton-proton collisions at  $\sqrt{s} = 13$  TeV”, 2024. arXiv:2403.09430. Submitted to JHEP.
- [113] CMS Collaboration, “Search for heavy resonances decaying to a pair of Lorentz-boosted higgs bosons in final states with leptons and a bottom quark pair at  $\sqrt{s} = 13$  TeV”, *JHEP* **05** (2022) 005, doi:10.1007/JHEP05(2022)005, arXiv:2112.03161.
- [114] CMS Collaboration, “Search for Higgs boson pairs decaying to WWWW, WW $\tau\tau$ , and  $\tau\tau\tau\tau$  in proton-proton collisions at  $\sqrt{s} = 13$  TeV”, *JHEP* **07** (2023) 095, doi:10.1007/JHEP07(2023)095, arXiv:2206.10268.
- [115] CMS Collaboration, “Search for a heavy Higgs boson decaying into two lighter Higgs bosons in the  $\tau\tau$ bb final state at 13 TeV”, *JHEP* **11** (2021) 057, doi:10.1007/JHEP11(2021)057, arXiv:2106.10361.
- [116] CMS Collaboration, “Search for a new resonance decaying into two spin-0 bosons in a final state with two photons and two bottom quarks in proton-proton collisions at  $\sqrt{s} = 13$  TeV”, 2023. arXiv:2310.01643.

- [117] CMS Collaboration, “Search for a massive scalar resonance decaying to a light scalar and a Higgs boson in the four b quarks final state with boosted topology”, *Phys. Lett. B* **842** (2023) 137392, doi:10.1016/j.physletb.2022.137392, arXiv:2204.12413.
- [118] M. Gouzevitch et al., “Scale-invariant resonance tagging in multijet events and new physics in Higgs pair production”, *JHEP* **07** (2013) 148, doi:10.1007/JHEP07(2013)148, arXiv:1303.6636.
- [119] A. J. Larkoski, I. Moult, and B. Nachman, “Jet substructure at the Large Hadron Collider: A review of recent advances in theory and machine learning”, *Phys. Rept.* **841** (2020) 1, doi:10.1016/j.physrep.2019.11.001, arXiv:1709.04464.
- [120] R. Kogler, B. Nachman, A. Schmidt (editors) et al., “Jet substructure at the Large Hadron Collider”, *Rev. Mod. Phys.* **91** (2019) 045003, doi:10.1103/RevModPhys.91.045003, arXiv:1803.06991.
- [121] R. Kogler, “Advances in jet substructure at the LHC: Algorithms, measurements and searches for new physical phenomena”, volume 284 of *Springer Tracts Mod. Phys.* Springer, 2021. doi:10.1007/978-3-030-72858-8, ISBN 978-3-030-72857-1, 978-3-030-72858-8.
- [122] CMS Collaboration, “The CMS experiment at the CERN LHC”, *JINST* **3** (2008) S08004, doi:10.1088/1748-0221/3/08/S08004.
- [123] CMS Collaboration, “Performance of the CMS Level-1 trigger in proton-proton collisions at  $\sqrt{s} = 13 \text{ TeV}$ ”, *JINST* **15** (2020) P10017, doi:10.1088/1748-0221/15/10/P10017, arXiv:2006.10165.
- [124] CMS Collaboration, “The CMS trigger system”, *JINST* **12** (2017) P01020, doi:10.1088/1748-0221/12/01/P01020, arXiv:1609.02366.
- [125] CMS Collaboration, “Particle-flow reconstruction and global event description with the CMS detector”, *JINST* **12** (2017) P10003, doi:10.1088/1748-0221/12/10/P10003, arXiv:1706.04965.
- [126] CMS Collaboration, “Technical proposal for the Phase-II upgrade of the Compact Muon Solenoid”, CMS Technical Proposal CMS-TDR-15-02, 2015.
- [127] M. Cacciari, G. P. Salam, and G. Soyez, “The anti- $k_T$  jet clustering algorithm”, *JHEP* **04** (2008) 063, doi:10.1088/1126-6708/2008/04/063, arXiv:0802.1189.
- [128] M. Cacciari, G. P. Salam, and G. Soyez, “FastJet user manual”, *Eur. Phys. J. C* **72** (2012) 1896, doi:10.1140/epjc/s10052-012-1896-2, arXiv:1111.6097.
- [129] CMS Collaboration, “Jet energy scale and resolution in the CMS experiment in pp collisions at 8 TeV”, *JINST* **12** (2017) P02014, doi:10.1088/1748-0221/12/02/P02014, arXiv:1607.03663.
- [130] D. Bertolini, P. Harris, M. Low, and N. Tran, “Pileup per particle identification”, *JHEP* **10** (2014) 59, doi:10.1007/JHEP10(2014)059, arXiv:1407.6013.
- [131] CMS Collaboration, “Pileup mitigation at CMS in 13 TeV data”, *JINST* **15** (2020) P09018, doi:10.1088/1748-0221/15/09/P09018, arXiv:2003.00503.

- [132] CMS Collaboration, “Performance of missing transverse momentum reconstruction in proton-proton collisions at  $\sqrt{s} = 13$  TeV using the CMS detector”, *JINST* **14** (2019) P07004, doi:[10.1088/1748-0221/14/07/P07004](https://doi.org/10.1088/1748-0221/14/07/P07004), arXiv:[1903.06078](https://arxiv.org/abs/1903.06078).
- [133] CMS Collaboration, “Jet algorithms performance in 13 TeV data”, CMS Physics Analysis Summary CMS-PAS-JME-16-003, 2017.
- [134] A. J. Larkoski, S. Marzani, G. Soyez, and J. Thaler, “Soft drop”, *JHEP* **05** (2014) 146, doi:[10.1007/JHEP05\(2014\)146](https://doi.org/10.1007/JHEP05(2014)146), arXiv:[1402.2657](https://arxiv.org/abs/1402.2657).
- [135] M. Dasgupta, A. Fregoso, S. Marzani, and G. P. Salam, “Towards an understanding of jet substructure”, *JHEP* **09** (2013) 029, doi:[10.1007/JHEP09\(2013\)029](https://doi.org/10.1007/JHEP09(2013)029), arXiv:[1307.0007](https://arxiv.org/abs/1307.0007).
- [136] J. M. Butterworth, A. R. Davison, M. Rubin, and G. P. Salam, “Jet substructure as a new Higgs search channel at the LHC”, *Phys. Rev. Lett.* **100** (2008) 242001, doi:[10.1103/PhysRevLett.100.242001](https://doi.org/10.1103/PhysRevLett.100.242001), arXiv:[0802.2470](https://arxiv.org/abs/0802.2470).
- [137] CMS Collaboration, “Identification of heavy-flavour jets with the CMS detector in pp collisions at 13 TeV”, *JINST* **13** (2018) P05011, doi:[10.1088/1748-0221/13/05/P05011](https://doi.org/10.1088/1748-0221/13/05/P05011), arXiv:[1712.07158](https://arxiv.org/abs/1712.07158).
- [138] E. Bols et al., “Jet flavour classification using DeepJet”, *JINST* **15** (2020) P12012, doi:[10.1088/1748-0221/15/12/P12012](https://doi.org/10.1088/1748-0221/15/12/P12012), arXiv:[2008.10519](https://arxiv.org/abs/2008.10519).
- [139] Y. L. Dokshitzer, G. D. Leder, S. Moretti, and B. R. Webber, “Better jet clustering algorithms”, *JHEP* **08** (1997) 001, doi:[10.1088/1126-6708/1997/08/001](https://doi.org/10.1088/1126-6708/1997/08/001), arXiv:[hep-ph/9707323](https://arxiv.org/abs/hep-ph/9707323).
- [140] M. Wobisch and T. Wengler, “Hadronization corrections to jet cross-sections in deep inelastic scattering”, in *Workshop on Monte Carlo Generators for HERA Physics*, p. 270. 1998. arXiv:[hep-ph/9907280](https://arxiv.org/abs/hep-ph/9907280).
- [141] CMS Collaboration, “Identification of heavy, energetic, hadronically decaying particles using machine-learning techniques”, *JINST* **15** (2020) P06005, doi:[10.1088/1748-0221/15/06/P06005](https://doi.org/10.1088/1748-0221/15/06/P06005), arXiv:[2004.08262](https://arxiv.org/abs/2004.08262).
- [142] H. Qu and L. Gouskos, “ParticleNet: Jet tagging via particle clouds”, *Phys. Rev. D* **101** (2020) 056019, doi:[10.1103/PhysRevD.101.056019](https://doi.org/10.1103/PhysRevD.101.056019), arXiv:[1902.08570](https://arxiv.org/abs/1902.08570).
- [143] CMS Collaboration, “Performance of the DeepJet b tagging algorithm using  $41.9 \text{ fb}^{-1}$  of data from proton-proton collisions at 13 TeV with Phase 1 CMS detector”, Detector performance note CMS-DP-2018-058, 2018.
- [144] J. Thaler and K. Van Tilburg, “Identifying boosted objects with N-subjettiness”, *JHEP* **03** (2011) 015, doi:[10.1007/JHEP03\(2011\)015](https://doi.org/10.1007/JHEP03(2011)015), arXiv:[1011.2268](https://arxiv.org/abs/1011.2268).
- [145] J. Dolen et al., “Thinking outside the ROCs: Designing decorrelated taggers (DDT) for jet substructure”, *JHEP* **05** (2016) 156, doi:[10.1007/JHEP05\(2016\)156](https://doi.org/10.1007/JHEP05(2016)156), arXiv:[1603.00027](https://arxiv.org/abs/1603.00027).
- [146] CMS Collaboration, “Performance of electron reconstruction and selection with the CMS detector in proton-proton collisions at  $\sqrt{s} = 8$  TeV”, *JINST* **10** (2015) P06005, doi:[10.1088/1748-0221/10/06/P06005](https://doi.org/10.1088/1748-0221/10/06/P06005), arXiv:[1502.02701](https://arxiv.org/abs/1502.02701).

- [147] CMS Collaboration, “Electron and photon reconstruction and identification with the CMS experiment at the CERN LHC”, *JINST* **16** (2021) P05014, doi:10.1088/1748-0221/16/05/P05014, arXiv:2012.06888.
- [148] CMS Collaboration, “Performance of CMS muon reconstruction in pp collision events at  $\sqrt{s} = 7$  TeV”, *JINST* **7** (2012) P10002, doi:10.1088/1748-0221/7/10/P10002, arXiv:1206.4071.
- [149] CMS Collaboration, “Performance of the CMS muon detector and muon reconstruction with proton-proton collisions at  $\sqrt{s} = 13$  TeV”, *JINST* **13** (2018) P06015, doi:10.1088/1748-0221/13/06/P06015, arXiv:1804.04528.
- [150] CMS Collaboration, “Performance of reconstruction and identification of  $\tau$  leptons decaying to hadrons and  $\nu_\tau$  in pp collisions at  $\sqrt{s} = 13$  TeV”, *JINST* **13** (2018) P10005, doi:10.1088/1748-0221/13/10/P10005, arXiv:1809.02816.
- [151] CMS Collaboration, “Identification of hadronic tau lepton decays using a deep neural network”, *JINST* **17** (2022) P07023, doi:10.1088/1748-0221/17/07/P07023, arXiv:2201.08458.
- [152] L. Bianchini et al., “Reconstruction of the Higgs mass in events with Higgs bosons decaying into a pair of  $\tau$  leptons using matrix element techniques”, *Nucl. Instrum. Meth. A* **862** (2017) 54, doi:10.1016/j.nima.2017.05.001, arXiv:1603.05910.
- [153] CMS Collaboration, “Combination of CMS searches for heavy resonances decaying to pairs of bosons or leptons”, *Phys. Lett. B* **798** (2019) 134952, doi:10.1016/j.physletb.2019.134952, arXiv:1906.00057.
- [154] CMS Collaboration, “Search for a heavy resonance decaying into a Z boson and a vector boson in the  $\nu\bar{\nu}q\bar{q}$  final state”, *JHEP* **07** (2018) 075, doi:10.1007/JHEP07(2018)075, arXiv:1803.03838.
- [155] CMS Collaboration, “Search for a heavy resonance decaying into a Z boson and a Z or W boson in  $2\ell 2q$  final states at  $\sqrt{s} = 13$  TeV”, *JHEP* **09** (2018) 101, doi:10.1007/JHEP09(2018)101, arXiv:1803.10093.
- [156] CMS Collaboration, “A multi-dimensional search for new heavy resonances decaying to boosted WW, WZ, or ZZ boson pairs in the dijet final state at 13 TeV”, *Eur. Phys. J. C* **80** (2020) 237, doi:10.1140/epjc/s10052-020-7773-5, arXiv:1906.05977.
- [157] M. Erdmann, E. Geiser, Y. Rath, and M. Rieger, “Lorentz boost networks: Autonomous physics-inspired feature engineering”, *JINST* **14** (2019) P06006, doi:10.1088/1748-0221/14/06/P06006, arXiv:1812.09722.
- [158] CMS Collaboration, “Evidence for associated production of a Higgs boson with a top quark pair in final states with electrons, muons, and hadronically decaying  $\tau$  leptons at  $\sqrt{s} = 13$  TeV”, *JHEP* **08** (2018) 066, doi:10.1007/JHEP08(2018)066, arXiv:1803.05485.
- [159] T. Huang et al., “Resonant di-Higgs boson production in the  $b\bar{b}WW$  channel: Probing the electroweak phase transition at the LHC”, *Phys. Rev. D* **96** (2017) 035007, doi:10.1103/PhysRevD.96.035007, arXiv:1701.04442.

- [160] CMS Collaboration, “Measurements of Higgs boson production in the decay channel with a pair of  $\tau$  leptons in proton-proton collisions at  $\sqrt{s} = 13$  TeV”, *Eur. Phys. J. C* **83** (2023) 562, doi:[10.1140/epjc/s10052-023-11452-8](https://doi.org/10.1140/epjc/s10052-023-11452-8), arXiv:[2204.12957](https://arxiv.org/abs/2204.12957).
- [161] CMS Collaboration, “A deep neural network for simultaneous estimation of b jet energy and resolution”, *Comput. Softw. Big Sci.* **4** (2020) 10, doi:[10.1007/s41781-020-00041-z](https://doi.org/10.1007/s41781-020-00041-z), arXiv:[1912.06046](https://arxiv.org/abs/1912.06046).
- [162] S. Wunsch, R. Friese, R. Wolf, and G. Quast, “Identifying the relevant dependencies of the neural network response on characteristics of the input space”, *Comput. Softw. Big Sci.* **2** (2018) 5, doi:[10.1007/s41781-018-0012-1](https://doi.org/10.1007/s41781-018-0012-1), arXiv:[1803.08782](https://arxiv.org/abs/1803.08782).
- [163] CMS Collaboration, “Observation of the diphoton decay of the Higgs boson and measurement of its properties”, *Eur. Phys. J. C* **74** (2014) 3076, doi:[10.1140/epjc/s10052-014-3076-z](https://doi.org/10.1140/epjc/s10052-014-3076-z), arXiv:[1407.0558](https://arxiv.org/abs/1407.0558).
- [164] CMS Collaboration, “Search for nonresonant Higgs boson pair production in final states with two bottom quarks and two photons in proton-proton collisions at  $\sqrt{s} = 13$  TeV”, *JHEP* **03** (2021) 257, doi:[10.1007/JHEP03\(2021\)257](https://doi.org/10.1007/JHEP03(2021)257), arXiv:[2011.12373](https://arxiv.org/abs/2011.12373).
- [165] T. Junk, “Confidence level computation for combining searches with small statistics”, *Nucl. Instrum. Meth. A* **434** (1999) 435, doi:[10.1016/S0168-9002\(99\)00498-2](https://doi.org/10.1016/S0168-9002(99)00498-2), arXiv:[hep-ex/9902006](https://arxiv.org/abs/hep-ex/9902006).
- [166] A. L. Read, “Presentation of search results: The  $CL_s$  technique”, *J. Phys. G* **28** (2002) 2693, doi:[10.1088/0954-3899/28/10/313](https://doi.org/10.1088/0954-3899/28/10/313).
- [167] G. Cowan, K. Cranmer, E. Gross, and O. Vitells, “Asymptotic formulae for likelihood-based tests of new physics”, *Eur. Phys. J. C* **71** (2011) 1554, doi:[10.1140/epjc/s10052-011-1554-0](https://doi.org/10.1140/epjc/s10052-011-1554-0), arXiv:[1007.1727](https://arxiv.org/abs/1007.1727). [Erratum: doi:[10.1140/epjc/s10052-013-2501-z](https://doi.org/10.1140/epjc/s10052-013-2501-z)].
- [168] ATLAS Collaboration, “Combination of searches for resonant Higgs boson pair production using pp collisions at  $\sqrt{s} = 13$  TeV with the ATLAS detector”, 2023. arXiv:[2311.15956](https://arxiv.org/abs/2311.15956).
- [169] CMS Collaboration, “Search for heavy Higgs bosons decaying to a top quark pair in proton-proton collisions at  $\sqrt{s} = 13$  TeV”, *JHEP* **04** (2020) 171, doi:[10.1007/JHEP04\(2020\)171](https://doi.org/10.1007/JHEP04(2020)171), arXiv:[1908.01115](https://arxiv.org/abs/1908.01115). [Erratum: doi:[10.1007/JHEP03\(2022\)187](https://doi.org/10.1007/JHEP03(2022)187)].
- [170] CMS Collaboration, “Search for a heavy Higgs boson decaying to a pair of W bosons in proton-proton collisions at  $\sqrt{s} = 13$  TeV”, *JHEP* **03** (2020) 034, doi:[10.1007/JHEP03\(2020\)034](https://doi.org/10.1007/JHEP03(2020)034), arXiv:[1912.01594](https://arxiv.org/abs/1912.01594).
- [171] A. Djouadi, J. Kalinowski, and M. Spira, “HDECAY: A Program for Higgs boson decays in the standard model and its supersymmetric extension”, *Comput. Phys. Commun.* **108** (1998) 56, doi:[10.1016/S0010-4655\(97\)00123-9](https://doi.org/10.1016/S0010-4655(97)00123-9), arXiv:[hep-ph/9704448](https://arxiv.org/abs/hep-ph/9704448).
- [172] A. Djouadi, J. Kalinowski, M. Mühlleitner, and M. Spira, “HDECAY: Twenty++ years after”, *Comput. Phys. Commun.* **238** (2019) 214, doi:[10.1016/j.cpc.2018.12.010](https://doi.org/10.1016/j.cpc.2018.12.010), arXiv:[1801.09506](https://arxiv.org/abs/1801.09506).

- [173] R. V. Harlander, S. Liebler, and H. Mantler, “SusHi: A program for the calculation of Higgs production in gluon fusion and bottom-quark annihilation in the standard model and the MSSM”, *Comput. Phys. Commun.* **184** (2013) 1605, doi:10.1016/j.cpc.2013.02.006, arXiv:1212.3249.
- [174] R. V. Harlander, S. Liebler, and H. Mantler, “SusHi bento: Beyond NNLO and the heavy-top limit”, *Comput. Phys. Commun.* **212** (2017) 239, doi:10.1016/j.cpc.2016.10.015, arXiv:1605.03190.
- [175] M. Spira, A. Djouadi, D. Graudenz, and P. M. Zerwas, “Higgs boson production at the LHC”, *Nucl. Phys. B* **453** (1995) 17, doi:10.1016/0550-3213(95)00379-7, arXiv:hep-ph/9504378.
- [176] R. Harlander and P. Kant, “Higgs production and decay: Analytic results at next-to-leading order QCD”, *JHEP* **12** (2005) 015, doi:10.1088/1126-6708/2005/12/015, arXiv:hep-ph/0509189.
- [177] R. V. Harlander and W. B. Kilgore, “Next-to-next-to-leading order Higgs production at hadron colliders”, *Phys. Rev. Lett.* **88** (2002) 201801, doi:10.1103/PhysRevLett.88.201801, arXiv:hep-ph/0201206.
- [178] C. Anastasiou and K. Melnikov, “Higgs boson production at hadron colliders in NNLO QCD”, *Nucl. Phys. B* **646** (2002) 220, doi:10.1016/S0550-3213(02)00837-4, arXiv:hep-ph/0207004.
- [179] V. Ravindran, J. Smith, and W. L. van Neerven, “NNLO corrections to the total cross-section for Higgs boson production in hadron hadron collisions”, *Nucl. Phys. B* **665** (2003) 325, doi:10.1016/S0550-3213(03)00457-7, arXiv:hep-ph/0302135.
- [180] R. V. Harlander and W. B. Kilgore, “Production of a pseudoscalar Higgs boson at hadron colliders at next-to-next-to leading order”, *JHEP* **10** (2002) 017, doi:10.1088/1126-6708/2002/10/017, arXiv:hep-ph/0208096.
- [181] C. Anastasiou and K. Melnikov, “Pseudoscalar Higgs boson production at hadron colliders in NNLO QCD”, *Phys. Rev. D* **67** (2003) 037501, doi:10.1103/PhysRevD.67.037501, arXiv:hep-ph/0208115.
- [182] U. Aglietti, R. Bonciani, G. Degrassi, and A. Vicini, “Two loop light fermion contribution to Higgs production and decays”, *Phys. Lett. B* **595** (2004) 432, doi:10.1016/j.physletb.2004.06.063, arXiv:hep-ph/0404071.
- [183] R. Bonciani, G. Degrassi, and A. Vicini, “On the generalized harmonic polylogarithms of one complex variable”, *Comput. Phys. Commun.* **182** (2011) 1253, doi:10.1016/j.cpc.2011.02.011, arXiv:1007.1891.
- [184] S. Heinemeyer, W. Hollik, and G. Weiglein, “FeynHiggs: A program for the calculation of the masses of the neutral CP even Higgs bosons in the MSSM”, *Comput. Phys. Commun.* **124** (2000) 76, doi:10.1016/S0010-4655(99)00364-1, arXiv:hep-ph/9812320.
- [185] S. Heinemeyer, W. Hollik, and G. Weiglein, “The masses of the neutral CP-even Higgs bosons in the MSSM: Accurate analysis at the two loop level”, *Eur. Phys. J. C* **9** (1999) 343, doi:10.1007/s100529900006, arXiv:hep-ph/9812472.

- [186] M. Frank et al., “The Higgs boson masses and mixings of the complex MSSM in the Feynman-diagrammatic approach”, *JHEP* **02** (2007) 047,  
`doi:10.1088/1126-6708/2007/02/047`, arXiv:[hep-ph/0611326](#).
- [187] T. Hahn et al., “High-precision predictions for the light CP-even Higgs boson mass of the minimal supersymmetric standard model”, *Phys. Rev. Lett.* **112** (2014) 141801,  
`doi:10.1103/PhysRevLett.112.141801`, arXiv:[1312.4937](#).
- [188] H. Bahl and W. Hollik, “Precise prediction for the light MSSM Higgs boson mass combining effective field theory and fixed-order calculations”, *Eur. Phys. J. C* **76** (2016) 499, `doi:10.1140/epjc/s10052-016-4354-8`, arXiv:[1608.01880](#).
- [189] H. Bahl, S. Heinemeyer, W. Hollik, and G. Weiglein, “Reconciling EFT and hybrid calculations of the light MSSM Higgs-boson mass”, *Eur. Phys. J. C* **78** (2018) 57,  
`doi:10.1140/epjc/s10052-018-5544-3`, arXiv:[1706.00346](#).
- [190] H. Bahl et al., “Precision calculations in the MSSM Higgs-boson sector with FeynHiggs 2.14”, *Comput. Phys. Commun.* **249** (2020) 107099,  
`doi:10.1016/j.cpc.2019.107099`, arXiv:[1811.09073](#).
- [191] A. Bredenstein, A. Denner, S. Dittmaier, and M. M. Weber, “Precise predictions for the Higgs-boson decay  $H \rightarrow WW/ZZ \rightarrow 4$  leptons”, *Phys. Rev. D* **74** (2006) 013004,  
`doi:10.1103/PhysRevD.74.013004`, arXiv:[hep-ph/0604011](#).
- [192] A. Bredenstein, A. Denner, S. Dittmaier, and M. M. Weber, “Radiative corrections to the semileptonic and hadronic Higgs-boson decays  $H \rightarrow WW/ZZ \rightarrow 4$  fermions”, *JHEP* **02** (2007) 080, `doi:10.1088/1126-6708/2007/02/080`, arXiv:[hep-ph/0611234](#).
- [193] U. Ellwanger and C. Hugonie, “Benchmark planes for Higgs-to-Higgs decays in the NMSSM”, *Eur. Phys. J. C* **82** (2022) 406,  
`doi:10.1140/epjc/s10052-022-10364-3`, arXiv:[2203.05049](#).
- [194] T. Robens, “TRSM benchmark planes – EPS-HEP2023 update”, in *2023 European Physical Society Conference on High Energy Physics*. 2023. arXiv:[2310.18045](#).
- [195] CMS Collaboration, “Search for a new scalar resonance decaying to a pair of Z bosons in proton-proton collisions at  $\sqrt{s} = 13$  TeV”, *JHEP* **06** (2018) 127,  
`doi:10.1007/JHEP06(2018)127`, arXiv:[1804.01939](#). [Erratum:  
`doi:10.1007/JHEP03(2019)128`].
- [196] CMS Collaboration, “Search for heavy resonances decaying to  $Z(\nu\bar{\nu})V(q\bar{q}')$  in proton-proton collisions at  $\sqrt{s} = 13$  TeV”, *Phys. Rev. D* **106** (2022) 012004,  
`doi:10.1103/PhysRevD.106.012004`, arXiv:[2109.08268](#).
- [197] CMS Collaboration, “Search for heavy resonances decaying to ZZ or ZW and axion-like particles mediating nonresonant ZZ or ZH production at  $\sqrt{s} = 13$  TeV”, *JHEP* **04** (2022) 087, `doi:10.1007/JHEP04(2022)087`, arXiv:[2111.13669](#).
- [198] CMS Collaboration, “Search for resonant and nonresonant new phenomena in high-mass dilepton final states at  $\sqrt{s} = 13$  TeV”, *JHEP* **07** (2021) 208,  
`doi:10.1007/JHEP07(2021)208`, arXiv:[2103.02708](#).
- [199] CMS Collaboration, “Search for W' bosons decaying to a top and a bottom quark at  $\sqrt{s} = 13$  TeV in the hadronic final state”, *Phys. Lett. B* **820** (2021) 136535,  
`doi:10.1016/j.physletb.2021.136535`, arXiv:[2104.04831](#).

- [200] CMS Collaboration, “Search for new physics in the lepton plus missing transverse momentum final state in proton-proton collisions at  $\sqrt{s} = 13$  TeV”, *JHEP* **07** (2022) 067, doi:10.1007/JHEP07(2022)067, arXiv:2202.06075.
- [201] CMS Collaboration, “Search for high mass dijet resonances with a new background prediction method in proton-proton collisions at  $\sqrt{s} = 13$  TeV”, *JHEP* **05** (2020) 033, doi:10.1007/JHEP05(2020)033, arXiv:1911.03947.
- [202] M. Carena, Z. Liu, and M. Riembau, “Probing the electroweak phase transition via enhanced di-Higgs boson production”, *Phys. Rev. D* **97** (2018) doi:10.1103/physrevd.97.095032.
- [203] R. Grober, M. Mühlleitner, and M. Spira, “Higgs pair production at NLO QCD for CP-violating Higgs sectors”, *Nucl. Phys. B* **925** (2017) 1, doi:10.1016/j.nuclphysb.2017.10.002, arXiv:1705.05314.
- [204] D. O’Connell, M. J. Ramsey-Musolf, and M. B. Wise, “Minimal Extension of the Standard Model Scalar Sector”, *Phys. Rev. D* **75** (2007) 037701, doi:10.1103/PhysRevD.75.037701, arXiv:hep-ph/0611014.
- [205] A. Papaefstathiou and G. White, “The electro-weak phase transition at colliders: confronting theoretical uncertainties and complementary channels”, *JHEP* **05** (2021) 099, doi:10.1007/JHEP05(2021)099, arXiv:2010.00597.
- [206] A. Papaefstathiou and G. White, “The Electro-Weak Phase Transition at Colliders: Discovery Post-Mortem”, *JHEP* **02** (2022) 185, doi:10.1007/JHEP02(2022)185, arXiv:2108.11394.
- [207] J. Alwall et al., “The automated computation of tree-level and next-to-leading order differential cross sections, and their matching to parton shower simulations”, *JHEP* **07** (2014) doi:10.1007/JHEP07(2014)079, arXiv:1405.0301.
- [208] A. Alloul et al., “FeynRules 2.0 – A complete toolbox for tree-level phenomenology”, *Comput. Phys. Commun.* **185** (2014) 2250, doi:10.1016/j.cpc.2014.04.012, arXiv:1310.1921.
- [209] R. Grober, M. Mühlleitner, M. Spira, and J. Streicher, “NLO QCD corrections to Higgs pair production including dimension-6 operators”, *JHEP* **09** (2015) 092, doi:10.1007/JHEP09(2015)092, arXiv:1504.06577.
- [210] M. Cepeda et al., “Report from Working Group 2: Higgs physics at the HL-LHC and HE-LHC”, *CERN Yellow Rep. Monogr.* **7** (2019) 221, doi:10.23731/CYRM-2019-007.221, arXiv:1902.00134.
- [211] I. Zurbano Fernandez et al., “High-Luminosity Large Hadron Collider (HL-LHC): Technical design report”, technical report, 2020. doi:10.23731/CYRM-2020-0010.
- [212] A. Dainese et al., eds., “Report on the Physics at the HL-LHC, and Perspectives for the HE-LHC”, volume 7/2019 of *CERN Yellow Reports: Monographs*. CERN, 2019. doi:10.23731/CYRM-2019-007, ISBN 978-92-9083-549-3.

## Glossary

<b>A, a</b>	$CP$ -odd Higgs bosons in extended Higgs sector models
<b>ATLAS</b>	A Toroidal LHC Apparatus
<b>BDT</b>	Boosted decision tree
<b>BSM</b>	Beyond the standard model
<b>CL</b>	Confidence level
<b>CMS</b>	Compact Muon Solenoid
<b>CP</b>	Charge-parity (symmetry)
<b>CR</b>	Control region
<b>DDT</b>	Designing decorrelated taggers (procedure)
<b>DNN</b>	Deep neural network
<b>DT</b>	Deep tau (identification algorithm)
<b>DY</b>	Drell–Yan (process)
<b>ECAL</b>	Electromagnetic calorimeter
<b>EFT</b>	Effective field theory
<b>EW</b>	Electroweak
<b>G</b>	Graviton
<b>ggF</b>	Gluon-gluon fusion (production process)
<b>HCAL</b>	Hadron calorimeter
<b>HH</b>	Higgs boson pair
<b>HL-LHC</b>	High-Luminosity Large Hadron Collider
<b>hMSSM</b>	Habent MSSM (scenario)
<b>HVT</b>	Heavy vector triplet (model)
<b>KK</b>	Kaluza-Klein (graviton)
<b>LHC</b>	Large Hadron Collider
<b>LO</b>	Leading order
<b>MC</b>	Monte Carlo (simulation)
<b>MSSM</b>	Minimal supersymmetric standard model
<b>MVA</b>	Multi-variate analysis
<b>NMSSM</b>	Next-to-minimal supersymmetric standard model
<b>NLO</b>	Next-to-leading order
<b>NN</b>	Neural network
<b>NWA</b>	Narrow-width approximation
<b>N2HDM</b>	Next-to-minimal 2HDM
<b>PF</b>	Particle flow (method of reconstructing particle candidates)
<b>pp</b>	Proton-proton
<b>PU</b>	Pileup
<b>PUPPI</b>	Pileup-per-particle identification (algorithm)
<b>QCD</b>	Quantum chromo-dynamics
<b>R</b>	Radion (graviscalar in the RS model), also distance in $(\Delta\eta, \Delta\phi)$ space
<b>RS</b>	Randall–Sundrum (model)
<b>Run 2</b>	The second run of the LHC, during the years 2015–2018
<b>SD</b>	Soft-drop (algorithm)
<b>SM</b>	Standard model
<b>SR</b>	Signal region
<b>SUSY</b>	Supersymmetry
<b><math>\sqrt{s}</math></b>	The centre-of-mass energy
<b>TRSM</b>	Two-real-singlet Model

<b>UFO</b>	Universal FeynRules output
<b>V</b>	Vector boson ( $W$ or $Z$ )
<b>VBF</b>	Vector boson fusion (production process)
<b>VH</b>	Vector plus Higgs boson (production process or decay channel)
<b>WED</b>	Warped extra dimensions (model)
<b>2HDM</b>	Two-Higgs-doublet Model
<b>2HDM+S</b>	Two-Higgs-doublet-plus-additional-singlet model



## A The CMS Collaboration

**Yerevan Physics Institute, Yerevan, Armenia**

A. Hayrapetyan, A. Tumasyan<sup>1</sup> 

**Institut für Hochenergiephysik, Vienna, Austria**

W. Adam , J.W. Andrejkovic, T. Bergauer , S. Chatterjee , K. Damanakis , M. Dragicevic , P.S. Hussain , M. Jeitler<sup>2</sup> , N. Krammer , A. Li , D. Liko , I. Mikulec , J. Schieck<sup>2</sup> , R. Schöfbeck , D. Schwarz , M. Sonawane , S. Templ , W. Waltenberger , C.-E. Wulz<sup>2</sup> 

**Universiteit Antwerpen, Antwerpen, Belgium**

M.R. Darwish<sup>3</sup> , T. Janssen , P. Van Mechelen 

**Vrije Universiteit Brussel, Brussel, Belgium**

N. Breugelmans, J. D'Hondt , S. Dansana , A. De Moor , M. Delcourt , F. Heyen, S. Lowette , I. Makarenko , D. Müller , S. Tavernier , M. Tytgat<sup>4</sup> , G.P. Van Onsem , S. Van Putte , D. Vannerom 

**Université Libre de Bruxelles, Bruxelles, Belgium**

B. Clerbaux , A.K. Das, G. De Lentdecker , H. Evard , L. Favart , P. Gianneios , D. Hohov , J. Jaramillo , A. Khalilzadeh, F.A. Khan , K. Lee , M. Mahdavikhorrami , A. Malara , S. Paredes , L. Thomas , M. Vanden Bemden , C. Vander Velde , P. Vanlaer 

**Ghent University, Ghent, Belgium**

M. De Coen , D. Dobur , G. Gokbulut , Y. Hong , J. Knolle , L. Lambrecht , D. Marckx , G. Mestdach, K. Mota Amarilo , C. Rendón, A. Samalan, K. Skovpen , N. Van Den Bossche , J. van der Linden , L. Wezenbeek 

**Université Catholique de Louvain, Louvain-la-Neuve, Belgium**

A. Benecke , A. Bethani , G. Bruno , C. Caputo , J. De Favereau De Jeneret , C. Delaere , I.S. Donertas , A. Giammanco , A.O. Guzel , Sa. Jain , V. Lemaitre, J. Lidrych , P. Mastrapasqua , T.T. Tran , S. Wertz 

**Centro Brasileiro de Pesquisas Fisicas, Rio de Janeiro, Brazil**

G.A. Alves , E. Coelho , C. Hensel , T. Menezes De Oliveira , A. Moraes , P. Rebello Teles , M. Soeiro, A. Vilela Pereira<sup>5</sup> 

**Universidade do Estado do Rio de Janeiro, Rio de Janeiro, Brazil**

W.L. Aldá Júnior , M. Alves Gallo Pereira , M. Barroso Ferreira Filho , H. Brandao Malbouisson , W. Carvalho , J. Chinellato<sup>6</sup>, E.M. Da Costa , G.G. Da Silveira<sup>7</sup> , D. De Jesus Damiao , S. Fonseca De Souza , R. Gomes De Souza, M. Macedo , J. Martins<sup>8</sup> , C. Mora Herrera , L. Mundim , H. Nogima , J.P. Pinheiro , A. Santoro , A. Sznajder , M. Thiel 

**Universidade Estadual Paulista, Universidade Federal do ABC, São Paulo, Brazil**

C.A. Bernardes<sup>7</sup> , L. Calligaris , T.R. Fernandez Perez Tomei , E.M. Gregores , I. Maietto Silverio , P.G. Mercadante , S.F. Novaes , B. Orzari , Sandra S. Padula 

**Institute for Nuclear Research and Nuclear Energy, Bulgarian Academy of Sciences, Sofia, Bulgaria**

A. Aleksandrov , G. Antchev , R. Hadjiiska , P. Iaydjiev , M. Misheva , M. Shopova , G. Sultanov 

**University of Sofia, Sofia, Bulgaria**

A. Dimitrov , L. Litov , B. Pavlov , P. Petkov , A. Petrov , E. Shumka 

**Instituto De Alta Investigación, Universidad de Tarapacá, Casilla 7 D, Arica, Chile**

S. Keshri , S. Thakur 

**Beihang University, Beijing, China**

T. Cheng , T. Javaid , L. Yuan 

**Department of Physics, Tsinghua University, Beijing, China**

Z. Hu , Z. Liang, J. Liu, K. Yi<sup>9,10</sup> 

**Institute of High Energy Physics, Beijing, China**

G.M. Chen<sup>11</sup> , H.S. Chen<sup>11</sup> , M. Chen<sup>11</sup> , F. Iemmi , C.H. Jiang, A. Kapoor<sup>12</sup> , H. Liao , Z.-A. Liu<sup>13</sup> , M.A. Shahzad<sup>11</sup>, R. Sharma<sup>14</sup> , J.N. Song<sup>13</sup>, J. Tao , C. Wang<sup>11</sup>, J. Wang , Z. Wang<sup>11</sup>, H. Zhang , J. Zhao 

**State Key Laboratory of Nuclear Physics and Technology, Peking University, Beijing, China**

A. Agapitos , Y. Ban , S. Deng , B. Guo, C. Jiang , A. Levin , C. Li , Q. Li , Y. Mao, S. Qian, S.J. Qian , X. Qin, X. Sun , D. Wang , H. Yang, L. Zhang , Y. Zhao, C. Zhou 

**Guangdong Provincial Key Laboratory of Nuclear Science and Guangdong-Hong Kong Joint Laboratory of Quantum Matter, South China Normal University, Guangzhou, China**

S. Yang 

**Sun Yat-Sen University, Guangzhou, China**

Z. You 

**University of Science and Technology of China, Hefei, China**

Z. Guo, K. Jaffel , N. Lu 

**Nanjing Normal University, Nanjing, China**

G. Bauer<sup>15</sup>, B. Li, J. Zhang 

**Institute of Modern Physics and Key Laboratory of Nuclear Physics and Ion-beam Application (MOE) - Fudan University, Shanghai, China**

X. Gao<sup>16</sup> 

**Zhejiang University, Hangzhou, Zhejiang, China**

Z. Lin , C. Lu , M. Xiao 

**Universidad de Los Andes, Bogota, Colombia**

C. Avila , D.A. Barbosa Trujillo, A. Cabrera , C. Florez , J. Fraga , J.A. Reyes Vega

**Universidad de Antioquia, Medellin, Colombia**

F. Ramirez , M. Rodriguez , A.A. Ruales Barbosa , J.D. Ruiz Alvarez 

**University of Split, Faculty of Electrical Engineering, Mechanical Engineering and Naval Architecture, Split, Croatia**

D. Giljanovic , N. Godinovic , D. Lelas , A. Sculac 

**University of Split, Faculty of Science, Split, Croatia**

M. Kovac , A. Petkovic, T. Sculac 

**Institute Rudjer Boskovic, Zagreb, Croatia**

P. Bargassa , V. Brigljevic , B.K. Chitroda , D. Ferencek , K. Jakovcic, S. Mishra , A. Starodumov<sup>17</sup> , T. Susa 

**University of Cyprus, Nicosia, Cyprus**

A. Attikis , K. Christoforou , A. Hadjiagapiou, A. Ioannou, C. Leonidou, J. Mousa , C. Nicolaou, L. Paizanos, F. Ptochos , P.A. Razis , H. Rykaczewski, H. Saka , A. Stepennov 

**Charles University, Prague, Czech Republic**

M. Finger , M. Finger Jr. , A. Kveton 

**Universidad San Francisco de Quito, Quito, Ecuador**

E. Carrera Jarrin 

**Academy of Scientific Research and Technology of the Arab Republic of Egypt, Egyptian Network of High Energy Physics, Cairo, Egypt**

Y. Assran<sup>18,19</sup>, B. El-mahdy, S. Elgammal<sup>19</sup>

**Center for High Energy Physics (CHEP-FU), Fayoum University, El-Fayoum, Egypt**

A. Lotfy , M.A. Mahmoud 

**National Institute of Chemical Physics and Biophysics, Tallinn, Estonia**

K. Ehataht , M. Kadastik, T. Lange , S. Nandan , C. Nielsen , J. Pata , M. Raidal , L. Tani , C. Veelken 

**Department of Physics, University of Helsinki, Helsinki, Finland**

H. Kirschenmann , K. Osterberg , M. Voutilainen 

**Helsinki Institute of Physics, Helsinki, Finland**

S. Bharthuar , N. Bin Norjoharuddeen , E. Brücke , F. Garcia , P. Inkaew , K.T.S. Kallonen , R. Kinnunen, T. Lampén , K. Lassila-Perini , S. Lehti , T. Lindén , L. Martikainen , M. Myllymäki , M.m. Rantanen , H. Siikonen , J. Tuominiemi 

**Lappeenranta-Lahti University of Technology, Lappeenranta, Finland**

P. Luukka , H. Petrow 

**IRFU, CEA, Université Paris-Saclay, Gif-sur-Yvette, France**

M. Besancon , F. Couderc , M. Dejardin , D. Denegri, J.L. Faure, F. Ferri , S. Ganjour , P. Gras , G. Hamel de Monchenault , V. Lohezic , J. Malcles , F. Orlandi , L. Portales , J. Rander, A. Rosowsky , M.Ö. Sahin , A. Savoy-Navarro<sup>20</sup> , P. Simkina , M. Titov , M. Tornago 

**Laboratoire Leprince-Ringuet, CNRS/IN2P3, Ecole Polytechnique, Institut Polytechnique de Paris, Palaiseau, France**

F. Beaudette , P. Busson , A. Cappati , C. Charlot , M. Chiusi , F. Damas , O. Davignon , A. De Wit , I.T. Ehle , B.A. Fontana Santos Alves , S. Ghosh , A. Gilbert , R. Granier de Cassagnac , A. Hakimi , B. Harikrishnan , L. Kalipoliti , G. Liu , M. Nguyen , C. Ochando , R. Salerno , J.B. Sauvan , Y. Sirois , L. Urda Gómez , E. Vernazza , A. Zabi , A. Zghiche 

**Université de Strasbourg, CNRS, IPHC UMR 7178, Strasbourg, France**

J.-L. Agram<sup>21</sup> , J. Andrea , D. Apparu , D. Bloch , J.-M. Brom , E.C. Chabert , C. Collard , S. Falke , U. Goerlach , R. Haeberle , A.-C. Le Bihan , M. Meena , O. Ponctet , G. Saha , M.A. Sessini , P. Van Hove , P. Vaucelle 

**Centre de Calcul de l'Institut National de Physique Nucléaire et de Physique des Particules, CNRS/IN2P3, Villeurbanne, France**

A. Di Florio 

**Institut de Physique des 2 Infinis de Lyon (IP2I ), Villeurbanne, France**

D. Amram, S. Beauceron , B. Blançon , G. Boudoul , N. Chanon , D. Contardo , P. Depasse , C. Dozen<sup>22</sup> , H. El Mamouni, J. Fay , S. Gascon , M. Gouzevitch , C. Greenberg, G. Grenier , B. Ille , E. Jourd'huy, I.B. Laktineh, M. Lethuillier , L. Mirabito, S. Perries, A. Purohit , M. Vander Donckt , P. Verdier , J. Xiao 

**Georgian Technical University, Tbilisi, Georgia**

G. Adamov, I. Lomidze , Z. Tsamalaidze<sup>17</sup> 

**RWTH Aachen University, I. Physikalisches Institut, Aachen, Germany**

V. Botta , L. Feld , K. Klein , M. Lipinski , D. Meuser , A. Pauls , D. Pérez Adán , N. Röwert , M. Teroerde 

**RWTH Aachen University, III. Physikalisches Institut A, Aachen, Germany**

S. Diekmann , A. Dodonova , N. Eich , D. Eliseev , F. Engelke , J. Erdmann , M. Erdmann , P. Fackeldey , B. Fischer , T. Hebbeker , K. Hoepfner , F. Ivone , A. Jung , M.y. Lee , F. Mausolf , M. Merschmeyer , A. Meyer , S. Mukherjee , D. Noll , F. Nowotny, A. Pozdnyakov , Y. Rath, W. Redjeb , F. Rehm, H. Reithler , V. Sarkisovi , A. Schmidt , A. Sharma , J.L. Spah , A. Stein , F. Torres Da Silva De Araujo<sup>23</sup> , S. Wiedenbeck , S. Zaleski

**RWTH Aachen University, III. Physikalisches Institut B, Aachen, Germany**

C. Dziwok , G. Flügge , T. Kress , A. Nowack , O. Pooth , A. Stahl , T. Ziemons , A. Zottz 

**Deutsches Elektronen-Synchrotron, Hamburg, Germany**

H. Aarup Petersen , M. Aldaya Martin , J. Alimena , S. Amoroso, Y. An , J. Bach , S. Baxter , M. Bayatmakou , H. Becerril Gonzalez , O. Behnke , A. Belvedere , S. Bhattacharya , F. Blekman<sup>24</sup> , K. Borras<sup>25</sup> , A. Campbell , A. Cardini , C. Cheng, F. Colombina , S. Consuegra Rodríguez , G. Correia Silva , M. De Silva , G. Eckerlin, D. Eckstein , L.I. Estevez Banos , O. Filatov , E. Gallo<sup>24</sup> , A. Geiser , V. Guglielmi , M. Guthoff , A. Hinzmann , L. Jeppe , B. Kaech , M. Kasemann , C. Kleinwort , R. Kogler , M. Komm , D. Krücker , W. Lange, D. Leyva Pernia , K. Lipka<sup>26</sup> , W. Lohmann<sup>27</sup> , F. Lorkowski , R. Mankel , I.-A. Melzer-Pellmann , M. Mendizabal Morentin , A.B. Meyer , G. Milella , K. Moral Figueroa , A. Mussgiller , L.P. Nair , J. Niedziela , A. Nürnberg , Y. Otarid, J. Park , E. Ranken , A. Raspereza , D. Rastorguev , J. Rübenach, L. Rygaard, A. Saggio , M. Scham<sup>28,25</sup> , S. Schnake<sup>25</sup> , P. Schütze , C. Schwanenberger<sup>24</sup> , D. Selivanova , K. Sharko , M. Shchedrolosiev , D. Stafford, F. Vazzoler , A. Ventura Barroso , R. Walsh , D. Wang , Q. Wang , Y. Wen , K. Wichmann, L. Wiens<sup>25</sup> , C. Wissing , Y. Yang , A. Zimmermann Castro Santos 

**University of Hamburg, Hamburg, Germany**

A. Albrecht , S. Albrecht , M. Antonello , S. Bein , L. Benato , S. Bollweg, M. Bonanomi , P. Connor , K. El Morabit , Y. Fischer , E. Garutti , A. Grohsjean , J. Haller , H.R. Jabusch , G. Kasieczka , P. Keicher, R. Klanner , W. Korcari , T. Kramer , C.c. Kuo, V. Kutzner , F. Labe , J. Lange , A. Lobanov , C. Matthies , L. Moureux , M. Mrowietz, A. Nigamova , Y. Nissan, A. Paasch , K.J. Pena Rodriguez , T. Quadfasel , B. Raciti , M. Rieger , D. Savoiu , J. Schindler , P. Schleper , M. Schröder , J. Schwandt , M. Sommerhalder , H. Stadie , G. Steinbrück , A. Tews, M. Wolf 

**Karlsruher Institut fuer Technologie, Karlsruhe, Germany**

S. Brommer [ID](#), M. Burkart, E. Butz [ID](#), T. Chwalek [ID](#), A. Dierlamm [ID](#), A. Droll, N. Faltermann [ID](#), M. Giffels [ID](#), A. Gottmann [ID](#), F. Hartmann<sup>29</sup> [ID](#), R. Hofsaess [ID](#), M. Horzela [ID](#), U. Husemann [ID](#), J. Kieseler [ID](#), M. Klute [ID](#), R. Koppenhöfer [ID](#), J.M. Lawhorn [ID](#), M. Link, A. Lintuluoto [ID](#), B. Maier [ID](#), S. Maier [ID](#), S. Mitra [ID](#), M. Mormile [ID](#), Th. Müller [ID](#), M. Neukum, M. Oh [ID](#), E. Pfeffer [ID](#), M. Presilla [ID](#), G. Quast [ID](#), K. Rabbertz [ID](#), B. Regnery [ID](#), N. Shadskiy [ID](#), I. Shvetsov [ID](#), H.J. Simonis [ID](#), L. Sowa, L. Stockmeier, K. Tauqueer, M. Toms [ID](#), N. Trevisani [ID](#), R.F. Von Cube [ID](#), M. Wassmer [ID](#), S. Wieland [ID](#), F. Wittig, R. Wolf [ID](#), X. Zuo [ID](#)

**Institute of Nuclear and Particle Physics (INPP), NCSR Demokritos, Aghia Paraskevi, Greece**

G. Anagnostou, G. Daskalakis [ID](#), A. Kyriakis, A. Papadopoulos<sup>29</sup>, A. Stakia [ID](#)

**National and Kapodistrian University of Athens, Athens, Greece**

P. Kontaxakis [ID](#), G. Melachroinos, Z. Painesis [ID](#), A. Panagiotou, I. Papavergou [ID](#), I. Paraskevas [ID](#), N. Saoulidou [ID](#), K. Theofilatos [ID](#), E. Tziaferi [ID](#), K. Vellidis [ID](#), I. Zisopoulos [ID](#)

**National Technical University of Athens, Athens, Greece**

G. Bakas [ID](#), T. Chatzistavrou, G. Karapostoli [ID](#), K. Kousouris [ID](#), I. Papakrivopoulos [ID](#), E. Siamarkou, G. Tsipolitis, A. Zacharopoulou

**University of Ioánnina, Ioánnina, Greece**

K. Adamidis, I. Bestintzanos, I. Evangelou [ID](#), C. Foudas, C. Kamtsikis, P. Katsoulis, P. Kokkas [ID](#), P.G. Kosmoglou Kioseoglou [ID](#), N. Manthos [ID](#), I. Papadopoulos [ID](#), J. Strologas [ID](#)

**HUN-REN Wigner Research Centre for Physics, Budapest, Hungary**

C. Hajdu [ID](#), D. Horvath<sup>30,31</sup> [ID](#), K. Márton, A.J. Rádl<sup>32</sup> [ID](#), F. Sikler [ID](#), V. Veszpremi [ID](#)

**MTA-ELTE Lendület CMS Particle and Nuclear Physics Group, Eötvös Loránd University, Budapest, Hungary**

M. Csand [ID](#), K. Farkas [ID](#), A. Fehrkuti<sup>33</sup> [ID](#), M.M.A. Gadallah<sup>34</sup> [ID](#), . Kadlecik [ID](#), P. Major [ID](#), G. Pasztor [ID](#), G.I. Veres [ID](#)

**Faculty of Informatics, University of Debrecen, Debrecen, Hungary**

P. Raics, B. Ujvari [ID](#), G. Zilizi [ID](#)

**Institute of Nuclear Research ATOMKI, Debrecen, Hungary**

G. Bencze, S. Czellar, J. Molnar, Z. Szillasi

**Karoly Robert Campus, MATE Institute of Technology, Gyongyos, Hungary**

T. Csorgo<sup>33</sup> [ID](#), T. Novak [ID](#)

**Panjab University, Chandigarh, India**

J. Babbar [ID](#), S. Bansal [ID](#), S.B. Beri, V. Bhatnagar [ID](#), G. Chaudhary [ID](#), S. Chauhan [ID](#), N. Dhingra<sup>35</sup> [ID](#), A. Kaur [ID](#), A. Kaur [ID](#), H. Kaur [ID](#), M. Kaur [ID](#), S. Kumar [ID](#), K. Sandeep [ID](#), T. Sheokand, J.B. Singh [ID](#), A. Singla [ID](#)

**University of Delhi, Delhi, India**

A. Ahmed [ID](#), A. Bhardwaj [ID](#), A. Chhetri [ID](#), B.C. Choudhary [ID](#), A. Kumar [ID](#), A. Kumar [ID](#), M. Naimuddin [ID](#), K. Ranjan [ID](#), M.K. Saini, S. Saumya [ID](#)

**Saha Institute of Nuclear Physics, HBNI, Kolkata, India**

S. Baradia [ID](#), S. Barman<sup>36</sup> [ID](#), S. Bhattacharya [ID](#), S. Das Gupta, S. Dutta [ID](#), S. Dutta, S. Sarkar

**Indian Institute of Technology Madras, Madras, India**

M.M. Ameen [ID](#), P.K. Behera [ID](#), S.C. Behera [ID](#), S. Chatterjee [ID](#), G. Dash [ID](#), P. Jana [ID](#), P. Kalbhor [ID](#), S. Kamble [ID](#), J.R. Komaragiri<sup>37</sup> [ID](#), D. Kumar<sup>37</sup> [ID](#), L. Panwar<sup>37</sup> [ID](#), P.R. Pujahari [ID](#),

N.R. Saha [ID](#), A. Sharma [ID](#), A.K. Sikdar [ID](#), R.K. Singh, P. Verma, S. Verma [ID](#), A. Vijay

**Tata Institute of Fundamental Research-A, Mumbai, India**

S. Dugad, M. Kumar [ID](#), G.B. Mohanty [ID](#), B. Parida [ID](#), M. Shelake, P. Suryadevara

**Tata Institute of Fundamental Research-B, Mumbai, India**

A. Bala [ID](#), S. Banerjee [ID](#), R.M. Chatterjee, M. Guchait [ID](#), Sh. Jain [ID](#), A. Jaiswal, S. Kumar [ID](#), G. Majumder [ID](#), K. Mazumdar [ID](#), S. Parolia [ID](#), A. Thachayath [ID](#)

**National Institute of Science Education and Research, An OCC of Homi Bhabha National Institute, Bhubaneswar, Odisha, India**

S. Bahinipati<sup>38</sup> [ID](#), C. Kar [ID](#), D. Maity<sup>39</sup> [ID](#), P. Mal [ID](#), T. Mishra [ID](#), V.K. Muraleedharan Nair Bindhu<sup>39</sup> [ID](#), K. Naskar<sup>39</sup> [ID](#), A. Nayak<sup>39</sup> [ID](#), S. Nayak, K. Pal, P. Sadangi, S.K. Swain [ID](#), S. Varghese<sup>39</sup> [ID](#), D. Vats<sup>39</sup> [ID](#)

**Indian Institute of Science Education and Research (IISER), Pune, India**

S. Acharya<sup>40</sup> [ID](#), A. Alpana [ID](#), S. Dube [ID](#), B. Gomber<sup>40</sup> [ID](#), P. Hazarika [ID](#), B. Kansal [ID](#), A. Laha [ID](#), B. Sahu<sup>40</sup> [ID](#), S. Sharma [ID](#), K.Y. Vaish [ID](#)

**Isfahan University of Technology, Isfahan, Iran**

H. Bakhshiansohi<sup>41</sup> [ID](#), A. Jafari<sup>42</sup> [ID](#), M. Zeinali<sup>43</sup> [ID](#)

**Institute for Research in Fundamental Sciences (IPM), Tehran, Iran**

S. Bashiri, S. Chenarani<sup>44</sup> [ID](#), S.M. Etesami [ID](#), Y. Hosseini [ID](#), M. Khakzad [ID](#), E. Khazaie<sup>45</sup> [ID](#), M. Mohammadi Najafabadi [ID](#), S. Tizchang [ID](#)

**University College Dublin, Dublin, Ireland**

M. Felcini [ID](#), M. Grunewald [ID](#)

**INFN Sezione di Bari<sup>a</sup>, Università di Bari<sup>b</sup>, Politecnico di Bari<sup>c</sup>, Bari, Italy**

M. Abbrescia<sup>a,b</sup> [ID](#), A. Colaleo<sup>a,b</sup> [ID](#), D. Creanza<sup>a,c</sup> [ID](#), B. D'Anzi<sup>a,b</sup> [ID](#), N. De Filippis<sup>a,c</sup> [ID](#), M. De Palma<sup>a,b</sup> [ID](#), L. Fiore<sup>a</sup> [ID](#), G. Iaselli<sup>a,c</sup> [ID](#), M. Louka<sup>a,b</sup> [ID](#), G. Maggi<sup>a,c</sup> [ID](#), M. Maggi<sup>a</sup> [ID](#), I. Margjeka<sup>a,b</sup> [ID](#), V. Mastrapasqua<sup>a,b</sup> [ID](#), S. My<sup>a,b</sup> [ID](#), S. Nuzzo<sup>a,b</sup> [ID](#), A. Pellecchia<sup>a,b</sup> [ID](#), A. Pompili<sup>a,b</sup> [ID](#), G. Pugliese<sup>a,c</sup> [ID](#), R. Radogna<sup>a</sup> [ID](#), D. Ramos<sup>a</sup> [ID](#), A. Ranieri<sup>a</sup> [ID](#), L. Silvestris<sup>a</sup> [ID](#), F.M. Simone<sup>a,b</sup> [ID](#), Ü. Sözbilir<sup>a</sup> [ID](#), A. Stamerra<sup>a</sup> [ID](#), D. Troiano<sup>a</sup> [ID](#), R. Venditti<sup>a</sup> [ID](#), P. Verwilligen<sup>a</sup> [ID](#), A. Zaza<sup>a,b</sup> [ID](#)

**INFN Sezione di Bologna<sup>a</sup>, Università di Bologna<sup>b</sup>, Bologna, Italy**

G. Abbiendi<sup>a</sup> [ID](#), C. Battilana<sup>a,b</sup> [ID](#), D. Bonacorsi<sup>a,b</sup> [ID](#), L. Borgonovi<sup>a</sup> [ID](#), P. Capiluppi<sup>a,b</sup> [ID](#), A. Castro<sup>a,b</sup> [ID](#), F.R. Cavallo<sup>a</sup> [ID](#), M. Cuffiani<sup>a,b</sup> [ID](#), G.M. Dallavalle<sup>a</sup> [ID](#), T. Diotalevi<sup>a,b</sup> [ID](#), F. Fabbri<sup>a</sup> [ID](#), A. Fanfani<sup>a,b</sup> [ID](#), D. Fasanella<sup>a,b</sup> [ID](#), P. Giacomelli<sup>a</sup> [ID](#), L. Giommi<sup>a,b</sup> [ID](#), C. Grandia<sup>a</sup> [ID](#), L. Guiducci<sup>a,b</sup> [ID](#), S. Lo Meo<sup>a,46</sup> [ID](#), M. Lorusso<sup>a,b</sup> [ID](#), L. Lunerti<sup>a</sup> [ID](#), S. Marcellini<sup>a</sup> [ID](#), G. Masetti<sup>a</sup> [ID](#), F.L. Navarria<sup>a,b</sup> [ID](#), G. Paggi<sup>a</sup> [ID](#), A. Perrotta<sup>a</sup> [ID](#), F. Primavera<sup>a,b</sup> [ID](#), A.M. Rossi<sup>a,b</sup> [ID](#), S. Rossi Tisbeni<sup>a,b</sup> [ID](#), T. Rovelli<sup>a,b</sup> [ID](#), G.P. Siroli<sup>a,b</sup> [ID](#)

**INFN Sezione di Catania<sup>a</sup>, Università di Catania<sup>b</sup>, Catania, Italy**

S. Costa<sup>a,b,47</sup> [ID](#), A. Di Mattia<sup>a</sup> [ID](#), R. Potenza<sup>a,b</sup>, A. Tricomi<sup>a,b,47</sup> [ID](#), C. Tuve<sup>a,b</sup> [ID](#)

**INFN Sezione di Firenze<sup>a</sup>, Università di Firenze<sup>b</sup>, Firenze, Italy**

P. Assiouras<sup>a</sup> [ID](#), G. Barbagli<sup>a</sup> [ID](#), G. Bardelli<sup>a,b</sup> [ID](#), B. Camaiani<sup>a,b</sup> [ID](#), A. Cassese<sup>a</sup> [ID](#), R. Ceccarelli<sup>a</sup> [ID](#), V. Ciulli<sup>a,b</sup> [ID](#), C. Civinini<sup>a</sup> [ID](#), R. D'Alessandro<sup>a,b</sup> [ID](#), E. Focardi<sup>a,b</sup> [ID](#), T. Kello<sup>a</sup>, G. Latino<sup>a,b</sup> [ID](#), P. Lenzi<sup>a,b</sup> [ID](#), M. Lizzo<sup>a</sup> [ID](#), M. Meschini<sup>a</sup> [ID](#), S. Paoletti<sup>a</sup> [ID](#), A. Papanastassiou<sup>a,b</sup> [ID](#), G. Sguazzoni<sup>a</sup> [ID](#), L. Viliani<sup>a</sup> [ID](#)

**INFN Laboratori Nazionali di Frascati, Frascati, Italy**

L. Benussi [ID](#), S. Bianco [ID](#), S. Meola<sup>48</sup> [ID](#), D. Piccolo [ID](#)

**INFN Sezione di Genova<sup>a</sup>, Università di Genova<sup>b</sup>, Genova, Italy**

P. Chatagnon<sup>a</sup> [ID](#), F. Ferro<sup>a</sup> [ID](#), E. Robutti<sup>a</sup> [ID](#), S. Tosi<sup>a,b</sup> [ID](#)

**INFN Sezione di Milano-Bicocca<sup>a</sup>, Università di Milano-Bicocca<sup>b</sup>, Milano, Italy**

A. Benaglia<sup>a</sup> [ID](#), G. Boldrini<sup>a,b</sup> [ID](#), F. Brivio<sup>a</sup> [ID](#), F. Cetorelli<sup>a</sup> [ID](#), F. De Guio<sup>a,b</sup> [ID](#), M.E. Dinardo<sup>a,b</sup> [ID](#), P. Dini<sup>a</sup> [ID](#), S. Gennai<sup>a</sup> [ID](#), R. Gerosa<sup>a,b</sup> [ID](#), A. Ghezzi<sup>a,b</sup> [ID](#), P. Govoni<sup>a,b</sup> [ID](#), L. Guzzi<sup>a</sup> [ID](#), M.T. Lucchini<sup>a,b</sup> [ID](#), M. Malberti<sup>a</sup> [ID](#), S. Malvezzi<sup>a</sup> [ID](#), A. Massironi<sup>a</sup> [ID](#), D. Menasce<sup>a</sup> [ID](#), L. Moroni<sup>a</sup> [ID](#), M. Paganoni<sup>a,b</sup> [ID](#), S. Palluotto<sup>a,b</sup> [ID](#), D. Pedrini<sup>a</sup> [ID](#), A. Perego<sup>a</sup> [ID](#), B.S. Pinolini<sup>a</sup>, G. Pizzati<sup>a,b</sup> [ID](#), S. Ragazzi<sup>a,b</sup> [ID](#), T. Tabarelli de Fatis<sup>a,b</sup> [ID](#)

**INFN Sezione di Napoli<sup>a</sup>, Università di Napoli 'Federico II'<sup>b</sup>, Napoli, Italy; Università della Basilicata<sup>c</sup>, Potenza, Italy; Scuola Superiore Meridionale (SSM)<sup>d</sup>, Napoli, Italy**

S. Buontempo<sup>a</sup> [ID](#), A. Cagnotta<sup>a,b</sup> [ID](#), F. Carnevali<sup>a,b</sup> [ID](#), N. Cavallo<sup>a,c</sup> [ID](#), F. Fabozzi<sup>a,c</sup> [ID](#), A.O.M. Iorio<sup>a,b</sup> [ID](#), L. Lista<sup>a,b,49</sup> [ID](#), P. Paolucci<sup>a,29</sup> [ID](#), B. Rossi<sup>a</sup> [ID](#), C. Sciacca<sup>a,b</sup> [ID](#)

**INFN Sezione di Padova<sup>a</sup>, Università di Padova<sup>b</sup>, Padova, Italy; Università di Trento<sup>c</sup>, Trento, Italy**

R. Ardino<sup>a</sup> [ID](#), P. Azzi<sup>a</sup> [ID](#), N. Bacchetta<sup>a,50</sup> [ID](#), M. Benettini<sup>a</sup> [ID](#), A. Bergnoli<sup>a</sup> [ID](#), D. Bisello<sup>a,b</sup> [ID](#), P. Bortignon<sup>a</sup> [ID](#), G. Bortolato<sup>a,b</sup> [ID](#), A. Bragagnolo<sup>a,b</sup> [ID](#), A.C.M. Bulla<sup>a</sup> [ID](#), P. Checchia<sup>a</sup> [ID](#), T. Dorigo<sup>a</sup> [ID](#), F. Gasparini<sup>a,b</sup> [ID](#), U. Gasparini<sup>a,b</sup> [ID](#), E. Lusiani<sup>a</sup> [ID](#), M. Margoni<sup>a,b</sup> [ID](#), A.T. Meneguzzo<sup>a,b</sup> [ID](#), M. Migliorini<sup>a,b</sup> [ID](#), J. Pazzini<sup>a,b</sup> [ID](#), P. Ronchese<sup>a,b</sup> [ID](#), R. Rossin<sup>a,b</sup> [ID](#), F. Simonetto<sup>a,b</sup> [ID](#), G. Strong<sup>a</sup> [ID](#), M. Tosi<sup>a,b</sup> [ID](#), A. Triossi<sup>a,b</sup> [ID](#), S. Ventura<sup>a</sup> [ID](#), M. Zanetti<sup>a,b</sup> [ID](#), P. Zotto<sup>a,b</sup> [ID](#), A. Zucchetta<sup>a,b</sup> [ID](#)

**INFN Sezione di Pavia<sup>a</sup>, Università di Pavia<sup>b</sup>, Pavia, Italy**

C. Aimè<sup>a</sup> [ID](#), A. Braghieri<sup>a</sup> [ID](#), S. Calzaferri<sup>a</sup> [ID](#), D. Fiorina<sup>a</sup> [ID](#), P. Montagna<sup>a,b</sup> [ID](#), V. Re<sup>a</sup> [ID](#), C. Riccardi<sup>a,b</sup> [ID](#), P. Salvini<sup>a</sup> [ID](#), I. Vai<sup>a,b</sup> [ID](#), P. Vitulo<sup>a,b</sup> [ID](#)

**INFN Sezione di Perugia<sup>a</sup>, Università di Perugia<sup>b</sup>, Perugia, Italy**

S. Ajmal<sup>a,b</sup> [ID](#), M.E. Ascoli<sup>a,b</sup> [ID](#), G.M. Bilei<sup>a</sup> [ID](#), C. Carrivale<sup>a,b</sup> [ID](#), D. Ciangottini<sup>a,b</sup> [ID](#), L. Fanò<sup>a,b</sup> [ID](#), M. Magherini<sup>a,b</sup> [ID](#), V. Mariani<sup>a,b</sup> [ID](#), M. Menichelli<sup>a</sup> [ID](#), F. Moscatelli<sup>a,51</sup> [ID](#), A. Rossi<sup>a,b</sup> [ID](#), A. Santocchia<sup>a,b</sup> [ID](#), D. Spiga<sup>a</sup> [ID](#), T. Tedeschi<sup>a,b</sup> [ID](#)

**INFN Sezione di Pisa<sup>a</sup>, Università di Pisa<sup>b</sup>, Scuola Normale Superiore di Pisa<sup>c</sup>, Pisa, Italy; Università di Siena<sup>d</sup>, Siena, Italy**

C.A. Alexe<sup>a,c</sup> [ID](#), P. Asenov<sup>a,b</sup> [ID](#), P. Azzurri<sup>a</sup> [ID](#), G. Bagliesi<sup>a</sup> [ID](#), R. Bhattacharya<sup>a</sup> [ID](#), L. Bianchini<sup>a,b</sup> [ID](#), T. Boccali<sup>a</sup> [ID](#), E. Bossini<sup>a</sup> [ID](#), D. Bruschini<sup>a,c</sup> [ID](#), R. Castaldi<sup>a</sup> [ID](#), M.A. Ciocci<sup>a,b</sup> [ID](#), M. Cipriani<sup>a,b</sup> [ID](#), V. D'Amante<sup>a,d</sup> [ID](#), R. Dell'Orso<sup>a</sup> [ID](#), S. Donato<sup>a</sup> [ID](#), A. Giassi<sup>a</sup> [ID](#), F. Ligabue<sup>a,c</sup> [ID](#), D. Matos Figueiredo<sup>a</sup> [ID](#), A. Messineo<sup>a,b</sup> [ID](#), M. Musich<sup>a,b</sup> [ID](#), F. Palla<sup>a</sup> [ID](#), A. Rizzi<sup>a,b</sup> [ID](#), G. Rolandi<sup>a,c</sup> [ID](#), S. Roy Chowdhury<sup>a</sup> [ID](#), T. Sarkar<sup>a</sup> [ID](#), A. Scribano<sup>a</sup> [ID](#), P. Spagnolo<sup>a</sup> [ID](#), R. Tenchini<sup>a</sup> [ID](#), G. Tonelli<sup>a,b</sup> [ID](#), N. Turini<sup>a,d</sup> [ID](#), F. Vaselli<sup>a,c</sup> [ID](#), A. Venturi<sup>a</sup> [ID](#), P.G. Verdini<sup>a</sup> [ID](#)

**INFN Sezione di Roma<sup>a</sup>, Sapienza Università di Roma<sup>b</sup>, Roma, Italy**

C. Baldenegro Barrera<sup>a,b</sup> [ID](#), P. Barria<sup>a</sup> [ID](#), C. Basile<sup>a,b</sup> [ID](#), M. Campana<sup>a,b</sup> [ID](#), F. Cavallari<sup>a</sup> [ID](#), L. Cunqueiro Mendez<sup>a,b</sup> [ID](#), D. Del Re<sup>a,b</sup> [ID](#), E. Di Marco<sup>a</sup> [ID](#), M. Diemoz<sup>a</sup> [ID](#), F. Errico<sup>a,b</sup> [ID](#), E. Longo<sup>a,b</sup> [ID](#), J. Mijuskovic<sup>a,b</sup> [ID](#), G. Organtini<sup>a,b</sup> [ID](#), F. Pandolfi<sup>a</sup> [ID](#), R. Paramatti<sup>a,b</sup> [ID](#), C. Quaranta<sup>a,b</sup> [ID](#), S. Rahatlou<sup>a,b</sup> [ID](#), C. Rovelli<sup>a</sup> [ID](#), F. Santanastasio<sup>a,b</sup> [ID](#), L. Soffi<sup>a</sup> [ID](#)

**INFN Sezione di Torino<sup>a</sup>, Università di Torino<sup>b</sup>, Torino, Italy; Università del Piemonte Orientale<sup>c</sup>, Novara, Italy**

N. Amapane<sup>a,b</sup> [ID](#), R. Arcidiacono<sup>a,c</sup> [ID](#), S. Argiro<sup>a,b</sup> [ID](#), M. Arneodo<sup>a,c</sup> [ID](#), N. Bartosik<sup>a</sup> [ID](#)

R. Bellan<sup>a,b</sup> , A. Bellora<sup>a,b</sup> , C. Biino<sup>a</sup> , C. Borca<sup>a,b</sup> , N. Cartiglia<sup>a</sup> , M. Costa<sup>a,b</sup> , R. Covarelli<sup>a,b</sup> , N. Demaria<sup>a</sup> , L. Finco<sup>a</sup> , M. Grippo<sup>a,b</sup> , B. Kiani<sup>a,b</sup> , F. Legger<sup>a</sup> , F. Luongo<sup>a,b</sup> , C. Mariotti<sup>a</sup> , L. Markovic<sup>a,b</sup> , S. Maselli<sup>a</sup> , A. Mecca<sup>a,b</sup> , L. Menzio<sup>a,b</sup> , P. Meridiani<sup>a</sup> , E. Migliore<sup>a,b</sup> , M. Monteno<sup>a</sup> , R. Mulargia<sup>a</sup> , M.M. Obertino<sup>a,b</sup> , G. Ortona<sup>a</sup> , L. Pacher<sup>a,b</sup> , N. Pastrone<sup>a</sup> , M. Pelliccioni<sup>a</sup> , M. Ruspa<sup>a,c</sup> , F. Siviero<sup>a,b</sup> , V. Sola<sup>a,b</sup> , A. Solano<sup>a,b</sup> , A. Staiano<sup>a</sup> , C. Tarricone<sup>a,b</sup> , D. Trocino<sup>a</sup> , G. Umoret<sup>a,b</sup> , E. Vlasov<sup>a,b</sup> , R. White<sup>a,b</sup> 

**INFN Sezione di Trieste<sup>a</sup>, Università di Trieste<sup>b</sup>, Trieste, Italy**

S. Belforte<sup>a</sup> , V. Candelise<sup>a,b</sup> , M. Casarsa<sup>a</sup> , F. Cossutti<sup>a</sup> , K. De Leo<sup>a</sup> , G. Della Ricca<sup>a,b</sup> 

**Kyungpook National University, Daegu, Korea**

S. Dogra , J. Hong , C. Huh , B. Kim , J. Kim, D. Lee, H. Lee, S.W. Lee , C.S. Moon , Y.D. Oh , M.S. Ryu , S. Sekmen , B. Tae, Y.C. Yang 

**Department of Mathematics and Physics - GWNU, Gangneung, Korea**

M.S. Kim 

**Chonnam National University, Institute for Universe and Elementary Particles, Kwangju, Korea**

G. Bak , P. Gwak , H. Kim , D.H. Moon 

**Hanyang University, Seoul, Korea**

E. Asilar , J. Choi , D. Kim , T.J. Kim , J.A. Merlin, Y. Ryou

**Korea University, Seoul, Korea**

S. Choi , S. Han, B. Hong , K. Lee, K.S. Lee , S. Lee , S.K. Park, J. Yoo 

**Kyung Hee University, Department of Physics, Seoul, Korea**

J. Goh , S. Yang 

**Sejong University, Seoul, Korea**

H. S. Kim , Y. Kim, S. Lee

**Seoul National University, Seoul, Korea**

J. Almond, J.H. Bhyun, J. Choi , J. Choi, W. Jun , J. Kim , S. Ko , H. Kwon , H. Lee , J. Lee , J. Lee , B.H. Oh , S.B. Oh , H. Seo , U.K. Yang, I. Yoon 

**University of Seoul, Seoul, Korea**

W. Jang , D.Y. Kang, Y. Kang , S. Kim , B. Ko, J.S.H. Lee , Y. Lee , I.C. Park , Y. Roh, I.J. Watson 

**Yonsei University, Department of Physics, Seoul, Korea**

S. Ha , H.D. Yoo 

**Sungkyunkwan University, Suwon, Korea**

M. Choi , M.R. Kim , H. Lee, Y. Lee , I. Yu 

**College of Engineering and Technology, American University of the Middle East (AUM), Dasman, Kuwait**

T. Beyrouthy

**Riga Technical University, Riga, Latvia**

K. Dreimanis , A. Gaile , G. Pikurs, A. Potrebko , M. Seidel , D. Sidiropoulos Kontos

**University of Latvia (LU), Riga, Latvia**

N.R. Strautnieks 

**Vilnius University, Vilnius, Lithuania**

M. Ambrozas , A. Juodagalvis , A. Rinkevicius , G. Tamulaitis 

**National Centre for Particle Physics, Universiti Malaya, Kuala Lumpur, Malaysia**

I. Yusuff<sup>52</sup> , Z. Zolkapli

**Universidad de Sonora (UNISON), Hermosillo, Mexico**

J.F. Benitez , A. Castaneda Hernandez , H.A. Encinas Acosta, L.G. Gallegos Maríñez, M. León Coello , J.A. Murillo Quijada , A. Sehrawat , L. Valencia Palomo 

**Centro de Investigacion y de Estudios Avanzados del IPN, Mexico City, Mexico**

G. Ayala , H. Castilla-Valdez , H. Crotte Ledesma, E. De La Cruz-Burelo , I. Heredia-De La Cruz<sup>53</sup> , R. Lopez-Fernandez , J. Mejia Guisao , C.A. Mondragon Herrera, A. Sánchez Hernández 

**Universidad Iberoamericana, Mexico City, Mexico**

C. Oropeza Barrera , D.L. Ramirez Guadarrama, M. Ramírez García 

**Benemerita Universidad Autonoma de Puebla, Puebla, Mexico**

I. Bautista , I. Pedraza , H.A. Salazar Ibarguen , C. Uribe Estrada 

**University of Montenegro, Podgorica, Montenegro**

I. Bubanja, N. Raicevic 

**University of Canterbury, Christchurch, New Zealand**

P.H. Butler 

**National Centre for Physics, Quaid-I-Azam University, Islamabad, Pakistan**

A. Ahmad , M.I. Asghar, A. Awais , M.I.M. Awan, H.R. Hoorani , W.A. Khan 

**AGH University of Krakow, Faculty of Computer Science, Electronics and Telecommunications, Krakow, Poland**

V. Avati, L. Grzanka , M. Malawski 

**National Centre for Nuclear Research, Swierk, Poland**

H. Bialkowska , M. Bluj , M. Górski , M. Kazana , M. Szleper , P. Zalewski 

**Institute of Experimental Physics, Faculty of Physics, University of Warsaw, Warsaw, Poland**

K. Bunkowski , K. Doroba , A. Kalinowski , M. Konecki , J. Krolikowski , A. Muhammad 

**Warsaw University of Technology, Warsaw, Poland**

K. Pozniak , W. Zabolotny 

**Laboratório de Instrumentação e Física Experimental de Partículas, Lisboa, Portugal**

M. Araujo , D. Bastos , C. Beirão Da Cruz E Silva , A. Boletti , M. Bozzo , T. Camporesi , G. Da Molin , P. Faccioli , M. Gallinaro , J. Hollar , N. Leonardo , G.B. Marozzo, T. Niknejad , A. Petrilli , M. Pisano , J. Seixas , J. Varela , J.W. Wulff

**Faculty of Physics, University of Belgrade, Belgrade, Serbia**

P. Adzic , P. Milenovic 

**VINCA Institute of Nuclear Sciences, University of Belgrade, Belgrade, Serbia**

M. Dordevic , J. Milosevic , L. Nadderd , V. Rekovic

**Centro de Investigaciones Energéticas Medioambientales y Tecnológicas (CIEMAT),**

**Madrid, Spain**

J. Alcaraz Maestre [ID](#), Cristina F. Bedoya [ID](#), Oliver M. Carretero [ID](#), M. Cepeda [ID](#), M. Cerrada [ID](#), N. Colino [ID](#), B. De La Cruz [ID](#), A. Delgado Peris [ID](#), A. Escalante Del Valle [ID](#), D. Fernández Del Val [ID](#), J.P. Fernández Ramos [ID](#), J. Flix [ID](#), M.C. Fouz [ID](#), O. Gonzalez Lopez [ID](#), S. Goy Lopez [ID](#), J.M. Hernandez [ID](#), M.I. Josa [ID](#), E. Martin Viscasillas [ID](#), D. Moran [ID](#), C. M. Morcillo Perez [ID](#), Á. Navarro Tobar [ID](#), C. Perez Dengra [ID](#), A. Pérez-Calero Yzquierdo [ID](#), J. Puerta Pelayo [ID](#), I. Redondo [ID](#), S. Sánchez Navas [ID](#), J. Sastre [ID](#), J. Vazquez Escobar [ID](#)

**Universidad Autónoma de Madrid, Madrid, Spain**

J.F. de Trocóniz [ID](#)

**Universidad de Oviedo, Instituto Universitario de Ciencias y Tecnologías Espaciales de Asturias (ICTEA), Oviedo, Spain**

B. Alvarez Gonzalez [ID](#), J. Cuevas [ID](#), J. Fernandez Menendez [ID](#), S. Folgueras [ID](#), I. Gonzalez Caballero [ID](#), J.R. González Fernández [ID](#), P. Leguina [ID](#), E. Palencia Cortezon [ID](#), C. Ramón Álvarez [ID](#), V. Rodríguez Bouza [ID](#), A. Soto Rodríguez [ID](#), A. Trapote [ID](#), C. Vico Villalba [ID](#), P. Vischia [ID](#)

**Instituto de Física de Cantabria (IFCA), CSIC-Universidad de Cantabria, Santander, Spain**

S. Bhowmik [ID](#), S. Blanco Fernández [ID](#), J.A. Brochero Cifuentes [ID](#), I.J. Cabrillo [ID](#), A. Calderon [ID](#), J. Duarte Campderros [ID](#), M. Fernandez [ID](#), G. Gomez [ID](#), C. Lasosa García [ID](#), R. Lopez Ruiz [ID](#), C. Martinez Rivero [ID](#), P. Martinez Ruiz del Arbol [ID](#), F. Matorras [ID](#), P. Matorras Cuevas [ID](#), E. Navarrete Ramos [ID](#), J. Piedra Gomez [ID](#), L. Scodellaro [ID](#), I. Vila [ID](#), J.M. Vizan Garcia [ID](#)

**University of Colombo, Colombo, Sri Lanka**

B. Kailasapathy<sup>54</sup> [ID](#), D.D.C. Wickramarathna [ID](#)

**University of Ruhuna, Department of Physics, Matara, Sri Lanka**

W.G.D. Dharmaratna<sup>55</sup> [ID](#), K. Liyanage [ID](#), N. Perera [ID](#)

**CERN, European Organization for Nuclear Research, Geneva, Switzerland**

D. Abbaneo [ID](#), C. Amendola [ID](#), E. Auffray [ID](#), G. Auzinger [ID](#), J. Baechler, D. Barney [ID](#), A. Bermúdez Martínez [ID](#), M. Bianco [ID](#), B. Bilin [ID](#), A.A. Bin Anuar [ID](#), A. Bocci [ID](#), C. Botta [ID](#), E. Brondolin [ID](#), C. Caillol [ID](#), G. Cerminara [ID](#), N. Chernyavskaya [ID](#), D. d'Enterria [ID](#), A. Dabrowski [ID](#), A. David [ID](#), A. De Roeck [ID](#), M.M. Defranchis [ID](#), M. Deile [ID](#), M. Dobson [ID](#), G. Franzoni [ID](#), W. Funk [ID](#), S. Giani, D. Gigi, K. Gill [ID](#), F. Glege [ID](#), L. Gouskos [ID](#), J. Hegeman [ID](#), J.K. Heikkilä [ID](#), B. Huber, V. Innocente [ID](#), T. James [ID](#), P. Janot [ID](#), O. Kaluzinska [ID](#), S. Laurila [ID](#), P. Lecoq [ID](#), E. Leutgeb [ID](#), C. Lourenço [ID](#), L. Malgeri [ID](#), M. Mannelli [ID](#), A.C. Marini [ID](#), M. Matthewman, A. Mehta [ID](#), F. Meijers [ID](#), S. Mersi [ID](#), E. Meschi [ID](#), V. Milosevic [ID](#), F. Monti [ID](#), F. Moortgat [ID](#), M. Mulders [ID](#), I. Neutelings [ID](#), S. Orfanelli, F. Pantaleo [ID](#), G. Petrucciani [ID](#), A. Pfeiffer [ID](#), M. Pierini [ID](#), H. Qu [ID](#), D. Rabady [ID](#), B. Ribeiro Lopes [ID](#), M. Rovere [ID](#), H. Sakulin [ID](#), S. Sanchez Cruz [ID](#), S. Scarfi [ID](#), C. Schwick, M. Selvaggi [ID](#), A. Sharma [ID](#), K. Shchelina [ID](#), P. Silva [ID](#), P. Sphicas<sup>56</sup> [ID](#), A.G. Stahl Leiton [ID](#), A. Steen [ID](#), S. Summers [ID](#), D. Treille [ID](#), P. Tropea [ID](#), D. Walter [ID](#), J. Wanczyk<sup>57</sup> [ID](#), J. Wang, S. Wuchterl [ID](#), P. Zehetner [ID](#), P. Zejdl [ID](#), W.D. Zeuner

**Paul Scherrer Institut, Villigen, Switzerland**

T. Bevilacqua<sup>58</sup> [ID](#), L. Caminada<sup>58</sup> [ID](#), A. Ebrahimi [ID](#), W. Erdmann [ID](#), R. Horisberger [ID](#), Q. Ingram [ID](#), H.C. Kaestli [ID](#), D. Kotlinski [ID](#), C. Lange [ID](#), M. Missiroli<sup>58</sup> [ID](#), L. Noehte<sup>58</sup> [ID](#), T. Rohe [ID](#)

**ETH Zurich - Institute for Particle Physics and Astrophysics (IPA), Zurich, Switzerland**

T.K. Arrestad [id](#), K. Androsov<sup>57</sup> [id](#), M. Backhaus [id](#), G. Bonomelli, A. Calandri [id](#), C. Cazzaniga [id](#), K. Datta [id](#), P. De Bryas Dexmiers D'archiac<sup>57</sup> [id](#), A. De Cosa [id](#), G. Dissertori [id](#), M. Dittmar, M. Donegà [id](#), F. Eble [id](#), M. Galli [id](#), K. Gedia [id](#), F. Glessgen [id](#), C. Grab [id](#), N. Härringer [id](#), T.G. Harte, D. Hits [id](#), W. Lustermann [id](#), A.-M. Lyon [id](#), R.A. Manzoni [id](#), M. Marchegiani [id](#), L. Marchese [id](#), C. Martin Perez [id](#), A. Mascellani<sup>57</sup> [id](#), F. Nessi-Tedaldi [id](#), F. Pauss [id](#), V. Perovic [id](#), S. Pigazzini [id](#), C. Reissel [id](#), T. Reitenspiess [id](#), B. Ristic [id](#), F. Riti [id](#), R. Seidita [id](#), J. Steggemann<sup>57</sup> [id](#), A. Tarabini [id](#), D. Valsecchi [id](#), R. Wallny [id](#)

#### **Universität Zürich, Zurich, Switzerland**

C. Amsler<sup>59</sup> [id](#), P. Bärtschi [id](#), M.F. Canelli [id](#), K. Cormier [id](#), M. Huwiler [id](#), W. Jin [id](#), A. Jofrehei [id](#), B. Kilminster [id](#), S. Leontsinis [id](#), S.P. Liechti [id](#), A. Macchiolo [id](#), P. Meiring [id](#), F. Meng [id](#), U. Molinatti [id](#), J. Motta [id](#), A. Reimers [id](#), P. Robmann, M. Senger [id](#), E. Shokr, F. Stäger [id](#), R. Tramontano [id](#)

#### **National Central University, Chung-Li, Taiwan**

C. Adloff<sup>60</sup>, D. Bhowmik, C.M. Kuo, W. Lin, P.K. Rout [id](#), P.C. Tiwari<sup>37</sup> [id](#), S.S. Yu [id](#)

#### **National Taiwan University (NTU), Taipei, Taiwan**

L. Ceard, K.F. Chen [id](#), P.s. Chen, Z.g. Chen, A. De Iorio [id](#), W.-S. Hou [id](#), T.h. Hsu, Y.w. Kao, S. Karmakar [id](#), G. Kole [id](#), Y.y. Li [id](#), R.-S. Lu [id](#), E. Paganis [id](#), X.f. Su [id](#), J. Thomas-Wilsker [id](#), L.s. Tsai, H.y. Wu, E. Yazgan [id](#)

#### **High Energy Physics Research Unit, Department of Physics, Faculty of Science, Chulalongkorn University, Bangkok, Thailand**

C. Asawatangtrakuldee [id](#), N. Srimanobhas [id](#), V. Wachirapusanand [id](#)

#### **Çukurova University, Physics Department, Science and Art Faculty, Adana, Turkey**

D. Agyel [id](#), F. Boran [id](#), F. Dolek [id](#), I. Dumanoglu<sup>61</sup> [id](#), E. Eskut [id](#), Y. Guler<sup>62</sup> [id](#), E. Gurpinar Guler<sup>62</sup> [id](#), C. Isik [id](#), O. Kara, A. Kayis Topaksu [id](#), U. Kiminsu [id](#), G. Onengut [id](#), K. Ozdemir<sup>63</sup> [id](#), A. Polatoz [id](#), B. Tali<sup>64</sup> [id](#), U.G. Tok [id](#), S. Turkcapar [id](#), E. Uslan [id](#), I.S. Zorbakir [id](#)

#### **Middle East Technical University, Physics Department, Ankara, Turkey**

G. Sokmen, M. Yalvac<sup>65</sup> [id](#)

#### **Bogazici University, Istanbul, Turkey**

B. Akgun [id](#), I.O. Atakisi [id](#), E. Gürmez [id](#), M. Kaya<sup>66</sup> [id](#), O. Kaya<sup>67</sup> [id](#), S. Tekten<sup>68</sup> [id](#)

#### **Istanbul Technical University, Istanbul, Turkey**

A. Cakir [id](#), K. Cankocak<sup>61,69</sup> [id](#), G.G. Dincer<sup>61</sup> [id](#), Y. Komurcu [id](#), S. Sen<sup>70</sup> [id](#)

#### **Istanbul University, Istanbul, Turkey**

O. Aydilek<sup>71</sup> [id](#), V. Epshteyn [id](#), B. Hacisahinoglu [id](#), I. Hos<sup>72</sup> [id](#), B. Kaynak [id](#), S. Ozkorucuklu [id](#), O. Potok [id](#), H. Sert [id](#), C. Simsek [id](#), C. Zorbilmez [id](#)

#### **Yildiz Technical University, Istanbul, Turkey**

S. Cerci<sup>64</sup> [id](#), B. Isildak<sup>73</sup> [id](#), D. Sunar Cerci [id](#), T. Yetkin [id](#)

#### **Institute for Scintillation Materials of National Academy of Science of Ukraine, Kharkiv, Ukraine**

A. Boyaryntsev [id](#), B. Grynyov [id](#)

#### **National Science Centre, Kharkiv Institute of Physics and Technology, Kharkiv, Ukraine**

L. Levchuk [id](#)

#### **University of Bristol, Bristol, United Kingdom**

D. Anthony [ID](#), J.J. Brooke [ID](#), A. Bundock [ID](#), F. Bury [ID](#), E. Clement [ID](#), D. Cussans [ID](#), H. Flacher [ID](#), M. Glowacki, J. Goldstein [ID](#), H.F. Heath [ID](#), M.-L. Holmberg [ID](#), L. Kreczko [ID](#), S. Paramesvaran [ID](#), L. Robertshaw, S. Seif El Nasr-Storey, V.J. Smith [ID](#), N. Stylianou<sup>74</sup> [ID](#), K. Walkingshaw Pass

#### **Rutherford Appleton Laboratory, Didcot, United Kingdom**

A.H. Ball, K.W. Bell [ID](#), A. Belyaev<sup>75</sup> [ID](#), C. Brew [ID](#), R.M. Brown [ID](#), D.J.A. Cockerill [ID](#), C. Cooke [ID](#), A. Elliot [ID](#), K.V. Ellis, K. Harder [ID](#), S. Harper [ID](#), J. Linacre [ID](#), K. Manolopoulos, D.M. Newbold [ID](#), E. Olaiya, D. Petyt [ID](#), T. Reis [ID](#), A.R. Sahasransu [ID](#), G. Salvi [ID](#), T. Schuh, C.H. Shepherd-Themistocleous [ID](#), I.R. Tomalin [ID](#), K.C. Whalen [ID](#), T. Williams [ID](#)

#### **Imperial College, London, United Kingdom**

I. Andreou [ID](#), R. Bainbridge [ID](#), P. Bloch [ID](#), C.E. Brown [ID](#), O. Buchmuller, V. Cacchio, C.A. Carrillo Montoya [ID](#), G.S. Chahal<sup>76</sup> [ID](#), D. Colling [ID](#), J.S. Dancu, I. Das [ID](#), P. Dauncey [ID](#), G. Davies [ID](#), J. Davies, M. Della Negra [ID](#), S. Fayer, G. Fedi [ID](#), G. Hall [ID](#), M.H. Hassanshahi [ID](#), A. Howard, G. Iles [ID](#), M. Knight [ID](#), J. Langford [ID](#), J. León Holgado [ID](#), L. Lyons [ID](#), A.-M. Magnan [ID](#), S. Mallios, M. Mieskolainen [ID](#), J. Nash<sup>77</sup> [ID](#), M. Pesaresi [ID](#), P.B. Pradeep, B.C. Radburn-Smith [ID](#), A. Richards, A. Rose [ID](#), K. Savva [ID](#), C. Seez [ID](#), R. Shukla [ID](#), A. Tapper [ID](#), K. Uchida [ID](#), G.P. Uttley [ID](#), L.H. Vage, T. Virdee<sup>29</sup> [ID](#), M. Vojinovic [ID](#), N. Wardle [ID](#), D. Winterbottom [ID](#)

#### **Brunel University, Uxbridge, United Kingdom**

K. Coldham, J.E. Cole [ID](#), A. Khan, P. Kyberd [ID](#), I.D. Reid [ID](#)

#### **Baylor University, Waco, Texas, USA**

S. Abdullin [ID](#), A. Brinkerhoff [ID](#), B. Caraway [ID](#), E. Collins [ID](#), J. Dittmann [ID](#), K. Hatakeyama [ID](#), J. Hiltbrand [ID](#), B. McMaster [ID](#), J. Samudio [ID](#), S. Sawant [ID](#), C. Sutantawibul [ID](#), J. Wilson [ID](#)

#### **Catholic University of America, Washington, DC, USA**

R. Bartek [ID](#), A. Dominguez [ID](#), C. Huerta Escamilla, A.E. Simsek [ID](#), R. Uniyal [ID](#), A.M. Vargas Hernandez [ID](#)

#### **The University of Alabama, Tuscaloosa, Alabama, USA**

B. Bam [ID](#), A. Buchot Perraguin [ID](#), R. Chudasama [ID](#), S.I. Cooper [ID](#), C. Crovella [ID](#), S.V. Gleyzer [ID](#), E. Pearson, C.U. Perez [ID](#), P. Rumerio<sup>78</sup> [ID](#), E. Usai [ID](#), R. Yi [ID](#)

#### **Boston University, Boston, Massachusetts, USA**

A. Akpinar [ID](#), C. Cosby [ID](#), G. De Castro, Z. Demiragli [ID](#), C. Erice [ID](#), C. Fangmeier [ID](#), C. Fernandez Madrazo [ID](#), E. Fontanesi [ID](#), D. Gastler [ID](#), F. Golf [ID](#), S. Jeon [ID](#), J. O'cain, I. Reed [ID](#), J. Rohlf [ID](#), K. Salyer [ID](#), D. Sperka [ID](#), D. Spitzbart [ID](#), I. Suarez [ID](#), A. Tsatsos [ID](#), A.G. Zecchinelli [ID](#)

#### **Brown University, Providence, Rhode Island, USA**

G. Benelli [ID](#), X. Coubez<sup>25</sup>, D. Cutts [ID](#), M. Hadley [ID](#), U. Heintz [ID](#), J.M. Hogan<sup>79</sup> [ID](#), T. Kwon [ID](#), G. Landsberg [ID](#), K.T. Lau [ID](#), D. Li [ID](#), J. Luo [ID](#), S. Mondal [ID](#), M. Narain<sup>†</sup> [ID](#), N. Pervan [ID](#), S. Sagir<sup>80</sup> [ID](#), F. Simpson [ID](#), M. Stamenkovic [ID](#), N. Venkatasubramanian, X. Yan [ID](#), W. Zhang

#### **University of California, Davis, Davis, California, USA**

S. Abbott [ID](#), J. Bonilla [ID](#), C. Brainerd [ID](#), R. Breedon [ID](#), H. Cai [ID](#), M. Calderon De La Barca Sanchez [ID](#), M. Chertok [ID](#), M. Citron [ID](#), J. Conway [ID](#), P.T. Cox [ID](#), R. Erbacher [ID](#), F. Jensen [ID](#), O. Kukral [ID](#), G. Mocellin [ID](#), M. Mulhearn [ID](#), S. Ostrom [ID](#), W. Wei [ID](#), Y. Yao [ID](#), S. Yoo [ID](#), F. Zhang [ID](#)

#### **University of California, Los Angeles, California, USA**

M. Bachtis [ID](#), R. Cousins [ID](#), A. Datta [ID](#), G. Flores Avila, J. Hauser [ID](#), M. Ignatenko [ID](#), M.A. Iqbal [ID](#), T. Lam [ID](#), E. Manca [ID](#), N. Mccoll [ID](#), A. Nunez Del Prado, D. Saltzberg [ID](#), B. Stone [ID](#), V. Valuev [ID](#)

**University of California, Riverside, Riverside, California, USA**

R. Clare [ID](#), J.W. Gary [ID](#), M. Gordon, G. Hanson [ID](#), W. Si [ID](#), S. Wimpenny<sup>†</sup> [ID](#)

**University of California, San Diego, La Jolla, California, USA**

A. Aportela, A. Arora [ID](#), J.G. Branson [ID](#), S. Cittolin [ID](#), S. Cooperstein [ID](#), D. Diaz [ID](#), J. Duarte [ID](#), L. Giannini [ID](#), Y. Gu, J. Guiang [ID](#), R. Kansal [ID](#), V. Krutelyov [ID](#), R. Lee [ID](#), J. Letts [ID](#), M. Masciovecchio [ID](#), F. Mokhtar [ID](#), S. Mukherjee [ID](#), M. Pieri [ID](#), M. Quinnan [ID](#), B.V. Sathia Narayanan [ID](#), V. Sharma [ID](#), M. Tadel [ID](#), E. Vourliotis [ID](#), F. Würthwein [ID](#), Y. Xiang [ID](#), A. Yagil [ID](#)

**University of California, Santa Barbara - Department of Physics, Santa Barbara, California, USA**

A. Barzdukas [ID](#), L. Brennan [ID](#), C. Campagnari [ID](#), K. Downham [ID](#), C. Grieco [ID](#), J. Incandela [ID](#), J. Kim [ID](#), A.J. Li [ID](#), P. Masterson [ID](#), H. Mei [ID](#), J. Richman [ID](#), S.N. Santpur [ID](#), U. Sarica [ID](#), R. Schmitz [ID](#), F. Setti [ID](#), J. Sheplock [ID](#), D. Stuart [ID](#), T.Á. Vámi [ID](#), S. Wang [ID](#), D. Zhang

**California Institute of Technology, Pasadena, California, USA**

A. Bornheim [ID](#), O. Cerri, A. Latorre, J. Mao [ID](#), H.B. Newman [ID](#), G. Reales Gutiérrez, M. Spiropulu [ID](#), J.R. Vlimant [ID](#), C. Wang [ID](#), S. Xie [ID](#), R.Y. Zhu [ID](#)

**Carnegie Mellon University, Pittsburgh, Pennsylvania, USA**

J. Alison [ID](#), S. An [ID](#), M.B. Andrews [ID](#), P. Bryant [ID](#), M. Cremonesi, V. Dutta [ID](#), T. Ferguson [ID](#), T.A. Gómez Espinosa [ID](#), A. Harilal [ID](#), A. Kallil Tharayil, C. Liu [ID](#), T. Mudholkar [ID](#), S. Murthy [ID](#), P. Palit [ID](#), K. Park, M. Paulini [ID](#), A. Roberts [ID](#), A. Sanchez [ID](#), W. Terrill [ID](#)

**University of Colorado Boulder, Boulder, Colorado, USA**

J.P. Cumalat [ID](#), W.T. Ford [ID](#), A. Hart [ID](#), A. Hassani [ID](#), G. Karathanasis [ID](#), N. Manganelli [ID](#), A. Perloff [ID](#), C. Savard [ID](#), N. Schonbeck [ID](#), K. Stenson [ID](#), K.A. Ulmer [ID](#), S.R. Wagner [ID](#), N. Zipper [ID](#), D. Zuolo [ID](#)

**Cornell University, Ithaca, New York, USA**

J. Alexander [ID](#), S. Bright-Thonney [ID](#), X. Chen [ID](#), D.J. Cranshaw [ID](#), J. Fan [ID](#), X. Fan [ID](#), S. Hogan [ID](#), P. Kotamnives, J. Monroy [ID](#), M. Oshiro [ID](#), J.R. Patterson [ID](#), M. Reid [ID](#), A. Ryd [ID](#), J. Thom [ID](#), P. Wittich [ID](#), R. Zou [ID](#)

**Fermi National Accelerator Laboratory, Batavia, Illinois, USA**

M. Albrow [ID](#), M. Alyari [ID](#), O. Amram [ID](#), G. Apollinari [ID](#), A. Apresyan [ID](#), L.A.T. Bauerick [ID](#), D. Berry [ID](#), J. Berryhill [ID](#), P.C. Bhat [ID](#), K. Burkett [ID](#), J.N. Butler [ID](#), A. Canepa [ID](#), G.B. Cerati [ID](#), H.W.K. Cheung [ID](#), F. Chlebana [ID](#), G. Cummings [ID](#), J. Dickinson [ID](#), I. Dutta [ID](#), V.D. Elvira [ID](#), Y. Feng [ID](#), J. Freeman [ID](#), A. Gandrakota [ID](#), Z. Gecse [ID](#), L. Gray [ID](#), D. Green, A. Grummer [ID](#), S. Grünendahl [ID](#), D. Guerrero [ID](#), O. Gutsche [ID](#), R.M. Harris [ID](#), R. Heller [ID](#), T.C. Herwig [ID](#), J. Hirschauer [ID](#), B. Jayatilaka [ID](#), S. Jindariani [ID](#), M. Johnson [ID](#), U. Joshi [ID](#), T. Klijnsma [ID](#), B. Klima [ID](#), K.H.M. Kwok [ID](#), S. Lammel [ID](#), D. Lincoln [ID](#), R. Lipton [ID](#), T. Liu [ID](#), C. Madrid [ID](#), K. Maeshima [ID](#), C. Mantilla [ID](#), D. Mason [ID](#), P. McBride [ID](#), P. Merkel [ID](#), S. Mrenna [ID](#), S. Nahn [ID](#), J. Ngadiuba [ID](#), D. Noonan [ID](#), S. Norberg, V. Papadimitriou [ID](#), N. Pastika [ID](#), K. Pedro [ID](#), C. Pena<sup>81</sup> [ID](#), F. Ravera [ID](#), A. Reinsvold Hall<sup>82</sup> [ID](#), L. Ristori [ID](#), M. Safdari [ID](#), E. Sexton-Kennedy [ID](#), N. Smith [ID](#), A. Soha [ID](#), L. Spiegel [ID](#), S. Stoynev [ID](#), J. Strait [ID](#), L. Taylor [ID](#), S. Tkaczyk [ID](#), N.V. Tran [ID](#), L. Uplegger [ID](#), E.W. Vaandering [ID](#), I. Zoi [ID](#)

**University of Florida, Gainesville, Florida, USA**

C. Aruta [ID](#), P. Avery [ID](#), D. Bourilkov [ID](#), P. Chang [ID](#), V. Cherepanov [ID](#), R.D. Field, E. Koenig [ID](#), M. Kolosova [ID](#), J. Konigsberg [ID](#), A. Korytov [ID](#), K. Matchev [ID](#), N. Menendez [ID](#), G. Mitselmakher [ID](#), K. Mohrman [ID](#), A. Muthirakalayil Madhu [ID](#), N. Rawal [ID](#), S. Rosenzweig [ID](#), Y. Takahashi [ID](#), J. Wang [ID](#)

**Florida State University, Tallahassee, Florida, USA**

T. Adams [ID](#), A. Al Kadhim [ID](#), A. Askew [ID](#), S. Bower [ID](#), R. Habibullah [ID](#), V. Hagopian [ID](#), R. Hashmi [ID](#), R.S. Kim [ID](#), S. Kim [ID](#), T. Kolberg [ID](#), G. Martinez, H. Prosper [ID](#), P.R. Prova, M. Wulansatiti [ID](#), R. Yohay [ID](#), J. Zhang

**Florida Institute of Technology, Melbourne, Florida, USA**

B. Alsufyani, M.M. Baarmand [ID](#), S. Butalla [ID](#), S. Das [ID](#), T. Elkafrawy<sup>83</sup> [ID](#), M. Hohlmann [ID](#), M. Rahmani, E. Yanes

**University of Illinois Chicago, Chicago, USA, Chicago, USA**

M.R. Adams [ID](#), A. Baty [ID](#), C. Bennett, R. Cavanaugh [ID](#), R. Escobar Franco [ID](#), O. Evdokimov [ID](#), C.E. Gerber [ID](#), M. Hawksworth, A. Hingrajiya, D.J. Hofman [ID](#), J.h. Lee [ID](#), D. S. Lemos [ID](#), A.H. Merrit [ID](#), C. Mills [ID](#), S. Nanda [ID](#), G. Oh [ID](#), B. Ozek [ID](#), D. Pilipovic [ID](#), R. Pradhan [ID](#), E. Prifti, T. Roy [ID](#), S. Rudrabhatla [ID](#), M.B. Tonjes [ID](#), N. Varelas [ID](#), M.A. Wadud [ID](#), Z. Ye [ID](#), J. Yoo [ID](#)

**The University of Iowa, Iowa City, Iowa, USA**

M. Alhusseini [ID](#), D. Blend, K. Dilsiz<sup>84</sup> [ID](#), L. Emediato [ID](#), G. Karaman [ID](#), O.K. Köseyan [ID](#), J.-P. Merlo, A. Mestvirishvili<sup>85</sup> [ID](#), O. Neogi, H. Ogul<sup>86</sup> [ID](#), Y. Onel [ID](#), A. Penzo [ID](#), C. Snyder, E. Tiras<sup>87</sup> [ID](#)

**Johns Hopkins University, Baltimore, Maryland, USA**

B. Blumenfeld [ID](#), L. Corcodilos [ID](#), J. Davis [ID](#), A.V. Gritsan [ID](#), L. Kang [ID](#), S. Kyriacou [ID](#), P. Maksimovic [ID](#), M. Roguljic [ID](#), J. Roskes [ID](#), S. Sekhar [ID](#), M. Swartz [ID](#)

**The University of Kansas, Lawrence, Kansas, USA**

A. Abreu [ID](#), L.F. Alcerro Alcerro [ID](#), J. Anguiano [ID](#), S. Arteaga Escatel [ID](#), P. Baringer [ID](#), A. Bean [ID](#), Z. Flowers [ID](#), D. Grove [ID](#), J. King [ID](#), G. Krintiras [ID](#), M. Lazarovits [ID](#), C. Le Mahieu [ID](#), J. Marquez [ID](#), N. Minafra [ID](#), M. Murray [ID](#), M. Nickel [ID](#), M. Pitt [ID](#), S. Popescu<sup>88</sup> [ID](#), C. Rogan [ID](#), C. Royon [ID](#), R. Salvatico [ID](#), S. Sanders [ID](#), C. Smith [ID](#), G. Wilson [ID](#)

**Kansas State University, Manhattan, Kansas, USA**

B. Allmond [ID](#), R. Guju Gurunadha [ID](#), A. Ivanov [ID](#), K. Kaadze [ID](#), Y. Maravin [ID](#), J. Natoli [ID](#), D. Roy [ID](#), G. Sorrentino [ID](#)

**University of Maryland, College Park, Maryland, USA**

A. Baden [ID](#), A. Belloni [ID](#), J. Bistany-riebman, Y.M. Chen [ID](#), S.C. Eno [ID](#), N.J. Hadley [ID](#), S. Jabeen [ID](#), R.G. Kellogg [ID](#), T. Koeth [ID](#), B. Kronheim, Y. Lai [ID](#), S. Lascio [ID](#), A.C. Mignerey [ID](#), S. Nabili [ID](#), C. Palmer [ID](#), C. Papageorgakis [ID](#), M.M. Paranjpe, L. Wang [ID](#)

**Massachusetts Institute of Technology, Cambridge, Massachusetts, USA**

J. Bendavid [ID](#), I.A. Cali [ID](#), P.c. Chou [ID](#), M. D'Alfonso [ID](#), J. Eysermans [ID](#), C. Freer [ID](#), G. Gomez-Ceballos [ID](#), M. Goncharov, G. Grossi, P. Harris, D. Hoang, D. Kovalevskyi [ID](#), J. Krupa [ID](#), L. Lavezzi [ID](#), Y.-J. Lee [ID](#), K. Long [ID](#), C. McGinn, A. Novak [ID](#), C. Paus [ID](#), D. Rankin [ID](#), C. Roland [ID](#), G. Roland [ID](#), S. Rothman [ID](#), G.S.F. Stephans [ID](#), Z. Wang [ID](#), B. Wyslouch [ID](#), T. J. Yang [ID](#)

**University of Minnesota, Minneapolis, Minnesota, USA**

B. Crossman [ID](#), B.M. Joshi [ID](#), C. Kapsiak [ID](#), M. Krohn [ID](#), D. Mahon [ID](#), J. Mans [ID](#),

B. Marzocchi [id](#), M. Revering [id](#), R. Rusack [id](#), R. Saradhy [id](#), N. Strobbe [id](#)

**University of Mississippi, Oxford, Mississippi, USA**

L.M. Cremaldi [id](#)

**University of Nebraska-Lincoln, Lincoln, Nebraska, USA**

K. Bloom [id](#), D.R. Claes [id](#), G. Haza [id](#), J. Hossain [id](#), C. Joo [id](#), I. Kravchenko [id](#), J.E. Siado [id](#), W. Tabb [id](#), A. Vagnerini [id](#), A. Wightman [id](#), F. Yan [id](#), D. Yu [id](#)

**State University of New York at Buffalo, Buffalo, New York, USA**

H. Bandyopadhyay [id](#), L. Hay [id](#), H.w. Hsia, I. Iashvili [id](#), A. Kalogeropoulos [id](#), A. Kharchilava [id](#), M. Morris [id](#), D. Nguyen [id](#), S. Rappoccio [id](#), H. Rejeb Sfar, A. Williams [id](#), P. Young [id](#)

**Northeastern University, Boston, Massachusetts, USA**

G. Alverson [id](#), E. Barberis [id](#), J. Dervan, Y. Haddad [id](#), Y. Han [id](#), A. Krishna [id](#), J. Li [id](#), M. Lu [id](#), G. Madigan [id](#), R. McCarthy [id](#), D.M. Morse [id](#), V. Nguyen [id](#), T. Orimoto [id](#), A. Parker [id](#), L. Skinnari [id](#), D. Wood [id](#)

**Northwestern University, Evanston, Illinois, USA**

J. Bueghly, S. Dittmer [id](#), K.A. Hahn [id](#), Y. Liu [id](#), Y. Miao [id](#), D.G. Monk [id](#), M.H. Schmitt [id](#), A. Taliercio [id](#), M. Velasco

**University of Notre Dame, Notre Dame, Indiana, USA**

G. Agarwal [id](#), R. Band [id](#), R. Bucci, S. Castells [id](#), A. Das [id](#), R. Goldouzian [id](#), M. Hildreth [id](#), K.W. Ho [id](#), K. Hurtado Anampa [id](#), T. Ivanov [id](#), C. Jessop [id](#), K. Lannon [id](#), J. Lawrence [id](#), N. Loukas [id](#), L. Lutton [id](#), J. Mariano, N. Marinelli, I. Mcalister, T. McCauley [id](#), C. McGrady [id](#), C. Moore [id](#), Y. Musienko<sup>17</sup> [id](#), H. Nelson [id](#), M. Osherson [id](#), A. Piccinelli [id](#), R. Ruchti [id](#), A. Townsend [id](#), Y. Wan, M. Wayne [id](#), H. Yockey, M. Zarucki [id](#), L. Zygala [id](#)

**The Ohio State University, Columbus, Ohio, USA**

A. Basnet [id](#), B. Bylsma, M. Carrigan [id](#), L.S. Durkin [id](#), C. Hill [id](#), M. Joyce [id](#), M. Nunez Ornelas [id](#), K. Wei, B.L. Winer [id](#), B. R. Yates [id](#)

**Princeton University, Princeton, New Jersey, USA**

H. Bouchamaoui [id](#), P. Das [id](#), G. Dezoort [id](#), P. Elmer [id](#), A. Frankenthal [id](#), B. Greenberg [id](#), N. Haubrich [id](#), K. Kennedy, G. Kopp [id](#), S. Kwan [id](#), D. Lange [id](#), A. Loeliger [id](#), D. Marlow [id](#), I. Ojalvo [id](#), J. Olsen [id](#), A. Shevelev [id](#), D. Stickland [id](#), C. Tully [id](#)

**University of Puerto Rico, Mayaguez, Puerto Rico, USA**

S. Malik [id](#)

**Purdue University, West Lafayette, Indiana, USA**

A.S. Bakshi [id](#), V.E. Barnes [id](#), S. Chandra [id](#), R. Chawla [id](#), A. Gu [id](#), L. Gutay, M. Jones [id](#), A.W. Jung [id](#), A.M. Koshy, M. Liu [id](#), G. Negro [id](#), N. Neumeister [id](#), G. Paspalaki [id](#), S. Piperov [id](#), V. Scheurer, J.F. Schulte [id](#), M. Stojanovic [id](#), J. Thieman [id](#), A. K. Virdi [id](#), F. Wang [id](#), W. Xie [id](#)

**Purdue University Northwest, Hammond, Indiana, USA**

J. Dolen [id](#), N. Parashar [id](#), A. Pathak [id](#)

**Rice University, Houston, Texas, USA**

D. Acosta [id](#), T. Carnahan [id](#), K.M. Ecklund [id](#), P.J. Fernández Manteca [id](#), S. Freed, P. Gardner, F.J.M. Geurts [id](#), W. Li [id](#), J. Lin [id](#), O. Miguel Colin [id](#), B.P. Padley [id](#), R. Redjimi, J. Rotter [id](#), E. Yigitbasi [id](#), Y. Zhang [id](#)

**University of Rochester, Rochester, New York, USA**

A. Bodek , P. de Barbaro , R. Demina , J.L. Dulemba , A. Garcia-Bellido , O. Hindrichs , A. Khukhunaishvili , N. Parmar, P. Parygin<sup>89</sup> , E. Popova<sup>89</sup> , R. Taus 

**The Rockefeller University, New York, New York, USA**

K. Goulian 

**Rutgers, The State University of New Jersey, Piscataway, New Jersey, USA**

B. Chiarito, J.P. Chou , S.V. Clark , D. Gadkari , Y. Gershtain , E. Halkiadakis , M. Heindl , C. Houghton , D. Jaroslawski , O. Karacheban<sup>27</sup> , S. Konstantinou , I. Laflotte , A. Lath , R. Montalvo, K. Nash, J. Reichert , H. Routray , P. Saha , S. Salur , S. Schnetzer, S. Somalwar , R. Stone , S.A. Thayil , S. Thomas, J. Vora , H. Wang 

**University of Tennessee, Knoxville, Tennessee, USA**

H. Acharya, D. Ally , A.G. Delannoy , S. Fiorendi , S. Higginbotham , T. Holmes , A.R. Kanuganti , N. Karunarathna , L. Lee , E. Nibigira , S. Spanier 

**Texas A&M University, College Station, Texas, USA**

D. Aebi , M. Ahmad , T. Akhter , O. Bouhali<sup>90</sup> , R. Eusebi , J. Gilmore , T. Huang , T. Kamon<sup>91</sup> , H. Kim , S. Luo , R. Mueller , D. Overton , D. Rathjens , A. Safonov 

**Texas Tech University, Lubbock, Texas, USA**

N. Akchurin , J. Damgov , N. Gogate , V. Hegde , A. Hussain , Y. Kazhykarim, K. Lamichhane , S.W. Lee , A. Mankel , T. Peltola , I. Volobouev 

**Vanderbilt University, Nashville, Tennessee, USA**

E. Appelt , Y. Chen , S. Greene, A. Gurrola , W. Johns , R. Kunnawalkam Elayavalli , A. Melo , F. Romeo , P. Sheldon , S. Tuo , J. Velkovska , J. Viinikainen 

**University of Virginia, Charlottesville, Virginia, USA**

B. Cardwell , B. Cox , J. Hakala , R. Hirosky , A. Ledovskoy , C. Neu 

**Wayne State University, Detroit, Michigan, USA**

S. Bhattacharya , P.E. Karchin 

**University of Wisconsin - Madison, Madison, Wisconsin, USA**

A. Aravind, S. Banerjee , K. Black , T. Bose , S. Dasu , I. De Bruyn , P. Everaerts , C. Galloni, H. He , M. Herndon , A. Herve , C.K. Koraka , A. Lanaro, R. Loveless , J. Madhusudanan Sreekala , A. Mallampalli , A. Mohammadi , S. Mondal, G. Parida , L. Pétré , D. Pinna, A. Savin, V. Shang , V. Sharma , W.H. Smith , D. Teague, H.F. Tsoi , W. Vetens , A. Warden 

**Authors affiliated with an institute or an international laboratory covered by a cooperation agreement with CERN**

S. Afanasiev , V. Alexakhin , V. Andreev , Yu. Andreev , T. Aushev , M. Azarkin , A. Babaev , V. Blinov<sup>92</sup> , E. Boos , V. Borshch , D. Budkouski , V. Bunichev , V. Chekhovsky, R. Chistov<sup>92</sup> , M. Danilov<sup>92</sup> , A. Dermenev , T. Dimova<sup>92</sup> , D. Druzhkin<sup>93</sup> , M. Dubinin<sup>81</sup> , L. Dudko , A. Ershov , G. Gavrilov , V. Gavrilov , S. Gninenko , V. Golovtcov , N. Golubev , I. Golutvin , I. Gorbunov , A. Gribushin , Y. Ivanov , V. Kachanov , V. Karjavine , A. Karneyeu , V. Kim<sup>92</sup> , M. Kirakosyan, D. Kirpichnikov , M. Kirsanov , V. Klyukhin , O. Kodolova<sup>94</sup> , D. Konstantinov , V. Korenkov , A. Kozyrev<sup>92</sup> , N. Krasnikov , A. Lanev , P. Levchenko<sup>95</sup> , N. Lychkovskaya , V. Makarenko , A. Malakhov , V. Matveev<sup>92</sup> , V. Murzin 

A. Nikitenko<sup>96,94</sup> , S. Obraztsov , V. Oreshkin , V. Palichik , V. Perelygin , S. Petrushanko , S. Polikarpov<sup>92</sup> , V. Popov , O. Radchenko<sup>92</sup> , M. Savina , V. Savrin , V. Shalaev , S. Shmatov , S. Shulha , Y. Skovpen<sup>92</sup> , S. Slabospitskii , V. Smirnov , A. Snigirev , D. Sosnov , V. Sulimov , E. Tcherniaev , A. Terkulov , O. Teryaev , I. Tlisova , A. Toropin , L. Uvarov , A. Uzunian , A. Vorobyev<sup>†</sup>, N. Voytishin , B.S. Yuldashev<sup>97</sup>, A. Zarubin , I. Zhizhin , A. Zhokin 

<sup>†</sup>: Deceased

<sup>1</sup>Also at Yerevan State University, Yerevan, Armenia

<sup>2</sup>Also at TU Wien, Vienna, Austria

<sup>3</sup>Also at Institute of Basic and Applied Sciences, Faculty of Engineering, Arab Academy for Science, Technology and Maritime Transport, Alexandria, Egypt

<sup>4</sup>Also at Ghent University, Ghent, Belgium

<sup>5</sup>Also at Universidade do Estado do Rio de Janeiro, Rio de Janeiro, Brazil

<sup>6</sup>Also at Universidade Estadual de Campinas, Campinas, Brazil

<sup>7</sup>Also at Federal University of Rio Grande do Sul, Porto Alegre, Brazil

<sup>8</sup>Also at UFMS, Nova Andradina, Brazil

<sup>9</sup>Also at Nanjing Normal University, Nanjing, China

<sup>10</sup>Now at The University of Iowa, Iowa City, Iowa, USA

<sup>11</sup>Also at University of Chinese Academy of Sciences, Beijing, China

<sup>12</sup>Also at China Center of Advanced Science and Technology, Beijing, China

<sup>13</sup>Also at University of Chinese Academy of Sciences, Beijing, China

<sup>14</sup>Also at China Spallation Neutron Source, Guangdong, China

<sup>15</sup>Now at Henan Normal University, Xinxiang, China

<sup>16</sup>Also at Université Libre de Bruxelles, Bruxelles, Belgium

<sup>17</sup>Also at an institute or an international laboratory covered by a cooperation agreement with CERN

<sup>18</sup>Also at Suez University, Suez, Egypt

<sup>19</sup>Now at British University in Egypt, Cairo, Egypt

<sup>20</sup>Also at Purdue University, West Lafayette, Indiana, USA

<sup>21</sup>Also at Université de Haute Alsace, Mulhouse, France

<sup>22</sup>Also at Department of Physics, Tsinghua University, Beijing, China

<sup>23</sup>Also at The University of the State of Amazonas, Manaus, Brazil

<sup>24</sup>Also at University of Hamburg, Hamburg, Germany

<sup>25</sup>Also at RWTH Aachen University, III. Physikalisches Institut A, Aachen, Germany

<sup>26</sup>Also at Bergische University Wuppertal (BUW), Wuppertal, Germany

<sup>27</sup>Also at Brandenburg University of Technology, Cottbus, Germany

<sup>28</sup>Also at Forschungszentrum Jülich, Juelich, Germany

<sup>29</sup>Also at CERN, European Organization for Nuclear Research, Geneva, Switzerland

<sup>30</sup>Also at Institute of Nuclear Research ATOMKI, Debrecen, Hungary

<sup>31</sup>Now at Universitatea Babes-Bolyai - Facultatea de Fizica, Cluj-Napoca, Romania

<sup>32</sup>Also at MTA-ELTE Lendület CMS Particle and Nuclear Physics Group, Eötvös Loránd University, Budapest, Hungary

<sup>33</sup>Also at HUN-REN Wigner Research Centre for Physics, Budapest, Hungary

<sup>34</sup>Also at Physics Department, Faculty of Science, Assiut University, Assiut, Egypt

<sup>35</sup>Also at Punjab Agricultural University, Ludhiana, India

<sup>36</sup>Also at University of Visva-Bharati, Santiniketan, India

<sup>37</sup>Also at Indian Institute of Science (IISc), Bangalore, India

<sup>38</sup>Also at IIT Bhubaneswar, Bhubaneswar, India

<sup>39</sup>Also at Institute of Physics, Bhubaneswar, India

- <sup>40</sup>Also at University of Hyderabad, Hyderabad, India  
<sup>41</sup>Also at Deutsches Elektronen-Synchrotron, Hamburg, Germany  
<sup>42</sup>Also at Isfahan University of Technology, Isfahan, Iran  
<sup>43</sup>Also at Sharif University of Technology, Tehran, Iran  
<sup>44</sup>Also at Department of Physics, University of Science and Technology of Mazandaran, Behshahr, Iran  
<sup>45</sup>Also at Department of Physics, Isfahan University of Technology, Isfahan, Iran  
<sup>46</sup>Also at Italian National Agency for New Technologies, Energy and Sustainable Economic Development, Bologna, Italy  
<sup>47</sup>Also at Centro Siciliano di Fisica Nucleare e di Struttura Della Materia, Catania, Italy  
<sup>48</sup>Also at Università degli Studi Guglielmo Marconi, Roma, Italy  
<sup>49</sup>Also at Scuola Superiore Meridionale, Università di Napoli 'Federico II', Napoli, Italy  
<sup>50</sup>Also at Fermi National Accelerator Laboratory, Batavia, Illinois, USA  
<sup>51</sup>Also at Consiglio Nazionale delle Ricerche - Istituto Officina dei Materiali, Perugia, Italy  
<sup>52</sup>Also at Department of Applied Physics, Faculty of Science and Technology, Universiti Kebangsaan Malaysia, Bangi, Malaysia  
<sup>53</sup>Also at Consejo Nacional de Ciencia y Tecnología, Mexico City, Mexico  
<sup>54</sup>Also at Trincomalee Campus, Eastern University, Sri Lanka, Nilaveli, Sri Lanka  
<sup>55</sup>Also at Saegis Campus, Nugegoda, Sri Lanka  
<sup>56</sup>Also at National and Kapodistrian University of Athens, Athens, Greece  
<sup>57</sup>Also at Ecole Polytechnique Fédérale Lausanne, Lausanne, Switzerland  
<sup>58</sup>Also at Universität Zürich, Zurich, Switzerland  
<sup>59</sup>Also at Stefan Meyer Institute for Subatomic Physics, Vienna, Austria  
<sup>60</sup>Also at Laboratoire d'Annecy-le-Vieux de Physique des Particules, IN2P3-CNRS, Annecy-le-Vieux, France  
<sup>61</sup>Also at Near East University, Research Center of Experimental Health Science, Mersin, Turkey  
<sup>62</sup>Also at Konya Technical University, Konya, Turkey  
<sup>63</sup>Also at Izmir Bakircay University, Izmir, Turkey  
<sup>64</sup>Also at Adiyaman University, Adiyaman, Turkey  
<sup>65</sup>Also at Bozok Universitetesi Rektörlüğü, Yozgat, Turkey  
<sup>66</sup>Also at Marmara University, Istanbul, Turkey  
<sup>67</sup>Also at Milli Savunma University, Istanbul, Turkey  
<sup>68</sup>Also at Kafkas University, Kars, Turkey  
<sup>69</sup>Now at stanbul Okan University, Istanbul, Turkey  
<sup>70</sup>Also at Hacettepe University, Ankara, Turkey  
<sup>71</sup>Also at Erzincan Binali Yıldırım University, Erzincan, Turkey  
<sup>72</sup>Also at Istanbul University - Cerrahpasa, Faculty of Engineering, Istanbul, Turkey  
<sup>73</sup>Also at Yildiz Technical University, Istanbul, Turkey  
<sup>74</sup>Also at Vrije Universiteit Brussel, Brussel, Belgium  
<sup>75</sup>Also at School of Physics and Astronomy, University of Southampton, Southampton, United Kingdom  
<sup>76</sup>Also at IPPP Durham University, Durham, United Kingdom  
<sup>77</sup>Also at Monash University, Faculty of Science, Clayton, Australia  
<sup>78</sup>Also at Università di Torino, Torino, Italy  
<sup>79</sup>Also at Bethel University, St. Paul, Minnesota, USA  
<sup>80</sup>Also at Karamanoğlu Mehmetbey University, Karaman, Turkey  
<sup>81</sup>Also at California Institute of Technology, Pasadena, California, USA  
<sup>82</sup>Also at United States Naval Academy, Annapolis, Maryland, USA

<sup>83</sup>Also at Ain Shams University, Cairo, Egypt

<sup>84</sup>Also at Bingol University, Bingol, Turkey

<sup>85</sup>Also at Georgian Technical University, Tbilisi, Georgia

<sup>86</sup>Also at Sinop University, Sinop, Turkey

<sup>87</sup>Also at Erciyes University, Kayseri, Turkey

<sup>88</sup>Also at Horia Hulubei National Institute of Physics and Nuclear Engineering (IFIN-HH), Bucharest, Romania

<sup>89</sup>Now at an institute or an international laboratory covered by a cooperation agreement with CERN

<sup>90</sup>Also at Texas A&M University at Qatar, Doha, Qatar

<sup>91</sup>Also at Kyungpook National University, Daegu, Korea

<sup>92</sup>Also at another institute or international laboratory covered by a cooperation agreement with CERN

<sup>93</sup>Also at Universiteit Antwerpen, Antwerpen, Belgium

<sup>94</sup>Also at Yerevan Physics Institute, Yerevan, Armenia

<sup>95</sup>Also at Northeastern University, Boston, Massachusetts, USA

<sup>96</sup>Also at Imperial College, London, United Kingdom

<sup>97</sup>Also at Institute of Nuclear Physics of the Uzbekistan Academy of Sciences, Tashkent, Uzbekistan